Analytical characterization of polyamide 11 and related polymers used for additive manufacturing

Dissertation

zur Erlangung des Doktorgrades der Naturwissenschaften

(Dr. rer. nat.)

der Fakultät Chemie und Pharmazie

der Universität Regensburg

vorgelegt von

Beate Theresia Scherer

aus **Deining - Oberbuchfeld**

April 2021

Die vorgelegte Dissertation entstand im Zeitraum von Dezember 2017 bis April 2021 in Kooperation des Instituts für Analytische Chemie, Chemo- und Biosensorik der naturwissenschaftlichen Fakultät IV der Universität Regensburg

und

der Technologie Werkstoff- und Verfahrensanalytik der BMW Group.

Die Arbeit wurde angeleitet von: Prof. Dr. habil. Frank-Michael Matysik und durchgeführt unter der Leitung von Johann Troffer.

Promotionsgesuch eingereicht am:	29.04.2021
Tag der mündlichen Prüfung:	13.07.2021

Prüfungsausschuss:

Vorsitzende:	Prof. Dr. Julia Rehbein
Erstgutachter:	Prof. Dr. Frank-Michael Matysik
Zweitgutachterin:	PD Dr. Katja Dettmer-Wilde
Drittprüfer:	Prof. Dr. Hubert Motschmann

AN DIESER STELLE MÖCHTE ICH MICH BEI ALLEN BEDANKEN, DIE MICH AUF DEM WEG ZUR PROMOTION UNTERSTÜTZT UND BEGLEITET HABEN.

Table of contents

List of publications

Dual detection for non-aqueous capillary electrophoresis combining contactless conductivity detection and mass spectrometry

Andrea Beutner, Beate Scherer, Frank-Michael Matysik

Talanta 183 (2018) 33-38

Abstract

Coupling of two detectors is a powerful tool to enhance the overall analytical performance generating complementary information and overcoming the limitations of the single detectors. In this work, capacitively coupled contactless conductivity detection (C^4D) and electrospray ionization mass spectrometry (ESI-MS) were coupled in conjunction with non-aqueous capillary electrophoresis (NACE). Non-aqueous electrolytes are highly compatible with ESI due to their volatility. Moreover, they exhibit low background conductivity, which is essential for the detection with C^4D. A NACE-C^4D-MS method was developed using an acetonitrile buffer containing 2 M HAc and 4 mM NH_4Ac as background electrolyte. The influence of the inner diameter of the separation capillary on the C^4D was studied and taken into account. A capillary with 50 µm inner diameter was found to be best suited. The complementarity of the two detectors was shown by determining a sample mixture containing choline, thiamine, nitrate, and chloride as well as bromide and acetylcholine as internal standards. The C^4D was the detector of choice for the inorganic ions, which were not detectable with the MS whereas the MS had much lower limits of detections for the organic biomolecules. The method was applied on an extract of a food supplement containing the model analytes.

Comparison of molar mass determination of poly(dimethylsiloxanes) by size exclusion chromatography and high-resolution polymer high-performance liquid chromatography based on a sawtooth gradient

Bernhard Durner, Beate Scherer, Thomas Ehmann, Frank-Michael Matysik

ACS Applied Polymer Materials 1 (2019) 2388-2397

Abstract

Polysiloxanes are used in a wide range of application fields, and extensive research is currently done to enhance product quality and performance. Therefore, more sophisticated analysis methods are necessary to monitor and support the polymer product optimization.

Based on different modes in polymer liquid chromatography, heart-cut polymer HPLC is one powerful analytical approach. Due to different distributions within polymer samples, separations according to chemical heterogeneities, molecular architecture, or molar mass differences are possible. With the recently introduced sawtooth gradient protocol a possibility for determining the polymer (micro-)structure on an analytical scale has been developed. Hence, the effect of various stationary phases with different particle based material and chemical modifications was investigated in the context of the separation of linear poly(dimethylsiloxane) in a molar mass range from 1,000 g mol^{-1} to 300,000 g mol^{-1}. The resulting chromatograms allowed a direct correlation between HPLC retention times and molar masses corresponding to separated peaks. Consequently, a detailed analysis of differences in the polymer structure, e.g. fingerprint analysis, is possible. This special technique could be used in the context of quality control to ensure the product stability of polymer samples.

Material characterization of polyamide 12 and related agents used in the multi jet fusion process: complementary application of high-resolution mass spectrometry and other advanced instrumental techniques

Beate Scherer, Ingo Leonard Kottenstedde, Frank-Michael Matysik

Monatshefte für Chemie - Chemical Monthly 151 (2020) 1203-1215

Abstract

The powder bed-based 3D printing process called multi jet fusion from HP is used in various industries for different applications. A polymer powder, the so-called fusing and detailing agents, and an IR source are needed. These novel materials offer some challenges for analytical characterization. High-resolution mass spectrometry in combination with a data base search was used as a tool for comprehensive characterization of the agents, the methanol extract of new polyamide 12 powder, and the methanol extract of a ground 3D printed part. In addition, thermogravimetric studies were carried out. Besides biocides and substances containing ethoxy units, 2-pyrrolidone and triethylene glycol were identified as organic solvents in the agents. The detailing agent contained 3.7% of 2-pyrrolidone and 11.1% of triethylene glycol. The fusing agent contained 18.7% of 2-pyrrolidone and 8.4% of triethylene glycol. Based on the agents' different functionalities, the water content of the detailing agent was 18% higher as compared to the fusing agent. In addition, the fusing agent contained a carbon black amount of 5.2%. The methanol extract of new polyamide 12 powder contained remaining monomer and oligomer compounds, as well as the oxidation stabilizer Irganox 1098. In the methanol extract of the ground 3D printed part the cyclic and linear

monomer, oligomers, and oxidation stabilizer were found. Moreover, ingredients of the agents were detected. Residues of 2-pyrrolidone, triethylene glycol, 3-benzisothiazolinone, and substances containing ethoxy units were identified in the methanol extract of the ground 3D printed part. In contrast, no 2-methyl-4-isothiazolin-3-one was observed.

Analytical characterization of polyamide 11 used in the context of selective laser sintering: Physico-chemical correlations

Beate Scherer, Ingo Leonard Kottenstedde, Wolfgang Bremser, Frank-Michael Matysik

Polymer Testing 91 (2020) 106786

Abstract

Polyamide 11 is an attractive material for additive manufacturing, however, in the selective laser sintering process it is subject to significant thermally induced stress. Suitable analytical methods are necessary to indicate any changes in the material properties. In this work, thermally stressed powder samples and printed tensile bars were analyzed by size exclusion chromatography – multi-angle laser light scattering and differential scanning calorimetry. Based on the molecular weight distribution, crystallization and melting temperatures, aging states of the investigated powders could be defined and transferred to the particles of the printed components. As a result, thermal stress led to an increase in molar mass and polydispersity. Moreover, calorimetric measurements indicated a delayed nucleation process as well as a decrease in polymorphism. Additionally, polymeric material with lower polydispersity values across the tensile bars could lead to decreasing elongation at break (ε_B) values. For the crystallization onset temperature the opposite effect on ε_B was observed.

Investigations of polymer samples of polyamide 11 concerning the content of monomer, oligomers, and the oxidation stabilizer Irganox 1098 by utilizing inverse gradient HPLC in combination with a triple detection system (diode array detection / mass spectrometry / charged aerosol detection)

Beate Scherer, Frank-Michael Matysik

Talanta Open 3 (2021) 100023

Abstract

The aim of this work was to develop a method to comprehensively characterize extracts from polyamide 11 powder samples used in the laser sintering process. Firstly, high-resolution mass spectrometry was applied to identify low molecular compounds in the material. Secondly, by means of an inverse gradient high-performance liquid chromatography (HPLC) in combination with a triple detection system consisting of a diode array detector (DAD), a mass spectrometer (MS), and a charged aerosol detector (CAD), a method was established to determine the amount of monomer and oligomers up to the linear tetramer and cyclic pentamer. Furthermore, the oxidation stabilizer identified as Irganox 1098 was determined. The DAD was utilized for the quantification of the UV-active oxidation stabilizer. Thus, to be able to extract the low molecular weight compounds, various protocols were studied and finally accelerated solvent extraction was used. As there is a lack of commercial standards of polyamide 11 related oligomers, these compounds were detected with the CAD, taking advantage of its uniform response behavior in conjunction with an inverse gradient HPLC protocol. In addition, the MS was utilized as a qualitative detector for peak identification. The information regarding low molecular weight compounds are required as the powder is subject to the thermal loading of the sintering process, which influences the composition of the low molecular weight compounds. Thus, the method was applied to new and oven-aged polyamide 11 samples. Finally, it was possible to monitor the change of low molecular weight compounds in stressed polyamide 11 powder samples.

Conference contributions

Oral presentations

15th International Students Conference “Modern Analytical Chemistry” 2019, September 19-20, 2019, Prague
Analytical investigations of fusing and detailing agents used in the context of multi jet fusion process in 3D printing
Beate Scherer, Frank-Michael Matysik

31. Doktorandenseminar des Arbeitskreises Separation Science der GDCh-Fachgruppe Analytische Chemie, January 11-12, 2021, online
Analytical investigations on polyamide 11 used for 3D printing
Beate Scherer, Frank-Michael Matysik

Poster presentations

ANAKON 2017, March 25-28, 2019, Münster
Analytical characterization of the aging of polyamide 11 powder used for 3D printing
Beate Scherer, Frank-Michael Matysik

ProMotion Dialogue Day of the BMW Group, September 17, 2020, virtual
Material analysis. Chemische Charakterisierung von Materialien für den 3D-Druck
Beate Scherer

Declaration of collaboration

Most of the theoretical and experimental work presented in this thesis was carried out solely by the author. In some cases, however, the practical implementation of concepts and the performance of measurements were carried out in collaboration with other researchers and individuals. In accordance with *§ 8 Abs. 1 Satz 7 of the Ordnung zum Erwerb des akademischen Grades eines Doktors der Naturwissenschaften (Dr. rer. nat.) an der Universität Regensburg vom 18. Juni 2009 (Änderungssatzung vom 6. Februar 2014)*, this section details the nature of these collaborations.

4.1 Comparison of molar mass determination of poly(dimethylsiloxanes) by size exclusion chromatography and high-resolution polymer high-performance liquid chromatography based on a sawtooth gradient

Experiments such as SEC analyses were conducted solely by the author. Experimental work regarding polymer HPLC was conducted by Bernhard Durner at the Corporate Analytics department of Wacker Chemie AG in Burghausen. The authors contributed equally to interpretation and writing. The research was carried out under supervision and guidance of Dr. Thomas Ehmann and Prof. Dr. Frank-Michael Matysik.

4.2 Development of a HRP-HPLC method by means of a sawtooth gradient profile for polyamide 11 and 12 samples in comparison to SEC-MALLS investigations

Measurements were done solely by the author. The research was done under supervision and guidance of Prof. Dr. Frank-Michael Matysik.

4.3 Material characterization of polyamide 12 and related agents used in the multi jet fusion process: complementary application of high-resolution mass spectrometry and other advanced instrumental techniques

Thermogravimetric measurements and the writing of the related sections were done by Ingo Leonard Kottenstedde at the business unit Technologie Werkstoff- und Verfahrensanalytik (TI-323) of the BMW Group in Dingolfing. HPLC-MS measurements were planned and performed solely by the author. The manuscript was written by the author except for the thermogravimetric part. The project was supervised by Prof. Dr. Frank-Michael Matysik.

4.4 Analytical characterization of polyamide 11 used in the context of selective laser sintering: Physico-chemical correlations

Experiments such as SEC analyses were conducted solely by the author. Experimental work regarding DSC was conducted by Ingo Leonard Kottenstedde at the business unit Technologie Werkstoff- und Verfahrensanalytik (TI-323) of the BMW Group in Dingolfing. The authors

contributed equally to interpretation and writing. The research was done under supervision and guidance of Prof. Dr. Wolfgang Bremser and Prof. Dr. Frank-Michael Matysik.

4.5 Investigations of polymer samples of polyamide 11 concerning the content of monomer, oligomers, and the oxidation stabilizer Irganox 1098 by utilizing inverse gradient HPLC in combination with a triple detection system (diode array detection / mass spectrometry / charged aerosol detection)

Measurements were performed solely by the author. The research was carried out under supervision and guidance of Prof. Dr. Frank-Michael Matysik.

List of abbreviations

AD	Analogue-digital
AM	Additive manufacturing
AUA	Aminoundecanoic acid
CV	Column volume
CAD	Charged aerosol detector
DAD	Diode array detector
dRI	Differential refractive index
DSC	Differential scanning calorimetry
ε_B	Elongation at break
ELSD	Evaporative light scattering detector
ESI	Electrospray ionization
FA	Formic acid
GC	Gas chromatography
GPEC	Gradient polymer elution chromatography
HFIP	1,1,1,3,3,3-Hexafluoroisopropanol
HFBA	Heptafluorobutyric acid
HPLC	High-performance liquid chromatography
HRP-HPLC	High-resolution polymer high-performance liquid chromatography
KTFAc	Potassium trifluoroacetate
LAC	Liquid adsorption chromatography
LC	Liquid chromatography
LCCC	Liquid chromatography under critical conditions
MALDI-ToF-MS	Matrix assisted laser desorption time-of-flight mass spectrometry
MALLS	Multi-angle laser light scattering
MFI	Melt flow index

M_n	Number average molar mass
M_p	Molar mass at peak maximum
MS	Mass spectrometry
M_w	Weight average molar mass
m/z	Mass-to-charge ratio
P	Polydispersity
PDMS	Poly(dimethylsiloxane)
PLC	Precipitation-redissolution chromatography
PMMA	Poly(methylmethacrylate)
PSD	particle size distribution
PVC	polyvinyl chloride
QTOF	quadrupole time-of-flight
RI	Refractive index
SAXS	Small-angle X-ray scattering
SEC	Size exclusion chromatography
TFA	Trifluoroacetic acid
THF	Tetrahydrofuran
TGA	Thermogravimetric analysis
UV-VIS	Ultraviolet-visible
WAXS	Wide-angle X-ray scattering

1 Introduction

Additive manufacturing (AM) also known as 3D printing enables the transfer of 3D models into physical objects on the basis of computer-aided designs [1]. Thereby, 3D data is transformed into slices of 2D data and transferred to a printing machine. After the setting of suitable build parameters, the printing takes place layer by layer without the need of molds. When the build job is finished and the printed parts are cooled down to a certain temperature if necessary, the parts are removed from the printing machine. This is often followed by post-processing steps to achieve the desired properties [1,2].

Typically, prototypes are produced with AM, however, as the next major step it is aimed to establish serial production. Therefore, ensuring consistent quality of the printed parts is important [3]. Especially within laser sintering and multi jet fusion, which are AM processes based on powder bed fusion of polymers, many different factors contribute to component quality and economic efficiency. The mentioned AM processes are applied in different industries such as medical, aerospace, and automotive industry [4,5]. The focus of the work at hand is on the analytical characterization of polyamide 11 and 12 powder samples used for powder bed fusion processes and printed parts.

The motivation was to study und reduce brittle fractures in printed parts. A high molar mass, thermal load or residual oxygen content in the printing process leading to material degradation were assumed as key points causing brittle fractures.

In literature, among others, melting and crystallization temperature, molecular weight, additives, monomer and oligomer content are described as factors with an impact on the quality of the final product of the printing process [5,6]. Different analytical methods can be utilized for material characterization, process control or failure analysis.

However, before suitable analytical techniques are applied, sampling and sample preparation are two crucial steps in order to receive reliable data. Consequently, it is important to consider the whole analytical process with respect to its robustness when interpreting the received results. Concerning the application of analytical methods for investigating different AM processes, it is necessary to know which material properties are the important ones to focus on. Different analytical tools need to be employed to gain the required knowledge [7].

For material characterization and investigation of quality related properties, different liquid chromatographic techniques are applied. Size exclusion chromatography (SEC) is very common to determine the molecular weight distribution of polymer samples [8–10]. In addition, high-resolution polymer high-performance liquid chromatography (HRP-HPLC) makes a

distinction of different process materials feasible [11–13]. Low molecular weight compounds included in polymer samples are identified by HPLC in combination with high-resolution mass spectrometry in order to receive information about ingredients of the powders such as oxidation stabilizers, monomers or oligomers [14]. Moreover, a quantitative determination of oligomers is achieved by the application of universal detectors like a charged aerosol detector as it is important to know how the oligomer content changes under the influence of thermal and thermo-oxidative aging [15–17]. Additionally, there is a risk of evaporation of the oligomers and the oxidation stabilizer which leads to a contamination of the machine resulting in parts of poor quality.

This thesis was based on the following objectives:

- Development of a sawtooth gradient in the context of HRP-HPLC to improve the separation efficiency for the analysis of polyamide 11 and 12 powder samples.
- Characterization of polyamide 12 and related agents used in the multi jet fusion process in terms of their ingredients by means of high-resolution mass spectrometry and other advanced instrumental techniques.
- Investigations of the correlation between the molar mass of thermally treated polyamide 11 powder samples and printed parts regarding their mechanical properties.
- Development and optimization of a protocol for the comprehensive characterization of polyamide 11 samples of different aging states by means of inverse gradient HPLC in combination with a triple detection system.

References

[1] S.C. Ligon, R. Liska, J. Stampfl, M. Gurr, R. Mülhaupt, Polymers for 3D printing and customized additive manufacturing, Chemical Reviews 117 (2017) 10212–10290. https://doi.org/10.1021/acs.chemrev.7b00074.

[2] I. Gibson, D. Rosen, B. Stucker, M. Khorasani, Introduction and basic principles, in: Additive Manufacturing Technologies, Springer International Publishing, Cham, 2021, pp. 1–21.

[3] P.V. Osswald, P. Obst, G.A.M. Capote, M. Friedrich, D. Rietzel, G. Witt, Failure criterion for PA 12 multi-jet fusion additive manufactured parts, Addit. Manuf. 37 (2021) 101668. https://doi.org/10.1016/j.addma.2020.101668.

[4] S. Yuan, F. Shen, C.K. Chua, K. Zhou, Polymeric composites for powder-based additive manufacturing: Materials and applications, Prog. Polym. Sci. 91 (2019) 141–168. https://doi.org/10.1016/j.progpolymsci.2018.11.001.

[5] A. Wegner, Theorie über die Fortführung von Aufschmelzvorgängen als Grundvoraussetzung für eine robuste Prozessführung beim Laser-Sintern von Thermoplasten. Dissertation, 2015.

[6] A. Wegner, R. Harder, G. Witt, D. Drummer, Determination of optimal processing conditions for the production of polyamide 11 parts using the laser sintering process, International Journal of Recent Contributions from Engineering, Science & IT 3 (2015) 5–12.

[7] W. Kupfer, Kunststoff-Analyse, Fresenius Z. Anal. Chem. 192 (1962) 219–248. https://doi.org/10.1007/BF00465766.

[8] C.-s. Wu (Ed.), Handbook of size exclusion chromatography, Marcel Dekker, New York, 1995.

[9] T.H. Mourey, T.G. Bryan, Size-exclusion chromatography in 1,1,1,3,3,3-hexafluoro-2-propanol, J. Chromatogr. A 964 (2002) 169–178. https://doi.org/10.1016/S0021-9673(02)00510-1.

[10] S. Laun, H. Pasch, N. Longiéras, C. Degoulet, Molar mass analysis of polyamides-11 and -12 by size exclusion chromatography in HFiP, Polymer 49 (2008) 4502–4509. https://doi.org/10.1016/j.polymer.2008.08.017.

[11] B. Durner, T. Ehmann, F.-M. Matysik, High-resolution polymer high performance liquid chromatography: Application of a saw tooth gradient for the separation of various polymers, J. Chromatogr. A 1587 (2019) 88–100. https://doi.org/10.1016/j.chroma.2018.11.075.

[12] B. Durner, T. Ehmann, F.-M. Matysik, High-resolution polymer high performance liquid chromatography: optimization of the saw tooth gradient profile for various stationary phases and separations on preparative scale, Anal. Methods 11 (2019) 4960–4968. https://doi.org/10.1039/C9AY00689C.

[13] B. Durner, T. Ehmann, F.-M. Matysik, Separation of linear and cyclic poly(dimethylsiloxanes) with polymer high-performance liquid chromatography, Monatsh. Chem. - Chemical Monthly 150 (2019) 1603–1610. https://doi.org/10.1007/s00706-019-02389-4.

[14] H. Wang, J. Yuan, Identification and quantification of unknown antioxidants in plastic materials by ultrasonic extraction and ultra-performance liquid chromatography coupled with quadrupole time-of-flight mass spectrometry, Eur. J. Mass Spectrom. 22 (2016) 19–29. https://doi.org/10.1255/ejms.1404.

[15] R.D. Cohen, L. Yong, Advances in aerosol-based detectors, in: E. Grushka, N. Grinber (Eds.), Advances in Chromatography: Volume 52, CRC, Boca Raton, 2014, pp. 1–53.

[16] P.H. Gamache (Ed.), Charged aerosol detection for liquid chromatography and related separation techniques, Wiley, Hoboken, 2017.

[17] J.H. Arndt, T. Macko, R. Brüll, Application of the evaporative light scattering detector to analytical problems in polymer science, J. Chromatogr. A 1310 (2013) 1–14. https://doi.org/10.1016/j.chroma.2013.08.041.

2 Fundamentals and background

2.1 Materials and processes

2.1.1 Polyamide 11 and 12

2.1.1.1 Synthesis

The general synthesis of polyamide 11 and 12 materials is described in this section. Since 1955 polyamide 11 is manufactured in large scale by polycondensation of 11-aminoundecanoic acid. The chemical synthesis of the monomer is shown in Figure 2.1.1. Ricinoleic acid out of the castor plant is esterified via thermal cleavage of castor oil and methanolysis [1]. Out of the product ricinoleic acid methyl ester, the undecylenic acid methyl ester and heptanal are synthesized [2]. The undecylenic acid methyl ester is hydrolyzed to undecylenic acid. Via radical addition of HBr followed by the substitution of the bromine by an amino group, the 11-aminoundecanoic acid is produced [1].

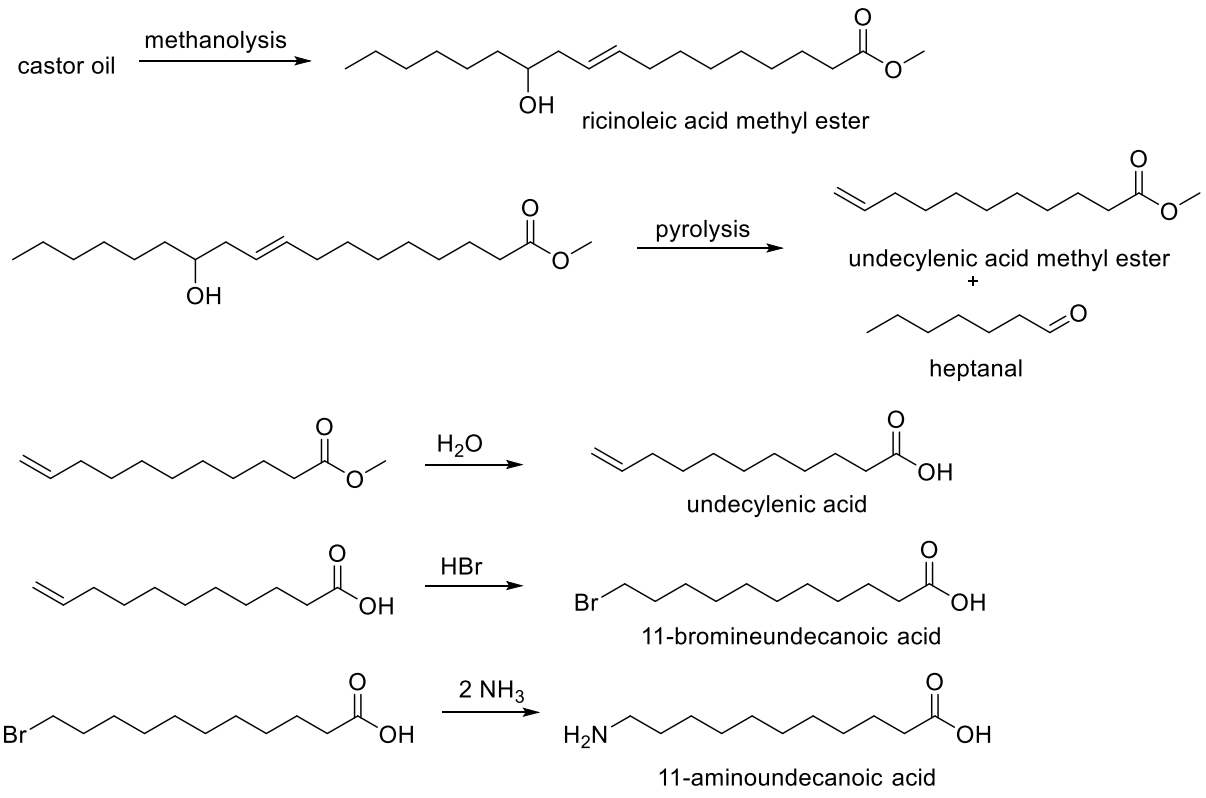

Figure 2.1.1 Synthesis of 11-aminoundecanoic acid [1].

The polycondensation of 11-aminoundecanoic acid is described as a 2nd order reaction [3] (see Figure 2.1.2) whereby phosphoric and phosphorus acid are utilized as catalysts to stabilize the degree of polymerization by blocking the NH_2-groups. The polymerization is conducted by melt condensation, followed by post-condensation in the solid phase to adjust

the molecular mass of the final product. Furthermore, based on the natural origin of the monomer, polyamide 11 is considered as a bio-based polymer [1,4].

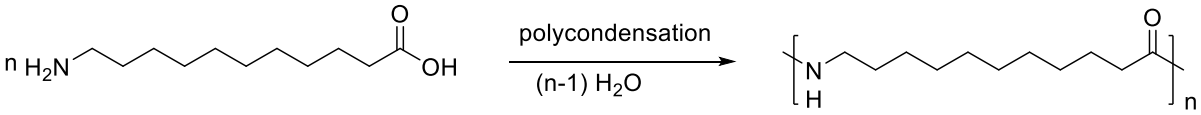

Figure 2.1.2 Polycondensation of 11-aminoundecanoic acid [1,5].

Different from the polycondensation of 11-aminoundecanoic acid, polyamide 12 is synthesized by ring-opening polymerization. The monomer is based on butadiene as a petrochemical raw material. The synthesis of laurolactam starts with the trimerization of butadiene leading to cyclododecatriene. This molecule is hydrated and oxidized yielding cyclododecanol and cyclododecanone. The cyclododecanol is dehydrated resulting also in the cyclododecanone. The alkanone reacts with hydroxylamine to the corresponding oxime and via Beckmann rearrangement to the laurolactam. The synthesis of the monomer of polyamide 12 is depicted in Figure 2.1.3 [5].

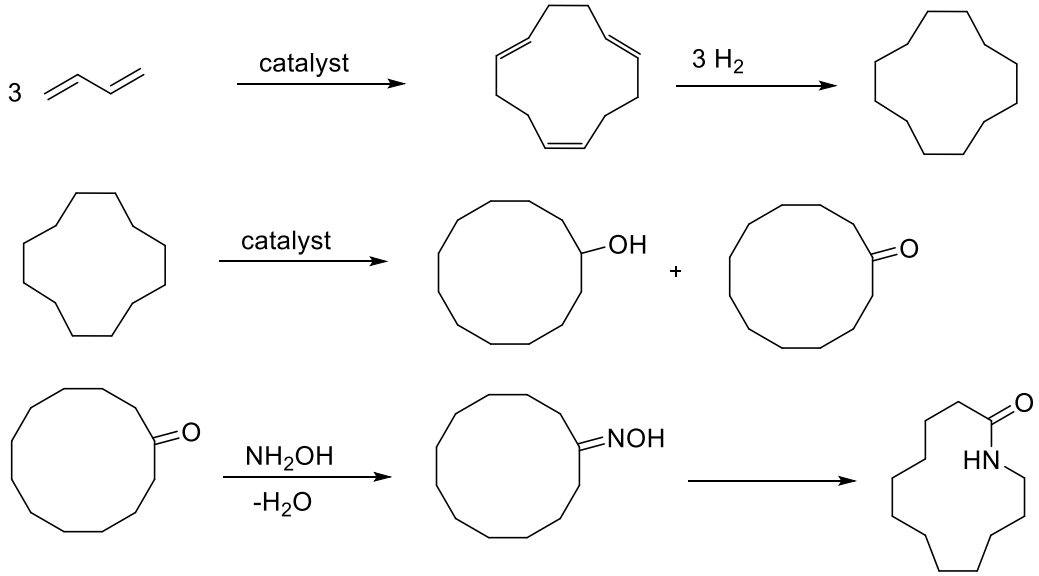

Figure 2.1.3 Scheme of laurolactam synthesis [5].

A second monomer, the 12-aminododecanoid acid plays only a minor role for the production of polyamide 12 as the 12-aminododecanoid acid is more complex to produce [6]. Instead the laurolactam is transformed to the 12-aminododecanoid acid via ring opening by using water under pressure and temperature followed by the polycondensation step. The corresponding scheme is depicted in Figure 2.1.4. The polymerization is executed via different large-scale processes. Just as the process of polyamide 11 a post-condensation in the solid state is conducted to adjust the molar mass for different applications. Besides the hydrolytic polymerization also cationic and anionic polymerizations are possible [5,7].

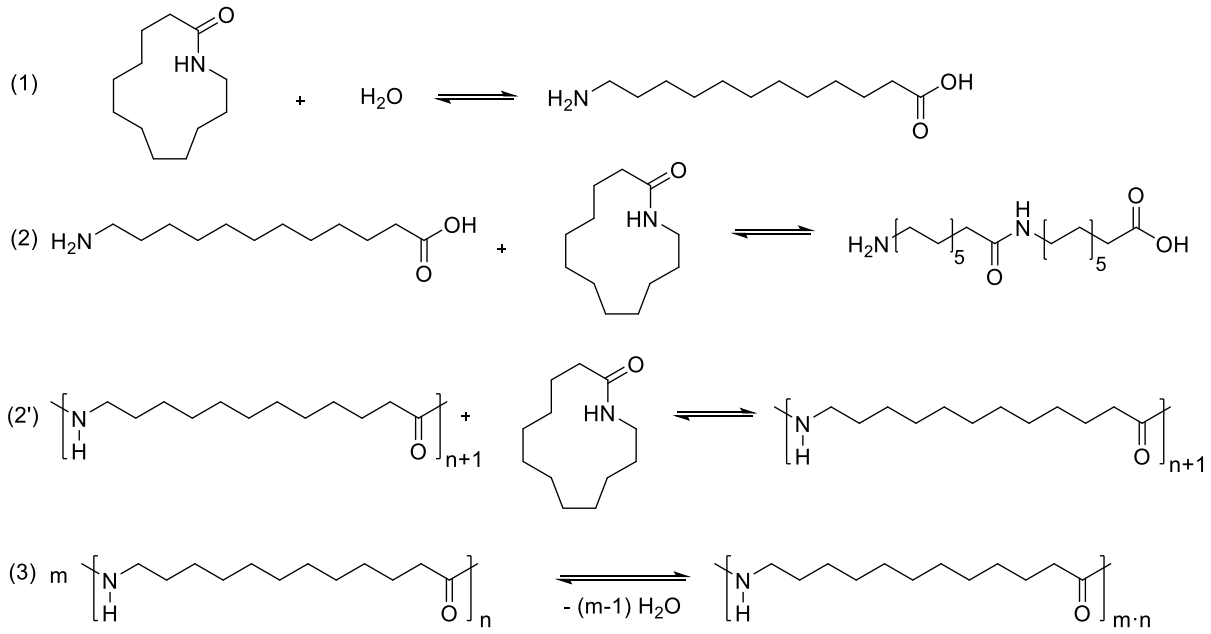

Figure 2.1.4 Hydrolytic polymerization of laurolactam [5].

2.1.1.2 Applications

Polyamide 11 and 12 are used in different fields for various applications such as the automotive, textile, oil, and gas industry [8]. Furthermore, powders based on polyamide 11 and 12 are employed for coating of metal parts suitable as protection against corrosion. Moreover, polyamide 12 is applicable in mechanical engineering. In this context, metal parts or other synthetic materials are replaced by polyamide 12 [5]. Due to its easy processing, polyamide 11 and 12 are applied for extrusion, extrusion-blow molding, injection molding, rotomolding, and 3D printing [8,9]. Besides that, the properties of polyamide 11 allow the use for internal insulation layers in flexible pipelines which are needed for offshore oilfield exploitation [10–13]. Concerning 3D printing, polyamide 11 and 12 are both mostly applied unfilled or filled as composites in powder bed fusion processes [14–17].

2.1.1.3 Material properties

Polyamide 11 belongs to the group of uneven polyamides and polyamide 12 to the even ones [18]. An overview of different properties of polyamide 11 and 12 is given in Table 2.1.1. The moisture absorption at 100% for both polyamides is relatively low with 1.9 and 1.6% compared to polyamide 6 (9.5%) due to the low ratio of carbonamide to methylene groups [5].

Table 2.1.1 Melting point, moisture absorption at 100% relative humidity and ratio of amide groups to CH_2 groups of polyamide 11 and 12.

property	polyamide 11	polyamide 12
melting point / °C [5]	185	178
Moisture absorption at 100% relative humidity / %[19]	1.9	1.6
Ratio of amide groups to CH_2 groups [20]	1:10	1:11

Furthermore, investigations have shown that different crystal forms can be observed for polyamide 11 and 12. Besides monoclinic β- and triclinic α- crystals, a pseudohexagonal δ phase can be received for polyamide 11. Thereby, the triclinic α phase reversibly transforms into the pseudohexagonal δ phase via the Brill transition during heating. Additionally, an α‘ phase was cited in literature very similar to the α phase. However, by quenching from the melt, the smectic δ‘ phase is formed which irreversibly transforms into the pseudohexagonal δ phase [19,21–25].

For polyamide 12 α, α‘, γ, and γ‘ phases are cited as possible crystal modifications in literature. The main crystallization phase is the hexagonal γ-form during moderate cooling rates from the melt. Quenching of the melt leads to the mesomorphic γ‘-phase which irreversibly transforms into the γ-phase by annealing. During cooling at pressure higher than 500 MPa, the α-phase was observed, whereby the α‘-phase was obtained at crystallization at high temperatures [26,27]. Dai et al. [28] observed a gradual transformation of the α-phase into the γ-phase which was designated to the Brill transition.

The focus of the work at hand is on polyamide 11 and 12 materials used for powder bed fusion 3D printing processes. For those materials an increase of the melting point and melting enthalpy can be achieved by treatment with water or steam without changing the crystallization temperature. The increase of the melting temperature results in an expanded sintering window for the laser sintering process [29]. Furthermore, the powder materials are also treated with e.g. phosphoric acid to establish a better reusability in the laser sintering process [30]. Within semi-crystalline polymers, it is assumed that the chain entanglement within the amorphous phase and especially the size of the amorphous regions between the crystalline lamellae are decisive for the ductile fracture behavior [31]. Moreover, mechanical properties are depending from the molecular weight, thermal treatment, and general manufacturing conditions, whereby a high elongation at break (ε_B) is typical for both polyamide 11 and 12. However, polyamide 11 is superior to polyamide 12 [5]. The molecular weight depends on the manufacturing conditions and the intended application. In this context, the reactive end groups of polyamide 11 and 12 result in the phenomenon of post-condensation under appropriate conditions such as high temperature and low humidity [32,33].

Unfortunately, the aging of polyamides leads to deterioration of mechanical and physical properties, whereby mostly an overlay of thermal and thermo-oxidative degradation processes occurs [34,35]. The thermal decomposition can be observed by a homolytic cleavage of the alkane group from the nitrogen of the amide group resulting in two radicals which react further to the terminal alkene and the carboxylic acid amide by disproportionation. Consequently, unsaturated nitriles under the release of water can result from the products of the disproportionation reaction. Additionally, the same products are received via a six-membered transition state followed by a *cis*-elimination. Furthermore, the formation of lower oligomers is possible by means of an intramolecular cyclization. However, the favored type of reaction depends on the experimental conditions [36]. In contrary to the thermal degradation, imides, alcohols, carboxylic acids, and esters are reported as products of the thermo-oxidative degradation [3]. Moreover, samples exposed to air typically show yellowing. Thereby, crotonaldehyde groups contribute to coloration and are developed during the oxidation of aliphatic polyamides [37,38]. Typically, the oxidation proceeds by radical chain reactions and it is commonly agreed that oxygen first attacks the methylene group next to the nitrogen of the amide group [34,36].

In order to prevent polymer degradation and increase service life, different types of stabilizers can be integrated within the polymer product in low concentration. Therefore, metal salts, aminic antioxidants, phosphites, and phenolic antioxidants are added individually or in stabilizer packages to prevent material degradation. The selection of stabilizers for polyamides depends on different factors such as the processing temperatures of the polyamides and the decomposition temperatures of the stabilizers. However, also the application type of the material e.g. food contact or not has an influence on the choice of stabilizer [35,39]. For polyamides sterically hindered phenols such as Irganox 1098 and Irganox 245 are reported as oxidation stabilizer typically in concentrations between 0.25 and 0.75% [5,35,40]. However, the formulation is not disclosed by the manufacturer. The hindered phenols act as H-donors and radical scavengers of the formed peroxy radicals and convert them to hydroperoxides. Possible reaction pathways are summarized in Figure 2.1.5. Steric hindrance in the 2,6-positions is crucial for the efficiency of H-donors. On the one hand, the lower the hindrance, the faster the hydrogen transfer and the higher the effectiveness. On the other hand, the stronger the hindrance, the higher is the stability of the intermediates. The drawn reactions of phenoxy radicals are an essential part of the stabilization mechanism of phenolic antioxidants. Most stabilizer types have in common that they are consumed in the process and thus thermo-oxidative degradations is inhibited [35,39,41].

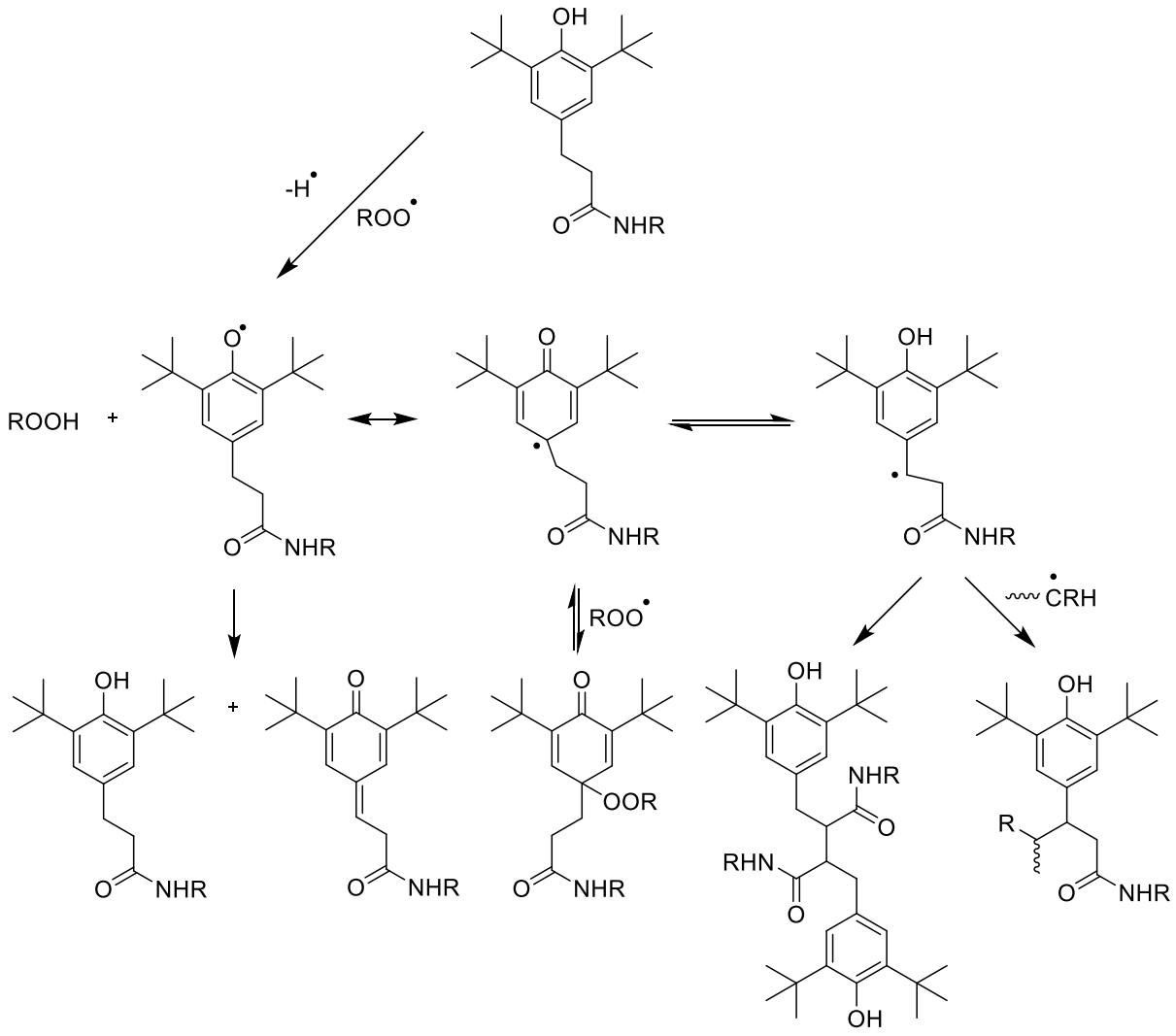

Figure 2.1.5 Inhibition reactions of sterically hindered phenols. Adapted from [39].

Besides the polymer itself and oxidation stabilizers, polymer powders contain flowing agents, possibly further additives, monomers, and oligomers [16]. An image of a polyamide 11 powder sample is shown in Figure 2.1.6.

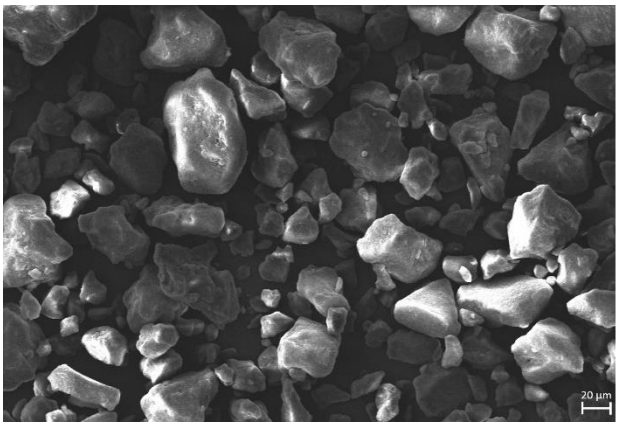

Figure 2.1.6 Scanning electron microscope image of a polyamide 11 powder sample provided by Ingo Leonard Kottenstedde.

Polyamides contain a certain percentage of linear and cyclic monomers and oligomers. However, the amount of those low molecular weight compounds is reported lower for polyamide 11 and 12 with approximately 2% compared to polyamide 6 (around 10%) [42]. The exact amount depends on the polymerization and post-treatment conditions such as applied extraction procedures to remove the low molecular weight compounds. Until now oligomer standards lack being commercially available, thus no quantitative determination via external calibration is possible [5,43].

2.1.2 Established characterization methods

In literature, several approaches are described to characterize polyamide 11 and polyamide 12 materials. This section provides an overview of applied methods:

Small angle and wide-angle X-ray scattering (SAXS, WAXS)

Small-angle and wide-angle X-ray scattering are demonstrated as tools to obtain information about the morphology and structure in correlation with the mechanical performance of the investigated materials. These experiments can be performed during application of constant strain rate of samples and set in relation to the reasons for brittle failure of the materials [8,44].

Differential scanning calorimetry (DSC)

Another method to investigate the melting and crystallization behavior is DSC. It is helpful to determine the sintering window and the related process conditions for the sintering process in 3D printing. Furthermore, DSC is applied to evaluate the degree of crystallinity and enthalpy requirements of the investigated samples. A correlation to phase transitions in the material can be drawn. In this context, the heating and cooling rates are important parameters which have influence on the resulting thermograms and the formation of different phases [17,45–50].

Thermogravimetric analysis (TGA)

Another thermal analysis technique is TGA which detects temperature-dependent changes in the sample mass. These changes may have several reasons such as moisture content, plasticizer content or other volatile components. TGA is used for quality control and to investigate the thermal stability under different atmospheres. Moreover, the method is applied to study the kinetics of the thermal decomposition of polymers [51–53].

Determination of melt flow index (MFI)

A relatively cheap and quick method to investigate rheological properties is to determine the melt flow rate. Within this procedure the molten polymer flow is measured at a particular shear stress related to the specific temperature and load conditions whereby the flow ability is

depending on the reactivity and the aging state of the polymer. The received MFI values give good indications regarding the flowability of single polymers. Unfortunately, different polymers hardly can be compared to each other. Furthermore, the operator has a direct influence on the determination of the MFI leading to an inaccurate value. Nevertheless, the MFI is often applied to receive information in terms of the aging state of the powders for laser sintering [16,54,55].

SEC

Furthermore, as a standard method SEC is used to determine the molar mass distribution of polyamide 11 and 12 samples. However, different SEC methods can be applied at ambient temperatures e.g. using solvent mixtures or at high temperatures using m-cresol or benzyl alcohol [56]. Moreover, common SEC solvents like THF can solely be used after trifluoroacetylation of the investigated polyamide 11 and 12 materials. However, for this reaction the contact with water or alcohols must be avoided. Furthermore, it has to be checked if the functionalization is nearly 100% [57–59]. Thus, at ambient temperature conditions commonly fluorocarbon containing solvents are applied such as 2,2,2-trifluoroethanol and 1,1,1,3,3,3-hexafluoroisopropanol (HFIP) despite being expensive [60,61].

Rheometry

In direct correlation to SEC are shear viscosity measurements, whereby the melt viscosity of polyamide 11 and 12 is characterized by capillary rheometry and rotational rheometry [13,62].

HPLC

Regarding the determination of low molecular weight compounds such as residual monomers, oligomers, and stabilizers often HPLC-UV is applied [63,64]. However, Mori et al [42] were able to determine the cyclic monomer and oligomers of polyamide 12 by reduction-gas chromatography.

Determination of water content

The effect of water absorption on polyamides is an important point for investigation as it affects the thermo-physical properties. Therefore, Karl Fischer titration is a possible method to determine the water content in polyamide samples [65,66].

Infrared spectroscopy

On the one hand, infrared spectroscopy is applied for material identification in quality control via the material related fingerprint. On the other hand, single bands can be investigated during material aging giving knowledge about material change during aging [67]. As an example,

Okamba-Diogo et al. [3] utilized infrared spectroscopy and UV-VIS spectrophotometry to monitor chemical structure changes and yellowing under aging of polyamide 11 samples. Especially the IR bands of the carbonyl species, which showed an increase under aging, were in the focus of investigations.

Determination of powder particle size distribution (PSD)

Polyamide 11 and 12 in powder form are characterized by their PSD as it has a direct influence on the processability in 3D printing. The PSD is determined by laser diffraction or imaging techniques. Additionally, the particle shape can be studied by means of scanning electron microscopy images and coalescence behavior by means of hot stage microscopy and thin sections. The PSD specifies the lowest feasible layer thickness of the print job and thus the resolution in z-direction [32,68–71].

2.1.3 Additive manufacturing

An overview of different processes belonging to 3D printing of polymer materials is shown in Figure 2.1.7 [72]. The additive manufacturing technologies are divided into different categories such as vat photopolymerization, material extrusion, material jetting, and powder bed fusion. Vat photopolymerization stands for 3D printing processes which utilize light-activated polymerization in a vat [73]. In contrary, material extrusion lays down materials of molten strings and within material jetting the polymer is cured by means of UV light. The focus of parts of the work at hand is on powder bed fusion techniques of polyamide 11 and 12 such as multi jet fusion (MJF) and laser beam - powder bed fusion - polymer also known as laser sintering (LB-PBF-P) [74–77]. The two powder bed-based processes will be described in more detail within the next sections.

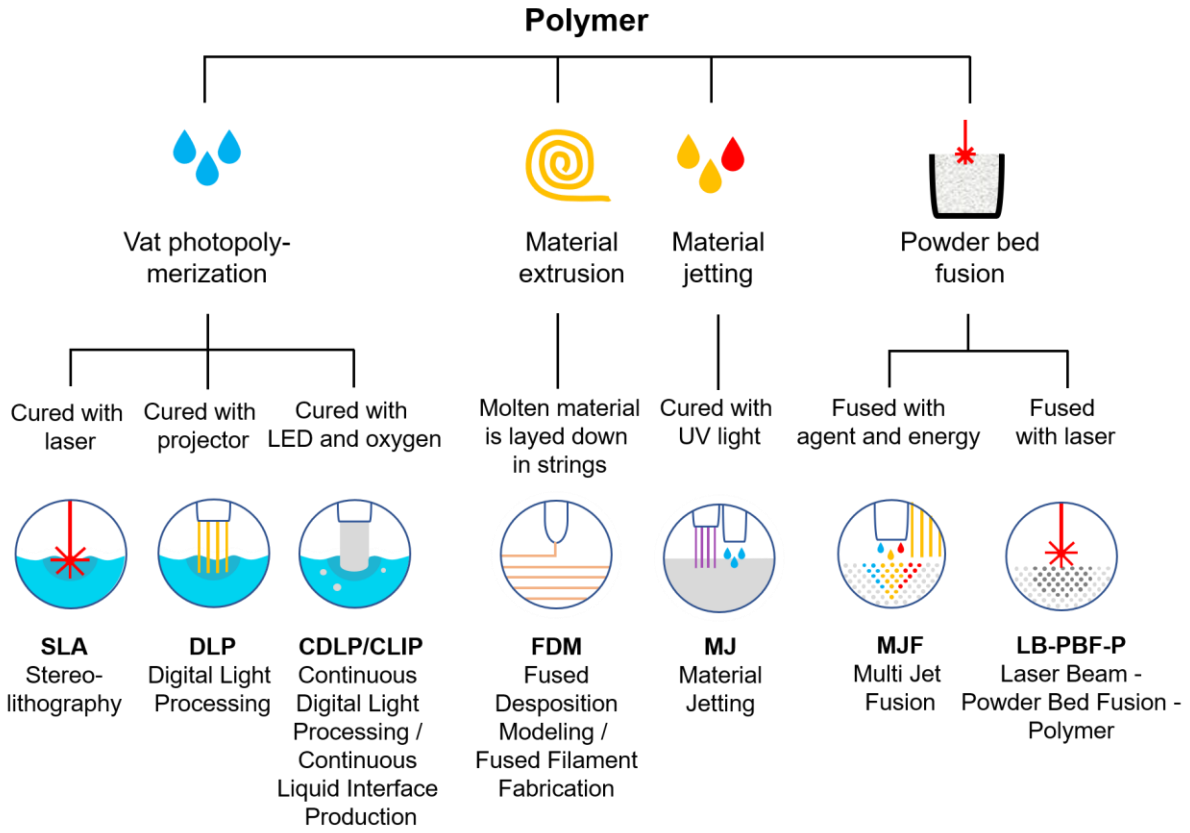

Figure 2.1.7 Additive manufacturing technologies for polymer. Adapted from [72,78].

2.1.4 Laser sintering

The main steps of the LB-PBF-P process are shown in Figure 2.1.8. At the beginning the build platform is lowered exactly by one layer thickness. The powder feedstock is applied by a coater from a feed region onto the build platform. By means of surface heating (IR radiation source) the powder layer is preheated to a temperature slightly below the melting temperature of the processed powder material. Afterwards, a CO_2-laser is directed with a deflection mirror onto the build surface where the powder particles need to be fused. The particles receive the energy input from the laser and coalesce. Afterwards the build platform is lowered again exactly by one layer thickness. The described steps are continually repeated until the print job is finished [15,16].

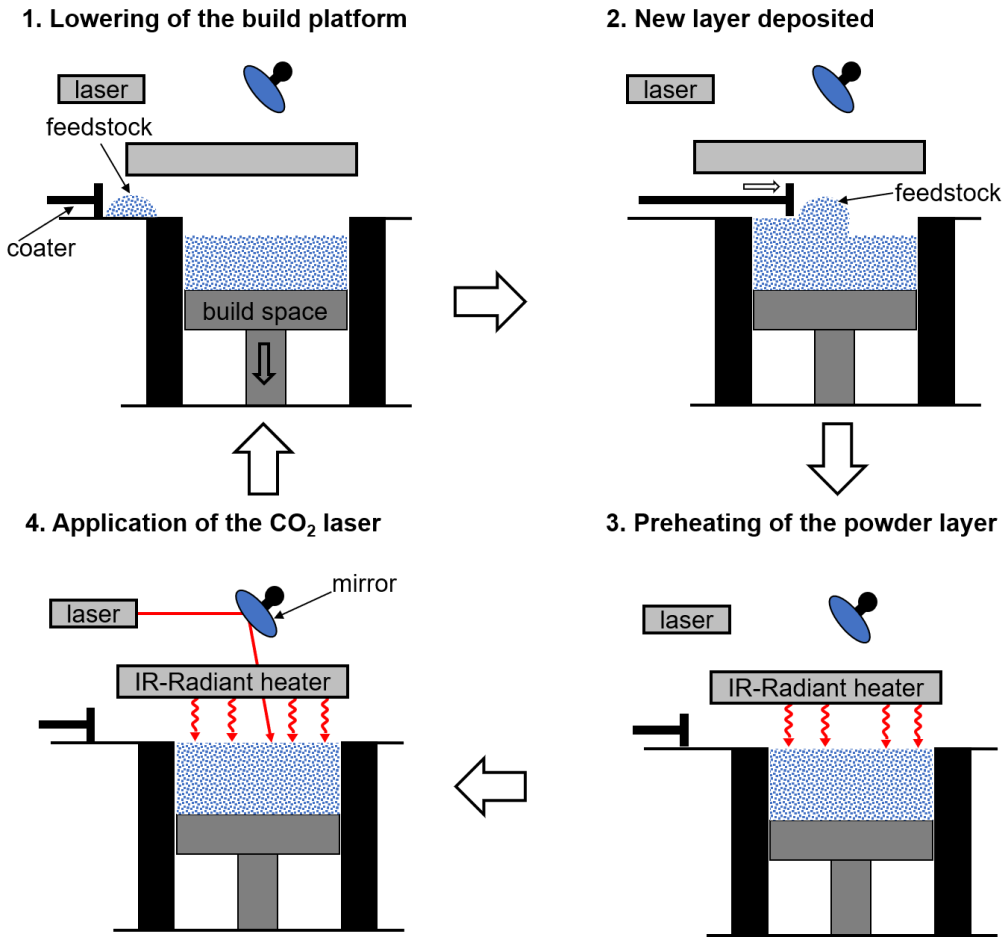

Figure 2.1.8 Schematic illustration of the laser sintering process [16].

The whole print job is done under N_2 atmosphere to prevent material degradation. When the sintering is completed, the part cake is slowly cooled down. It is important to prevent part deformation and surface defects such as orange peel. Moreover, the layer adhesion needs to be assured and the build of pores has to be as low as possible to obtain high quality parts. After curing of the printed parts, the part cake is unpacked and the parts can be post-processed to improve the surface properties. In the light of financial aspects and sustainability, powder reusability is an important topic. Consequently, it is aimed to keep the refresh rate as low as possible whereby it mainly depends on the aging state of the used powder. A mixed powder including a virgin powder rate of up to 60% is needed to ensure still good part properties. For quality control, test specimen are printed next to the parts and investigated e.g. in terms of their Young's modulus, maximum tensile strength, and ε_B. Especially concerning the ε_B values polyamide 11 is superior to other materials although the ε_B values for laser sintering are worse compared to injection molding as the starting material is a powder for the LB-PBF-P process [15–17,68,79,80].

2.1.5 Multi jet fusion

The MJF process, shown in Figure 2.1.9, is similar to laser sintering as both are powder bed-based AM techniques. The difference of the two techniques, however, is that the curing within LB-PBF-P is achieved by applying a laser. In contrary, an agent system and energy mostly in terms of infrared radiation are used for building up structures in the MJF process. The technique is similar to conventional ink-jet printing. For MJF the so called detailing and fusing agents are applied on the top layer powder surface. Thereby, the fusing agent is deposited on regions where the powder particles should be fused. Instead, the water-based detailing agent is sprayed around the contours of the printed part to improve the resolution. Detailing agent can also be jetted onto areas with fusing agent to prohibit extreme thermal accumulation. An infrared source is moved across the build surface and infrared radiation energy is absorbed where the fusing agent was deposited in the step before [77,81].

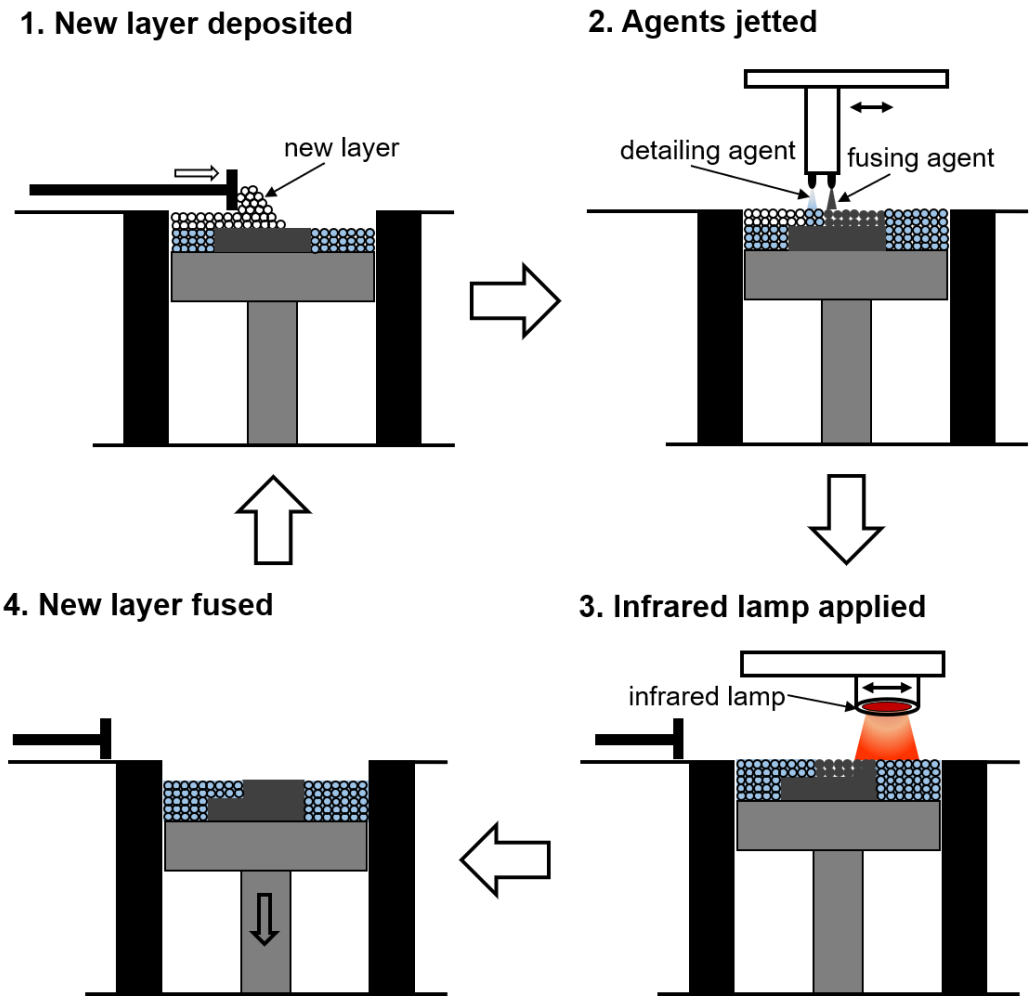

Figure 2.1.9 Schematic illustration of the MJF process [77].

The process is conducted under normal air and without an inert gas atmosphere. Consequently, the powder material can be the same as for laser sintering, but it has to

withstand the different process conditions for example by including a different stabilizer package. Due to the scanning of the whole surface area with the infrared radiation source at a given speed, the scan times for MJF are faster compared to the time-consuming laser scanning for LB-PBF-P. With the application of the agents, however, residues of the agents might remain in the parts and could influence the part quality [82–84]

2.2 Analytical techniques

2.2.1 Fundamentals of polymer liquid chromatography

Synthetic polymers consist of a number of individual molecules. This fact is caused by the synthesis of macromolecules based on a statistical process as it is for example the case for linear condensation of polymers [85]. The resulting molecules may differ in mass, chemical composition, and other properties [86,87]. As the corresponding molecular distributions have impact on the end-use properties, proper characterization methods are necessary [87]. Thus, different types of LC are applied for the molecular characterization of polymers such as SEC, liquid chromatography under critical conditions (LCCC), or interactive chromatography. Special techniques of the latter are gradient polymer elution chromatography (GPEC), barrier-techniques, temperature gradient interaction chromatography, and precipitation-redissolution chromatography (PLC) [86,87]. The separation of PLC is caused by the different solubilities of the analytes in the mobile phase. Therefore, the polymer sample is precipitated after injection based on poor solvent conditions. Afterwards, the ratio of a suitable solvent is increased step by step leading to dissolution of the precipitated molecules. However, it can hardly be determined if the separation occurs solely due to solubility effects [86].

Generally, the behavior of synthetic polymers in interactive chromatography differs from those of small molecules and can be described by thermodynamics as follows [87,88]: the retention of solute molecules in interaction chromatography is caused by the selective interactions of analyte molecules with the surface of the stationary phase. This includes interaction both inside and outside of the pores [89]. In liquid adsorption chromatography the conformational changes of the analytes are zero and the separation is mainly based on enthalpic interaction. However, in ideal SEC, which will be discussed in detail in section 2.2.3, entropic interactions are predominant. This means that the separation is driven by conformational changes of the analyte molecules [88]. In interactive chromatography, SEC and LAC are often used in mixed-modes with predominance of entropic or enthalpic interactions [89]. In the critical mode, the adsorption forces are exactly equalized by the entropy losses resulting in a region called the critical point of adsorption [88]. Moreover, critical conditions lead to analytes eluting independently of their molecular weight at the same time. As steric interactions are completely

counterbalanced by attractive forces, solely one single peak appears in the chromatogram [86]. This very narrow range between SEC and adsorptive modes is very sensitive towards changes in temperature and mobile phase composition [88]. A scheme representing the chromatographic behavior of the analytes in the different modes of SEC, LCCC, and LAC modes is given in Figure 2.2.1.

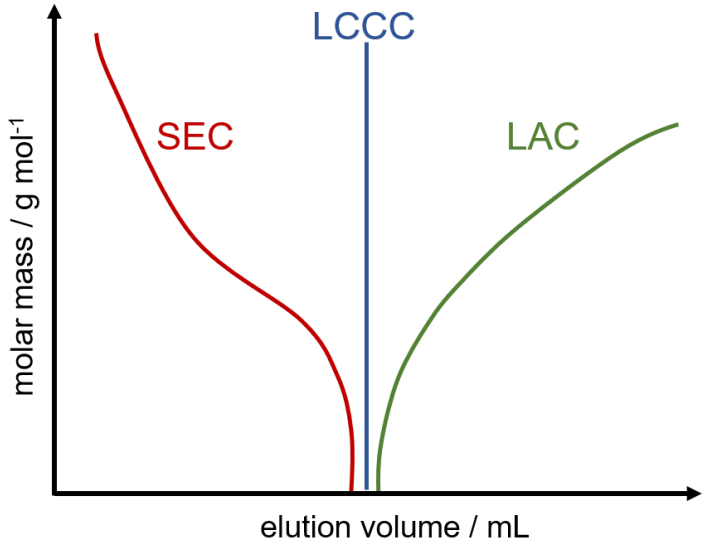

Figure 2.2.1 Chromatographic behavior of molar mass vs. elution volume in different chromatographic modes such as SEC, LCCC, and LAC [88].

In GPEC many effects might influence the separation simultaneously such as adsorption, partition, exclusion, precipitation, and redissolution. Basically, after injection the analyte molecules are held back due to the initial composition of the mobile phase leading to precipitation or at least a very strong adsorption of the polymer sample. Step by step, the amount of thermodynamically good solvent in the mobile phase is increased resulting in the elution and separation of the analyte molecules [87]. Elution under isocratic conditions usually only works for low molar mass samples. Anyway, the strength of the mobile phase is very crucial in LAC as a polymer chain is retained in the stationary phase as long as still one repeat unit of the analyte molecule is adsorbed [89].

As synthetic polymers contain macromolecules of different sizes, characteristic values are utilized to describe polymer samples. Therefore, mean values for the number average M_n and the weight average M_w are expressed based on the degree of polymerization and defined in the following formulas [90].

$$M_n = \frac{\sum n_i M_i}{\sum n_i}, \qquad M_w = \frac{\sum n_i M_i^2}{\sum n_i M_i}, \qquad [88,90].$$

The M_n value is defined as the weight of the sample divided by the total number of chains present where n_i is the number of polymers of molar mass M_i. M_n can be also assessed by colligative property methods and is mostly influenced by the species at the lower end of the molar mass distribution. M_w can be determined by static light scattering (see section 2.2.3), and ultracentrifugation and is particularly influenced by the high-molar mass species [91]. Furthermore, the heterogeneity of a polymer sample is described by the polydispersity P:

$$P = \frac{M_w}{M_n} \qquad [88,90],$$

which was also referred to as non-uniformity coefficient by Glöckner [90]. The difference of M_n and M_w resembles the width of the particular distribution [92]. In this work, also the peak average molar mass M_p will be encountered. M_p is the molar mass of the slice eluting at the peak apex in the SEC chromatogram and therefore is only determinable by SEC. M_p is helpful as calibration curves are constructed based on the M_p values of narrow molecular weight standards [91].

2.2.2 High-resolution polymer HPLC

Durner et al [93] developed a novel gradient protocol primarily based on GPEC. They started with linear gradients and stepwise gradients. However, not until the application of a periodic sawtooth gradient profile, the separation performance of a PVC sample became improved. An overview of the investigated parameters, which form one single step in the sawtooth gradient, is given in section 4.2.1 [93]. Briefly, one effective step length is composed of the height of the negative backward gradient step for the drop of the mobile phase A, the effective step height B, the retardation of negative slope C, the duration of the lower plateau D, and the retardation of the positive slope E. The experiments were started based on the interstitial column volumes using the column volume as scale up or down factor. The parameter B as the effective step height relates directly to the number of steps and to the separation performance of the resulting chromatogram. Consequently, B correlates with the run time of one measurement. For a high number of peaks, a rather long measuring time has to be accepted. Furthermore, the implementation of the sawtooth gradient steps into the chromatographic software program is an important point and difficult to implement into Agilent software products, whereby it is no problem for Thermo Fischers' Chromeleon software [93]. The oligomers elute step by step and a continuous increase in molar mass was observed as long as the critical point of adsorption was not reached and potentially possible chemical differences are excluded [93,94]. The separation was investigated by heart-cut HRP-HPLC and MALDI-ToF-MS, including decreasing P values obtained by fractionation with a sawtooth gradient [93]. Furthermore, single fractions were investigated by SEC to be able to establish a direct

correlation between molar mass values and retention times of single fractions in the sawtooth gradient protocol [94]. So far, the sawtooth gradient was successfully applied to PVC, PMMA, PDMS, polypropylene glycol, and in this work to different polyamide 11 and 12 samples [93]. Additionally, the protocol was improved in terms of total run time and separation performance. The increase in flow rate and a down-to-zero approach, which means that the content of desorption promoting solvent was set to 0% at the end of each step, were applied. Moreover, based on a modification of the mobile phase composition a ternary and a multicomponent approach were developed. In the ternary sawtooth gradient, the whole gradient elution was repeated with two adequate pairs of non-solvents and desorption promoting solvents. Consequently, mixtures containing diverse polymer components could be separated leading to fingerprint analysis of complex polymer mixtures [95].

2.2.3 Size exclusion chromatography

In SEC, molecules are separated according to their molecular dimension, which is their hydrodynamic volume, regardless of their functionality (see Figure 2.2.2). In contrary to polymer HPLC, larger molecules are detected first (compare the purple polymer in Figure 2.2.2) based on macromolecules' diffusion into pores of different size [86,89]. Consequently, the entropy-driven steric interactions lead to steric exclusion of analyte molecules from the packing material [86,87]. SEC is applied as a standard technique to determine molecular mass distribution of polymers and the related mean molar mass values [88].

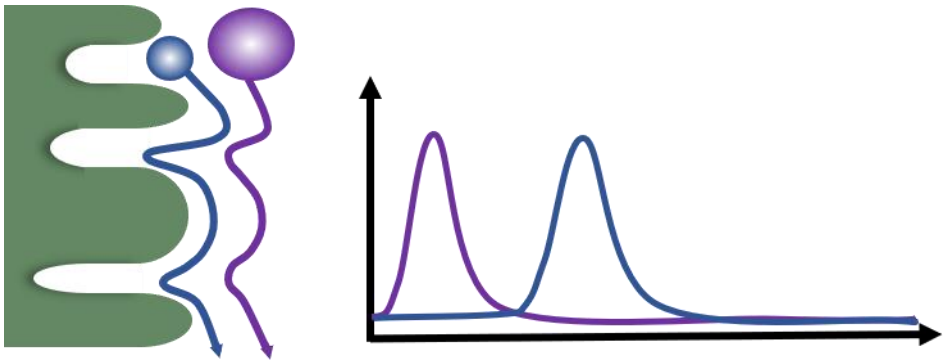

Figure 2.2.2 Scheme of separation process in size exclusion chromatography.

However, due to the separation according to size no differentiation in chemical structure or other properties is possible which might lead to the coelution of macromolecules of different compositions and architectures [90,92]. Furthermore, surrounded by solvent linear polymer strands can adopt different conformations such as a compact sphere, a random coil, or a rod-like conformation whereby additional conformations in between are possible depending on the thermodynamic properties of solvent and solute polymer. Synthetic linear polymers mainly

adopt a random coil in their appropriate solvent which corresponds to the statistically most probable conformation. However, hydrodynamic volume changes have to be considered in data interpretation. This is the case especially if the conformation and composition are varied although the molar mass stays the same [91,96]. In SEC, the choice of stationary and mobile phases is most important. The mobile phase, normally a single solvent, has to be a thermodynamically good solvent which dissolves macromolecules and excludes interactions with the stationary phase at the same time. Most frequently used solvents are tetrahydrofuran (THF), toluene, esters, and dimethylformamide. Furthermore, salt additives are common for rather polar polymers to eliminate non-exclusion effects [88]. Stationary phases are made from different materials depending on their applications in aqueous or non-aqueous solvents. Either porous silica, crosslinked organic gels such as styrene and divinylbenzene, modified silica, or crosslinked hydrophilic polymers are in use [88,90]. Furthermore, SEC columns are characterized by their total exclusion and total permeation volume [97]. At the total exclusion volume polymer coils elute which are larger than the largest pores of the packing. In contrary, small molecules having access to the entire pore volume are detected within the total permeation volume [88]. Typically, SEC is combined with a dRI detector as it responds well to most common polymeric samples provided that the dRI of the mobile phase and analyte molecules differ. Furthermore, the dRI signal is equally proportional to the polymer concentration [97]. In most experiments a calibration is established via narrow molar mass standards which is termed conventional calibration. Therefore, monodisperse calibration standards with known molar masses are taken. If available, standards of the polymer, which should be analyzed, are used or of another polymer resulting in molar masses determined as equivalents of the standard polymer. Consequently, each elution slice of a sample can be converted into a molar mass slice. The molar mass values and the height of each slice are converted to receive M_n, M_w, and M_p. One disadvantage is that the molar mass determination is possibly incorrect for samples with different chemistries as for those of the calibrants [91]. Another more complex possibility is to determine molar masses absolutely by applying static light scattering such as multi-angle laser light scattering (MALLS) [96,98]. MALLS instruments are available in different angle setups and can be utilized to obtain information not just about the molar mass but also regarding the size of a polymer via the value of the radius of gyration. However, an additional concentration detector such as an dRI or an UV detector is needed except for off-line experiments. In case of an UV detector it needs to be provided that the analyte molecules are absorbing in the ultraviolet but not the solvent. Especially for the radius determination the solutes have to have at least the radius of one twentieth of the wavelength of the laser.

In general, the Rayleigh ratio R (θ) is proportional to the molar mass (M), the concentration (c), and the squared refractive index increment $(\frac{dn}{dc})^2$. As the scattering signal is depending on both the molar mass and the concentration, a concentration detector is needed in addition to the MALLS instrument:

$$R(\theta) \propto M \cdot c \cdot (\frac{dn}{dc})^2 \quad [96,99].$$

For the investigations of polyamides by means of SEC special eluents need to be used as polyamides show poor or rather lack solubility in many solvents. The amide groups of polyamides favor to associate via hydrogen bonding resulting in intermolecular associates. For dissolution and to avoid non-exclusion effects fluorinated eluents like HFIP together with salt additives are utilized as mobile phases. Moreover, no polyamide standards are commercially available so far. Thus, either molar masses are determined in equivalents of PMMA or absolutely [61,100].

2.2.4 Fundamentals of evaporative light scattering detection and charged aerosol detection

Aerosol-based detection techniques are applied as universal detectors in polymer analysis. They are used for detection of compounds without chromophores or lacking the possibility of ionization for MS detection or possess too high molar masses for LC-MS [101]. In this section, the focus will be on the evaporative light scattering detector (ELSD) and charged aerosol detector (CAD). In contrast to UV and MS, the ELSD and CAD work the following way: The eluent of the HPLC column enters the detector and is evaporated and nebulized with nitrogen. This is followed by solvent evaporation in a drift tube to produce an aerosol residue. Then the working principle of both detectors differs. Concerning the ELSD, the remaining solid fraction is introduced into a measurement cell where a light beam becomes scattered by the analyte particles. A photomultiplier generates a signal proportional to the number of scattered photons [101,102]. Consequently, the aerosol particles are detected by its light scattering properties depending on the ratio of the diameter of the particle (d) to the wavelength of the incident light (λ). Several mechanisms contribute to the light scattering process which are Rayleigh scattering, Mie scattering, reflection and refraction [103,104]. Rayleigh scattering is caused by particles with a small diameter $(\frac{d}{\lambda} < 0.1)$ which corresponds to particles less than about 100 nm. Mie scattering is related to intermediate particles and reflection-refraction are occurring for the largest particles. An example for an ELSD is depicted in Figure 2.2.3 [105]. The signal response is influenced by several factors such as the flow rate and composition of the mobile phase, the type of nebulizer, the evaporation temperature, and types of different

nebulization gases. Moreover, the chemical and physical properties of the investigated analyte itself contribute to the signal response [106]. As a constraint, the ELSD shows limitations such as a non-linear response and provides no information regarding compound identification. Furthermore, volatile or semi-volatile analytes are hardly detectable [105]. Nevertheless, the robustness of evaporative light scattering detection, the acceptable precision, the relatively low costs, and a multitude of available models are attractive for purchase [105]. In general, highest signal responses are achieved with low flow rates of the mobile phase [107].

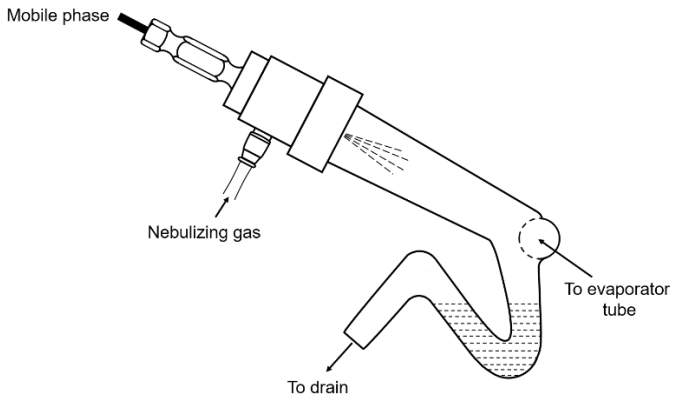

Figure 2.2.3 Scheme of a SEDEX ELSD nebulization chamber. Large droplets are diverted to waste before the evaporator drift tube. Adapted from [105].

For charged aerosol detection the aerosol residue encounters a secondary flow of nitrogen, which is positively charged by a corona needle in combination with high voltage. This charged nitrogen is mixed with the stream of the aerosol causing a charge migration to the particles of the aerosol. The charged sample particles reach a collector where an electrometer produces a signal proportional to the mass of the sample, but independent of its chemical structure. The measured current leads to an equal response for equal mass amounts [103,108]. This response is inherently non-linear and has to be fitted properly [109]. A scheme of a CAD is depicted in Figure 2.2.4. Consequently, the CAD is differently operating compared to the principle of MS ion sources. For MS, ionized analyte molecules are generated in the gas phase whereas for charged aerosol detection charged aerosol particles are generated [105].

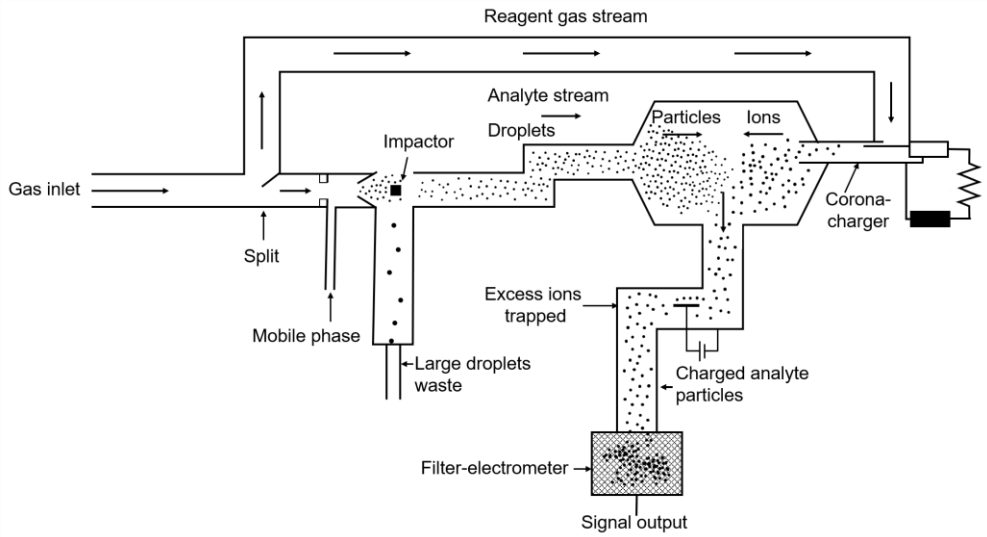

Figure 2.2.4 Conceptual setup of a CAD, adapted from [110].

For both detectors, the signal responses can be described by a power law function with a variable exponent but no linear response behavior [103]. The CAD is reported to offer a better system repeatability than the ELSD and is also more sensitive [101]. As a consequence, the CAD is not as robust against unknown samples or impurities as the ELSD. However, the CAD offers the improved detection limits which is based on the reason that aerosol charging can be efficiently transferred to particles smaller than 100 nm. Generally, for aerosol-based detectors mobile phase additives must be volatile such as formic acid (FA), acetic acid or trifluoroacetic acid (TFA) [105].

2.3 References

[1] M. Genas, Rilsan (Polyamid 11), Synthese und Eigenschaften, Angew. Chem. (1962) 535–540. https://doi.org/10.1002/ange.19620741504.

[2] B. Sreenivasan, N.R. Kamath, J.G. Kane, Studies on castor oil. I. Fatty acid composition of castor oil, J. Am. Oil Chem. Soc. 33 (1956) 61–66. https://doi.org/10.1007/BF02612549.

[3] O. Okamba-Diogo, E. Richaud, J. Verdu, F. Fernagut, J. Guilment, B. Fayolle, Molecular and macromolecular structure changes in polyamide 11 during thermal oxidation, Polym. Degrad. and Stab. (2014) 123–132. https://doi.org/10.1016/j.polymdegradstab.2014.05.028.

[4] J. Pagacz, K.N. Raftoppoulos, A. Leszczynska, K. Pielichowski, Bio-polyamides based on renewable raw materials, J. Therm. Anal. Calorim. (2016) 1225–1237. https://doi.org/10.1007/s10973-015-4929-x.

[5] G.W. Becker, D. Braun (Eds.), Technische Thermoplaste Polyamide: Kunststoff Handbuch ¾, Hanser, München, 1998.

[6] G.B. Apgar, M.J. Koskoski, The history of development of nylons 11 and 12, in: R.B. Seymour, G.S. Kirshenbaum (Eds.), High performance polymer: Their origin and development, Elsevier, New York, 1986, pp. 55–65.

[7] R. Feldmann, R. Feinauer, Polykondensationsgleichgewicht bei Polylaurinlactam, Angew. Makromol. Chemie 54 (1976) 1–13. https://doi.org/10.1002/apmc.1976.050540101.

[8] S. Tencé-Girault, S. Lebreton, O. Bunau, P. Dang, F. Bargain, Simultaneous SAXS-WAXS experiments on semi-crystalline polymers: Example of PA11 and its brill transition, Crystals (2019) 271–288. https://doi.org/10.3390/cryst9050271.

[9] B. van Hooreweder, D. Moens, R. Boonen, J.-P. Kruth, P. Sas, On the difference in material structure and fatigue properties of nylon specimens produced by injection molding and selective laser sintering, Polymer Testing 32 (2013) 972–981. https://doi.org/10.1016/j.polymertesting.2013.04.014.

[10] W. Romão, E.V.R. Castro, E.A.S. Filho, R.C.L. Guimarães, A.L.N. Silva, S.C.S. Teixeira, M.-A. de Paoli, G.L. de Sena, Ageing of polyamide 11 used in the manufacture of flexible piping, J. Appl. Polym. Sci. 114 (2009) 1777–1783. https://doi.org/10.1002/app.30793.

[11] B. Jacques, M. Werth, I. Merdas, F. Thominette, J. Verdu, Hydrolytic ageing of polyamide 11. 1. Hydrolysis kinetics in water, Polymer 43 (2002) 6439–6447. https://doi.org/10.1016/S0032-3861(02)00583-9.

[12] J.O. Bello, R.J.K. Wood, Grooving micro-abrasion of polyamide 11 coated carbon steel tubulars for downhole application, Wear 255 (2003) 1157–1167. https://doi.org/10.1016/S0043-1648(03)00226-6.

[13] S. Maïza, X. Lefebvre, N. Brusselle-Dupend, M.-H. Klopffer, L. Cangémi, S. Castagnet, J.-C. Grandidier, Physicochemical and mechanical degradation of polyamide 11 induced by hydrolysis and thermal aging, J. Appl. Polym. Sci. 136 (2019) 47628–47638. https://doi.org/10.1002/app.47628.

[14] M.A. Dechet, A. Goblirsch, S. Romeis, M. Zhao, F.J. Lanyi, J. Kaschta, D.W. Schubert, D. Drummer, W. Peukert, J. Schmidt, Production of polyamide 11 microparticles for additive manufacturing by liquid-liquid phase separation and precipitation, Chem. Eng. Sci. 197 (2019) 11–25. https://doi.org/10.1016/j.ces.2018.11.051.

[15] M. Schmid, Additive Fertigung mit Selektivem Lasersintern (SLS): Prozess- und Werkstoffüberblick, Springer, Wiesbaden, 2015.

[16] M. Schmid, Selektives Lasersintern (SLS) mit Kunststoffen: Technologie, Prozesse und Werkstoffe, Hanser, München, 2015.

[17] K. Schubert, J. Kolb, F. Wohlgemuth, D. Lellinger, I. Alig, Thermische Alterung und Eigenschaften von Polymermaterialien für das Selektive Lasersintern, in: H.A. Richard, B. Schramm, T. Zipsner (Eds.), Additive Fertigung von Bauteilen und Struktuen, pp. 159–172.

[18] J.H. Magill, Formation of spherulities in polyamides. IV. Even–odd polyamides and poly(ω-aminocarboxylic acids), J. Polym. Sci. Part A-2: Polym. Phys. 7 (1969) 123–142. https://doi.org/10.1002/pol.1969.160070110.

[19] K. Jariyavidyanont, W. Focke, R. Androsch, Thermal Properties of Biobased Polyamide 11, in: M.L. Di Lorenzo, R. Androsch (Eds.), Thermal Properties of Bio-based Polymers, Springer International Publishing, Cham, 2019, pp. 143–187.

[20] Y. Kinoshita, An investigation of the structures of polyamide series, Die Makromolekulare Chemie 33 (1959) 1–20. https://doi.org/10.1002/macp.1959.020330101.

[21] S. Rhee, J.L. White, Crystalline structure and morphology of biaxially oriented polyamide-11 films, J. Polym. Sci. B Polym. Phys. 40 (2002) 2624–2640. https://doi.org/10.1002/polb.10330.

[22] J. Pepin, V. Miri, J.-M. Lefebvre, New Insights into the Brill transition in polyamide 11 and polyamide 6, Macromolecules 49 (2016) 564–573. https://doi.org/10.1021/acs.macromol.5b01701.

[23] W.P. Slichter, Crystal structures in polyamides made from ω-amino acids, J. Polym. Sci. 36 (1959) 259–266. https://doi.org/10.1002/pol.1959.1203613020.

[24] L.J. Mathias, D.G. Powell, J.P. Autran, R.S. Porter, Nitrogen-15 NMR characterization of multiple crystal forms and phase transitions in polyundecanamide (nylon 11), Macromolecules 23 (1990) 963–967. https://doi.org/10.1021/ma00206a012.

[25] K.G. Kim, B.A. Newman, J.I. Scheinbeim, Temperature dependence of the crystal structures of nylon 11, J. Polym. Sci. B Polym. Phys. 23 (1985) 2477–2482. https://doi.org/10.1002/pol.1985.180231206.

[26] C. Fischer, A. Seefried, D. Drummer, Crystallization and component properties of polyamide 12 at processing-relevant cooling conditions, Polym. Eng. Sci. 57 (2017) 450–457. https://doi.org/10.1002/pen.24441.

[27] F. Paolucci, D. Baeten, P.C. Roozemond, B. Goderis, G.W.M. Peters, Quantification of isothermal crystallization of polyamide 12: Modelling of crystallization kinetics and phase composition, Polymer 155 (2018) 187–198. https://doi.org/10.1016/j.polymer.2018.09.037.

[28] R. Dai, M. Huang, L. Ma, W. Liu, S. He, H. Liu, C. Zhu, Y. Wang, Z. Zhang, A. Sun, Study on crystal structure and phase transitions of polyamide 12 via wide-angle X-ray diffraction with variable temperature, Advanced Composites and Hybrid Materials 3 (2020) 522–529. https://doi.org/10.1007/s42114-020-00192-y.

[29] J.-P. Allen, P. Blondel, P. Douais, Verfahren zur Erhöhung des Schmelzpunktes und der Schmelzenthalpie von Polyamiden, DE 60303275 T2.

[30] A. Lemaitre, C. Mathieu, Verfahren zur Erhöhung der Recyclingfähigkeit eines Polyamids, das zum Sintern benutzt wird, EP 2530121 B1.

[31] S.J.A. Hocker, W.T. Kim, H.C. Schniepp, D.E. Kranbuehl, Polymer crystallinity and the ductile to brittle transition, Polymer 158 (2018) 72–76. https://doi.org/10.1016/j.polymer.2018.10.031.

[32] L. Verbelen, S. Dadbakhsh, van den Eynde, Characterization of polyamide powders for determination of laser sintering processability, Europ. Polym. J. 75 (2016) 163–174. https://doi.org/10.1016/j.eurpolymj.2015.12.014.

[33] B. Scherer, I.L. Kottenstedde, W. Bremser, F.-M. Matysik, Analytical characterization of polyamide 11 used in the context of selective laser sintering: Physico-chemical correlations, Polymer Testing 91 (2020) 106786. https://doi.org/10.1016/j.polymertesting.2020.106786.

[34] O. Okamba-Diogo, E. Richaud, J. Verdu, F. Fernagut, J. Guilment, B. Fayolle, Investigation of polyamide 11 embrittlement during oxidative degradation, Polymer 82 (2016) 49–56. https://doi.org/10.1016/j.polymer.2015.11.025.

[35] G.W. Ehrenstein, S. Pongratz, Beständigkeit von Kunststoffen: Band 1, Hanser, München, 2007.

[36] S.V. Levchik, E.D. Weil, M. Lewin, Thermal decomposition of aliphatic nylons, Polym. Int. 48 (1999) 532–557. https://doi.org/10.1002/(SICI)1097-0126(199907)48:7<532:AID-PI214>3.0.CO;2-R.

[37] D. Fromageot, A. Roger, J. Lemaire, Thermooxidation yellowing of aliphatic polyamides, Angew. Makromol. Chemie 170 (1989) 71–85. https://doi.org/10.1002/apmc.1989.051700105.

[38] A. Roger, D. Sallet, J. Lemaire, Photochemistry of aliphatic polyamides. 4. Mechanisms of photooxidation of polyamides 6, 11, and 12 at long wavelengths, Macromolecules 19 (1986) 579–584. https://doi.org/10.1021/ma00157a015.

[39] A. Wegmann, A. Le Gal, D. Müller, Antioxidantien, in: R.D. Maier, M. Schiller (Eds.), Handbuch Kunststoff-Additive, 4th ed., Hanser, München, 2016, pp. 1–153.

[40] C. Mathieu, G. Filou, A. Lemaitre, Verfahren zur Herstellung eines recycelbaren Polyamidpulvers, EP 2488572 B1.

[41] H. Zweifel, Stabilization of polymeric materials, Springer, Berlin, 1997.

[42] S. Mori, M. Furusawa, T. Takeuchi, Reduction-gas chromatographic determination of cyclic monomer and oligomers in polyamides, Anal. Chem. 42 (1970) 661–662. https://doi.org/10.1021/ac60288a037.

[43] M. Heimrich, M. Bönsch, H. Nickl, T.J. Simat, Cyclic oligomers in polyamide for food contact material: quantification by HPLC-CLND and single-substance calibration, Food Addit. Contam. Part A 29 (2012) 846–860. https://doi.org/10.1080/19440049.2011.649496.

[44] F. Paolucci, L. Govaert, G. Peters, In situ WAXD and SAXS during tensile deformation of moulded and sintered polyamide, Polymers (2019) 1001–1019. https://doi.org/10.3390/polym11061001.

[45] K. Jariyavidyanont, A. Janke, R. Androsch, Crystal self-nucleation in polyamide 11, Thermochim. Acta 677 (2019) 139–143. https://doi.org/10.1016/j.tca.2019.02.006.

[46] A. Mollova, R. Androsch, D. Mileva, C. Schick, A. Benhamida, Effect of supercooling on crystallization of polyamide 11, Macromolecules 46 (2013) 828–835. https://doi.org/10.1021/ma302238r.

[47] F. Neugebauer, V. Ploshikhin, J. Ambrosy, G. Witt, Isothermal and non-isothermal crystallization kinetics of polyamide 12 used in laser sintering, J. Therm. Anal. Calorim. 124 (2016) 925–933. https://doi.org/10.1007/s10973-015-5214-8.

[48] K. Wudy, D. Drummer, Aging effects of polyamide 12 in selective laser sintering: Molecular weight distribution and thermal properties, Addit. Manuf. 25 (2019) 1–9. https://doi.org/10.1016/j.addma.2018.11.007.

[49] Q. Zhang, Z. Mo, S. Liu, H. Zhang, Influence of annealing on structure of nylon 11, Macromolecules 33 (2000) 5999–6005. https://doi.org/10.1021/ma000298d.

[50] A. Xenopoulos, B. Wunderlich, Thermodynamic properties of liquid and semicrystalline linear aliphatic polyamides, J. Polym. Sci. B Polym. Phys. 28 (1990) 2271–2290. https://doi.org/10.1002/polb.1990.090281209.

[51] M. Herrera, G. Matuschek, A. Kettrup, Main products and kinetics of the thermal degradation of polyamides, Chemosphere (2001) 601–607. https://doi.org/10.1016/S0045-6535(00)00233-2.

[52] O.P. Korobeinichev, A.A. Paletsky, M.B. Gonchikzhapov, R.K. Glaznev, I.E. Gerasimov, Y.K. Naganovsky, I.K. Shundrina, A.Y. Snegirev, R. Vinu, Kinetics of thermal decomposition of PMMA at different heating rates and in a wide temperature range, Thermochim. Acta 671 (2019) 17–25. https://doi.org/10.1016/j.tca.2018.10.019.

[53] A. Nadal Gisbert, J.E. Crespo Amorós, J. López Martínez, A. Macias Garcia, Study of thermal degradation kinetics of elastomeric powder (ground tire rubber), Polymer-Plastics Technology and Engineering 47 (2007) 36–39. https://doi.org/10.1080/03602550701580870.

[54] D.T. Pham, K.D. Dotchev, W.A.Y. Yusoff, Deterioration of polyamide powder properties in the laser sintering process, Proceedings of the Institution of Mechanical Engineers, Part C: Journal of Mechanical Engineering Science 222 (2008) 2163–2176. https://doi.org/10.1243/09544062JMES839.

[55] DIN EN ISO, Kunststoffe - Bestimmung der Schmelze-Massefließrate (MFR) und der Schmelze-Volumenfließrate (MVR) von Thermoplasten: Teil 2: Verfahren für Materialien, die

empfindlich gegen eine zeit- bzw. temperaturabhängige Vorgeschichte und/oder Feuche sind, 2011.

[56] J. Chen, W. Radke, H. Pasch, Analysis of polyamides by size exclusion chromatography and laser light scattering, Macromol. Symp. 193 (2003) 107–118. https://doi.org/10.1002/masy.200390044.

[57] K. Weisskopf, Determination of molecular weight averages and molecular weight distribution by g.p.c. of N-trifluoroacetylated polyamides, Polymer 26 (1985) 1187–1190. https://doi.org/10.1016/0032-3861(85)90250-2.

[58] E. Jacobi, H. Schuttenberg, R.C. Schulz, A new method for gel permeation chromatography of polyamides, Die Makromolekul. Chem. Rapid Comm. 1 (1980) 397–402. https://doi.org/10.1002/marc.1980.030010609.

[59] V. Girardon, M. Tessier, E. Maréchal, Characterization of functional aliphatic oligoamides using N-trifluoroacetylation—II. size exclusion chromatography, Eur. Polym. J. 34 (1998) 1325–1330. https://doi.org/10.1016/S0014-3057(97)00267-X.

[60] P.J. Wang, R.J. Rivard, Characterization of nylons by gel permeation chromatography and low angle laser light scattering in 2,2,2-trifluoroethanol, J. Liq. Chromatogr. 10 (1987) 3059–3071. https://doi.org/10.1080/01483918708068297.

[61] T.H. Mourey, T.G. Bryan, Size-exclusion chromatography in 1,1,1,3,3,3-hexafluoro-2-propanol, J. Chromatogr. A 964 (2002) 169–178. https://doi.org/10.1016/S0021-9673(02)00510-1.

[62] B. Haworth, N. Hopkinson, D. Hitt, X. Zhong, Shear viscosity measurements on polyamide-12 polymers for laser sintering, Rapid Prototyp. J. 19 (2013) 28–36. https://doi.org/10.1108/13552541311292709.

[63] O. Okamba-Diogo, E. Richaud, J. Verdu, F. Fernagut, J. Guilment, F. Pery, B. Fayolle, Quantification of hindered phenols in polyamide 11 during thermal aging, Polymer Testing 52 (2016) 63–70. https://doi.org/10.1016/j.polymertesting.2016.03.023.

[64] V. Krajník, P. Božek, J. Kondelíková, J. Králíček, High-performance liquid chromatography of 12-dodecanelactam and its cyclic oligomers present in polymide 12, J. Chromatogr. A 250 (1982) 138–140. https://doi.org/10.1016/S0021-9673(00)95224-5.

[65] R. Aro, M.W. Ben Ayoub, I. Leito, É. Georgin, Moisture in Solids: Comparison between evolved water vapor and vaporization coulometric Karl Fischer methods, Int. J. Thermophys. 41 (2020) 113. https://doi.org/10.1007/s10765-020-02697-6.

[66] R. Seltzer, de la Escalera, Federico Martín, J. Segurado, Effect of water conditioning on the fracture behavior of PA12 composites processed by selective laser sintering, Mater. Sci. Eng. A 528 (2011) 6927–6933. https://doi.org/10.1016/j.msea.2011.05.045.

[67] C.A. Wilkie, TGA/FTIR: an extremely useful technique for studying polymer degradation, Polym. Degrad. and Stab. 66 (1999) 301–306. https://doi.org/10.1016/S0141-3910(99)00054-3.

[68] D. Rietzel, Werkstoffverhalten und Prozessanalyse beim Laser-Sintern von Thermoplasten. Dissertation, Erlangen-Nürnberg, 2011.

[69] M. Schmid, A. Amado, K. Wegener, Polymer powders for selective laser sintering (SLS), AIP Conference Proceedings 1664 (2015) 160009. https://doi.org/10.1063/1.4918516.

[70] ISO, Particle size analysis - imaga analysis methods: Part 2: Dynamic image analysis methods, 2006.

[71] ISO, Particle size analysis - image analysis methods: Part 1: Static image analysis methods, 2014.

[72] DIN EN ISO/ASTM, Additive Fertigung - Grundlagen - Terminologie, 2017.

[73] International Organization for Standardization (ISO), ISO/ASTM 52900: Additive manufacturing - general priciples - terminology: International, Geneva, 2015.

[74] A. Gebhardt, Generative Fertigungsverfahren. Additive Manufacturing und 3D Drucken für Prototyping - Tooling - Produktion, 4th ed., Hanser, München.

[75] S.C. Ligon, R. Liska, J. Stampfl, M. Gurr, R. Mülhaupt, Polymers for 3D printing and customized additive manufacturing, Chem. Rev. 117 (2017) 10212–10290. https://doi.org/10.1021/acs.chemrev.7b00074.

[76] H. Bika, P. Stavropoulos, G. Chryssolouris, Additive manufacturing methods and modelling approaches: a critical review, Int. J. Adv. Manuf. Technol. (2016) 389–405.

[77] C. Cai, W.S. Tey, J. Chen, W. Zhu, X. Liu, T. Liu, L. Zhao, K. Zhou, Comparative study on 3D printing of polyamide 12 by selective laser sintering and multi jet fusion, J. Mater. Process. Technol. 288 (2021) 116882. https://doi.org/10.1016/j.jmatprotec.2020.116882.

[78] 3D Hubs, Additive manufacturing technologies: An overview, https://www.3dhubs.com/knowledge-base/additive-manufacturing-technologies-overview/, accessed 10 January 2021.

[79] A. Wegner, Theorie über die Fortführung von Aufschmelzvorgängen als Grundvoraussetzung für eine robuste Prozessführung beim Laser-Sintern von Thermoplasten. Dissertation, 2015.

[80] A. Wegner, R. Harder, G. Witt, D. Drummer, Determination of optimal processing conditions for the production of polyamide 11 parts using the laser sintering process, International Journal of Recent Contributions from Engineering, Science & IT 3 (2015) 5–12.

[81] J. Riedelbauch, D. Rietzel, G. Witt, Analysis of material aging and the influence on the mechanical properties of polyamide 12 in the multi jet fusion process, Additive Manufacturing 27 (2019) 259–266. https://doi.org/10.1016/j.addma.2019.03.002.

[82] A.J.K. Väisänen, M. Hyttinen, S. Ylönen, L. Alonen, Occupational exposure to gaseous and particulate contaminants originating from additive manufacturing of liquid, powdered and filament plastic materials and related post-processes, Journal of Occupational and Environmental Hygiene (2019) 258–271. https://doi.org/10.1080/15459624.2018.1557784.

[83] M. Mele, G.L. Monti, G. Pisaneschi, G. Campana, Investigation into effects of cooling rate on properties of polyamide 12 parts in the multi jet fusion process, Rapid Prototyp. J. 26 (2020) 1789–1795. https://doi.org/10.1108/RPJ-04-2020-0080.

[84] F. Sillani, R.G. Kleijnen, M. Vetterli, M. Schmid, K. Wegener, Selective laser sintering and multi jet fusion: Process-induced modification of the raw materials and analyses of parts performance, Addit. Manuf. 27 (2019) 32–41. https://doi.org/10.1016/j.addma.2019.02.004.

[85] P.J. Flory, Molecular size distribution in linear condensation polymers, J. Am. Chem. Soc. 58 (1936) 1877–1885. https://doi.org/10.1021/ja01301a016.

[86] E. Uliyanchenko, S. van der Wal, P.J. Schoenmakers, Challenges in polymer analysis by liquid chromatography, Polym. Chem. 3 (2012) 2313–2335. https://doi.org/10.1039/C2PY20274C.

[87] Y. Brun, C.J. Rasmussen, Interaction polymer chromatography, in: S. Fanali, P.R. Haddad, Poole C. F., M.-L. Riekkolo (Eds.), Liquid chromatography: Fundamentals and instrumentation, 2nd ed., Elsevier, Amsterdam, 2017, pp. 275–318.

[88] H. Pasch, B. Trathnigg, HPLC of polymers, Springer, Berlin, 1998.

[89] H. Pasch, B. Trathnigg, Multidimensional HPLC of polymers, Springer, Berlin, 2013.

[90] G. Glöckner, Polymer characterization by liquid chromatography, Elsevier, Amsterdam, 1987.

[91] A.M. Striegel, W.W. Yau, J.J. Kirkland, D.D. Bly, Modern size-exclusion liquid chromatography: Practice of gel permation and gel filtration chromatography, John Wiley & Sons, Hoboken, New Jersey, 2009.

[92] D. Corradini (Ed.), Handbook of HPLC: Second Edition, CRC, Boca Raton, 2011.

[93] B. Durner, T. Ehmann, F.-M. Matysik, High-resolution polymer high performance liquid chromatography: Application of a saw tooth gradient for the separation of various polymers, J. Chromatogr. A 1587 (2019) 88–100. https://doi.org/10.1016/j.chroma.2018.11.075.

[94] B. Durner, B. Scherer, T. Ehmann, F.-M. Matysik, Comparison of molar mass determination of poly(dimethylsiloxanes) by size exclusion chromatography and high-resolution polymer high performance liquid chromatography based on a sawtooth gradient, ACS Appl. Polym. Mater. 1 (2019) 2388–2397. https://doi.org/10.1021/acsapm.9b00483.

[95] B. Durner, T. Ehmann, F.-M. Matysik, High-resolution polymer high performance liquid chromatography: optimization of the saw tooth gradient profile for various stationary phases and separations on preparative scale, Anal. Methods 11 (2019) 4960–4968. https://doi.org/10.1039/C9AY00689C.

[96] S. Podzimek, Light scattering, size exclusion chromatography and asymmetric flow field flow fractionation: Powerful tools for the characterization of polymers, proteins, and nanoparticles, Wiley, Hoboken, New Jersey, 2011.

[97] C.-s. Wu (Ed.), Handbook of size exclusion chromatography, Marcel Dekker, New York, 1995.

[98] P.J. Wyatt, Multiangle light scattering: The basic tool for macromolecular characterization, Instrum. Sci. Technol. 25 (1997) 1–18. https://doi.org/10.1080/10739149709351443.

[99] P.J. Wyatt, Light scattering and the absolute characterization of macromolecules, Anal. Chim. Acta (1992) 1–40.

[100] C. Dauwe, Size exclusion chromatography of polyamides, polyester, and fluoropolymers, in: C.-s. Wu (Ed.), Handbook of size exclusion chromatography, 2nd ed., Marcel Dekker, New York, 2004.

[101] N. Vervoort, D. Daemen, G. Török, Performance evaluation of evaporative light scattering detection and charged aerosol detection in reversed phase liquid chromatography, J. Chromatogr. A 1189 (2008) 92–100. https://doi.org/10.1016/j.chroma.2007.10.111.

[102] G. Glöckner, Gradient HPLC of copolymers and chromatographic cross-fractionation, Springer, Berlin, 1991.

[103] P.H. Gamache (Ed.), Charged aerosol detection for liquid chromatography and related separation techniques, Wiley, Hoboken, 2017.

[104] M. Righezza, G. Guiochon, Effects of the nature of the solvent and solutes on the response of a light-scattering detector, J. Liq. Chromatogr. 11 (1988) 1967–2004. https://doi.org/10.1080/01483918808069036.

[105] R.D. Cohen, L. Yong, Advances in aerosol-based detectors, in: E. Grushka, N. Grinber (Eds.), Advances in Chromatography: Volume 52, CRC, Boca Raton, 2014, pp. 1–53.

[106] B. Durner, T. Ehmann, F.-M. Matysik, Adaption of a parallel-path poly(tetrafluoroethylene) nebulizer to an evaporative light scattering detector: Optimization and application to studies of poly(dimethylsiloxane) oligomers as a model polymer, J. Chromatogr. A 1564 (2018) 214–223. https://doi.org/10.1016/j.chroma.2018.06.008.

[107] J.H. Arndt, T. Macko, R. Brüll, Application of the evaporative light scattering detector to analytical problems in polymer science, J. Chromatogr. A 1310 (2013) 1–14. https://doi.org/10.1016/j.chroma.2013.08.041.

[108] M. Plaza, J. Kariuki, C. Turner, Quantification of individual phenolic compounds' contribution to antioxidant capacity in apple: A novel analytical tool based on liquid chromatography with diode array, electrochemical, and charged aerosol detection, J. Agric. Food Chem. 62 (2014) 409–418. https://doi.org/10.1021/jf404263k.

[109] R.D. Cohen, Y. Liu, X. Gong, Analysis of volatile bases by high performance liquid chromatography with aerosol-based detection, J. Chromatogr. A 1229 (2012) 172–179. https://doi.org/10.1016/j.chroma.2012.01.036.

[110] P.H. Gamache, R.S. McCarthy, S.M. Freeto, D.J. Asa, M.J. Woodcock, K. Laws, R.O. Cole, HPLC analysis of nonvolatile analytes using charged aerosol detection, LC GC Eur. 18 (2005) 150–161.

3 Experimental

In this chapter, an overview of the chemicals, materials, and instruments is given. Instrumental setups and general procedures are briefly described. Exact details of the experiments are given in the respective results sections.

3.1 Chemicals and materials

HFIP (99%) was purchased from Chempur (Karlsruhe, Germany). Potassium trifluoroacetate (KTFAc) was purchased from Alfa Aesar (Kandel, Germany). For HPLC-ESI-QTOF measurements, all solvents were LC-MS grade. All other used solvents were at least HPLC grade and were used without further purification. Isopropanol, acetonitrile, tetrahydrofuran, methanol, ethanol, and toluene were purchased from Merck (Darmstadt, Germany). 2-Pyrrolidone for synthesis was also purchased from Merck. The internal standard diethylene glycol monobutyl ether also for synthesis was obtained from Merck-Schuchardt (Hohenbrunn, Germany). Triethylene glycol (99%) was purchased from Thermo Fisher (Karlsruhe, Germany). Formic acid (FA, 98-100%) and heptafluorobutyric acid (HFBA, for synthesis) were also acquired from Merck. Trifluoroacetic acid (TFA, HiPErSolv CHROMANORM) was used with 100% purity and was purchased from VWR (Darmstadt, Germany). Furthermore, uracil of analytical grade was obtained from Fluka (Buchs, Schweiz) and AUA from Sigma-Aldrich with a purity of 97%. Moreover, ultrapure water (18.2 MΩ cm) prepared by a Sartorius Stedim Biotech system was used. All investigated polymer samples, polymer standards, and stationary phases are separately stated in the appropriate chapters.

3.2 Preparation of polymer samples

3.2.1 Powder aging

PA 1101 powder was thermally and thermo-oxidatively aged. 1 g of powder were filled in an aluminum crinkle and inserted into a Micro-Chamber M-CTE250 (Markes, Offenbach am Main, Germany) at defined temperatures. The used micro-chamber is shown in Figure 3.2.1. The temperature was checked with a calibrated RS 1316 dual data logger thermometer. The aging was done by applying a nitrogen gas flow and a compressed air gas flow of 10 mL min^{-1}, respectively. A nitrogen gas flow was used to eliminate the influence of oxygen and to observe a pure thermal aging behavior. The samples were cooled in the chamber to 40 °C and afterwards stored in argon atmosphere. The exact aging conditions are stated in the respective chapters.

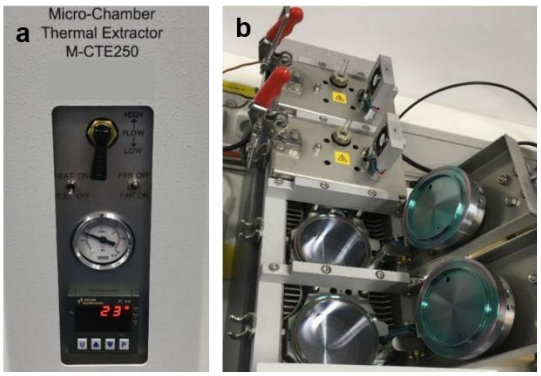

Figure 3.2.1 Micro-chamber used for artificial powder aging **a**) front view, **b**) view from above.

3.2.2 Extraction procedures

3.2.2.1 Ultrasonic extraction

The necessary amount of powder sample was weighed and a defined volume of extraction solvent was added. Afterwards, the sample was ultrasonicated for at least 15 min, followed by filtration using a 0.2 µm PTFE syringe filter from VWR.

3.2.2.2 Soxhlet extraction

For the Soxhlet extractions, the automated extraction system B-811 from Büchi (Essen, Germany) was used. The defined number of extraction cycles and the heat rate were adjusted to the properties of the chosen extraction solvents according to the user manual provided by the manufacturer [1]. An amount of powder (the exact quantity was noted) was filled into extraction thimbles (603 Standard Cellulose Extraction Thimbles) manufactured from high-quality cellulose with a size of 33 mm x 94 mm from VWR (Darmstadt, Germany), respectively. The cooling system was a recirculating chiller F-114 from Büchi. The exact extraction conditions are described in section 4.5.2.3.

3.2.2.3 Accelerated solvent extraction (ASE)

For accelerated solvent extraction the ASE 200 accelerated solvent extractor from Dionex (Dreieich, Germany) was used. The sample was loaded into an extraction cell with a volume of 11 mL together with Ottawa sand and sodium sulphate. The solvent was pumped into the preheated cell followed by the extraction under a defined pressure and static extraction time. Afterwards, the cell was flushed. The procedure was repeated three times and the extracts were collected. The applied extraction conditions are given in section 4.5.2.3.

3.3 Liquid chromatographic methods

3.3.1 High-resolution polymer HPLC

A chromatographic Agilent series 1100 system equipped with a quaternary pump was used. The system was connected to a SEDEX 85 LT ELSD detector purchased from ERC (Riemerling, Germany). All devices were controlled with the software ChemStation version B.0403 SP1. Due to the limited amount of editable positions in the gradient program of the software, several ChemStation methods were combined to one sawtooth gradient protocol to be able to perform the necessary number of steps.

3.3.2 HPLC-ESI-QTOF

HPLC–ESI–QTOF experiments were carried out using a 1260 Infinity LC system in combination with an electrospray ionization (ESI) source and a 6530 Accurate-Mass QTOF detector from Agilent Technologies (Waldbronn, Germany). The ESI source was operated in positive ion mode. MS data were received in the range of *m/z* 20 to 1500. Additionally, spectra with different collision energies of 20 eV, 30 eV, and 40 eV were recorded. Therefore, MS scans with the listed collision energies were conducted within one HPLC run. For data evaluation, the Agilent MassHunter Qualitative Analysis Navigator B.08.00 and the Agilent MassHunter Qualitative Analysis Workflow B.08.00 in combination with a database research were applied.

3.3.3 Size exclusion chromatography

A chromatography system Agilent Series 1260 Infinity equipped with an isocratic pump, a 4-channel degasser (PSS, Mainz, Germany), an autosampler, and a column oven (either from PSS or Waters, Eschborn, Germany) was used. The RI detector Optilab Tr-EX and the MALLS detector Dawn HELEOS II were manufactured by Wyatt Technologies (Santa Barbara, U.S.A.). All SEC measurements and data evaluation were performed by using the ASTRA 7 and HPLC Manager software (Wyatt Technologies, Santa Barbara, U.S.A.).

3.3.4 HPLC-DAD/MS/CAD

The HPLC-DAD/MS/CAD measurements were controlled with the software OpenLab CDS Version 2.4 from Agilent. For establishing a separation gradient, a 1290 pump (Agilent Technologies) was applied. For the inverse gradient, which was applied post-column after the DAD, a second pump (1200, Agilent) was installed. The injection system, the column oven, and the DAD were 1290 systems. A flow splitter (Analytical Scientific Instruments, model-No.: 600-PO10-06) purchased from Thermo Fisher (Germering, Germany) was installed before the

MS and CAD. An AD converter (1200 Infinity Universal Interface Box II, Agilent Technologies) was used to integrate the CAD signal into the OpenLab software. The MS signals were recorded using the single quadrupole 6130 LC-MS system in combination with an ESI source from Agilent. The CAD was a Corona Veo purchased from Thermo Fisher Scientific Dionex (Germering, Germany). The scheme of the overall setup is shown in Figure 4.5.1. The two streams of the mobile phase were combined before the splitter, but after the DAD. The second stream was supplied by the additionally installed pump. Mixing took place in a T-piece. The lines from the two pumps were connected to the opposite arms of the T-piece, and the line to the splitter was connected to the perpendicular arm. This setup is shown in detail in Figure 3.3.1.

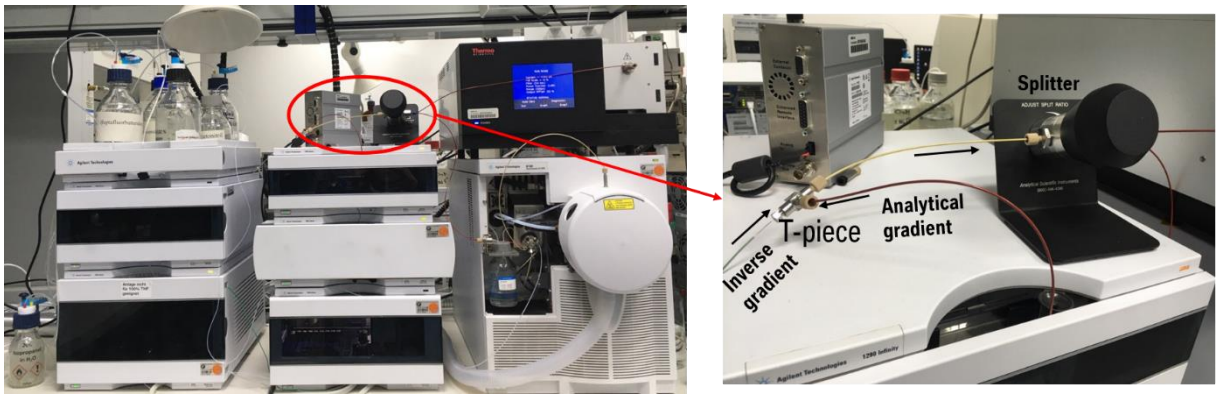

Figure 3.3.1 Inverse gradient HPLC in combination with a triple detection system (DAD / MS / CAD).

3.4 References

[1] Büchi (Ed.), Betriebsanleitung Extraktionssystem B-811, 2016.

4 Results and discussion

4.1 Comparison of molar mass determination of poly(dimethylsiloxanes) by size exclusion chromatography and high-resolution polymer high-performance liquid chromatography based on a sawtooth gradient

This subchapter was published in the journal *ACS Applied Polymer Materials*. The layout specifications of the journal were changed for uniformity. The corresponding text is adapted from:

B. Durner, B. Scherer, T. Ehmann, F.-M. Matysik, *ACS Applied Polymer Materials* **2019**, 1 2388-2397

Abstract

Polysiloxanes are used in a wide range of application fields, and extensive research is currently done to enhance product quality and performance. Therefore, more sophisticated analysis methods are necessary to monitor and support the polymer product optimization. Based on different modes in polymer liquid chromatography, heart-cut polymer HPLC is one powerful analytical approach. Due to different distributions within polymer samples, separations according to chemical heterogeneities, molecular architecture, or molar mass differences are possible. With the recently introduced sawtooth gradient protocol a possibility for determining the polymer (micro-)structure on an analytical scale has been developed. Hence, the effect of various stationary phases with different particle based material and chemical modifications was investigated in the context of the separation of linear poly(dimethylsiloxane) in a molar mass range from 1,000 g mol^{-1} to 300,000 g mol^{-1}. The resulting chromatograms allowed a direct correlation between HPLC retention times and molar masses corresponding to separated peaks. Consequently, a detailed analysis of differences in the polymer structure, e.g. fingerprint analysis, is possible. This special technique could be used in the context of quality control to ensure the product stability of polymer samples.

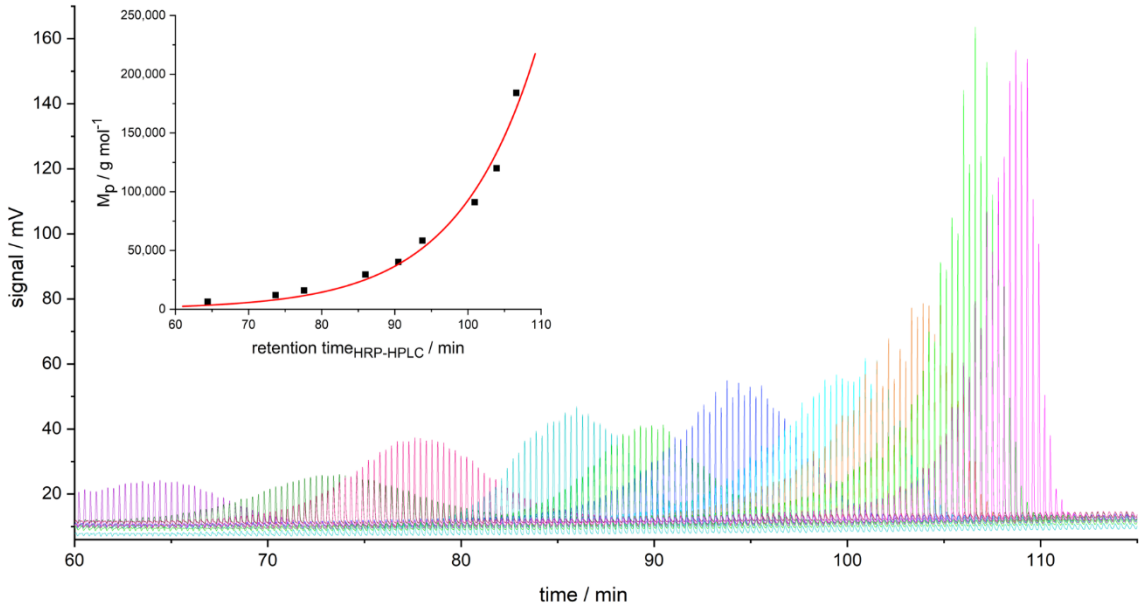

Graphical abstract Connection between molar mass and retention time in polymer HPLC.

4.1.1 Introduction

Since their first synthesis by Müller and Rochow [1], siloxanes have been applied in a broad variety of different application areas, e.g., automotive, electronic, construction, or health care industries. The versatile use of siloxanes stems from their inorganic and organic character of the polymer backbone, depending on modification of the number and type of organofunctional groups at the side chains. Based on the microscopic conditions and the cross-linking density, siloxanes are distinguished in silicone dispersions, elastomers, resins, or rubbers [2-7]. One of the most important representatives of this polymer class is poly(dimethylsiloxane) (PDMS) containing silicon and oxygen atoms as well as methylene groups in the backbone. Therefore, PDMS is used as a release agent, heat transfer liquid, antifoam, or coating or in the pharmaceutical or medical industry [8]. Further information about siloxane polymers and their applications are given in refs [9-15].

As with most synthetic polymers, siloxanes vary in some properties like molecular weight, chemical composition, and chain architecture. Therefore, it is necessary to obtain detailed information about these characteristics [16]. Various analytical methods can be applied including size exclusion chromatography (SEC), liquid chromatography at critical conditions (LCCC), and polymer HPLC [17,18]. Regarding thermodynamics, SEC is ideally dominated by entropic effects without any impact of chemical interactions. In polymer HPLC or more specifically liquid adsorption chromatography (LAC), the separation is driven by enthalpic

interactions. For LCCC, enthalpic and entropic interactions equalize each other and allow a separation independent of the molar mass of the investigated polymer. Armstrong et al. [19] were able to separate polystyrene in a molar mass region up to 10^7 g mol^{-1} based on gradient separation by precipitation mechanisms. Furthermore, polymers can be separated due to the application of gentle solvent gradients at near critical conditions (SG-NCC). Apel et al. [20] described a SG-NCC method for the separation of polycarbonate according to end groups using a mobile phase gradient that changes only slightly around the critical point of adsorption. Another possibility improving polymer separation with liquid chromatography was introduced by Chang and coworkers [21,22] and is called temperature gradient interaction chromatography (TGIC). For instance, they applied TGIC for the separation of polyvinyl chloride up to a molar mass of 1,800,000 g mol^{-1} by only changing the column temperature from 25 to 48 °C [23] or the analysis of anionic polymerized PDMS samples [24]. Each technique has its own advantages and disadvantages; however, this study focuses on comparing SEC and polymer HPLC in combination with sawtooth gradients. Further information concerning LCCC can be found in refs [25-28]. Typical detectors used in SEC and polymer HPLC are refractive index (RI) or/and multi-angle laser light scattering (MALLS) detectors in isocratic elution or evaporative light scattering detectors (ELSD) for gradient elution [29-32]. Moreover, the coupling to matrix assisted laser desorption ionization time-of-flight mass spectrometry can also be performed [33,34].

In SEC the hydrodynamic volume is assumed to be proportional to a fractional power of molecular weight enabling the determination of molar mass distributions. SEC is performed isocratically [35,36]. However, Schollenberger and Radke [37] introduced an SEC-gradient method which is an alternative approach to polymer gradient chromatography. Constraints of SEC are enthalpic interactions, as they often cannot be excluded completely, tending to lead to inaccurate molecular weight distributions. Nevertheless, SEC can offer enhanced resolution especially in the high-molecular mass range when compared to liquid adsorption chromatography (LAC) [32,38,39]. In order to enhance the performance of polymer HPLC, we recently introduced a newly developed sawtooth gradient protocol [40]. Applying a sawtooth gradient profile to polymer separations allows highly resolved analytical and (semi-)preparative measurements. Therefore, the back and forth of the sawtooth gradient enables a very detailed characterization of various polymer samples and is thus superior to normal gradient elution.

Often a combination of the above modes of polymer liquid chromatography is used for an enhanced separation, especially in the case of polymer HPLC. Therefore, heart-cut techniques of e.g. polymer HPLC or LCCC coupled to SEC are a powerful approach [38].

Combining with high-resolution polymer HPLC (HRP-HPLC), a very powerful preparative fractionation is achieved. Compared to classical preparative HPLC approaches [41,42], the method upscale based on a sawtooth gradient is simplified. Therefore, the optimized gradient profile can be used similarly in analytical and (semi-)preparative systems; only the effective step length has to be adjusted. Furthermore, concentration and volume overloading can easily be adapted to the separation system, and as far as for gradient polymer elution chromatography (GPEC), the injection always occurs in 100% adsorption promoting or, rather, nonsolvent. Thus, peak broadening effects can be avoided. Therefore, we recently [43] optimized a hybrid HPLC system which allowed the overall application of the sawtooth gradient and analyzed a PDMS sample with a weight average molar mass of approximately 20,000 g mol^{-1}. In this study, the investigated molar mass range is extended and the impact of different stationary phases on separation performance was analyzed. Additionally, after fraction collection of a polydisperse PDMS sample, the molar masses of the single fractions were correlated to retention times in polymer HPLC. This connection between retention time and molar mass in polymer HPLC is easily achieved through the firmly fractionated polymer peaks generated through the sawtooth gradient profile.

4.1.2 Material and methods

4.1.2.1 Mobile phase components and polymer standards

All used solvents were HPLC grade, except for toluene (analytical grade >99.9%). Acetonitrile, methanol, nonstabilized tetrahydrofuran (THF), and toluene were purchased from Merck (Darmstadt, Germany) and were used without further purification. All PDMS standards with viscosities of 5 mPa s, 20 mPa s, 200 mPa s, 8,000 mPa s, and 1,000,000 mPa s were obtained from Wacker Chemie AG (Burghausen, Germany). The mixtures of various PDMS polymers for preparative HRP-HPLC contained 5 mPa s, 20 mPa s, 200 mPa s, 8,000 mPa s, and 1,000,000 mPa s in a ratio of 1:3:4:4:4 dissolved in THF with an overall PDMS concentration of 100 mg mL^{-1} resulting in a molar mass distribution of a polydispersity of 18. The molecular weight distribution of the PDMS sample mixture is shown in the section 4.1.6 (Figure 4.1.8). The linear PDMS oligomers of Si10, Si22, Si30, and Si40 were isolated as described previously [44]. In this study, a concentration of 1 mg mL^{-1} for each linear PDMS oligomer (dissolved in THF) was used.

4.1.2.2 Preparative HRP-HPLC based on a sawtooth gradient

Preparative HRP-HPLC was performed by coupling a Thermo Fisher Scientific (Waltham, U.S.A.) Ultimate 3000 HPLC (with binary pump, autosampler, and column oven) to an Agilent (Waldbronn, Germany) 1260 fraction collector equipped with an Agilent LAN Interface Card.

For determination of the cutting pattern an Agilent 385 ELSD modified with a parallel path poly(tetrafluoroethylene) (PTFE) nebulizer was used (40 °C evaporator temperature, 90 °C nebulizer temperature and a gas flow rate of 1.6 standard liters per minute [31]). For fraction collection, an additional (but inactive) Agilent 1100 HPLC pump and autosampler were necessary. The Agilent autosampler had to be deactivated in the script editor of the chromatographic data system Chromeleon (Thermo Fisher Scientific, version 7.2) by using the command "LCSystem.ALS.Position" set to a value of "1".

For the preparative separations, acetonitrile was used as an adsorption promoting or, rather, nonsolvent (in the following referred to as adsorption promoting solvent independently of influences of precipitation and redissolution effects) and THF as desorption promoting solvent. The first set of fraction collections was performed on a Hypersil Gold C18 aQ (100 mm × 10 mm, 5 µm) with an overall fractionated amount of 1200 mg PDMS (24 injections at 50 mg). Thus, the injection volume was 100 µL. The used sawtooth gradient had an effective step length of 2.25 min, an effective step height of 1.0%, a height of the negative backward gradient step of 40%, and a LC flow rate of 4.0 mL min^{-1}. The second set of fraction collections was performed on an Agilent PLgel MIXED-C SEC column (300 mm × 5 mm, 5 µm) with an overall fractionated amount of 800 mg of PDMS (16 injections at 50 mg). The injection volume again was 100 µL. The used sawtooth gradient had an effective step length of 3.0 min, an effective step height of 1.0%, a height of the negative backward gradient step of 100%, and a LC flow rate of 3.0 mL min^{-1}.

4.1.2.3 SEC equipment and measurements

For conventional calibration by a RI detector a set of Agilent polystyrene standards between 580 and 2,698,000 g mol^{-1} was used with a concentration of 0.50% (w/v). All SEC measurements were performed according to ISO 16014-3 and ISO 16014-5 [45,46]. A chromatography system Agilent Series 1260 Infinity equipped with an isocratic pump, a 4-channel degasser (PSS, Mainz, Germany), an autosampler, and a column oven (T = 45 °C, Waters, Eschborn, Germany) was used. The RI detector Optilab Tr-EX and the MALLS detector Dawn HELEOS II were manufactured by Wyatt Technologies (Santa Barbara, U.S.A.). The Optilab Tr-EX detector was set to 45 °C. All SEC measurements and data evaluation were performed by using ASTRA 7 and HPLC Manager software (Wyatt Technologies, Santa Barbara, U.S.A.). The light scattering measurements and the measurements for the conventional calibration were performed with an injection volume of 20 µL, a flow rate of 0.3 mL min^{-1}, toluene as eluent, and a sample concentration of 3 mg mL^{-1}. An Agilent PLgel MiniMIX-C Guard column (50 mm × 4.6 mm, 5 µm) and three

Agilent PLgel MiniMIX-C columns (250 mm × 4.6 mm, 5 µm) were used as the stationary phase.

4.1.2.4 Analytical HRP-HPLC based on a highly resolved sawtooth gradient

The analytical HRP-HPLC measurements were performed on a Thermo Fisher Scientific Ultimate 3000 HPLC (quaternary pump, autosampler, column oven) equipped with an Agilent 385 ELSD modified with a parallel path PTFE nebulizer (see above). Methanol was used as adsorption promoting solvent and THF as desorption promoting solvent. The sawtooth gradient (for methodical details see ref [40]), with an effective step height of 0.2%, an effective step length of 0.3 min, a height of the negative backward gradient step of 40%, and an LC flow rate of 3.0 mL min^{-1}, started at 100% methanol and ended at 100% THF. The measurements were performed on a Thermo Fisher Scientific Accucore C18 (50 mm × 4.6 mm, 2.6 µm) and a ZirChrom (Anoka, U.S.A.) Diamondbond C18 (150 mm × 4.6 mm, 5 µm). The injection volumes were 8 µL for each analyzed sample.

4.1.3 Results and discussion

In addition to the previously reported results [40], whereby the sawtooth gradient showed a better performance compared to conventional gradient elution, further investigations with preparative high-resolution polymer HPLC (HRP-HPLC) based on a sawtooth gradient were performed. With a model mixture of linear PDMS composed of silicone oils with different viscosities and thus molar masses from 300 g mol^{-1} up to over 300,000 g mol^{-1} (see section 4.1.6), the separation capability of the sawtooth gradient is discussed. Furthermore, reanalysis of samples fractionated by applying a high-resolution sawtooth gradient on two appropriate stationary phases (refer to ref [43]) allowed the correlation of average molar mass at peak maximum to retention times of HRP-HPLC.

4.1.3.1 Preparative HRP-HPLC for PDMS fractionation and SEC data evaluation

Comparing two completely different stationary phases, the separation efficiency of the used sawtooth gradients is discussed. Initially, a Hypersil Gold C18 aQ (100 mm × 10 mm, 5 µm) was used to separate the PDMS mixture specified above in 22 consecutive fractions (Figure 4.1.1). Therefore, acetonitrile was used as adsorption promoting or, rather, nonsolvent for the investigated PDMS mixture and THF as desorption promoting solvent. The polymer sample was introduced in the separation system by multiple injection (5 times) of 100 µL of the above PDMS mixture at a low flow rate of 0.2 mL min^{-1} in 100% of adsorption promoting solvent. The advantage of this injection procedure is that the injection loop did not have to be changed. Thus, volume overloading effects were reduced, and the peak width remained small

because the sample precipitated or was strongly adsorbed on the column head. This procedure was very beneficial for scaling up from analytical [40] to (semi-)preparative sawtooth gradients.

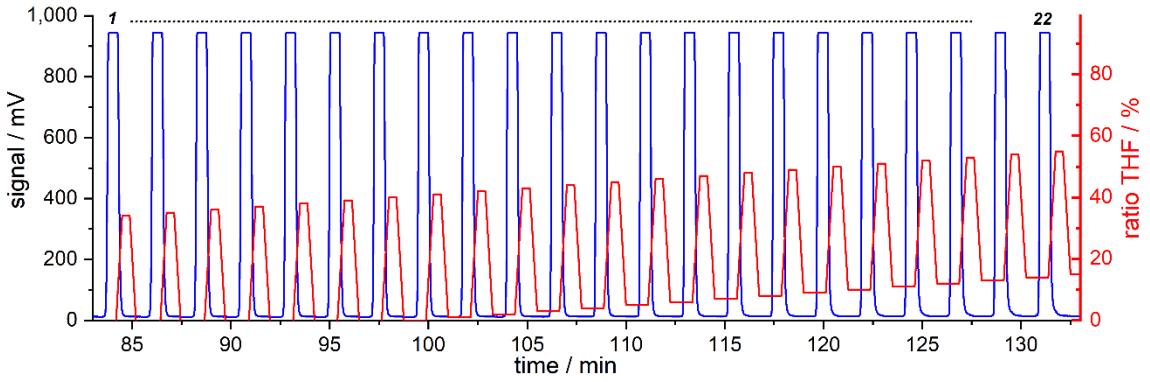

Figure 4.1.1 Measurement for preparative separation of a linear PDMS sample mixture containing silicone oils with viscosities of 5 mPa s, 20 mPa s, 200 mPa s, 8,000 mPa s, and 1,000,000 mPa s, dissolved in THF with a mixing ratio of 1:3:4:4:4 and an overall PDMS concentration of 100 mg mL^{-1}. A Hypersil Gold C18 aQ column (100 mm × 10 mm, 5 µm), acetonitrile as the nonsolvent, and THF as the desorption promoting solvent were used with a sawtooth gradient of 40% height of the negative backward gradient step, 1% effective step height, and 2.25 min effective step length. The collected fractions are numbered from 1 to 22.

The sample amount per fraction is depicted in Table 4.1.1. Furthermore, an overview of the number average molecular weight M_n, the weight average molecular weight M_w, the average molar mass at peak maximum M_p, and the polydispersity (M_w/M_n) of fractions 1 to 22 is also given. Elugrams of each fraction were evaluated by means of conventional calibration as equivalents of polystyrene standards using only the RI detector and retention times (see Table 4.1.1). Moreover, the absolute masses were determined by using MALLS detection with RI detection for determining the concentration for each fraction. These results are also given in Table 4.1.1 as MALLS results. Therefore, 100% recovery is assumed for calculating the distinct refractive index increments dn/dc from the RI signals. In calculating the absolute molar mass, dn/dc is used as the square in the corresponding equation emphasizing the importance of reliable values for dn/dc. In general, SEC measurements show a continuously increasing molar mass with increasing fraction number. But by evaluation based on absolute molar mass determination the number and weight average molecular masses did not consistently increase from fractions 1 up to 22. Referring to the average molecular masses the polydispersity index also fluctuated. However, the M_p values of MALLS and RI increased throughout from fraction 1 up to fraction 22 with just one exception of fraction 2 when assessed by MALLS detection. One possible reason why the molar masses obtained by MALLS were not monotonously increasing, e.g., at fractions 2, 9, 10, 12, and 19, could be caused by the inappropriate

assumption of 100% mass recovery and its impact on the dn/dc calculation. Nevertheless, values evaluated by conventional calibration showed continuous increase of M_w, M_n, and M_p values. Regarding the polydispersity, fractions 1 up to 17 are highly monodisperse with values ranging from 1.04 to 1.07. Polydispersity indices of fraction 18, 19, 20, and 21 showed a remarkable increase followed by the more than doubled polydispersity index of fraction 22 compared to that of 21. This could be seen as an indicator that the column used for fraction collection probably had to be optimized to achieve an ideal separation.

Table 4.1.1 Results of the SEC measurements of the first set of fraction collection (compare Figure 4.1.1)[a].

Fraction number	Weight of fraction /mg	M_w /g mol^{-1}		M_n /g mol^{-1}		M_p /g mol^{-1}		Polydispersity	
		MALLS	RI	MALS	RI	MALLS	RI	MALLS	RI
FC1	5.5	4,600	4,300	4,500	4,200	4,400	4,600	1.02	1.04
FC2	5.8	4,300	5,200	4,200	4,900	4,300	5,500	1.01	1.05
FC3	5.8	4,600	5,400	4,600	5,200	4,600	5,800	1.01	1.04
FC4	6.2	4,800	5,600	4,800	5,400	5,000	6,000	1.01	1.04
FC5	6.1	4,900	5,900	4,800	5,600	5,100	6,300	1.01	1.05
FC6	6.4	5,000	6,100	4,900	5,900	5,200	6,600	1.02	1.04
FC7	6.7	5,600	6,500	5,600	6,200	5,600	7,000	1.00	1.04
FC8	7.0	6,700	6,800	6,300	6,400	6,200	7,300	1.08	1.05
FC9	7.4	6,600	7,200	6,400	6,900	6,500	7,800	1.04	1.05
FC10	8.0	6,200	7,800	5,900	7,500	6,600	8,400	1.05	1.05
FC11	8.8	8,000	8,300	7,800	7,900	7,600	9,100	1.04	1.06
FC12	9.3	7,400	9,000	7,100	8,500	7,900	9,800	1.04	1.06
FC13	10.1	8,000	9,700	7,800	9,100	8,400	10,500	1.02	1.06
FC14	11.4	8,600	10,600	8,300	9,900	9,200	11,500	1.03	1.07
FC15	12.4	9,900	11,700	9,700	11,000	10,400	12,600	1.02	1.06
FC16	13.9	10,700	12,700	10,000	11,900	11,600	13,800	1.07	1.07
FC17	15.3	12,100	14,000	11,000	13,100	13,200	15,200	1.10	1.07
FC18	17.2	15,500	15,500	15,000	13,200	15,300	17,100	1.03	1.18
FC19	19.0	14,700	17,600	13,200	16,000	16,300	19,300	1.11	1.10
FC20	21.2	20,100	20,100	19,800	15,100	20,300	22,400	1.01	1.34
FC21	83.0	162,700	161,700	119,600	102,800	125,800	125,600	1.36	1.57
FC22	81.4	335,000	269,000	128,400	82,100	499,100	392,900	2.61	3.27

[a]SEC was performed with 3 MiniMIX C SEC columns (250 mm x 4.6 mm, 5 µm) and toluene as eluent; the values for the weight average molar mass M_w, the number average molar mass M_n, and the average molar mass at peak maximum M_p were evaluated by an RI and a MALLS detector.

The RI detector is the most common detector in SEC as most of the polymers can be detected. If standards for mass calibration of the respective polymer are available, the assessed molar masses directly refer to the investigated polymer. If not, the molar mass averages are determined as equivalents of certain available polymer standards e.g. polystyrene or

poly(methyl methacrylate). For PDMS, toluene is used as the eluent because THF and PDMS are nearly isorefractive resulting in a very poor signal [47].

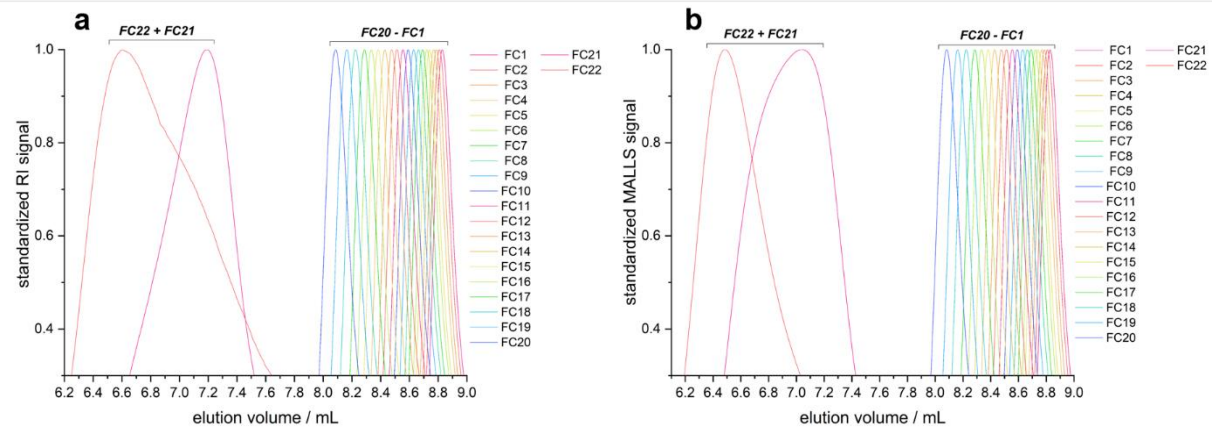

Figure 4.1.2 SEC results of the preparative separation depicted in Figure 4.1.1; each elugram shows a standardized y axis for (**a**) the RI signal and (**b**) the MALLS signal. The fraction numbers are shown and are color coded in the legend.

In Figure 4.1.2 the normalized signals obtained by MALLS (a) and RI detection (b) are depicted. Each fraction is color coded. The peak maxima of lower fractions are located directly next to each other. The peak maxima of the first fractions are very close to each other, and with increasing fraction number the distance slightly increases. But fractions 21 and 22 showed an atypical behavior. Therefore, for subsequent measurements only the RI detector was used for assessing the molar mass distributions. The large distance between the peak maximum of fraction 20 and that of fraction 21 could be explained by the failure of the applied stationary phase in appropriately separating the high molecular mass components of the sample by the sawtooth gradient approach. It could be assumed that fractions 21 and 22 eluted very close to the point of critical adsorption. This limiting condition for the application of a preparative sawtooth gradient could be overcome by applying a different stationary phase. Additionally, for the analyzed PDMS mixture RI detection was sufficient and was solely used in subsequent measurements.

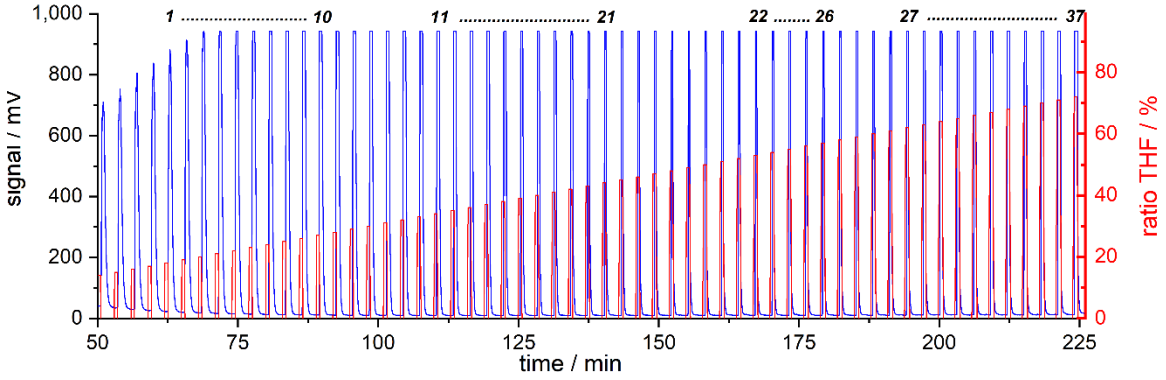

Figure 4.1.3 Chromatogram of preparative separation of a synthetic mixture of linear PDMS containing silicone oils with viscosities of 5 mPa s, 20 mPa s, 200 mPa s, 8,000 mPa s, and 1,000,000 mPa s, dissolved in THF with a mixing ratio of 1:3:4:4:4 and an overall PDMS concentration of 100 mg mL^{-1}. A PLgel MIXED-C SEC column (300 mm × 5 mm, 5 µm), acetonitrile as the nonsolvent, and THF as the desorption promoting solvent were used with a sawtooth gradient of 100% height of the negative backward gradient step, 1% effective step height, and 3.0 min effective step length. The collected fractions are assigned from 1 to 37 over the chromatogram.

In a following preparative HRP-HPLC separation (Figure 4.1.3) a PLgel MIXED-C (300 × 5 mm, 5 µm) SEC column was used with acetonitrile and THF as mobile phase components again. The different base material of the stationary phase increased the working range for the separation based on the sawtooth gradient. As already depicted in ref [43], operating a sawtooth gradient on a SEC column worked pretty well. Fraction collection was performed for 37 fractions, with several time jumps covering certain ranges of the total distribution of the synthetic PDMS mixture. Additionally, a sawtooth gradient down to zero (with 100% height of the negative backward gradient step) was applied to enhance the separation performance. Compared to the aforementioned fraction collection, more peaks could be resolved and collected.

The molar mass distribution of SEC (Figure 4.1.4) showed the same gaps in the molar mass distribution as depicted in the cutting pattern (Figure 4.1.3). Similar to the first set of fraction collections, the molar masses increased with growing fraction number but with an improved peak resolution for high molecular components. Particularly, for fraction numbers 27 to 37 the MIXED-C column showed an enhanced separation performance suggesting that the critical point of adsorption was shifted to even higher molecular masses. In summary, a MIXED-C SEC column offered an improved separation range compared to Hypersil Gold C18 aQ for applying a sawtooth gradient on extremely polydisperse synthetic PDMS mixtures.

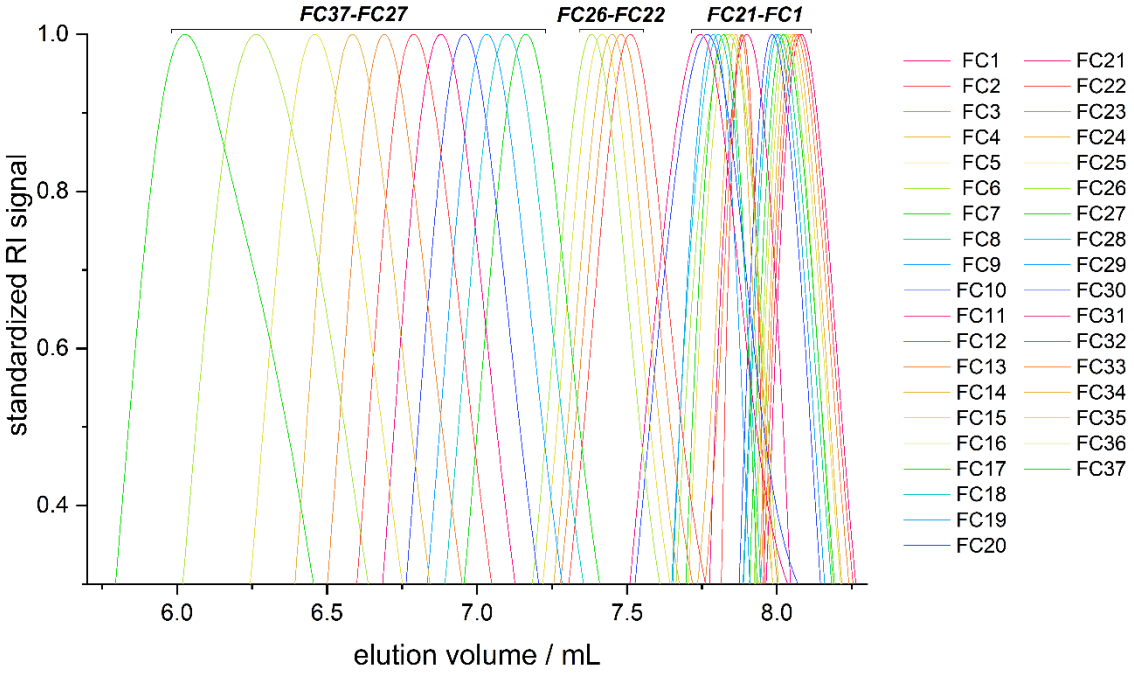

Figure 4.1.4 SEC results for the preparative separation depicted in Figure 4.1.3. The y axis shows the standardized RI signal, and the fraction numbering correlates to the numbers in Figure 4.1.3; a further overlay with the original PDMS sample mix is shown in Figure 4.1.9.

The results for M_w, M_n, and M_p are presented in Table 4.1.2. Compared to the Hypersil Gold C18 aQ, the values for M_w, M_n, and M_p showed a monotonous rise with the fraction number. M_p starts from 3,400 g mol^{-1} at fraction 1 and ends at 311,000 g mol^{-1} for fraction 37, M_w from 2,900 g mol^{-1} to 231,000 g mol^{-1}, and M_n from 2,500 g mol^{-1} to 170,400 g mol^{-1}.

Table 4.1.2 Results of the SEC measurements of the second fraction collection (compare Figure 4.1.3)[a].

Fraction number	Weight of fraction /mg	M_w /g mol^{-1}	M_n /g mol^{-1}	M_p /g mol^{-1}
FC1	1.6	2,900	2,500	3,400
FC2	1.5	3,000	2,500	3,500
FC3	1.6	3,100	2,600	3,600
FC4	1.9	3,100	2,700	3,600
FC5	1.7	3,200	2,700	3,700
FC6	2.1	3,300	2,800	3,800
FC7	1.7	3,400	2,800	3,900
FC8	1.5	3,500	2,900	4,000
FC9	2.4	3,500	2,900	4,100
FC10	2.3	3,600	3,000	4,200
FC11	3.0	4,400	3,500	5,100
FC12	4.9	4,600	3,700	5,300
FC13	4.5	4,600	3,700	5,300
FC14	5.4	4,900	3,800	5,500
FC15	2.7	5,000	3,900	5,700
FC16	1.9	5,200	4,000	5,900
FC17	3.3	5,400	4,200	6,100
FC18	2.3	5,500	4,400	6,300
FC19	2.7	5,700	4,600	6,500
FC20	2.6	6,000	4,900	6,800
FC21	2.7	6,200	5,000	7,100
FC22	4.4	10,000	7,700	12,000
FC23	4.4	10,800	8,600	12,800
FC24	5.3	11,500	9,500	13,800
FC25	4.4	12,400	10,200	14,800
FC26	4.3	13,200	10,300	15,900
FC27	7.0	25,500	20,600	2,500
FC28	5.8	26,500	21,800	29,500
FC29	8.5	29,100	23,900	34,100
FC30	9.5	33,100	25,700	40,200
FC31	9.7	39,600	29,600	48,100
FC32	9.8	47,600	36,800	58,400
FC33	10.6	63,300	47,800	71,900
FC34	11.7	73,800	56,700	91,100
FC35	11.7	99,700	77,300	120,000
FC36	11.8	144,800	110,700	184,000
FC37	17.2	231,000	170,400	311,000

[a]SEC was performed with 3 MiniMIX-C SEC columns (250 mm x 4.6 mm, 5 µm) and toluene as eluent; the values for the weight average molar mass M_w, the number average molar mass M_n, and the average molar mass at peak maximum M_p were evaluated by an RI detector.

4.1.3.2 Correlation of average molar masses to HRP-HPLC retention times

Based on the measurement series on the PLgel MIXED-C column, reanalysis of the fractionated PDMS samples by applying a high-resolution sawtooth gradient (0.2% effective step height) was performed on a ZirChrom Diamondbond C18 column (Figure 4.1.5) showing a good separation performance for PDMS over a broad molar mass range in previous measurements [43]. Under these conditions, no chromatography under critical conditions occurred in the investigated molar mass range. Thus, even the highest masses of PDMS (up to 300,000 g mol^{-1}) could be separated with good resolution.

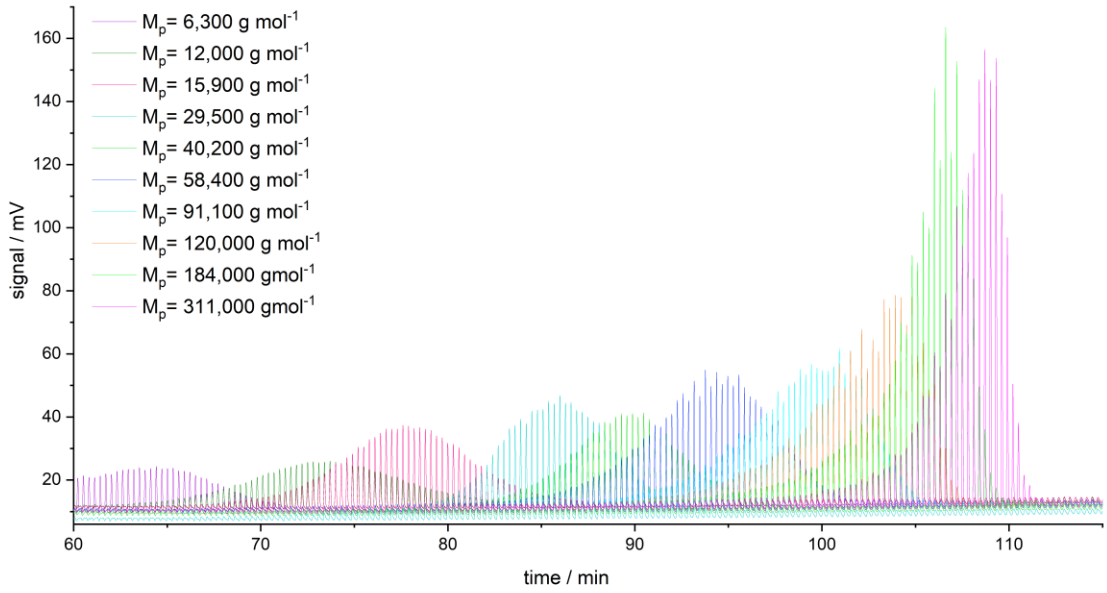

Figure 4.1.5 Correlation of average molar masses of the fractionated PDMS sample to retention times in HRP-HPLC by performing a sawtooth gradient (effective step height: 0.2%, effective step length: 0.3 min, height of the negative backward gradient step: 40%) with methanol as the adsorption promoting solvent and THF as the desorption promoting solvent applying a ZirChrom Diamondbond C18 column (150 mm × 4.6 mm, 5 µm).

In addition to this high molar mass separation, an Accucore C18 column (Figure 4.1.6) was chosen in order to analyze the low molar mass PDMS polymers which were insufficiently separated (extremely broad distribution) on the Diamondbond C18. For all fractionated samples down to fraction 1 a good separation was achievable. Furthermore, linear PDMS oligomer standards Si10, Si22, Si30, and Si40 were used to show the limits of the separation based on the applied sawtooth gradient. Furthermore, applying these oligomer standards with exactly defined molar masses to the separation was in very good accordance with the average molar mass corresponding to peak maximum values obtained from SEC. However, peak splitting of the pure oligomer samples showed the limitation of the sawtooth gradient for low molar mass compounds. Peak splitting originated from mass overloading of the single gradient steps. Consequently, a sawtooth gradient either with an extended effective step length or with

a reduced sample amount would be necessary. Apart from that, referring to the single oligomers the molar masses of HRP-HPLC correlated pretty good to those of SEC, even for the lower mass range. Generally, for molar masses up to 2,000 g mol^{-1} other separation techniques are preferred as shown in the separation of cyclic from linear PDMS [44,48].

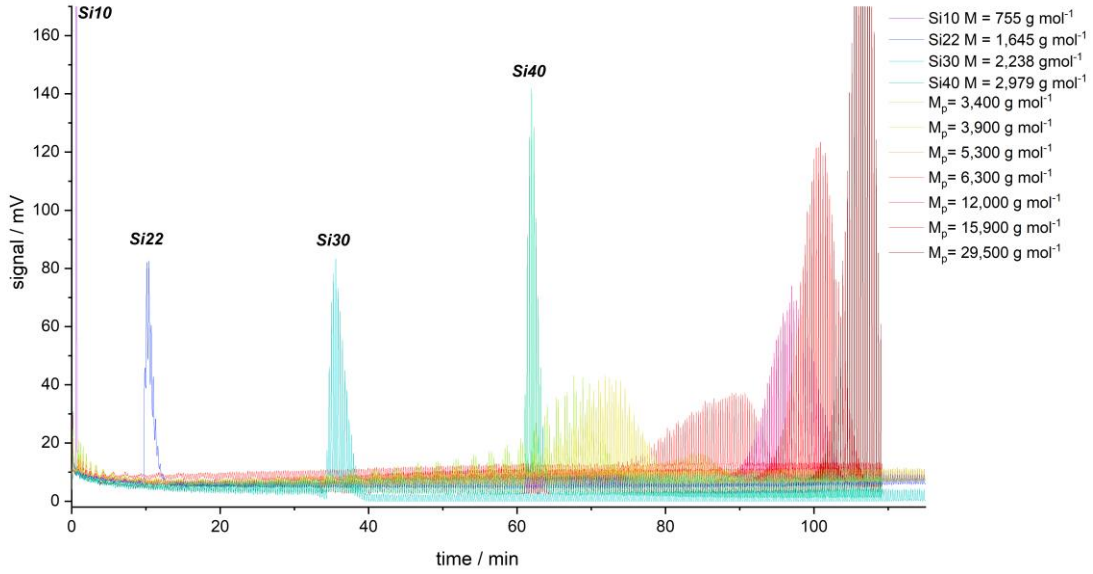

Figure 4.1.6 Correlation of average molar masses of the fractionated PDMS sample and linear PDMS oligomers Si10, Si22, Si30, and Si40 to HR-PHPLC retention times by applying a sawtooth gradient (effective step height: 0.2%, effective step length: 0.3 min, height of the negative backward gradient step: 40%) with methanol as the adsorption promoting solvent and THF as the desorption promoting solvent using a Thermo Fisher Scientific Accucore C18 column (50 mm × 4.6 mm, 2.6 µm).

Based on analytical HRP-HPLC applying a high-resolution sawtooth gradient, the molar masses of each PDMS fraction were correlated to retention times in HRP-HPLC. Thus, the molar mass at peak maximum obtained by SEC was related to the highest peak of the peak distribution, and the corresponding retention time was determined. Table 4.1.3 summarizes molar masses at peak maximum and the retention times. Employing an Accucore C18 and a Diamondbond C18 as stationary phases, the mass range between 6,000 g mol^{-1} and 16,000 g mol^{-1} overlapped; thus, by combining both stationary phases a molar mass range from <1,000 g mol^{-1} up to 300,000 g mol^{-1} could be covered.

Table 4.1.3 Correlation of HRP-HPLC retention time to average molar mass at peak maximum M_p for several fractionated PDMS samples and linear PDMS oligomers Si10, Si22, Si40, and Si48 isolated as described in reference [44][a].

HPLC column	sample name	M_p /g mol^{-1}	retention time /min
Accucore C18	Si10	755	0.7
	Si22	1,645	10.1
	Si30	2,238	35.6
	Si40	2,979	62.0
	Si48	3,572	71.0
	FC1	3,400	67.7
	FC7	3,900	71.9
	FC12	5,300	83.5
	FC18	6,300	89.5
	FC22	12,000	97.6
	FC26	15,900	100.9
Diamondbond C18	FC18	6,300	64.4
	FC22	12,000	73.7
	FC26	15,900	77.6
	FC28	29,500	86.0
	FC30	40,200	90.5
	FC32	58,400	93.8
	FC34	91,100	100.9
	FC35	120,000	103.9
	FC36	184,000	106.6
	FC37	311,000	108.7

[a]For covering the complete molar mass range, two HPLC columns, Accucore C18 (50 mm × 4.6 mm, 2.6 µm) and Diamondbond C18 (150 mm × 4.6 mm, 5 µm), were used for analytical measurements.

Based on the values of Table 4.1.3 a calibration model for the Diamondbond C18 (Figure 4.1.7 a) and for the Accucore C18 (Figure 4.1.7 b) was established correlating the retention times to molar masses.

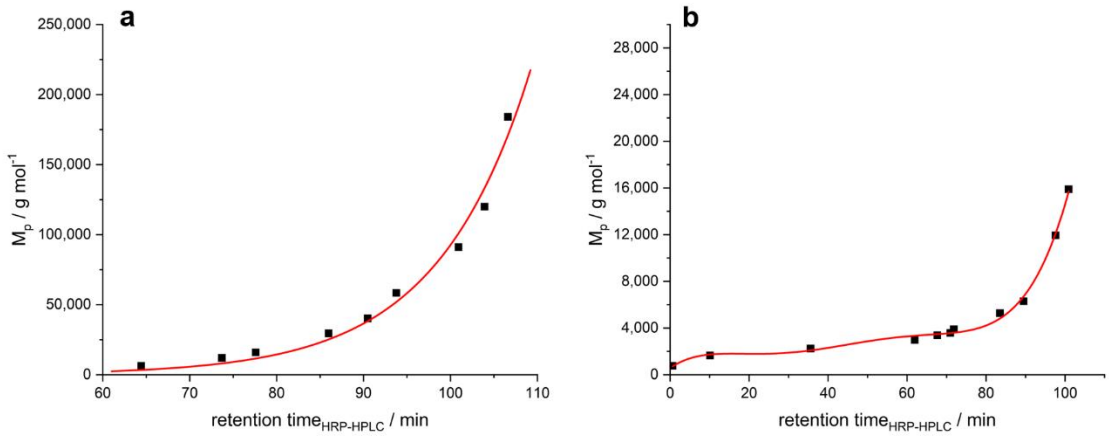

Figure 4.1.7 Calibration curves for average molar mass correlation to retention time in HRP-HPLC. (**a**) Exponential fit [$M_p = 8.62 \cdot \exp(0.0928 \cdot t)$] in the high molar mass range on a Diamondbond C18 column, (**b**) fifth order polynomial fit [$M_p = 3.1 \times 10^{-5} \cdot t^5 + 6.5 \times 10^{-3} \cdot t^4 + 0.5 \cdot t^3 - 16.5 \cdot t^2 + 237.4 \cdot t + 567.5$] in the low molar mass range on an Accucore C18 column; the uncertainties and the resulting error bars for each data point (three repetitions) are smaller than the data symbols.

For the Diamondbond C18 column, the best fit was an exponential curve with the following equation ($M_p = 8.62 \cdot \exp(0.0928 \cdot t)$), and for the Accucore C18 column a fifth-order polynomial equation ($M_p = 3.1 \times 10^{-5} \cdot t^5 + 6.5 \times 10^{-3} \cdot t^4 + 0.5 \cdot t^3 - 16.5 \cdot t^2 + 237.4 \cdot t + 567.5$) was an appropriate fit model. Based on these models, a more thorough characterization of investigated PDMS samples could be generated. For instance, small differences in the polymer distributions of various samples could be compared with respect to the exact molar masses. However, as shown by employing two different stationary phases, the shape and the type of the fitting curve highly depends on the type of the stationary phase. These findings were in accordance with literature describing liquid chromatography at critical conditions [28]. Therefore, already small changes of mobile or stationary phases lead to a big change of the critical conditions. In case of Diamondbond C18 and Accucore C18, zircon-based particles are compared to silica-based particles. Presumably, changes in the composition of the mobile phase and the temperature setting also influence the fit function. Therefore, choosing the overall separation system in advance is helpful to keep the efforts as small as possible. Comparing the molar mass determination in SEC with that in HRP-HPLC, the major advantage of SEC is the nearly polymer independent conventional calibration when applying the polymer equivalent approach. But with HRP-HPLC an essentially improved resolution of the polymer distribution is achieved, facilitating the distinction of small differences within polymer samples. For correlating molar mass to retention time in HRP-HPLC, the type of the polymer has to be known as well as the chemical functionality. Anyway, the measurements in HRP-HPLC are highly reproducible and only showed minor uncertainties in determining the retention times. The nonlinear fit functions were calculated from highly reproducible data points, and therefore

with modern calculation software an ideal best suited fit function could be generated. With respect to the high molar mass range of the investigated sample the critical point of adsorption limited the application of the sawtooth gradient. However, the comparison of Accucore C18 and Diamondbond C18 columns showed the big differences between critical adsorption conditions in several separation systems. Therefore, choosing a well-suited stationary phase in advance enables still good separation results.

4.1.4 Conclusion

Two sets of preparative HRP-HPLC measurements for PDMS were compared with respect to separation performance of the used sawtooth gradient and impact of the used stationary phases. Therefore, based on heart-cut preparative HRP-HPLC, using a PLgel MIXED-C column allowed a considerably improved separation result. By reanalyzing the collected fractions with SEC, a consecutive increase of molar mass with the fraction number was found.

Molar masses obtained by absolute molar mass evaluation applying a MALLS detector showed some deviation from a monotonous increase presumably due to uncertainties in the calculation of dn/dc for each fraction. When assessing the molar masses by an RI detector and conventional calibration as equivalents of polystyrene, the results steadily increased from fraction to fraction. Consequently, for the second set of fraction collection by using the sawtooth gradient only RI detection and evaluation was applied for reanalyzing with SEC. A constant increase of molecular weight due to the fraction number and a correlation between molecular weights and retention times of the analyzed fractions were obtained. Reanalysis with a high-resolution sawtooth gradient showed good results over the whole investigated molar mass range. Consequently, two different stationary phases, an Accucore C18 and a Diamondbond C18, were used for covering either the low or the high molar mass range. The Diamondbond C18 column showed a superior separation performance for the high molar mass range because the CPA did not affect the separation. The correlation between molar masses and retention times in HRP-HPLC enabled an enhanced characterization of polymers. Based on the calibration model, information about the polymer (micro-)structure was measurable and comparable especially for high molar mass polymer samples. Comparing with SEC, one drawback is the susceptibility of HRP-HPLC to simultaneous changes of chemical and molar mass distribution of the investigated polymers. Thus, for each kind of polymer differing in more than one molecular distribution property, a proprietary optimization is necessary. Nevertheless, the high-resolution of HRP-HPLC up to molar masses of 300,000 g mol^{-1} and the possibility to generate quantitative results at the molecular level make this technique very attractive.

4.1.5 References

[1] E.G. Rochow, An introduction to the chemistry of silicones, Wiley, New York, 1947.

[2] A.M. Muzafarov, A. Bockholt (Eds.), Silicon polymers, Springer, Berlin, 2011.

[3] W. Noll, Chemie und Technologie der Silicone, 2nd ed., Verlag Chemie GmbH, Weinheim, 1968.

[4] B. Pachaly, F. Achenbach, C. Herzig, K. Mautner, Silicone, in: Winnacker, Küchler (Eds.), Chemische Technik: Prozesse und Produkte: Organische Zwischenverbindungen, Polymere, 5th ed., Wiley-VCH, Weinheim, 2005.

[5] A. Tiwari, M.D. Soucek (Eds.), Concise encyclopedia of high performance silicones, John Wiley & Sons, Inc, Hoboken, NJ, USA, 2014.

[6] G. Koerner, M. Schulze, J. Weis, Silicone: Chemie und Technologie; Symposium am 28. April 1989, Vulkan-Verl., Essen, 1989.

[7] Y. Liu (Ed.), Silicone dispersions, CRC Press, Boca Raton, 2017.

[8] Smithers Rapra Technology, High Performance Plastics 2011: Cologne, Germany, 23-24 February 2011, iSmithers, Shawbury, U.K., 2011.

[9] N. Auner, J. Weis (Eds.), Organosilicon chemistry II: From molecules to materials, VCH, Weinheim, 1996.

[10] N. Auner, J. Weis (Eds.), Organosilicon chemistry IV: From molecules to materials, Wiley-VCH, Weinheim, 2000.

[11] N. Auner, J. Weis (Eds.), Organosilicon chemistry V: From molecules to materials, Wiley-VCH, Weinheim, 2003.

[12] N. Auner, J. Weis (Eds.), Organosilicon chemistry VI: From Molecules to materials, Wiley-VCH, Weinheim, 2005.

[13] N. Auner, J. Weis (Eds.), Organosilicon Chemistry III: From Molecules to materials, Wiley, Weinheim, 2008.

[14] N. Auner, J. Weis (Eds.), Organosilicon Chemistry I: From Molecules to materials, Wiley, Weinheim, 2011.

[15] S.J. Clarson, J.A. Semlyen, Siloxane polymers, Prentice Hall, Englewood Cliffs, NJ, 1993.

[16] K. Mojsiewicz-Pieńkowska, Size exclusion chromatography with evaporative light scattering detection as a method for speciation analysis of polydimethylsiloxanes. II. Validation of the method for analysis of pharmaceutical formulations, J. Pharm. Biomed. Anal. 56 (2011) 851–858. https://doi.org/10.1016/j.jpba.2011.07.021.

[17] M.I. Malik, P. Sinha, G.M. Bayley, P.E. Mallon, H. Pasch, Characterization of polydimethylsiloxane-block-polystyrene (PDMS-b-PS) copolymers by liquid chromatography at critical conditions, Macromol. Chem. Phys. 212 (2011) 1221–1228. https://doi.org/10.1002/macp.201000711

[18] H. Pasch, B. Trathnigg, Multidimensional HPLC of polymers, Springer, Berlin, 2013.

[19] D.W. Armstrong, K.H. Bui, Nonaqueous reversed-phase liquid chromatographic fractionation of polystyrene, Anal. Chem. 54 (1982) 706–708. https://doi.org/10.1021/ac00241a024

[20] N. Apel, E. Uliyanchenko, S. Moyses, S. Rommens, C. Wold, T. Macko, R. Brüll, Separation of branched poly(bisphenol A carbonate) structures by solvent gradient at near-critical conditions and two-dimensional liquid Chromatography, Anal. Chem. 90 (2018) 5422–5429. https://doi.org/10.1021/acs.analchem.8b00618

[21] H.C. Lee, W. Lee, T. Chang, Characterization of polymers by temperature gradient interaction chromatography, Korea Polym. J. 4 (1996) 160–165.

[22] H.C. Lee, T. Chang, Polymer molecular weight characterization by temperature gradient high performance liquid chromatography, Polymer 37 (1996) 5747–5749. https://doi.org/10.1016/S0032-3861(96)00510-1

[23] S. Park, C. Ko, H. Choi, K. Kwon, T. Chang, Characterization of polydisperse poly(vinyl chloride) by temperature gradient interaction chromatography, J. Chromatogr. A 1123 (2006) 22–25. https://doi.org/10.1016/j.chroma.2006.04.095

[24] H. Choi, K. Im, T. Chang, Fractionation of poly(dimethyl siloxane) by interaction chromatography, Macromol. Res. (20) 2012 101–105. https://doi.org/10.1007/s13233-012-0006-5

[25] Y. Brun, P. Alden, Gradient separation of polymers at critical point of adsorption, J. Chromatogr. A 966 (2002) 25–40. https://doi.org/10.1016/S0021-9673(02)00705-7

[26] Y. Brun, C.J. Rasmussen, Interaction polymer chromatography, in: S. Fanali, P.R. Haddad, C.F. Poole, M.-L. Riekkola (Eds.), Liquid chromatography: Fundamentals and instrumentation, 2nd ed., Elsevier, Amsterdam, 2017, pp. 275–318.

[27] D. Berek, Polymer HPLC, in: D. Corradini (Ed.), Handbook of HPLC, 2nd ed., Taylor & Francis, Boca Raton, FL, 2010, pp. 447–504.

[28] A. Abe, A.-C. Albertsson, H.-J. Cantow, K. Dusek, S. Edwards., H. Höcker, J.F. Joanny, H.-H. Kausch, S. Kobayashi, K.-S. Lee, I. Manners, O. Nuyken, S.I. Stupp, U.W. Suter, G. Wegner, R. Bhargava (Eds.), Liquid chromatography / FTIR microspectroscopy / microwave assisted synthesis, Springer, Berlin, 2003.

[29] K. Mojsiewicz-Pieńkowska, Size-exclusion chromatography with evaporative light scattering detection: Method for determination of polydimethylsiloxanes. I. Testing dependence of molecular weight of polydimethylsiloxanes and injected mass upon the detector signal, J. Chromatogr. B 865 (2008) 1–6. https://doi.org/10.1016/j.jchromb.2008.02.021

[30] K. Mojsiewicz-Pieńkowska, Size exclusion chromatography with evaporative light scattering detection: Method for the determination of polydimethylsiloxanes. II.

Application of TSK-GEL H HR GMH HR -M column to determine and separate molecular weight of linear polydimethylsiloxanes, J. Chromatogr. B 865 (2008) 7–12. https://doi.org/10.1016/j.jchromb.2007.12.029

[31] B. Durner, T. Ehmann, F.-M. Matysik, Adaption of a parallel-path poly(tetrafluoroethylene) nebulizer to an evaporative light scattering detector: Optimization and application to studies of poly(dimethylsiloxane) oligomers as a model polymer, J. Chromatogr. A 1564 (2018) 214–223. https://doi.org/10.1016/j.chroma.2018.06.008

[32] A.M. Striegel, W.W. Yau, J.J. Kirkland, D.D. Bly, Modern size-exclusion liquid chromatography: Practice of gel permeation and gel filtration chromatography, 2nd ed., John Wiley & Sons, Inc., Hoboken, NJ, USA, 2009.

[33] M.S. Montaudo, C. Puglisi, F. Samperi, G. Montaudo, Application of size exclusion chromatography matrix-assisted laser desorption/ionization time-of-flight to the determination of molecular masses in polydisperse polymers, Rapid Commun. Mass Spectrom. 12 (1998) 519–528. https://doi.org/10.1002/(SICI)1097-0231(19980515)12:9<519::AID-RCM186>3.0.CO;2-L

[34] G. Montaudo, M.S. Montaudo, C. Puglisi, F. Samperi, Molecular weight distribution of poly(dimethylsiloxane) by combining matrix-assisted laser desorption/ionization time-of-flight mass spectrometry with gel-permeation chromatography fractionation, Rapid Commun. Mass Spectrom. 9 (1995) 1158–1163. https://doi.org/10.1002/rcm.1290091215

[35] S. Mori, H.G. Barth (Eds.), Size exclusion chromatography, Springer, Berlin, 1999.

[36] L.R. Snyder, J.J. Kirkland, J.W. Dolan, Introduction to modern liquid chromatography, 3rd ed., John Wiley & Sons, Inc., Hoboken, NJ, USA, 2010.

[37] M. Schollenberger, W. Radke, SEC-Gradients, an alternative approach to polymer gradient chromatography: 1. Proof of the concept, Polymer 52 (2011) 3259–3262. https://doi.org/10.1016/j.polymer.2011.05.047

[38] E. Uliyanchenko, S. van der Wal, P.J. Schoenmakers, Challenges in polymer analysis by liquid chromatography, Polym. Chem. 3 (2012) 2313-2335. https://doi.org/10.1039/C2PY20274C

[39] C.-s. Wu (Ed.), Handbook of size exclusion chromatography, Dekker, New York, 1995.

[40] B. Durner, T. Ehmann. F.-M. Matysik, High-resolution polymer high performance liquid chromatography: Application of a saw tooth gradient for the separation of various polymers, J. Chromatogr. A 1587 (2018) 88-100. https://doi.org/10.1016/j.chroma.2018.11.075

[41] U. Huber, R.E. Majors, Principles in preparative HPLC: A Primer 2007, https://www.agilent.com/cs/library/primers/Public/5989-6639EN.pdf, accessed 10 July 2019.

[42] P. Penduff, Analytical to preparative HPLC method transfer: Technical overview - An easy way to scale up from UHPLC to preparative HPLC using focused gradients, 2013, http://www.ingenieria-analitica.com/downloads/dl/file/id/1903/product/300/analytical_to_preparative_hplc_method_transfer.pdf, accessed 10 July 2019.

[43] B. Durner, T. Ehmann, F.-M. Matysik, High-resolution polymer high performance liquid chromatography: Optimization of the saw tooth gradient profile for various stationary phases and separations on preparative scale, Anal. Methods 39 (2019) 4953-5072. https://doi.org/10.1039/C9AY00689C.

[44] B. Durner, T. Ehmann, F.-M. Matysik, Separation of linear and cyclic poly(dimethylsiloxanes) with polymer high-performance liquid chromatography, Monatsh. Chem. - Chemical monthly 150 (2019) 1603-1610. https://doi.org/10.1007/s00706-019-02389-4.

[45] ISO16014-3:2012, Plastics Determination of average molecular mass and molecular mass distribution of polymers using size exclusion chromatography Part 3, 2012.

[46] ISO16014-5:2012, Plastics Determination of average molecular mass and molecular mass distribution of polymers using size exclusion chromatography Part 5, 2012.

[47] P. Kilz, D. Held, Tips & Tricks: GPC/SEC Understanding positive and negative detector signals, The Column 4 (2008) 17–20.

[48] B. Durner, T. Ehmann, F.-M. Matysik, Separation of linear and cyclic poly(dimethylsiloxanes) with interactive chromatography, in: K. Nesmerak (Ed.), Proceedings of the 14th International Students Conference “Modern Analytical Chemistry”: Prague, 20-21 September 2018, Faculty of Science, Charles University Prague, 2018, pp 7-13. ISSN: 1434-4475.

4.1.6 Supporting information

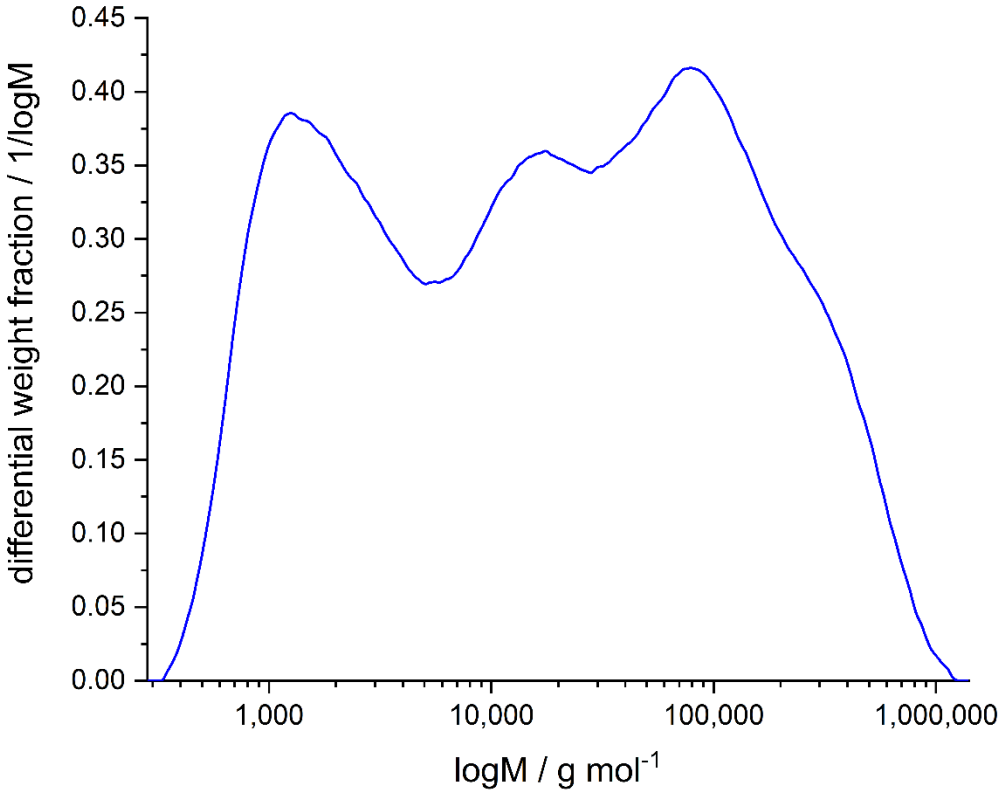

Figure 4.1.8 SEC chromatogram of a linear PDMS sample mixture containing silicone oils with viscosities of 5 mPa s, 20 mPa s, 200 mPa s, 8,000 mPa s, 1,000,000 mPa s. The mixture was dissolved in THF with a mixing ratio of 1:3:4:4:4 and an overall PDMS concentration of 100 mg mL^{-1} and diluted further to an overall PDMS concentration of 3 mg mL^{-1} in toluene. The molar mass distribution of the sample mixture is plotted as differential weight fraction against molar mass in logarithmic scale. The SEC measurement was performed with an injection volume of 20 µL, a flow rate of 0.3 mL min^{-1}, toluene as eluent as it was the case for the fractionated samples. An Agilent PLgel MiniMIX-C Guard column (50 mm x 4.6 mm, 5 µm) and three Agilent PLgel MiniMIX C columns (250 mm x 4.6 mm, 5 µm) were used as stationary phase. The elugram was evaluated by means of conventional calibration as equivalents of polystyrene standards using only the refractive index detector and retention times.

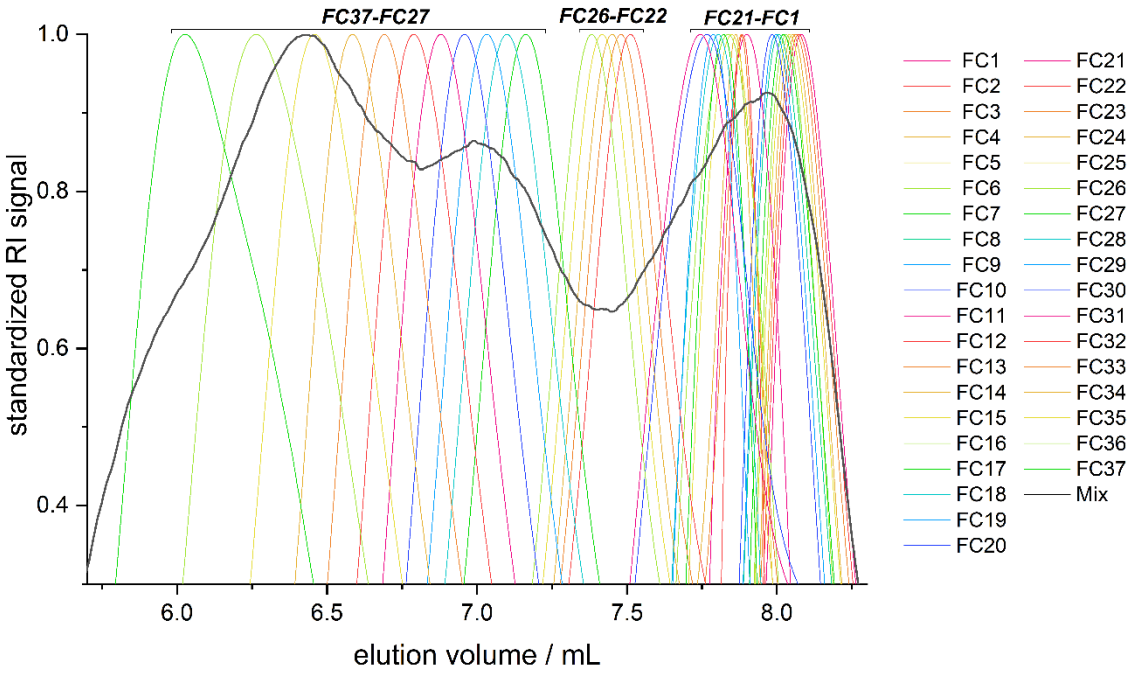

Figure 4.1.9 Comparison of SEC of a linear PDMS sample mixture (Mix) and the SECs of the associated fractionated samples FC1 up to FC37. The y axis shows the standardized RI signal and the fraction numbering correlates to the numbers in Figure 4.1.3. The fractions were obtained by the following sawtooth gradient protocol: A PLgel MIXED-C SEC column (300 mm x 5 mm, 5 µm), acetonitrile as non-solvent, and THF as desorption promoting solvent were used with a sawtooth gradient of 100% height of the negative backward gradient step, 1% effective step height, and 3.0 min effective step length. The PDMS mixture contains silicone oils with viscosities of 5 mPa s, 20 mPa s, 200 mPa s, 8,000 mPa s, 1,000,000 mPa s. The mixture was dissolved in THF with a mixing ratio of 1:3:4:4:4 and an overall PDMS concentration of 100 mg mL^{-1} and diluted further to an overall PDMS concentration of 3 mg mL^{-1} in toluene.

4.2 Development of a HRP-HPLC method by means of a sawtooth gradient profile for polyamide 11 and 12 samples in comparison to SEC-MALLS investigations

4.2.1 Introduction

Simple and distributed properties of polymers are referred to as important for their performance including e.g. the residual monomer or oligomer content which were determined for PA 1101 in section 4.5. The distribution of functional groups, the molar mass distribution or the polymer chemistry in general belong to the distributed properties. [1].

LC techniques are very commonly used to characterize polymers on a molecular base. However, the analysis of macromolecules is challenging due to many factors, such as chemical heterogeneity, poor solubility of many polymers in common chromatographic solvents and polymer dispersity [2]. SEC, liquid adsorption chromatography (LAC), liquid chromatography under critical conditions (LCCC), and precipitation-redissolution chromatography (PLC) are applied for polymer analysis, whereby any chromatographic process is based on the selective distribution of the analyte between the mobile and the stationary phase of a chromatographic system [1,2]. The different chromatographic techniques are described in more detail in the fundamental part (compare section 2.2.1) of this work, respectively.

However, in polymer HPLC the separation performance is limited to linear gradient techniques. Thus, starting with linear and stepwise gradients, Durner et al. [3] developed a periodic sawtooth gradient profile. This technique was termed high-resolution polymer HPLC (HRP-HPLC). Within the sawtooth gradient a negative gradient slope as an additional step interrupts the elution of the polymer resulting in an enhanced separation performance. One complete sawtooth gradient profile can be cut down to one single effective step length described by different parameters. An example of one effective step length and the related parameters are shown in Figure 4.2.1 [3]. The column volume (CV) corresponds to a scaling factor within the sawtooth gradient. The effective CV is obtained by dividing of the CV value by the flow rate. The parameter B within the sawtooth gradient profile represents the effective step height between the consecutive upper plateaus. Moreover, parameter A determines the height of the negative backward gradient step and parameter C depicts the step length of the retardation of the negative slope. Furthermore, the parameters D and E correspond to the step length of the lower plateau and the one of the retardation to the positive slope. The amount of obtained peaks is dependent on the effective gradient step height [3]. Consequently, the effective

gradient step height and the effective CV have the highest impact on the length of one single measurement.

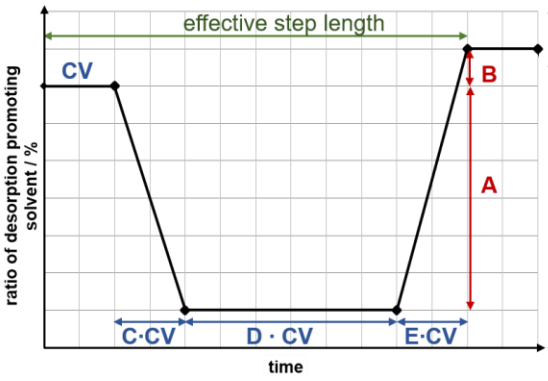

parameter	explanation
CV	Column volume
C	Retardation of negative slope
D	Duration of the lower plateau
E	Retardation of the positive slope
A	Height of the negative backward gradient step
B	Effective step height

Figure 4.2.1 Example for one effective step length of a sawtooth gradient protocol [3].

The polymer is dissolved in the desorption promoting solvent and injected into the chromatographic system at usually strong adsorption promoting conditions. This procedure leads to precipitation or at least strong adsorption of the analytes on the head of the column [3–6]. By increasing the ratio of desorption promoting solvent the analytes elute from low to high molar masses provided the critical point of adsorption is not reached [7]. The separation is primarily based on adsorption effects to the stationary phase and precipitation effects related to the solubility of the analytes in the mobile phase. However, beyond the point of critical adsorption no separation according to the molar mass of the polymer can be achieved resulting in a limited resolution of HPLC in the high molar mass region of polymers. Based on the back and forth strategy of the sawtooth shape, selective elution of different polymer fractions is possible and applications to different polymers such as polystyrene, polyvinylchloride, PDMS, PMMA, and polypropylene glycol have proven the separation performance of the HRP-HPLC [3,8,9].

However, so far polyamide 11 and 12 have not been investigated by HRP-HPLC as they offer some challenges such as the lack of solubility in common HPLC solvents. For the dissolution of polyamides, fluorinated solvents like HFIP are needed which is cost intensive [10]. The HFIP must not remain in the HPLC device without a flow for a longer time as this leads to damage to the HPLC system. Additionally, the dissolution of thermally stressed powders can be problematic as it is demonstrated in section 4.4. So far polyamides are commonly analyzed and characterized by means of SEC including the in section 2.2.3 described limitations [11,12].

The aim of this project was the development of a preferably universal sawtooth gradient protocol which allows HRP-HPLC of polyamide 11 and 12 samples in comparison with SEC measurements.

4.2.2 Experimental

4.2.2.1 Equipment for HRP-HPLC

A chromatographic Agilent series 1100 system (Waldbronn, Germany) equipped with a quaternary pump was used. The system was connected to a SEDEX 85 LT ELSD detector purchased from ERC (Riemerling, Germany). The ELSD was operated at a temperature of 30 °C and a N_2 pressure of 3.5 bar. All devices were integrated into the Software ChemStation version B.0403 SP1. The column Symmetry C18 (4.6 mm x 75 mm, 3.5 µm) from Waters was used for the development of sawtooth gradients and for the measurements of the powder samples.

4.2.2.2 SEC equipment and measurement

An Agilent 1260 Infinity system was connected to a MALLS detector Dawn HELEOS II (Wyatt Technologies, Santa Barbara, USA) and a RI detector Optilab T-rEx (Wyatt Technologies). The RI detector was operated at 40 °C. Furthermore, a column oven from PSS was included and used at 40 °C. The softwares ASTRA 7 and HPLC Manager were applied for SEC measurements and data evaluation.

4.2.2.2.1 Columns solely applied for the comparison of the polyamide 12 variants

2 PFG analytical linear XL columns (8 mm x 300 mm, 7 µm) from PSS were applied at a flow rate of 1 mL min^{-1} of the eluent HFIP + 0.05 M KTFAc. The sample concentration was 2 g L^{-1} and the injection volume was 50 µL.

4.2.2.2.2 Columns for all other SEC experiments

2 Phenogel linear columns (300 mm x 4.6 mm, 5 µm) from Phenomenex (Aschaffenburg, Germany) were used at a flow rate of 0.35 mL min^{-1} of the eluent HFIP + 0.05 M KTFAc. The sample concentration was 5 g L^{-1} and the injection volume was 15 µL.

4.2.2.3 Polyamide samples and chemicals

4.2.2.3.1 Powder samples

Different polyamide 11 powder samples applied in powder bed-based 3D printing processes were investigated: PA 1101 (EOS, Germany), Adsint PA 11 (BASF, Germany), HP 3D High Reusability Polyamide 11 (HP PA11, HP, Paolo Alto) und Rilsan Invent Natural (RIN, ARKEMA, France). Additionally, the following polyamide 12 powders were investigated: PA 2200 (EOS) and HP 3D High Reusability Polyamide 12 (HP PA12, HP). Within the PA 1101 different powder samples were measured: PA 1101 virgin powder, mixed powder,

and used powder. The term used PA 1101 powder describes powder which was already used in the sintering process but was not sintered and can thus again be added to the sintering process. The term mixed powder also called feedstock includes 40% of used powder and 60% of virgin powder and describes the powder material which was used for the standard sintering process.

4.2.2.3.2 Chemicals

HFIP (99%) was received from Chempur (Karlsruhe, Germany). KTFAc was purchased from Alfa Aesar (Kandel, Germany) and gradient grade isopropanol from Merck (Darmstadt, Germany).

4.2.2.4 Gradient protocols

Starting point for the development of a sawtooth gradient was the linear gradient shown in Table 4.2.1 to identify at which percentage of HFIP in the eluent the PA 1101 virgin powder sample eluted. Afterwards, the steps of the sawtooth gradient were developed around this range. Thus, 25% HFIP was chosen as starting point for the sawtooth shaped elution steps. The effective CV was varied to optimize the method length. Furthermore, the influence of different HFIP concentrations at the beginning of the chromatographic separation were investigated. At the starting condition of 0% HFIP a linear gradient was used within 2.4 min up to 27% HFIP, from there the sawtooth gradient was applied. At the starting condition of 15% HFIP a linear gradient was used up to 26% HFIP within 1.2 min. At the starting condition of 35% HFIP the method directly started with the sawtooth gradient at 35% HFIP. Additionally, a direct comparison between a linear gradient and the established sawtooth gradient profile was conducted. An overview of the linear gradients is given in Table 4.2.1. The sawtooth gradients are depicted in Table 4.2.2.

Table 4.2.1 Settings of the linear gradients i.e. the linear gradient as starting point for the development of a sawtooth gradient profile and the linear gradient for direct comparison to the sawtooth gradient with isopropanol as adsorption promoting and HFIP as desorption promoting solvent.

	linear gradient protocols	
	starting gradient	compared to sawtooth gradient
method length / min	15	71.8
gradient description	0 - 100% HFIP	25 - 78% HFIP
sample concentration / g L^{-1}	5	10
injection volume / µL	10	10
flow rate / mL min^{-1}	1.0	1.0

Table 4.2.2 Overview of the settings of the different sawtooth gradient protocols with isopropanol as adsorption promoting and HFIP as desorption promoting solvent.

	sawtooth gradient protocols					
	protocol development					*standard protocol*
	influence of step length		influence of starting condition			
sample concentration / g L^{-1}	25	25	25	25	25	25/10
injection volume / µL	40	40	40	40	40	40
flow rate / mL min^{-1}	1.0	1.0	1.0	1.0	1.0	1.0
effective column volume / min	0.4	0.2	0.2	0.2	0.2	0.2
starting condition / % HFIP	25	25	0	15	35	25
A: height of the negative backward gradient step / %	6	6	6	6	6	6
B: effective step height / %	1.0	1.0	1.0	1.0	1.0	1.0
C: retardation of negative slope	1	1	1	1	1	1
D: lower Plateau	3	3	3	3	3	3
E: retardation of positive slope	1	1	1	1	1	1

4.2.3 Results and discussion

For all experiments HFIP was chosen as desorption promoting solvent for polyamide 11 and 12 (analogous to SEC experiments but without the addition of salt). As adsorption promoting solvent isopropanol was chosen representing the unfluorinated version of HFIP.

4.2.3.1 Linear gradient protocol

As a first experiment, a linear gradient protocol was conducted. For this purpose, a dissolved PA 1101 sample was injected and analyzed by applying a linear gradient from 0 to 100% HFIP within 15 min (Figure 4.2.2). The elution of sample was observed in a range between 58 and 80% HFIP.

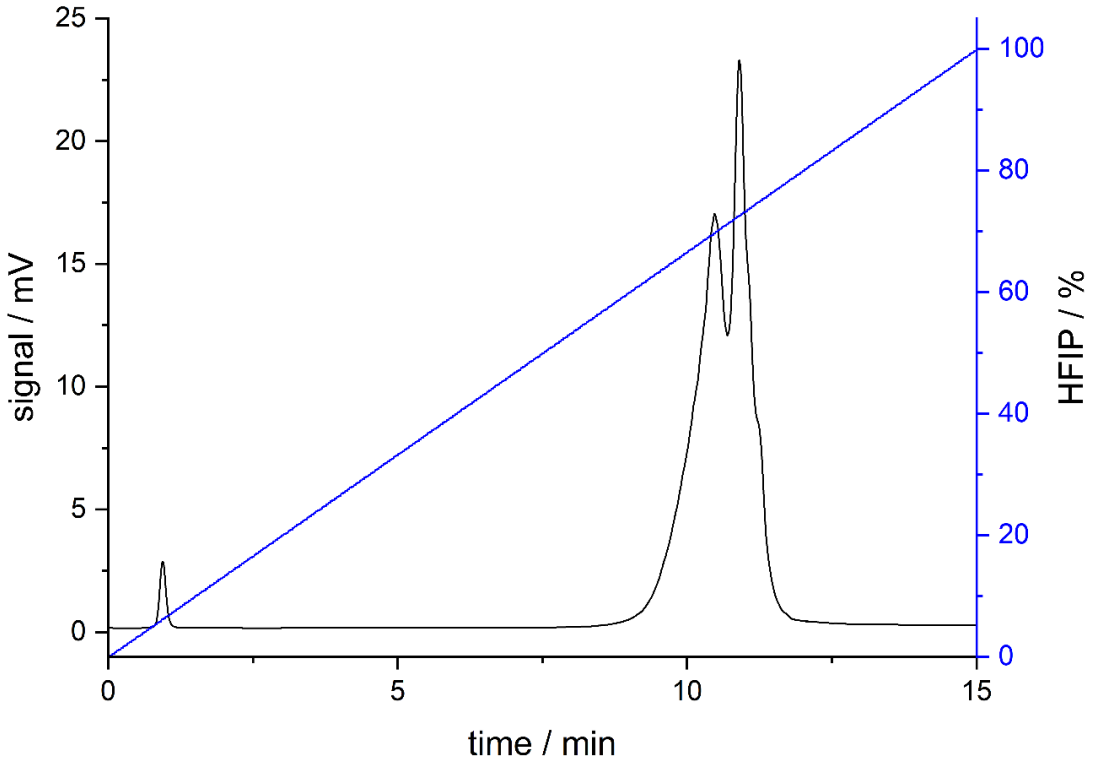

Figure 4.2.2 Application of a linear gradient to a new PA 1101 powder sample with isopropanol as adsorption promoting and HFIP as desorption promoting solvent. The detailed parameters are listed in Table 4.2.1.

4.2.3.2 Development of a sawtooth gradient protocol

Starting from the linear gradient experiment the parameters of the sawtooth gradient were set or optimized in a way to receive resolved peaks within a reasonable time frame. In doing so, the amount of editable positions for the gradient program in the ChemStation method was limited to 40. Hence, four ChemStation methods were combined to one sawtooth gradient protocol to be able to perform enough steps. In order to connect the single methods smoothly the flow was set to zero at the end of one method and adjusted again to the proper flow rate at the beginning of the following method. In the next sections different parameters of the sawtooth gradient protocol were varied and the influence on the resulting chromatograms was investigated.

4.2.3.2.1 Influence of the effective CV

The effective CV and its influence on the length of a sawtooth gradient protocol was varied to establish a reasonable length of the sawtooth gradient protocol. Reducing the effective CV from 0.4 min to 0.2 min resulted in a method running twice as fast which can be seen in Figure 4.2.3. As a starting condition 25% HFIP were chosen. By taking a closer look to the dead volume peak it became obvious that the additive Irganox 1098 eluted with the dead

volume peak. Irganox 1098 is used as an oxidation stabilizer in the formulation of PA 1101. The oxidation stabilizer was identified by its UV-spectrum and by comparison with the retention behavior of the pure substance Irganox 1098. Additionally, other soluble parts included in the polymer probably elute within that time range as well as e.g. the monomer and oligomers.

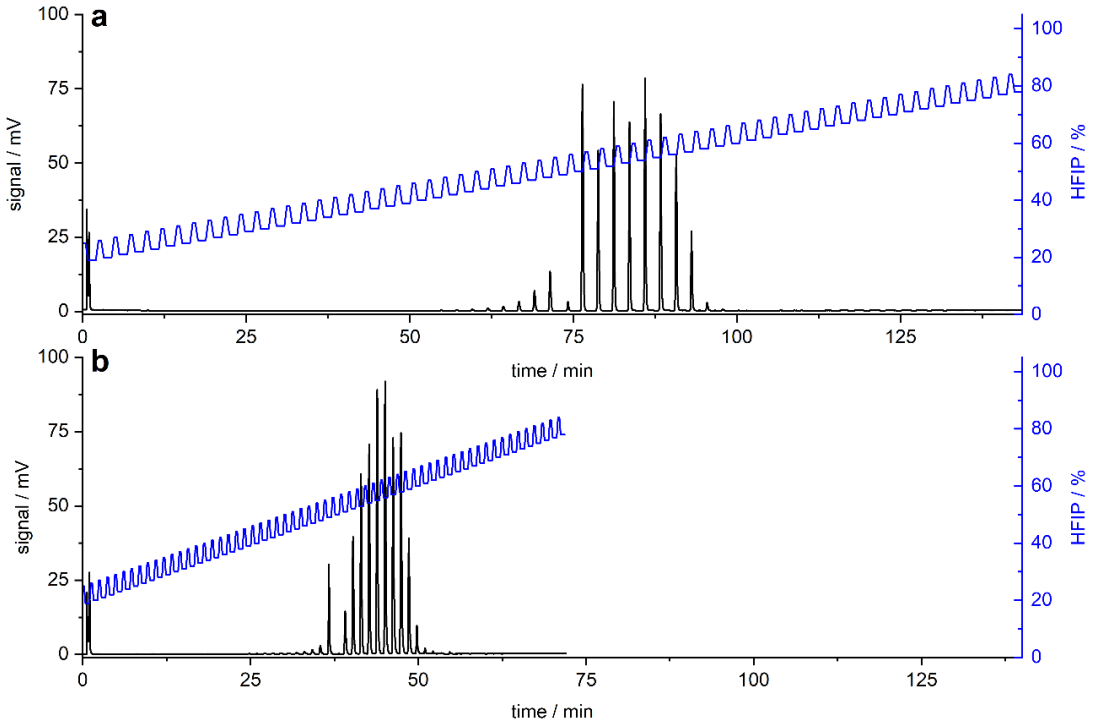

Figure 4.2.3 Influence of the effective CV on the chromatogram of a PA 1101 virgin powder with effective column volumes of (a) 0.4 min and (b) 0.2 min with isopropanol as adsorption promoting and HFIP as desorption promoting solvent. The detailed parameters are listed in Table 4.2.2.

4.2.3.2.2 Influence of starting conditions (variation of the solvent content of HFIP during the injection)

Furthermore, the amount of HFIP at the beginning of the sawtooth gradient protocol was varied, and its impact on the chromatograms was investigated. The resulting chromatograms are shown in Figure 4.2.4 and the corresponding gradient parameters are depicted in Table 4.2.2. At 0% HFIP as starting condition the HPLC system was prone to clogging by precipitation of the sample in the HPLC system or on the column. In contrary, at 35% HFIP starting condition a higher amount of the polymer sample eluted already within the dead volume peak. Additionally, all other peaks were shifted to earlier retention times in comparison with 0% and 15% HFIP as starting condition. Moreover, 0% and 15% showed no differences in the retention times of the peaks though within the distribution of the peak intensities. For all further measurements, 25% HFIP were chosen as starting condition (the same as in

Figure 4.2.3) due to low risk for clogging and the shorter measurement duration compared to 15% HFIP as starting condition.

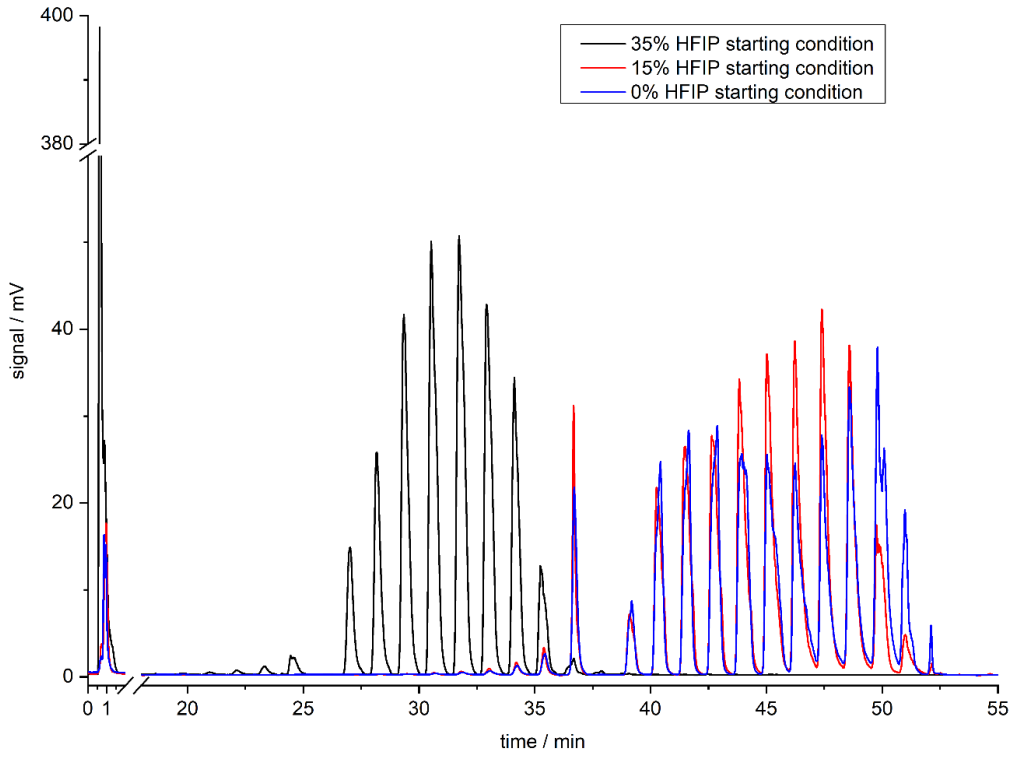

Figure 4.2.4 Influence of starting conditions (% HFIP) on the chromatograms obtained by a sawtooth gradient with isopropanol as adsorption promoting and HFIP as desorption promoting solvent. The detailed parameters are listed in Table 4.2.2.

4.2.3.3 Application of the established sawtooth gradient protocol to various polyamide 11 and 12 samples in comparison to SEC measurements

4.2.3.3.1 Application of the sawtooth gradient protocol and SEC to various polyamide 11 samples

In Figure 4.2.5 different polyamide 11 powders, which are used in powder bed-based 3D printing processes, were investigated by the application of the standard sawtooth gradient protocol depicted in Table 4.2.2. The powders of interest were HP PA11, RIN, Adsint PA11, and PA 1101. Peaks were detected at the same retention times, but small differences within the peak intensities became visible. Thus, it was concluded that all the powder materials could originate from a production process of similar conditions.

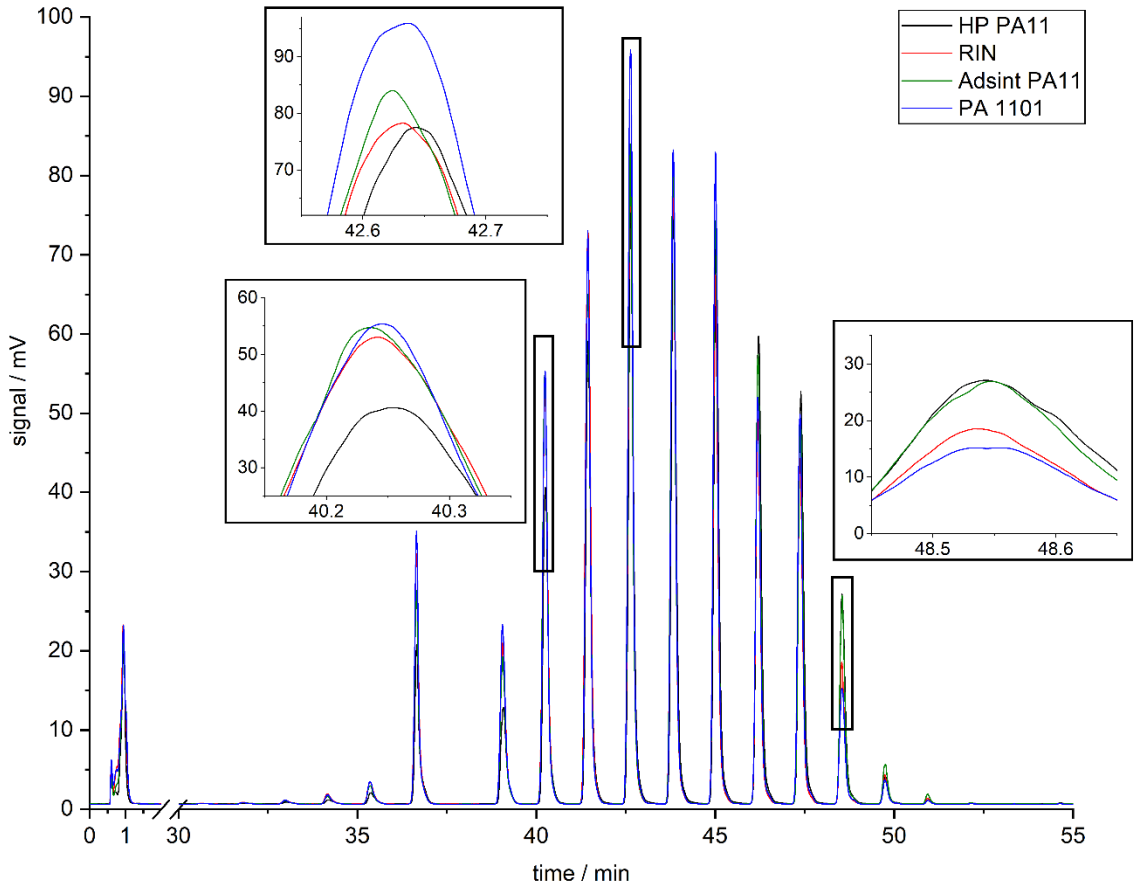

Figure 4.2.5 Overlay of chromatograms of different polyamide 11 materials (HP PA11, RIN, Adsint PA11, PA 1101) under application of the same sawtooth gradient protocol with isopropanol as adsorption promoting and HFIP as desorption promoting solvent. The detailed parameters of the standard sawtooth gradient protocol are listed in Table 4.2.2.

Additionally, the different polyamide 11 powder samples were investigated by SEC-MALLS. It was aimed to directly compare the SEC-MALLS results to the chromatograms received by application of the sawtooth gradient protocol. With reference to SEC-MALLS, a conclusion can be drawn about the different average molar mass values such as the weight average molar mass M_w, the number average molar mass M_n, the average molar mass at peak maximum M_p, and the polydispersity P which are shown in Table 4.2.3. Furthermore, the light scattering signal at 90°, the dRI signal and the molecular weight distribution are depicted in Figure 4.2.6 a-c. Adsint PA11 and PA 1101 showed an almost complete overlay except for the lower part of the molecular weight distribution. In general, the molecular weight distribution showed fluctuations in the low molar mass region and up to approximately 12,000 g mol^{-1} which is related to the characteristics of the MALLS detector (marked with a grey box in Figure 4.2.6). The values for M_w, M_n, and M_p of Adsint PA11 and PA 1101 were close together. In general, the P values of all polyamide 11 samples were similar. The lowest values for M_w,

M_n, and M_p were observed for RIN whereas HP PA11 revealed the highest values in comparison. This is in accordance with the corresponding light scattering and dRI curves. Consequently, the SEC reveals additional information to the HRP-HPLC in terms of average molar mass values. By solely considering the sawtooth gradient experiments, it would not be possible to draw these conclusions.

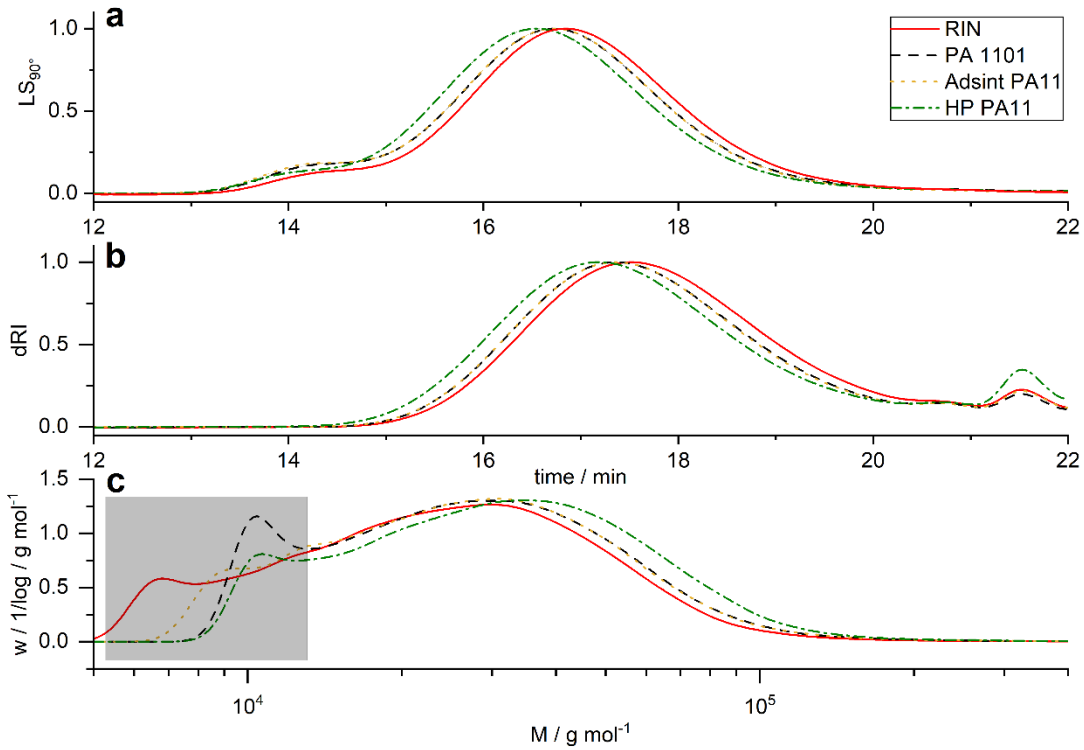

Figure 4.2.6 a $LS_{90°}$, **b** dRI signal, and **c** molecular weight distribution of different polyamide 11 powder samples such as RIN, PA 1101, Adsint PA11, and HP PA11. The dRI and LS signals were normalized to the respective plots. The curves show the example of one measurement and no average, respectively.

Table 4.2.3 The values for the weight average molar mass M_w, the number average molar mass M_n, the average molar mass at peak maximum M_p, and the polydispersity P of different polyamide 11 powders are listed as an average of three measurements.

Material type	M_n / g mol^{-1}	σ / %	M_p / g mol^{-1}	σ / %	M_w / g mol^{-1}	σ / %	P	σ / %
HP PA11	24,961	1.4	34,131	0.3	38,811	0.4	1.55	1.6
RIN	19,257	4.2	26,938	1.0	30,439	0.4	1.58	3.8
Adsint PA11	21,260	3.6	29,723	0.3	34,139	0.8	1.61	3.3
PA 1101	21,863	1.7	29,561	1.0	34,664	1.2	1.59	0.7

4.2.3.3.2 Application of the sawtooth gradient protocol and SEC to two polyamide 12 samples

In addition to different types of polyamide 11 powders, HP PA12 and PA 2200 were compared to each other in the sawtooth gradient chromatograms shown in Figure 4.2.7. While the chromatograms of the polyamide 11 samples looked quite similar, the HP PA12 differed from the PA 2200 in the sawtooth gradient chromatogram. Based on the sawtooth gradient experiments HP PA12 seemed to have a major amount of higher molar masses. Hence, it was concluded that HP PA12 and PA 2200 were not originating from the same manufacturer as differences are clearly visible in the sawtooth gradient chromatograms.

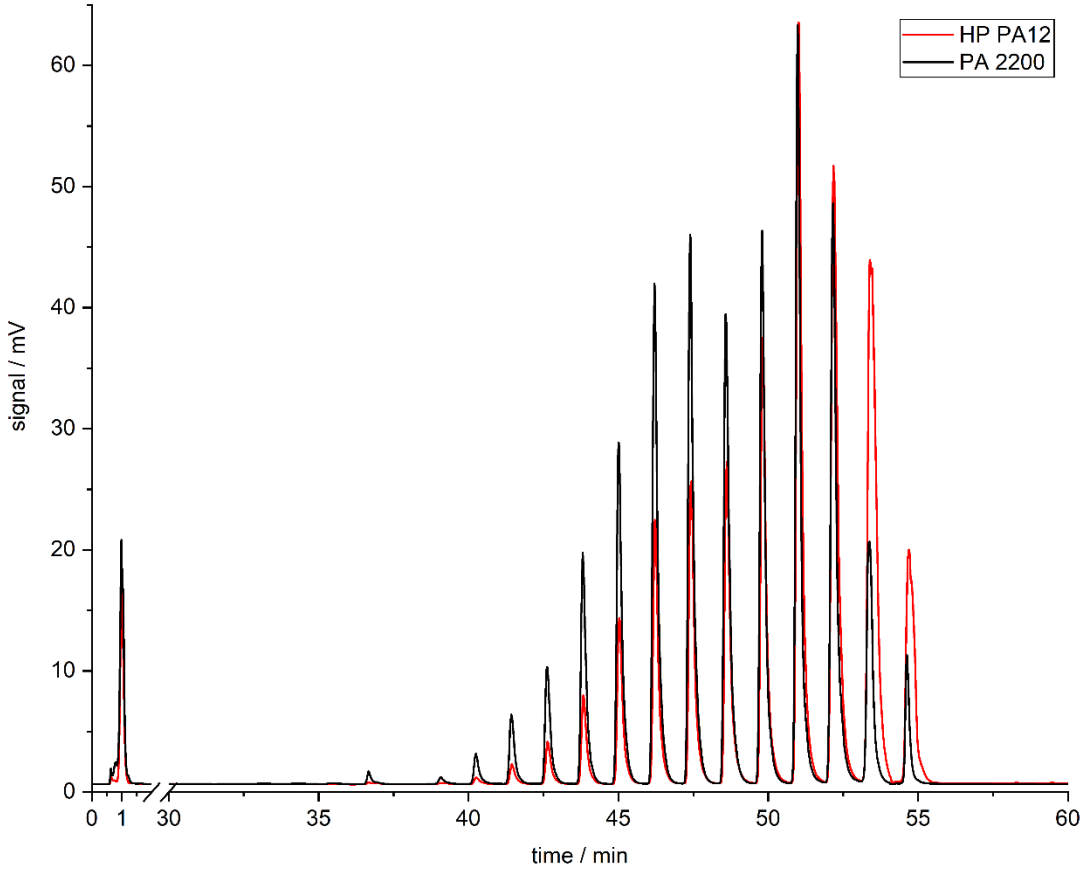

Figure 4.2.7 Chromatograms of two different polyamide 12 powder materials (HP PA12 and PA 2200) under application of the same sawtooth gradient protocol with isopropanol as adsorption promoting and HFIP as desorption promoting solvent. The detailed parameters of the standard sawtooth gradient protocol are listed in Table 4.2.2.

The SEC-MALLS results depicted in Figure 4.2.8 and Table 4.2.4 were in good correlation with the results of the sawtooth gradient experiments. For HP PA12 higher values for the average molar masses are listed when compared to PA 2200. Additionally, the P values differed by 0.4. The SEC results of the two polyamide 12 samples showed a relatively high standard deviation based on the high background noise.

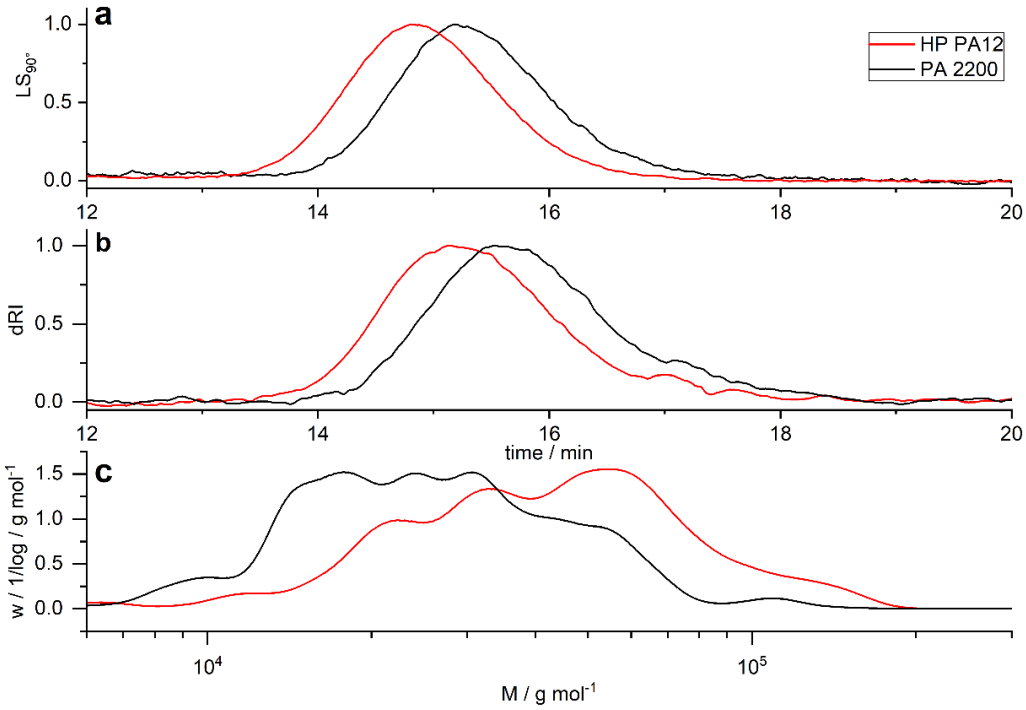

Figure 4.2.8 a $LS_{90°}$, **b** dRI signals, and **c** molecular weight distribution of HP PA12 and PA 2200. The dRI and LS signals were normalized to the respective plots.

Table 4.2.4 The values for the weight average molar mass M_w, the number average molar mass M_n, the average molar mass at peak maximum M_p, and the polydispersity P of HP PA12 and PA 2200 powders are listed.

type of material	M_n / g mol^{-1}	σ / %	M_p / g mol^{-1}	σ / %	M_w / g mol^{-1}	σ / %	P	σ / %
HP PA12	28,519	8.29	45,529	9.11	48,266	3.22	1.70	9.24
PA 2200	22,138	17.75	30,907	7.66	30,363	4.34	1.37	21.54

4.2.3.4 Comparison of the chromatograms of polyamide 11 powder samples in different aging stages in terms of sawtooth and linear gradient protocols

In this section, the performance of the sawtooth gradient was directly compared to a linear gradient with the same method length. Therefore, PA 1101 virgin, mixed, and used powder samples were investigated by the developed sawtooth gradient protocol and by a comparable linear gradient protocol. The corresponding chromatograms are shown in Figure 4.2.9. In Figure 4.2.9 a the standard sawtooth gradient protocol was applied and in part b the linear

gradient was used in the range from 25% up to 78% HFIP within 71.8 min. Both protocols revealed chromatograms which were showing the intensity differences regarding the virgin, mixed, and used powder. In Figure 4.2.9 a the virgin powder sample showed the highest intensities up to the peaks at 42.7 min. From there a reversal of the intensities of the powder samples was observed resulting in increasing peak intensities for used and mixed powder. Figure 4.2.9 b showed the same tendencies but with worse resolution as the linear gradient led solely to one broadly distributed peak, respectively. Consequently, the separation performance is higher by applying a sawtooth gradient protocol compared to a linear gradient one. Based on this observation, the saw tooth gradient setup might be used preferably in order to compare the qualities of different batches of PA 1101.

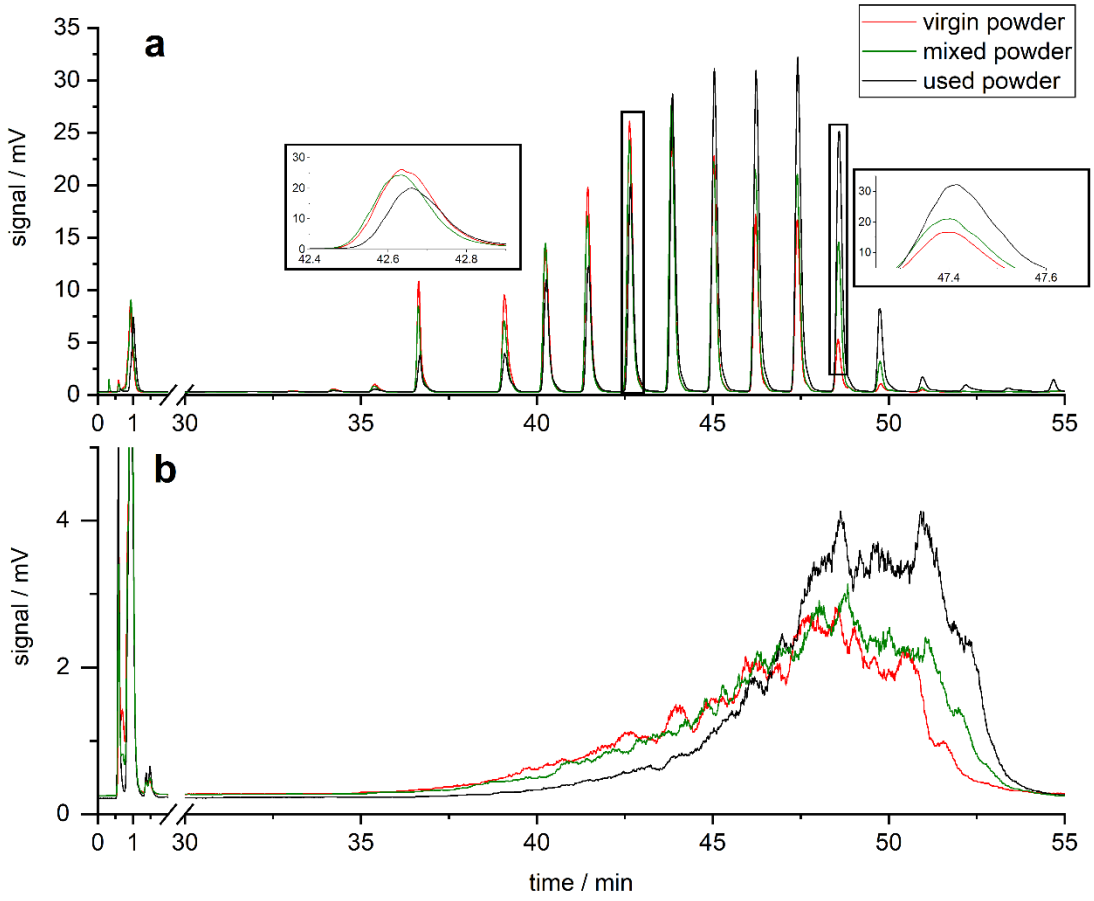

Figure 4.2.9 Comparison of the chromatograms of different PA 1101 powder samples out of the laser sintering process obtained by (a) a sawtooth gradient protocol and (b) a linear gradient application in the same time range with isopropanol as adsorption promoting and HFIP as desorption promoting solvent. The detailed parameters of the standard sawtooth gradient protocol are listed in Table 4.2.2 and for the linear gradient in Table 4.2.1.

4.2.3.5 Comparison of results of SEC and HRP-HPLC of PA 1101 and PA 2200 samples

In this part, the SEC-MALLS and the sawtooth gradient results of virgin PA 1101 and PA 2200 powder which are both applied in laser sintering were directly compared to each other in Figure 4.2.10 a and b. Within the SEC-MALLS experiments, PA 1101 eluted earlier compared to PA 2200 which corresponded to higher molar masses for PA 1101. However, in the sawtooth gradient chromatogram PA 1101 eluted again earlier as PA 2200. This proves, that the sawtooth gradient applied for HRP-HPLC does not lead to a separation solely by molar masses. Instead, other properties of the samples such as differences in their molecular structure could have influence on the retention behavior. Polyamide 11 and 12 both belong to the group of aliphatic polyamides. However, polyamide 11 holds 10 CH_2 groups and 1 amide group, polyamide 12 has 11 CH_2 groups and 1 amide group resulting in a higher ratio of amide groups for polyamide 11 [13]. However, it has to be investigated in more detail if the difference in one CH_2 group leads to the deviation in the retention behavior or if different structures of the polymer strands in solution are the reason.

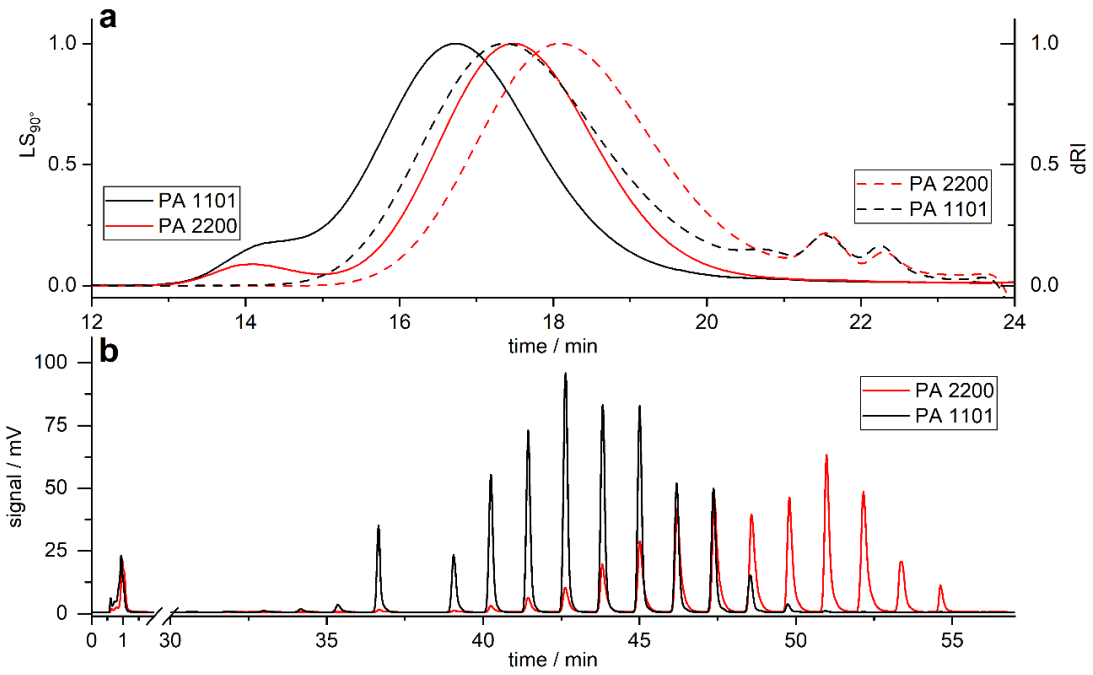

Figure 4.2.10 Comparison of (**a**) SEC and (**b**) HRP-HPLC measurements of virgin PA 1101 and PA 2200 powder samples.

4.2.4 Conclusion

In this project, sawtooth gradient protocols were applied to different polyamide 11 and 12 samples dissolved in HFIP. In this context, the sawtooth gradient has been proven to be a valuable tool to differentiate between different PA 1101 process powders such as virgin, mixed, and used powder samples. Complementary with the SEC-MALLS measurements information regarding the molar mass distribution of the samples could be obtained.

SEC-MALLS is useful to receive information regarding the molar mass distribution of polymer samples whereby an adsorptive interaction with the stationary phase must be avoided. However, only broadly distributed signals are obtained for polymers that originate from a statistical manufacturing process as this is the case for polyamide 11 and 12. At this point HRP-HPLC comes into play which offers an improved separation performance. Additionally, the resolution is adjustable via the single parameters of one step of the sawtooth gradient protocol. Consequently, it becomes easier to determine differences in polymer samples which show similar results in SEC-MALLS.

Furthermore, heart-cut polymer HPLC is a useful approach to receive further information regarding the analyte properties. However, proper analytical methods are needed to receive and reinvestigate the single fractions [7]. Depending on the type of stationary phase the separation can be based on molar mass of the polymers so that a direct correlation between retention time and molar mass of the sample can be drawn. However, a prerequisite is that no overloading of the column is obtained. If the column is overloaded, it has to be considered for data interpretation. Thus, a reduction of the injected sample amount in combination with a higher number of fractionation collection runs by using an automatized approach for fraction collection would be helpful.

HRP-HPLC is one complementary technique to SEC and the combination of those in 2D-separations could result in in-depth information for complex polymer samples [14]. Especially the selective control of the amount of obtained peaks via the effective peak height for HRP-HPLC is outstanding.

Acknowledgements

The author thanks the BMW AG for funding analytical equipment and financial support which is gratefully acknowledged. Many thanks are addressed to Bernhard Durner (Wacker Chemie AG, Munich) for the inspiring discussions and support.

4.2.5 References

[1] H. Pasch, B. Trathnigg, Multidimensional HPLC of polymers, Springer, Berlin, 2013.

[2] E. Uliyanchenko, S. van der Wal, P.J. Schoenmakers, Challenges in polymer analysis by liquid chromatography, Polym. Chem. 3 (2012) 2313–2335. https://doi.org/10.1039/C2PY20274C.

[3] B. Durner, T. Ehmann, F.-M. Matysik, High-resolution polymer high performance liquid chromatography: Application of a saw tooth gradient for the separation of various polymers, J. Chromatogr. A 1587 (2019) 88–100. https://doi.org/10.1016/j.chroma.2018.11.075.

[4] D. Berek, Liquid chromatography of macromolecules at the point of exclusion — Adsorption transition. Principle, experimental procedures and queries concerning feasibility of method, Macromol. Symp. 110 (1996) 33–56. https://doi.org/10.1002/masy.19961100104.

[5] G. Glöckner, Characterization of copolymers by means of liquidchromatography, Pure Appl. Chem. 55 (1983) 1553–1562.

[6] G. Glöckner, van der Berg, J.H.M., Precipitation and adsorption phenomena in polymer chromatography, J. Chromatogr. A 352 (1986) 511–522. https://doi.org/10.1016/S0021-9673(01)83405-1.

[7] B. Durner, B. Scherer, T. Ehmann, F.-M. Matysik, Comparison of molar mass determination of poly(dimethylsiloxanes) by size exclusion chromatography and high-resolution polymer high performance liquid chromatography based on a sawtooth gradient, ACS Appl. Polym. Mater. 1 (2019) 2388–2397. https://doi.org/10.1021/acsapm.9b00483.

[8] B. Durner, T. Ehmann, F.-M. Matysik, High-resolution polymer high performance liquid chromatography: optimization of the saw tooth gradient profile for various stationary phases and separations on preparative scale, Anal. Methods 11 (2019) 4960–4968. https://doi.org/10.1039/C9AY00689C.

[9] B. Durner, Analyzing the chemical heterogeneity of poly(dimethylsiloxanes) and other polymers: Development and optimization of a polymer HPLC method. Dissertation, Regensburg, 2019.

[10] T.H. Mourey, T.G. Bryan, Size-exclusion chromatography in 1,1,1,3,3,3-hexafluoro-2-propanol, J. Chromatogr. A 964 (2002) 169–178. https://doi.org/10.1016/S0021-9673(02)00510-1.

[11] C.-s. Wu (Ed.), Handbook of size exclusion chromatography, Marcel Dekker, New York, 1995.

[12] D. Berek, Size exclusion chromatography – A blessing and a curse of science and technology of synthetic polymers, J. Sep. Sci. 33 (2010) 315–335. https://doi.org/10.1002/jssc.200900709.

[13] G.W. Becker, D. Braun (Eds.), Technische Thermoplaste Polyamide: Kunststoffhandbuch ¾, Hanser, München, 1998.

[14] S. Fanali, P.R. Haddad, Poole C. F., Riekkola M.-L. (Eds.), Liquid chromatography: Fundamentals and instrumentation, 2nd ed., Elsevier, Amsterdam, 2017.

4.3 Material characterization of polyamide 12 and related agents used in the multi jet fusion process: complementary application of high-resolution mass spectrometry and other advanced instrumental techniques

This subchapter was published in the journal *Monatshefte für Chemie - Chemical Monthly*. The layout specifications of the journal were changed for uniformity. The corresponding text is adapted from:

Beate Scherer, Ingo Leonard Kottenstedde, Frank-Michael Matysik, *Monatshefte für Chemie - Chemical Monthly* **2020**, 151 1203-1215

Abstract

The powder bed-based 3D printing process called multi jet fusion from HP is used in various industries for different applications. A polymer powder, the so-called fusing and detailing agents, and an IR source are needed. These novel materials offer some challenges for analytical characterization. High-resolution mass spectrometry in combination with a data base search was used as a tool for comprehensive characterization of the agents, the methanol extract of new polyamide 12 powder, and the methanol extract of a ground 3D printed part. In addition, thermogravimetric studies were carried out. Besides biocides and substances containing ethoxy units, 2-pyrrolidone and triethylene glycol were identified as organic solvents in the agents. The detailing agent contained 3.7% of 2-pyrrolidone and 11.1% of triethylene glycol. The fusing agent contained 18.7% of 2-pyrrolidone and 8.4% of triethylene glycol. Based on the agents' different functionalities, the water content of the detailing agent was 18% higher as compared to the fusing agent. In addition, the fusing agent contained a carbon black amount of 5.2%. The methanol extract of new polyamide 12 powder contained remaining monomer and oligomer compounds, as well as the oxidation stabilizer Irganox 1098. In the methanol extract of the ground 3D printed part the cyclic and linear monomer, oligomers, and oxidation stabilizer were found. Moreover, ingredients of the agents were detected. Residues of 2-pyrrolidone, triethylene glycol, 3-benzisothiazolinone, and substances containing ethoxy units were identified in the methanol extract of the ground 3D printed part. In contrast, no 2-methyl-4-isothiazolin-3-one was observed.

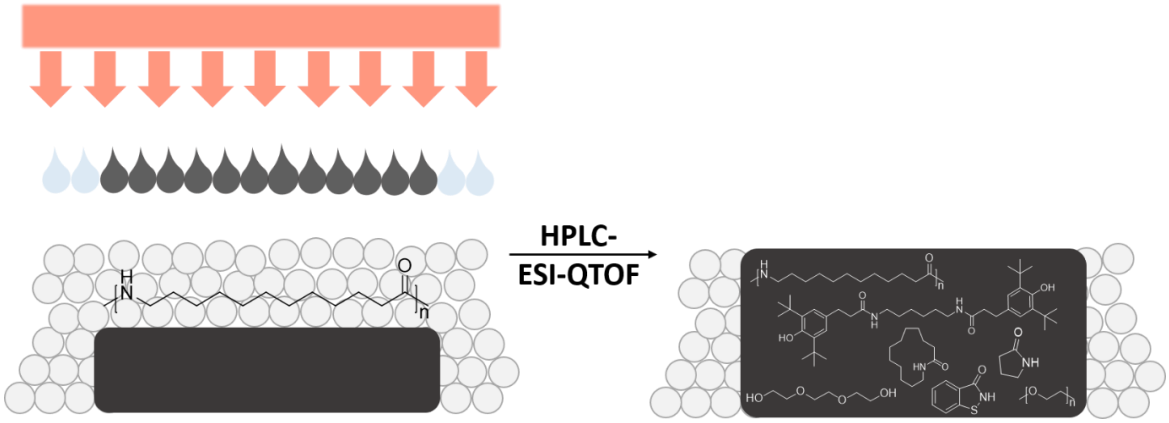

Graphical Abstract Multi jet fusion process and received information applying HPLC-ESI-QTOF.

4.3.1 Introduction

The importance of additive manufacturing is increasing, involving applications in automotive, aerospace, and medical industry [1]. Over the years, several different technologies have been developed to satisfy the needs of the various application areas. Powder-based techniques are categorized as being among the most important ones in additive manufacturing [2]. As one of the advantages powder is only fused in positions where needed and the remaining powder can be recycled.

In 2016, the new technology named multi jet fusion was commercially introduced by the company HP [3, 4]. A simplified process chain is shown in Figure 4.3.1. The process starts with a controlled deposition of a thin layer of pre-heated powder particles, whereby the thickness of one layer is 80 µm [5]. Then, a combination of agents is applied by printheads. First, a black fusing agent is distributed selectively on the polymer surface where the powder is determined to coalesce. In a second step, the detailing agent is deposited on the adjacent bulk powder. The detailing agent improves the accuracy and surface quality of the printed parts by absorbing heat due to its high water content [4]. IR radiation is applied to the powder bed by means of an IR lamp that is moved across the powder surface. It melts the powder material, which is covered with fusing agent as solely the fusing agent is able to absorb IR radiation. These steps are repeated layer by layer until the printing process is completed [3, 6]. Besides HP 3D High Reusability Polyamide 12 (HP PA12), available powder materials are polyamide 12 (PA 12) filled with glass beads, and polyamide 11 (PA 11), whereby the focus on this study is on HP PA12 [6]. PA 11 and PA 12 both offer good properties regarding 3D printing and are commonly used in powder bed fusion processes [3]. PA 12 is synthesized by ring opening polyaddition between azacyclotridecan-2-one (laurolactam) and water [7]. The recyclability and reusability of the polymer powder are considered as key points for the

industrialization of multi jet fusion and selective laser sintering. Changing properties of the material during the printing process may affect processing and thus the reusability of the polymer [2].

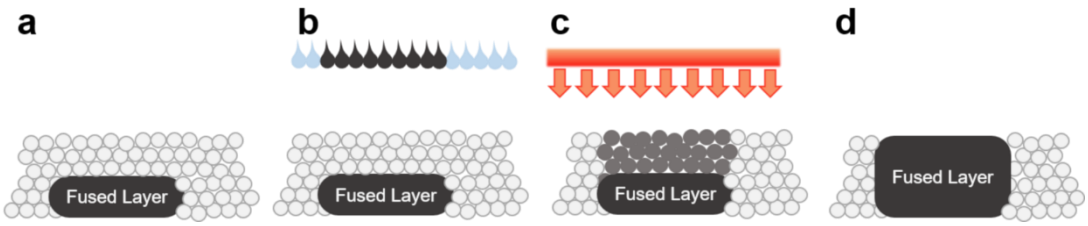

Figure 4.3.1 Scheme of the multi jet fusion process. **a** applied layer of polymer powder, **b** application of the agents (black: fusing agent, light blue: detailing agent), **c** energy delivery by IR radiation, and **d** fused layer [6].

In general, polyamides (PAs) are sensitive to oxygen and deterioration of properties, resulting in yellowing and embrittlement likely to occur due to oxidation. Corresponding studies found that the oxidation of PAs is proceeded by a free-radical chain reaction [8, 9]. Consequently, different types of stabilizers in low concentration are added to the polymer material to protect the polymer itself against temperature, light, and oxygen. Phenols are most often used as antioxidants, followed by phosphites and sulfur compounds. The choice of stabilizers for PAs primarily depends on the processing temperatures of the materials and the decomposition temperatures of the stabilizers [10]. Copper salts in combination with halogen or phosphorous compounds are efficient at temperatures higher than 140 °C. However, the mechanism of the copper stabilization is not fully understood. It is assumed that a redox reaction interferes with the radical chain reaction [10, 11]. Aromatic amines show a stabilizing effect up to 140 °C whereby a color change may occur. Furthermore, they are of toxicological concern. Phosphites are applied as co-stabilizers for phenolic oxidation stabilizers and show synergistic effects [10, 12]. Sterically hindered phenols act as radical scavengers resulting in the use of compounds such as different Irganox types [13, 14].

Besides molecules added for stabilization, residues of monomers and oligomers, too, can be found in the polymer as equilibrium products of the polymerization process. However, in literature, the analysis of cyclic oligomers of *ε*-caprolactam is most often quoted [15]. Mengerink et al. [16] determined cyclic and linear polyamide 6 (PA 6) oligomers by gradient elution chromatography, whereby formic acid was used as a modifier on a reversed phase. The majority of the condensation products was linear but cyclic structures were detected in the low molecular mass region as well. Linear oligomers were determined in the range of the hexamer up to the tetracontamer [16]. Another study investigated cyclic and linear monomers and oligomers in PA 6, PA 66, and PA 12. In total, 1.5% cyclic oligomers in PA 12 as compared to 10.1% in PA 6 were observed [17]. Moreover, the formation of cyclic monomers and

oligomers depends on the thermodynamic stability of the ring and the distance of the end groups which have to react with each other. Consequently, the amount of monomers and oligomers is much lower in case of PA 12 compared to PA 6 [18].

Väisänen et al. [19] investigated the multi jet fusion process regarding gaseous and particulate contaminants. In their studies pyrrolidin-2-one (2-pyrrolidone) (549–564 µg m^{-3}) and 2-[2-(2-hydroxyethoxy)ethoxy]ethanol (triethylene glycol) (201–211 µg m^{-3}) were found besides acetone, formaldehyde, and butan-2-one which were detected in concentrations ranging from 14 µg m^{-3} up to 41 µg m^{-3} [19].

So far, in the literature, little information about the analytical characterization of the agents applied in multi jet fusion process is reported. The scope of this work was to investigate the agents and the methanol extracts of new HP PA12 powder and a ground 3D printed part, as all these materials are important for the quality control of the multi jet fusion process. The investigation of these materials is associated with various analytical challenges. First characterization was achieved by means of high-performance liquid chromatography (HPLC) in combination with high-resolution time-of-flight mass spectrometry. As the agents are used as processing aids, remaining components might still be present in printed parts and influence the properties of the final product. Therefore, the present work aimed to identify and to determine ingredients of the agents in real samples of printed parts.

4.3.2 Experimental

4.3.2.1 Reagents and chemicals

Ethanol and methanol were of HPLC grade. Acetonitrile and non-stabilized tetrahydrofuran were of LC–MS quality. All solvents were purchased from Merck (Darmstadt, Germany) and used without further purification. Furthermore, ultrapure water (18.2 MΩ cm) generated from a Sartorius Stedim Biotech system was used. The Karl Fischer reagent for water content determination was Hydronal™-Coulomat AG-Oven from Fluka (Seelze, Germany). 2-Pyrrolidone for synthesis was purchased from Merck. The internal standard diethylene glycol monobutyl ether also used for synthesis was obtained from Merck-Schuchardt (Hohenbrunn, Germany). Triethylene glycol (99%) was purchased from Thermo Fisher (Karlsruhe, Germany). The 3D agents (fusing and detailing agent) 3D700 were obtained from HP (Palo Alto, USA).

4.3.2.2 Instrumentation and measurement conditions

HPLC–ESI–QTOF experiments were carried out using a 1260 Infinity LC system in combination with an electrospray ionization (ESI) source and a 6530 Accurate-Mass QTOF

detector from Agilent Technologies (Waldbronn, Germany). 1 mm^3 of sample solution was injected into the system and was separated on a reversed-phase SB-C18, RRHD column (2.1 mm × 150 mm, 1.8 µm) from Agilent Technologies. Chromatographic separation was realized using gradient elution containing 0.02% formic acid in water as solvent A and acetonitrile/ tetrahydrofuran (70/30, v/v) as solvent B. The flow rate was set to 0.45 $cm^3\,min^{-1}$. LC gradient was: 0 min: 95% of solvent A + 5% solvent B, 1 min: 95% A + 5% B, 15 min: 100% B until 20 min, followed by reconditioning of the system applying initial conditions. Column oven temperature was set to 45 °C. UV/VIS spectra were recorded in the range of 200-640 nm. The ESI source was operated in positive ion mode. Source parameters were 250 °C gas temperature, 8 $dm^3\,min^{-1}$ drying gas flow, 35 psi nebulizer pressure, 350 °C sheath gas temperature, and 11 $dm^3\,min^{-1}$ sheath gas flow (N_2). As a capillary voltage 3,000 V were applied and a fragmentor voltage of 80 V was used. The skimmer voltage was set to 65 V. MS data were received in the range of *m/z* 20 to 1,500 with an acquisition rate of 2 spectra/s and an acquisition time of 500 ms/spectrum. Additionally, spectra with different collision energies of 20 eV, 30 eV, and 40 eV were recorded. Therefore, MS scans with the listed collision energies were conducted within one HPLC run. For data evaluation, the Agilent MassHunter Qualitative Analysis Navigator B.08.00 and the Agilent MassHunter Qualitative Analysis Workflow B.08.00 in combination with a database research (Agilent accurate mass personal compound database and library for extractables and leachables) were applied.

Thermogravimetric measurements were performed with a NETZSCH TGA 209 F1 Libra in accordance with DIN EN ISO 11358. For this purpose, the samples were first held at 28 °C for 15 min isothermally and then heated to 800 °C at a heating rate of 10 K min^{-1}. After another isothermal phase of 10 min, the purge gas was changed from nitrogen to oxygen and the sample was heated to 950 °C at a heating rate of 10 K min^{-1}. Subsequently, this temperature was also maintained isothermally for 10 min. The purge gas flow rate was 25 $cm^3\,min^{-1}$ during the entire measurement. The coulometric determination of water content of the agents was achieved by Karl Fischer titration using a 774 Oven Sample Processor from Metrohm (Herisau, Switzerland) according to DIN EN ISO 12937. Quantitative analyses of triethylene glycol and 2-pyrrolidone were performed using a GC-FID 7890A system (Agilent Technologies). The injector temperature was set to 280 °C. Injection volume was 1 mm^3 in split mode (25:1). Helium was used as a carrier gas at a constant flow rate of 1.688 $cm^3\,min^{-1}$. Chromatographic separation was carried out on a HP-5MS 5% phenyl methyl polysiloxane (30 m × 250 µm × 0.25 µm) capillary column from Agilent Technologies. The oven temperature was set to 40 °C for 4 min followed by a temperature gradient up to 300 °C at a rate of 10 °C min^{-1}. The temperature was held for 10 min. Total analysis time was 40 min. FID

parameters were 320 °C heater temperature, 30 $cm^3\,min^{-1}$ H_2 flow, 400 $cm^3\,min^{-1}$ air flow, and 25 $cm^3\,min^{-1}$ makeup gas flow.

4.3.2.3 Sample preparation for HPLC-ESI-QTOF investigations

A complete cross-section of the 3D printed part was grinded using a CryoMill from Retsch with a defined grinding process: 5 min precooling at 5 Hz, followed by 3 cycles of 2 min grinding at 30 Hz with 1 min cooling time between each cycle. The ground material was stored in the desiccator for at least one night before further preparation. 250 mg of powder samples and agents were dissolved in 5 cm^3 methanol and placed in an ultrasonic bath for 10–15 min, respectively. Fusing agent and powder samples were filtrated using a MS syringe filter (0.2 µm WWPTFE) from Acrodise (Westborough, USA).

4.3.2.4 Sample preparation for GC-FID measurements

For GC-FID measurements, standard stock solutions of 100 mg dm^{-3} of reference materials and the internal standard were prepared. Solutions from 1 up to 10 mg dm^{-3} were prepared for calibration by diluting the stock solution. Fusing agent samples were filtrated with a MS syringe filter (0.2 µm WWPTFE) from Acrodise (Westborough, USA).

4.3.2.5 Sample preparation for TGA measurements

For TGA measurements, the agents were conditioned at room temperature until they reached mass consistency (approx. 48 h). For this purpose, 2 g of each sample were weighed in and stored in an open petri dish. Subsequently, samples were weighed in an 85 mm^3 Al_2O_3 crucible to 10.5 ± 0.5 mg.

4.3.2.6 Quantification of 2-pyrrolidone and triethylene glycol by GC-FID

The amount of water in the agents was determined by Karl Fischer titration. 2-Pyrrolidone and triethylene glycol were quantified by GC-FID measurements. The results are summarized in Table 4.3.1. For quantitative determination of 2-pyrrolidone and triethylene glycol in the agents, GC was chosen since the substances can be transferred to the gas phase quite easily. External calibration was conducted with internal standard for 2-pyrrolidone and triethylene glycol. As an internal standard diethylene glycol monobutyl ether was used. All calibration curves showed a strictly linear behavior. Quantification was confirmed by calculating the recovery of the test sample. A recovery of 100.2% was achieved for triethylene glycol. The detailing agent contained 3.7% 2-pyrrolidone and 11.1% of triethylene glycol. The fusing agent contained 18.7% of 2-pyrrolidone and 8.4% of triethylene glycol.

Table 4.3.1 Overview of the results of the quantitative determination of water content, 2-pyrrolidone, triethylene glycol, and carbon black by Karl Fischer titration, GC-FID measurements, and thermogravimetric analysis.

Substance	Calibration type	Recovery of test sample / %	Amount in detailing agent / %	Amount in fusing agent / %
water	Karl Fischer titration	-	83 ± 0.1	65 ± 0.4
2-pyrrolidone	external calibration with ISTD	97.98 ± 0.20	3.67 ± 0.01	18.74 ± 0.02
triethylene glycol	external calibration with ISTD	100.24 ± 0.02	11.08 ± 0.03	8.36 ± 0.02
carbon black	TGA	-	0	5.2 ± 0.1

standard deviations calculated on number of measurements (n=2 for Karl Fischer titration, n=3 for all other determinations)

4.3.2.7 Quantification of carbon black by TGA

The carbon black content in both agents was quantified using TGA. The conditioning of the samples resulted in a preliminary mass loss of 82.2% for the detailing agent and 61.5% for the fusing agent. No carbon black content could be determined for the detailing agent from the subsequent thermogravimetric measurements. In the case of the fusing agent, a relative carbon black content of 5.2% was obtained.

4.3.3 Results and discussion

4.3.3.1 Qualitative investigations of detailing and fusing agents

For qualitative investigations of the agents, HPLC in combination with positive electrospray ionization-quadrupole-time-of-flight (HPLC-ESI-QTOF) experiments were conducted.

The total-ion chromatograms (TICs) of both agents are illustrated in Figure 4.3.2 a, b. In the retention time window up to 2.5 min, the shape of the TIC traces looked similar. After 2.5 min, however, the chromatograms differed from each other. The first peak (1.1 min) was integrated for both agents and two mass traces occurring in both agents were identified. The application of Agilents' library for extractables and leachables and the characteristic isotopic pattern helped to identity 2-pyrrolidone and triethylene glycol as organic solvents in both agents. The calculated $[M + H]^+$ values of both substances (2-pyrrolidone: *m/z* 86.060, triethylene glycol: *m/z* 151.097) were extracted from the TIC with a mass range interval of ± 20 ppm. The corresponding extracted ion chromatograms (EICs) for detailing and fusing agents are shown in Figure 4.3.2 c–f. The intensities of the EIC curves differed for both substances and agents.

The positive mode of ESI was chosen as it offered better response compared to the negative mode. Besides the extraction solvent methanol, acetonitrile/tetrahydrofuran (9:1, v/v) was tested as well, but led to a lower number of signals. Consequently, methanol was chosen as the extraction solvent for all experiments.

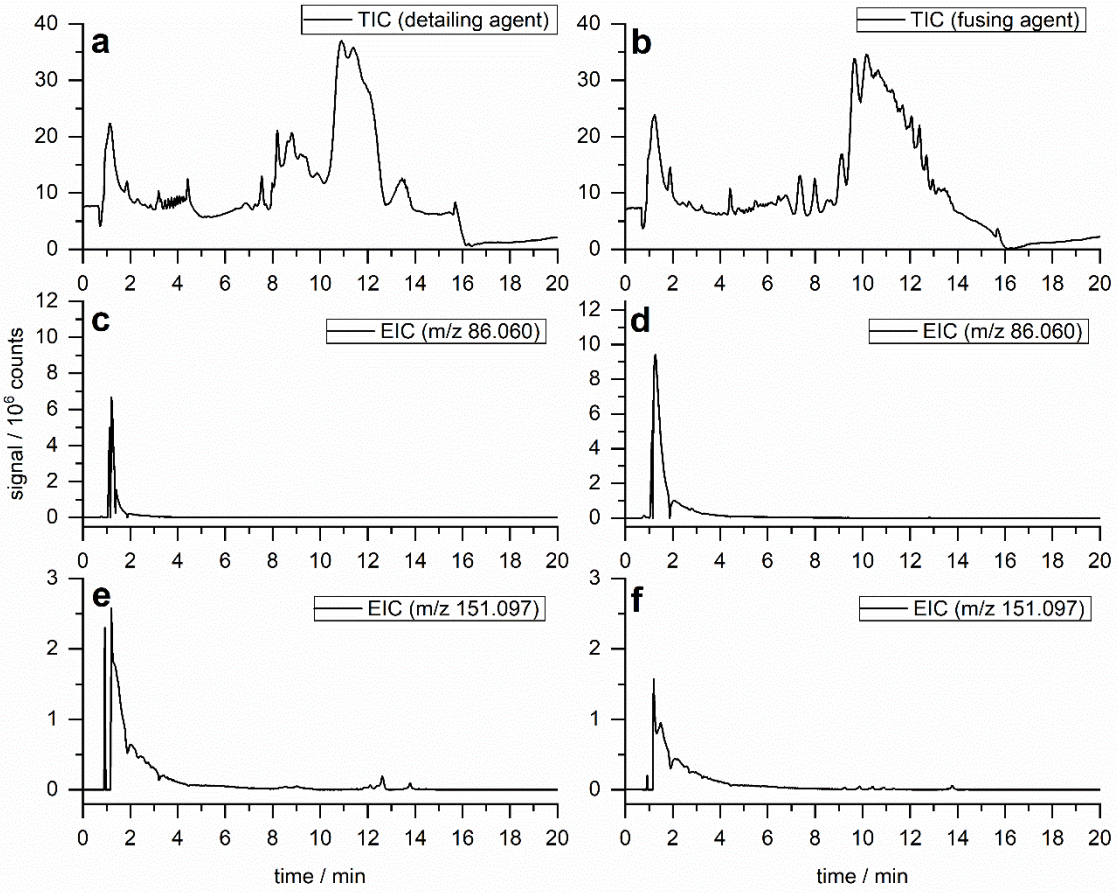

Figure 4.3.2 a, **b** Total ion chromatograms (TICs) of detailing and fusing agents. Extracted ion chromatograms (EICs) of *m/z* 86.060 ($[M+H]^+$ of 2-pyrrolidone) contained in detailing (**c**) and fusing (**d**) agents. EIC traces of *m/z* 151.097 ($[M+H]^+$ of triethylene glycol) detected in both agents (**e**, **f**). The chromatograms **c-f** were extracted with a mass range interval of ±20 ppm from the TIC traces above, respectively.

One reason for including 2-pyrrolidone in the formulations of the agents could be the high boiling point of 251 °C, resulting in a low tendency for outgassing [20]. In addition, triethylene glycol is a water soluble and colorless additive with low volatility and a very high boiling point (288 °C). Furthermore, the application of triethylene glycol in printing inks, cleaning compounds, and heat-transfer fluids is reported in the literature [21].

The detailing agent contained 3.7% of 2-pyrrolidone and 11.1% triethylene glycol, quantified by GC-FID. The fusing agent contained 18.7% of 2-pyrrolidone and 8.4% of triethylene glycol. Besides organic solvents, the fusing and detailing agents included a certain amount of water. The water content of the agent was measured by Karl Fischer titration and was determined as

83% in detailing agent and 65% in fusing agent. The high water content of the detailing agent has a local cooling effect based on the evaporation energy being removed. Consequently, during the printing process contours become sharper and the surface quality is increased. In addition, detailing agent can be applied on the same area as the fusing agent to establish a better heat control [4]. The water content of the fusing agent is lower since its aim is to obtain proper IR absorption resulting in coalescing polymer. In addition, the aqueous nature of the fusing agent permits partial penetration into the layer of the powder material. For a homogeneous distribution of carbon black in the liquid, surfactants and organic co-solvents are required. These ingredients provide a desirable wetting behavior [22, 23].

Besides the main components, it was more difficult to identify the ingredients with lower content. In Figure 4.3.3 c, d, g, h, the EIC of 2-methyl-1,2-thiazol-3-one (2-methyl-4-isothiazolin-3-one) and 1,2-benzothiazol-3-one (3-benzisothiazolinone) both extracted from the TIC traces of the agents, respectively, are depicted. These types of biocides are UV-active based on their molecular structure including a conjugated π-electron system. The UV activity of 2-methyl-4-isothiazolin-3-one was confirmed by the corresponding UV signal at a wavelength of 280 nm (see Figure 4.3.3 e, f). The UV signal of 3-benzisothiazolinone at a wavelength of 250 nm is depicted in Figure 4.3.3 i, j. The fusing agent showed lower intensities of 2-methyl-4-isothiazolin-3-one and 3-benzisothiazolinone. These biocides are added to the agents to prevent biocidal contaminations and bacterial growth during storage and the period of use. Thus, the water content of the agents is probably in direct correlation with biocide concentration. In [24], it is reported that halogen-free isothiazolinones were used in combination of two or more isothiazolinones to ensure storage stability over time and at increased temperatures. The safety data sheets of the agents declare that biocides are included in a quantity of < 0.1% in the agents. Furthermore, 2-pyrrolidone and carbon black have to be listed, respectively [25, 26].

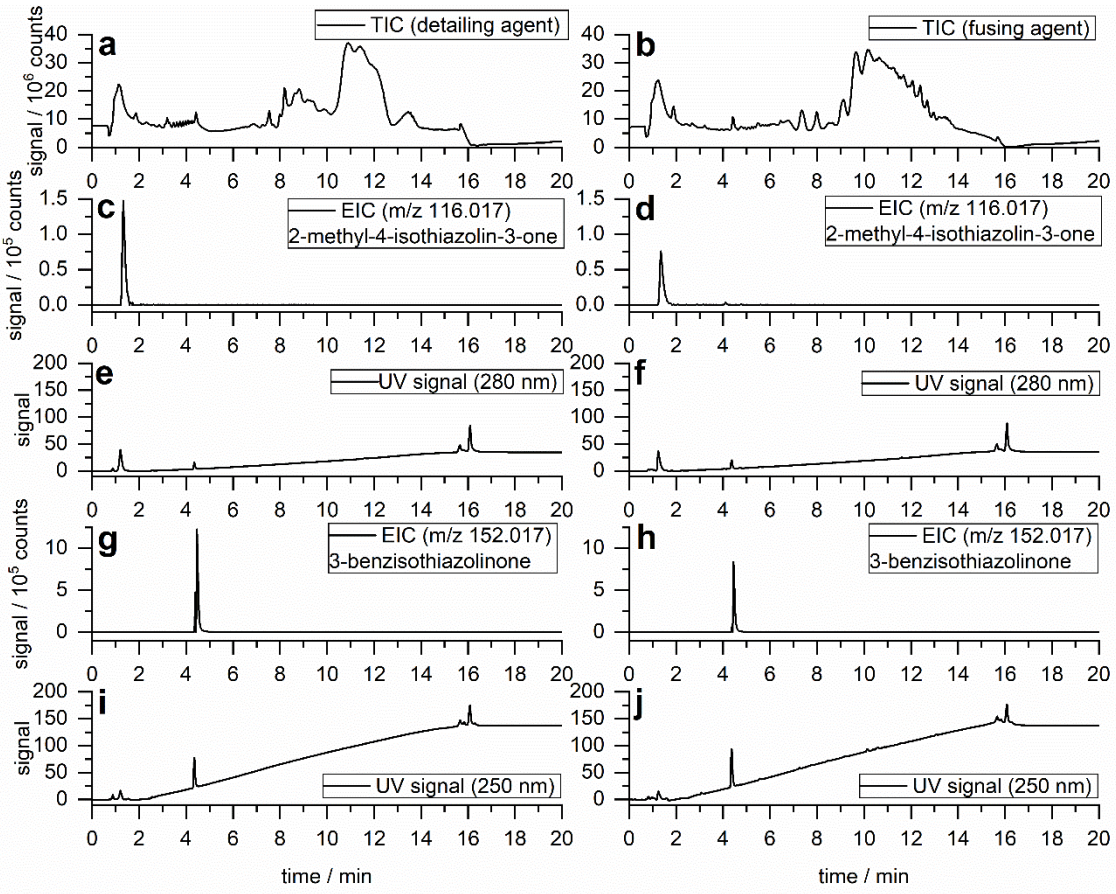

Figure 4.3.3 a, b TIC traces of detailing and fusing agents. EIC traces of 2-methyl-4-isothiazolin-3-one (*m/z* 116.017) contained in detailing (**c**) and fusing (**d**) agents. EIC of 3-benzisothiazolinone (*m/z* 152.017) detected in both agents (**g, h**). In **e**, **f**, **i**, and **j** UV signals at a wavelength of 280 nm and 250 nm are depicted and confirm the biocidal compounds. The EIC traces were extracted with a mass range interval of ±100 ppm.

The identification of molecules containing ethoxy units in detailing agent is illustrated in Figure 4.3.4 and Figure 4.3.5. In Figure 4.3.4 a–d, average mass spectra of the peak area from 3.1 to 4.6 min of the TIC of detailing agent at different collision energies are depicted, i.e. mass spectra with the following collision energies: 0 eV (a), 20 eV (b), 30 eV (c), and 40 eV (d). As Figure 4.3.4 a depicts the MS spectrum without collision energy, a homogeneous distribution of *m/z* signals in the range of *m/z* 380 up to almost *m/z* 900 is recognizable. In Figure 4.3.4 b the MS spectrum with 20 eV collision energy is shown. Consequently, the intensity of mass traces in the range of *m/z* 380 up to *m/z* 900 became smaller, resulting in peaks that were hardly visible at collision energies of 30 eV and 40 eV (compare Figure 4.3.4 c, d). Instead, the intensity of fragmentation products increased resulting in peaks appearing in the range of *m/z* 80 up to *m/z* 150. The mass trace *m/z* 177.11 arose at a collision energy of 20 eV, but the intensity decreased at a collision energy of 30 eV and disappeared

at the collision energy of 40 eV. Moreover, the intensity of the mass trace *m/z* 133.08 decreased for a collision energy of 40 eV to about half of its value at 30 eV.

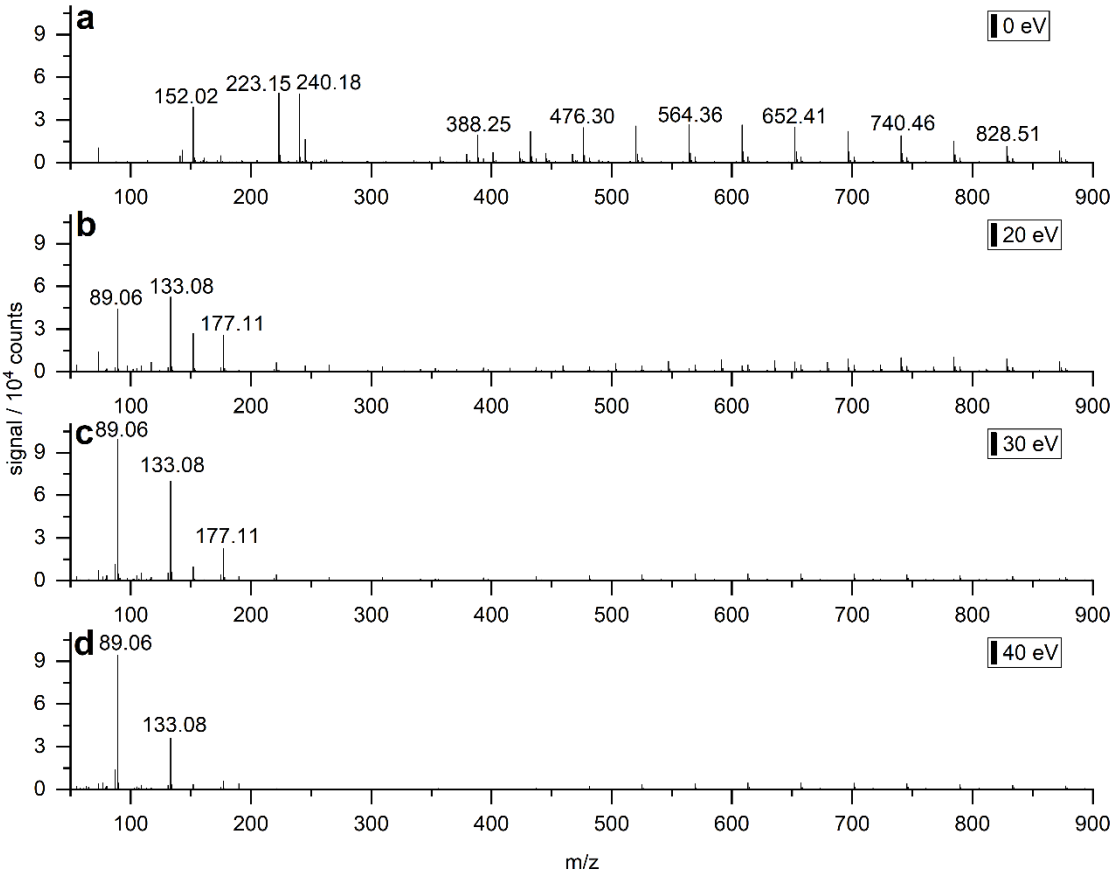

Figure 4.3.4 a-d Average mass spectra of the peak area from 3.1-4.6 min of the TIC of detailing agent at different collision energies. Collision energies **a**, 0 eV; **b**, 20 eV; **c**, 30 eV; **d**, 40 eV.

Figure 4.3.5 a, b provides more detailed information about the average mass spectra of the peak area from 3.1 to 4.6 min without collision (a) and with a collision energy of 20 eV (b). The average MS spectrum without collision energy shows a difference of 44.03 g mol^{-1} of the signals in the range of *m/z* 380 up to *m/z* 900, which is an indicator for ethoxy units. The assumption of molecules in the detailing agent which include ethoxy units was confirmed by the MS spectrum with a collision energy of 20 eV. High intensities of *m/z* 89.06 and *m/z* 133.08 can be seen in Figure 4.3.5 b. Those two *m/z* values equal the chemical formulas of 2 ($[C_4H_8O_2 + H]^+$) and 3 ($[C_6H_{12}O_3 + H]^+$) ethoxy units and confirm the assumption of compounds containing ethoxy units in detailing agent. The calculated corresponding masses were *m/z* 89.059 and *m/z* 133.086 for two and three protonated ethoxy units. The ethoxy units could be part of polyethylene glycols (PEG) which usually show a distinct molar mass distribution (see Figure 4.3.5 a). Comparing the distribution curves of the higher *m/z* values of Figure 4.3.5 a and b, a change of the local maxima in the range of *m/z* 380 to *m/z* 900 from around *m/z* 600 to *m/z* 750 could be observed. As non-ionic surfactants PEGs help to ensure

homogenous solutions of water, organic solvents, and further additives. Moreover, they can be used to adjust the viscosity of the detailing agent.

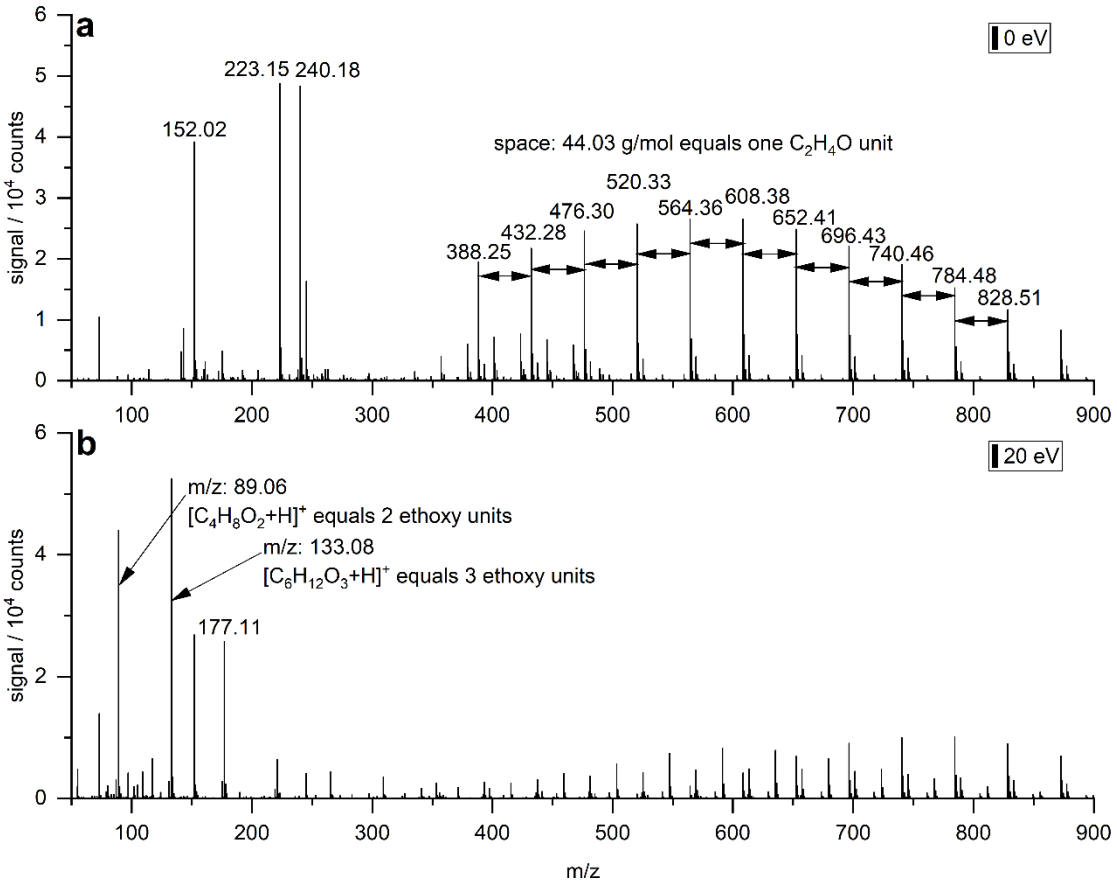

Figure 4.3.5 Identification of compounds containing ethoxy units in detailing agent. Average mass spectra of the peak area from 3.1-4.6 min (**a**) without collision and (**b**) with a collision energy of 20 eV.

Figure 4.3.6 a–d shows the EIC traces of *m/z* 89.060 and *m/z* 133.086 extracted out of all scans with different collision energies for fusing and detailing agents. Thus, the intensities of the mass traces obtained from experiments with different collision energies (0 eV, 20 eV, 30 eV, and 40 eV) were added, respectively. Consequently, the higher intensities were caused by molecules including a larger number of ethoxy units. Moreover, it becomes obvious that compounds with 2 and 3 ethoxy units were included in both agents and distributed over the complete chromatograms. The EIC traces of *m/z* 89.060 and 133.086 of detailing and fusing agents varied slightly. Furthermore, the intensity in the detailing agent was higher as compared to the fusing agent. Additionally, the distribution of the curves of detailing and fusing agents differed. Comparing the EIC traces of detailing and fusing agents, the chromatograms showed that the signals in the retention time window from 3 to 9.5 min appearing in detailing agent are missing in the EIC curves of fusing agent. This was one indicator that the composition of those agents varied regarding their compounds with ethoxy units which could, e.g. be different molar mass distributions of polyethylene glycols or non-ionic surfactants

differing in their functional groups. However, based on Figure 4.3.6, it was not possible to draw a conclusion regarding the distinct compounds containing the ethoxy units. Therefore, a closer evaluation of mass distribution in dependence of the retention time would be necessary.

All the detected compounds in this section are included in fusing and detailing agents, but by having a closer look at the chromatograms and mass spectra, differences in the chromatograms themselves and in the intensities of the EIC traces could be seen.

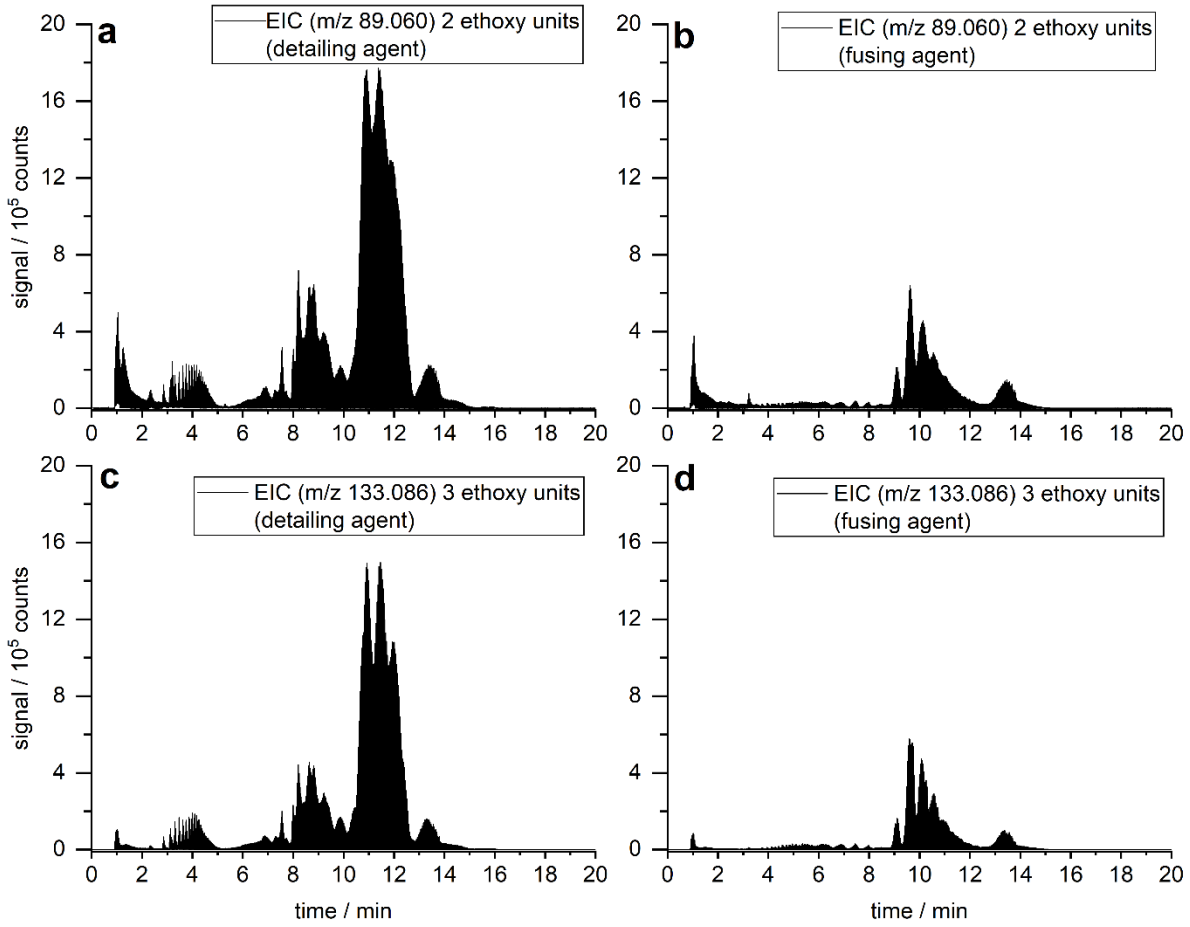

Figure 4.3.6 a-d EIC of *m/z* 89.060 (equals 2 ethoxy units) and *m/z* 133.086 (equals 3 ethoxy units) of detailing and fusing agents. The intensities of the mass traces obtained at different collision energies (0 eV, 20 eV, 30 eV, and 40 eV) were summed up. The chromatograms were extracted with a mass range interval of ±100 ppm.

By performing thermogravimetric analysis (TGA), the amount of carbon black in both agents could be investigated. Therefore, mass losses at different temperatures and gas atmospheres led to information on the material composition of the agents. The corresponding measurement curves are shown in Figure 4.3.7. The samples were conditioned before the measurements. Preliminary mass losses of 82.2% and 61.5% for detailing and fusing agents were found. In the following, we discuss the TGA results of conditioned samples in detail. At first, an

isothermal segment at 28 °C in nitrogen atmosphere allowed to detect the amount of adsorbed moisture contained in the samples. Water molecules were desorbed by convection resulting in a slight mass loss of 2.4% and 2.5% for detailing and fusing agent, respectively. The following heating phase to 800 °C at 10 K min^{-1} showed a two-step thermal degradation of the ingredients triethylene glycol, 2-pyrrolidone, and other additives of higher thermal resistance for both samples in the range of 100 to 450 °C. The next heating phase from 800 to 950 °C at 10 K min^{-1} took place in a pure oxygen atmosphere. Carbon black or pyrolysis products were oxidized by oxygen in this temperature segment. Clear differences between the samples could be observed. The detailing agent showed no mass loss under oxygen atmosphere. All components were already evaporated or completely decomposed without the formation of char by pyrolysis. However, a mass loss of 13.6% was detected in the fusing agent. This was due to the amount of carbon black present in the formulation. By taking the mass loss of the conditioning step into consideration, the amount of carbon black was calculated as 5.2%.

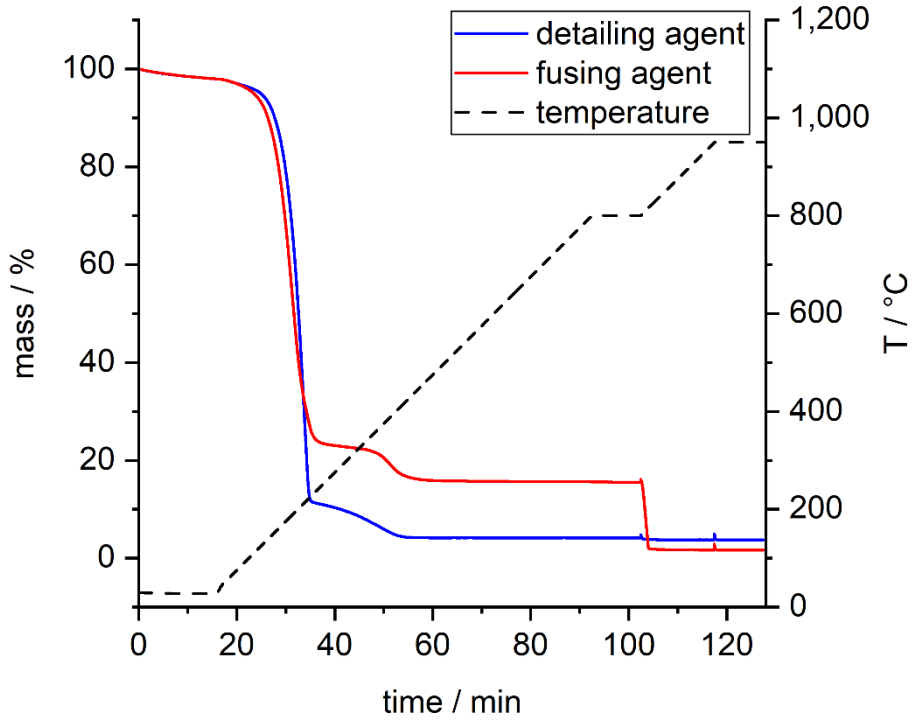

Figure 4.3.7 Thermogravimetric measurements of detailing and fusing agents as a function of time in reference to the temperature profile.

4.3.3.2 Qualitative investigations of HP PA12 powder

Besides the agents, the methanol extract of the virgin HP PA12 powder was investigated. The corresponding TIC curve is depicted in Figure 4.3.8 a. An overview of detected monomers and oligomers together with their molecular structures is shown in Figure 4.3.8 b–k. The calculated masses of the cyclic (b) and the linear (e) dimer were extracted as $[M + H]^+$ which equaled

m/z values of 395.363 and 413.374, respectively. However, within the EIC of the cyclic dimer (b) more peaks were detected in the EIC starting with the first peak at the retention time of the linear dimer. Thus, the linear dimer could also form the cyclic dimer during the ionization process in the ESI spray chamber. In this case, more complicated situations of other species may contribute. In Figure 4.3.8 c the EIC of the cyclic PA 12 monomer laurolactam is depicted. Thus, residues of the laurolactam could be found in intensities of up to $5 \cdot 10^6$ counts. Moreover, the linear monomer and other oligomers are also side products of the polymerization process. Figure 4.3.8 g shows one single peak of the cyclic trimer with an intensity of $4 \cdot 10^6$ counts which is in the range of the intensities of the cyclic dimer and monomer.

In Figure 4.3.8 f the EIC of the identified oxidation stabilizer Irganox 1098 is depicted. Its identity could be proven by comparison of the UV-spectra and the retention time of a reference standard. Okamba et al. [13] investigated three phenol stabilizers in PA 11. These were *N,N′*-1,6-hexanediylbis[3,5-bis(1,1-dimethylethyl)-4-hydroxyphenylpropanamide (Irganox 1098), [3-[3-(3,5-di*tert*-butyl-4-hydroxyphenyl)propanoyloxy]-2,2-bis[3-(3,5-di-*tert*-butyl-4-hydroxy-phenyl)propanoyloxymethyl]propyl] 3-(3,5-di-*tert*-butyl-4-hydroxyphenyl)propanoate (Irganox 1010), and 2-[2-[2-[3-(3-*tert*-butyl-4-hydroxy-5-methylphenyl)propanoyloxy] ethoxy] -ethoxy]ethyl3-(3-*tert*-butyl-4-hydroxy-5-methylphenyl)propanoate (Irganox 245), whereby Irganox 1098 is commonly used for the stabilization of PAs [27]. In general, for the application of stabilizers in PA 12 in the multi jet fusion process, the stabilizer needs to be applicable for the polymer itself. Furthermore, the stabilizer has to withstand high temperatures during the printing process. In literature [9], it is shown that Irganox 1098 offers sufficient thermal long-term stability.

The linear monomer 12-aminolauric acid (compare Figure 4.3.8 g, RT 5.9 min) eluted earlier from the column as compared to the cyclic monomer (RT 7.9 min) due to higher polarity. The linear oligomers tended to elute earlier compared to the cyclic ones, which is caused by the higher hydrophilicity of the linear forms. Figure 4.3.8 k shows the linear PA 12 pentamer, whereby the cyclic pentamer could not be detected anymore. A decreasing intensity of the higher oligomers was observed. However, the cyclic oligomers always showed higher intensities compared to the corresponding linear oligomers, whereby the highest intensities were observed within the peak of the cyclic dimer (b). A closer look at the retention times showed that the current HPLC method was not able to separate all the monomers and oligomers from each other. Laurolactam showed a partial coelution with the linear dimer. Furthermore, a limited resolution of Irganox 1098, the cyclic tetramer, and the linear pentamer could be noticed as all of these substances eluted at retention times around 12 min. Moreover, the cyclic trimer coeluted with the linear tetramer at 11.3 min and the cyclic dimer with the

linear trimer at 10 min. Further method development would be necessary to achieve a complete separation by reversed-phase HPLC. For the investigation of higher oligomers other detection principles, such as evaporative light scattering detection or charged aerosol detection in combination with gradient elution chromatography, could be helpful [16].

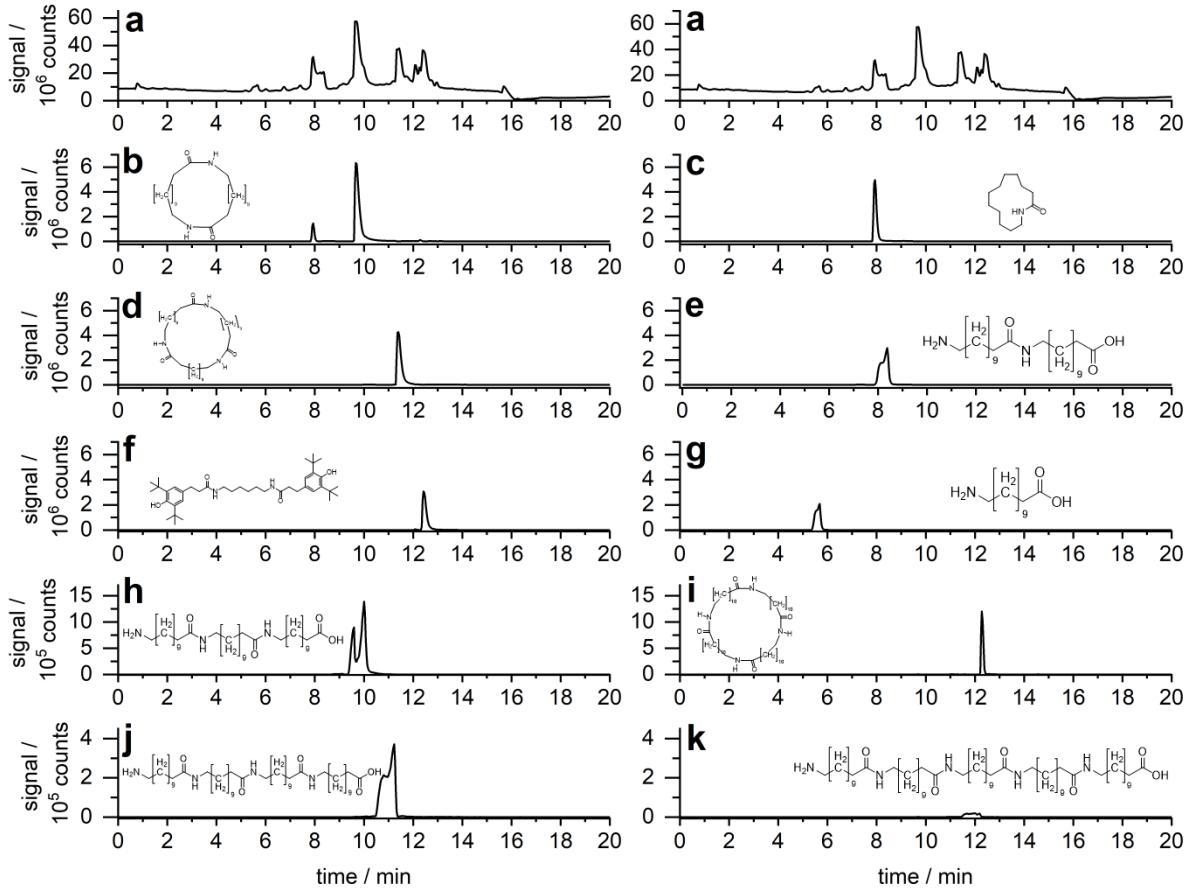

Figure 4.3.8 a TIC of a methanol extract of new PA 12 powder from HP. The EIC traces of the monomers, oligomers, and the oxidation stabilizer are depicted: **b** cyclic dimer (*m/z* 395.348); **c** laurolactam (*m/z* 198.185); **d** cyclic trimer (*m/z* 592.541); **e** linear dimer (*m/z* 413.374); **f** Irganox 1098 (*m/z* 637.494); **g** 12-aminolauric acid (*m/z* 216.196); **h** linear trimer (*m/z* 610.552); **i** cyclic tetramer (*m/z* 789.719); **j** linear tetramer (*m/z* 807.730); **k** linear pentamer (*m/z* 1,004.908). The EIC traces were extracted with a mass range interval of ±100 ppm.

4.3.3.3 Investigations of printed parts

Besides the pure agents and the methanol extract of a new polymer powder, the methanol extract of a printed part was investigated to obtain information on whether residues of the agents could be detected in the printed part. The TIC of a HP PA12 virgin powder sample extracted with methanol (red line) and an overlay with the TIC of a methanol extract of a printed part (blue line) is shown in Figure 4.3.9. Differences in the TIC traces can be seen. Higher intensities in the retention time window (0.7–1.5 min) were obtained concerning the HP PA12 component. Additionally, the peak pattern in the range of 1.7–4.5 min showed similarities with

the TIC recording of detailing agent in the same retention time window, which was interpreted as a first indicator for parts of the detailing agent remaining in the printed part. Furthermore, the peak between 13 and 14 min could only be seen in the TIC trace corresponding to the printed part. Again, the TIC trace of the detailing agent showed a peak with similar shape in the same retention time window between 13 and 14 min (compare Figure 4.3.2 a). The EIC traces of detailing agent of 2 and 3 ethoxy units (see Figure 4.3.5 a–d) depicted a peak at the same retention time and again with similar curve, which indicated the peak between 13 and 14 min in the TIC recording of the printed part caused by compounds containing ethoxy units. In Table 4.3.2, the compounds found in the methanol extract of new HP PA12 powder and the methanol extract of a printed part with their corresponding molecular formulas and calculated $[M + H]^+$ values are summarized. Obviously, the monomers, oligomers, and the stabilizer Irganox 1098 could be detected in the new HP PA12 powder and in the printed part. Furthermore, all substances observed in the agents were detected in the printed part except the biocide 2-methyl-4-isothiazolin-3-one. This is due to the fact that the boiling point of 2-methyl-4-thiazolin-3-one (93 °C [28]) is much lower compared to the temperature during the energy input that causes the polymer melting. Consequently, the 2-methyl-4-thiazolin-3-one evaporated during the printing process. Instead, the other biocide 3-benzisothiazolinone was reported to show low volatility [28].

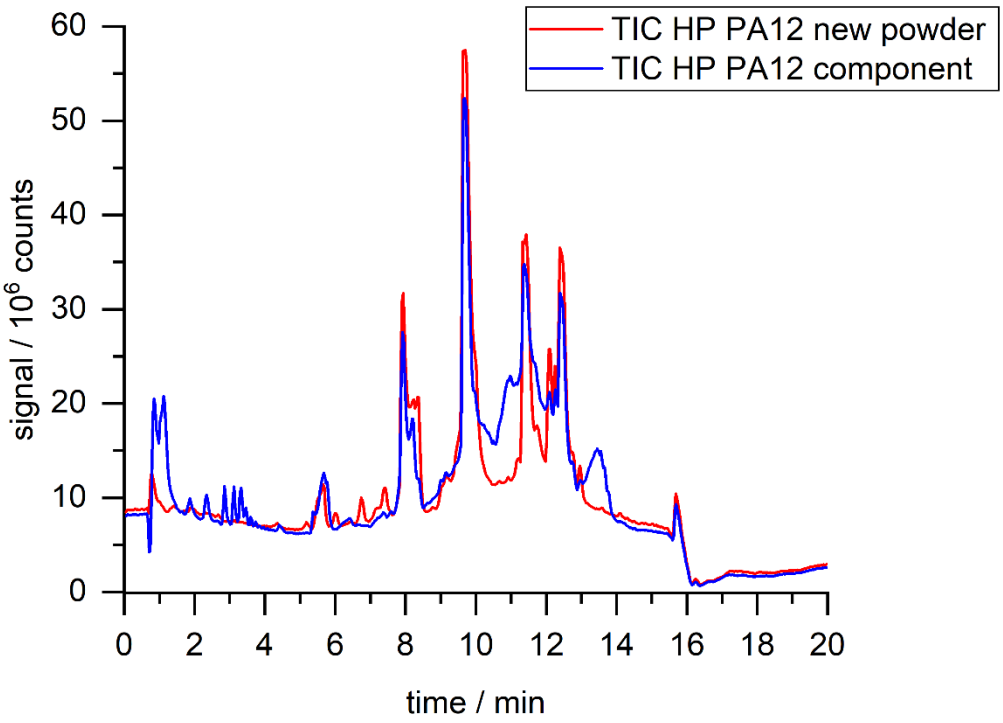

Figure 4.3.9 TIC comparison of the methanol extract of new HP PA12 powder (red curve) and a grinded 3D printed part fabricated from HP PA12 powder (blue curve).

Table 4.3.2 Overview of substances detected in the methanol extracts of new HP PA12 powder and of a printed part with their corresponding molecular formulas and calculated $[M+H]^+$ results.

Compound	Molecular formula	$[M+H]^+$	Virgin powder	Printed part
laurolactam	$C_{12}H_{23}NO$	198.185	yes	yes
12-aminolauric acid	$C_{12}H_{25}NO_2$	216.196	yes	yes
linear dimer of PA 12	$C_{24}H_{48}N_2O_3$	413.374	yes	yes
cyclic dimer of PA 12	$C_{24}H_{46}N_2O_2$	395.363	yes	yes
linear trimer of PA 12	$C_{36}H_{71}N_3O_4$	610.552	yes	yes
cyclic trimer of PA 12	$C_{36}H_{69}N_3O_3$	592.541	yes	yes
linear tetramer of PA 12	$C_{48}H_{94}N_4O_5$	807.730	yes	yes
cyclic tetramer of PA 12	$C_{48}H_{92}N_4O_4$	789.719	yes	yes
linear pentamer of PA 12	$C_{60}H_{117}N_5O_6$	1,004.908	yes	yes
Irganox 1098	$C_{40}H_{64}N_2O_4$	637.494	yes	yes
2-pyrrolidone	C_4H_7NO	86.060	no	yes
triethylene glycol	$C_6H_{14}O_4$	151.097	no	yes
2-methl-4-isothiazolin-3-one	C_4H_5NOS	116.017	no	no
3-benzisothiazolinone	C_7H_5NOS	152.017	no	yes
compounds with 2 ethoxy units	$C_4H_8O_2$	89.060	no	yes
compounds with 3 ethoxy units	$C_6H_{12}O_3$	133.086	no	yes

Furthermore, Figure 4.3.10 a, b show that the printed part also contained compounds including 2 and 3 ethoxy groups as it was the case for the agents. Since there were also signals within the range of 2–8 min retention time, it was confirmed that components of the detailing agent were detected in the methanol extract of the printed part. Thus, detailing agent was applied on the fused polymer and not solely traces of the fusing agent (compare Figure 4.3.6 a, c).

Another reason might be that the detailing agent remained in the reused polymer powder due to the suggested refresh rate of 80% recycled HP PA12 powder and 20% virgin powder. Consequently, both scenarios may be responsible for compounds of the detailing agent detected in the printed part [4].

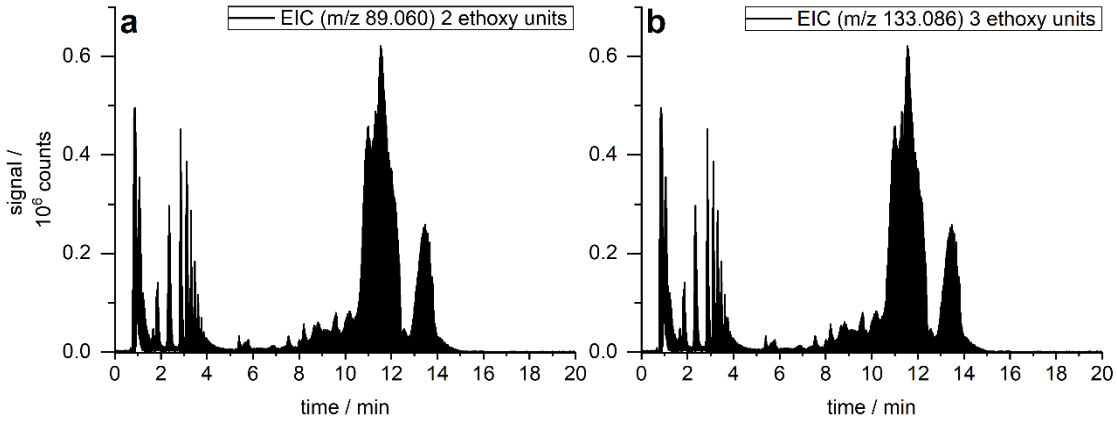

Figure 4.3.10 EIC of **a** *m/z* 89.060 (equals 2 ethoxy units) and **b** *m/z* 133.086 (equals 3 ethoxy units) of a methanol extract of a ground part of HP PA12. The chromatograms were extracted with a mass range interval of ± 100 ppm.

4.3.4 Conclusion

Fusing agent, detailing agent, new HP PA12 powder, and a ground 3D printed part were analytically investigated regarding their ingredients by HPLC–ESI–QTOF screening measurements. In addition, GC-FID and TGA experiments were applied for further characterization of the agents. Both investigated agents contained 2-pyrrolidone and triethylene glycol. Furthermore, a combination of two biocides was used in the formulations to prevent bacterial contaminations. Moreover, substances containing two or more ethoxy units could be detected and verified by experiments with the quadrupole applying different collision energies. Those substances could be utilized to adjust the viscosity of the agents, ensure homogenous agents, and the wettability of the polymer powder. However, it was not possible to determine the exact ethoxylated molecules, as those substances are applied with a homogeneous molar mass distribution. In order to guarantee the best possible processing during the printing process and part quality, the composition of the agents varied in the quantities of the detected ingredients. In the methanol extract of the new HP PA12 powder residues of cyclic and linear monomers and oligomers were detected. The laurolactam showed the highest intensity as it is applied as a monomer in the polymerization process. In general, higher intensities for the cyclic oligomers were observed compared to the linear ones. Moreover, the oxidation stabilizer Irganox 1098 was detected in HP PA12 [13, 14]. All compounds detected in the agents except the 2-methyl-4-isothiazolin-3-one could be found in the methanol extract of the printed part. The 2-methyl-4-isothiazolin-3-one evaporated during the printing process as the boiling point is below the processing temperature of the multi jet

fusion process. The influence of the remaining substances of the agents observed in the printed parts has to be further investigated. Besides changes after longer periods of thermal loads, especially, the impact on mechanical properties of the printed parts needs to be examined. Using HPLC as a method for separation according to the chemical selectivity in combination with high-resolution mass spectrometry, it was possible to identify those substances based on their characteristic isotopic pattern.

High-resolution mass spectrometry in combination with collision experiments is a powerful tool for screening measurements. Useful information about soluble and ionizable compounds in unknown samples can be obtained with the chosen ion source. Furthermore, distinct fragmentation experiments and the separation according to the chemical selectivity reveal even more details regarding the detected compounds.

Acknowledgements

We are grateful to BMW AG for funding analytical equipment and financial support. Many thanks go to Gabriele Fruhmann (BMW AG, Munich) for inspiring discussions and Julius Riedelbauch (BMW AG, Munich) for providing various samples.

4.3.5 References

[1] S. Yuan, F. Shen, C.K. Chua, K. Zhou, Polymeric composites for powder-based additive manufacturing: Materials and applications, Prog. Polym. Sci. 91 (2019) 141–168. https://doi.org/10.1016/j.progpolymsci.2018.11.001.

[2] F. Sillani, R.G. Kleijnen, M. Vetterli, M. Schmid, K. Wegener, Selective laser sintering and multi jet fusion: Process-induced modification of the raw materials and analyses of parts performance, Addit. Manuf. 27 (2019) 32–41. https://doi.org/10.1016/j.addma.2019.02.004.

[3] S.C. Ligon, R. Liska, J. Stampfl, M. Gurr, R. Mülhaupt, Polymers for 3D printing and customized additive manufacturing, Chem. Rev. 117 (2017) 10212–10290. https://doi.org/10.1021/acs.chemrev.7b00074.

[4] J. Riedelbauch, D. Rietzel, G. Witt, Analysis of material aging and the influence on the mechanical properties of polyamide 12 in the Multi Jet Fusion process, Addit. Manuf. 27 (2019) 259–266. https://doi.org/10.1016/j.addma.2019.03.002.

[5] S. Morales-Planas, J. Minguella-Canela, J. Lluma-Fuentes, J.A. Travieso-Rodriguez, A.-A. García-Granada, Multi jet fusion PA12 manufacturing parameters for watertightness, strength and tolerances, Materials 11 (2018) 1472–1482. https://doi.org/10.3390/ma11081472.

[6] H.J. O'Connor, A.N. Dickson, D.P. Dowling, Evaluation of the mechanical performance of polymer parts fabricated using a production scale multi jet fusion printing process, Addit. Manuf. 22 (2018) 381–387. https://doi.org/10.1016/j.addma.2018.05.035.

[7] S.M. Aharoni, n-Nylons: Their Synthesis, Structure and Properties, Wiley, New York, 1997.

[8] D. Forsström, B. Terselius, Thermo oxidative stability of polyamide 6 films I. Mechanical and chemical characterisation, Polym. Degrad. Stab. 67 (2000) 69–78. https://doi.org/10.1016/S0141-3910(99)00122-6.

[9] R. D. Maier, M. Schiller (Ed.), Handbuch Kunststoff-Additive, 4th ed., Hanser, München, 2016.

[10] G. W Ehrenstein, S. Pongratz, Beständigkeit von Kunststoffen: Band 1, Hanser, München, 2007.

[11] K. Janssen, P. Gijsman, D. Tummers, Mechanistic aspects of the stabilization of polyamides by combinations of metal and halogen salts, Polym. Degrad. Stab. 49 (1995) 127–133. https://doi.org/10.1016/0141-3910(95)00065-T.

[12] J. Barret, P. Gijsman, J. Swagten, R.F.M. Lange, A molecular study towards the interaction of phenolic anti-oxidants, aromatic amines and HALS stabilizers in a thermo-

oxidative ageing process, Polym. Degrad. Stab. 76 (2002) 441–448. https://doi.org/10.1016/S0141-3910(02)00047-2.

[13] O. Okamba-Diogo, E. Richaud, J. Verdu, F. Fernagut, J. Guilment, F. Pery, B. Fayolle, Quantification of hindered phenols in polyamide 11 during thermal aging, Polym. Test. 52 (2016) 63–70. https://doi.org/10.1016/j.polymertesting.2016.03.023.

[14] R.B. Fish JR., Y. Brun, High flow, thoughened, weatherable polyamide compositions containing a blend of stabilizers (2004).

[15] V. Krajník, P. Božek, J. Kondelíková, j. Králíček, High-performance liquid chromatography of 12-dodecanelactam and its cyclic oligomers present in polymide 12, J. Chromatogr. A 250 (1982) 138–140. https://doi.org/10.1016/S0021-9673(00)95224-5.

[16] Y. Mengerink, S. van der Wal, H.A. Claessens, C.A. Cramers, Analysis of higher polyamide-6 oligomers on a silica-based reversed-phase column with a gradient of formic acid as compared with hexafluoroisopropanol, J. Chromatogr. A 871 (2000) 259–268. https://doi.org/10.1016/S0021-9673(99)01072-9.

[17] S. Mori, M. Furusawa, T. Takeuchi, Reduction-gas chromatographic determination of cyclic monomer and oligomers in polyamides, Anal. Chem. 42 (1970) 661–662. https://doi.org/10.1021/ac60288a037.

[18] V.R. Feldmann, R. Feinauer, Cyclische Monomere und Oligomere in Polyamid-11 und Polyamid-12, Angew. Makromol. Chem. 34 (1973) 9–18. https://doi.org/10.1002/apmc.1973.050340102.

[19] A.J.K. Väisänen, M. Hyttinen, S. Ylönen, L. Alonen, Occupational exposure to gaseous and particulate contaminants originating from additive manufacturing of liquid, powdered and filament plastic materials and related post-processes, J. Occup. Environ. Hyg. (2019) 258–271. https://doi.org/10.1080/15459624.2018.1557784.

[20] R. C. Weast (Ed.), Handbook of Chemistry and Physics: A Ready-Reference Book of Chemical and Physical Data, 58th ed., CRC Press, Inc, Cleveland, Ohio, 1977.

[21] M.W. Forkner, J.H. Robson, W.M. Snellings, A.E. Martin, F.H. Murphy, T.E. Parsons, Glycols, Kirk-Othmer Encyclopedia of Chemical Technology. https://doi.org/10.1002/0471238961.0520082506151811.a01.pub2.

[22] A. Emamjomeh, K.A. Prasad, M.A. Novick, E.M. Fung, Detailing agent for three-dimensional (3D) printing (2015), Hewlett-Packard Development Company, L. P.

[23] M. Mele, G. Campana, G.L. Monti, Modelling of the capillarity effect in Multi Jet Fusion technology, Addit. Manuf. 30 (2019) 100879–100887. https://doi.org/10.1016/j.addma.2019.100879.

[24] H. Uhr, Biozide Mittel (2009), Lanxess Deutschland GmbH.

[25] HP Deutschland GmbH, SDS V1Q61Series: Detailing Agent, 2020, http://h22235.www2.hp.com/hpinfo/globalcitizenship/environment/productdata/Countries/de/3d_v1q61series_de_eng_v37.pdf, accessed 28 January 2020.

[26] HP Deutschland GmbH, SDS V1Q60Series: Fusing Agent, 2020, http://h22235.www2.hp.com/hpinfo/globalcitizenship/environment/productdata/Countries/de/3d_v1q60series_de_eng_v47.pdf, accessed 28 January 2020.

[27] W. Dong, P. Gijsman, The diffusion and solubility of Irganox® 1098 in polyamide 6, Polym. Degrad. Stab. 95 (2010) 955–959. https://doi.org/10.1016/j.polymdegradstab.2010.03.020.

[28] A. Wypych, G. Wypych, Databook of Biocides, Elsevier Science, Toronto, 2015.

4.4 Analytical characterization of polyamide 11 used in the context of selective laser sintering: Physico-chemical correlations

This subchapter was published in the journal *Polymer Testing*. The layout specifications of the journal were changed for uniformity. The corresponding text is adapted from:

B. Scherer, I. L. Kottenstedde, W. Bremser, F.-M. Matysik, *Polymer Testing* **2020,** 91, 106786

Abstract

Polyamide 11 is an attractive material for additive manufacturing, however, in the selective laser sintering process it is subject to significant thermally induced stress. Suitable analytical methods are necessary to indicate any changes in the material properties. In this work, thermally stressed powder samples and printed tensile bars were analyzed by size exclusion chromatography – multi-angle laser light scattering and differential scanning calorimetry. Based on the molecular weight distribution, crystallization and melting temperatures, aging states of the investigated powders could be defined and transferred to the particles of the printed components. As a result, thermal stress led to an increase in molar mass and polydispersity. Moreover, calorimetric measurements indicated a delayed nucleation process as well as a decrease in polymorphism. Additionally, polymeric material with lower polydispersity values across the tensile bars could lead to decreasing elongation at break (ε_B) values. For the crystallization onset temperature the opposite effect on ε_B was observed.

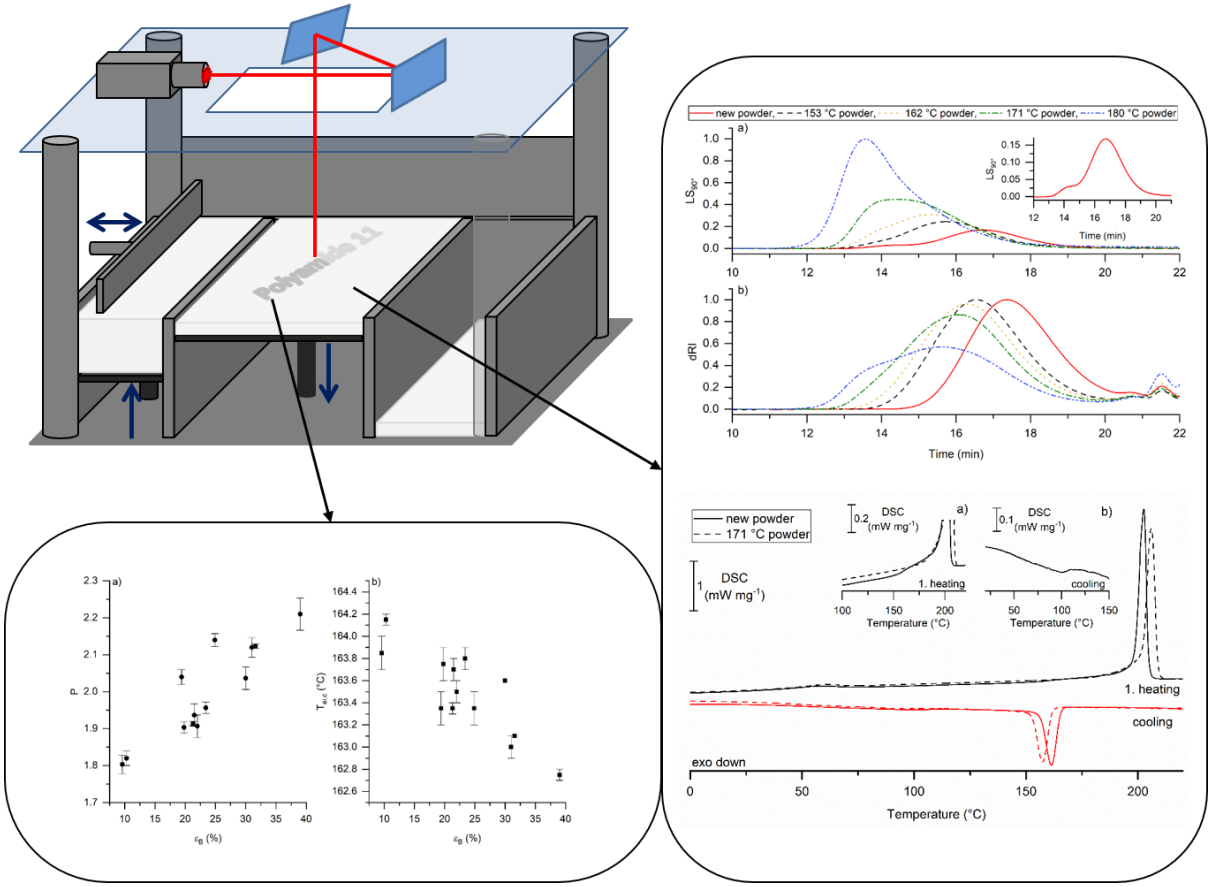

Graphical Abstract Physico-chemical correlations of polyamide 11 powder used for laser sintering.

4.4.1 Introduction

The technology of additive manufacturing (AM) combines many different processes for the layer-by-layer fabrication (layer thicknesses from 15 µm to 500 µm). These include, for example, extrusion processes such as fused deposition modelling (FDM) or laser-based powder bed fusion of polymers such as laser sintering (LB-PBF-P) [1]. In these types of processes, parts can be produced directly from 3D data without the need for molds [2]. In addition, AM offers a high degree of flexibility as parts with different geometries can be generated during the same build job [2]. AM is often used in the fields of rapid prototyping and rapid manufacturing. Thereby, rapid prototyping includes functional prototypes, which can considerably reduce the scope of development in industry. Rapid manufacturing, on the other hand, describes the production of components in small series, e.g. individual interior and exterior components in the automotive aftersales [3,4].

LB-PBF-P was first developed during the second half of the 1980s and has since become one of the most widely used AM processes [2]. The entire process takes place in the build

chamber, which is equipped with an IR light source to preheat the powder bed. The top layer of the powder is heated up to a temperature slightly below the melting temperature of the sintered polymer [5]. The sintering process consists of a repeated powder deposition, where the preheated particles are selectively melted by a CO_2 laser between each powder application. The selective melting of the powder particles connects the individual layers with each other and ensures a material bond. Afterwards, the build platform is lowered depending on the thickness of the defined layer. These steps are repeated until all layers of the manufactured parts are sintered. The detailed steps of the LB-PBF-P build process are described in literature [6]. For LB-PBF-P processing, mainly semi-crystalline thermoplastics are used. Established materials are polyamides (polyamide 6, polyamide 6.13, polyamide 11, and polyamide 12), thermoplastic elastomers, and polyether ether ketones. These polymers can be processed unfilled and filled [6,7]. Recent studies by Yang et al. [8] showed an innovative implementation of the LB-PBF-P process and polyamide 12 material to manufacture multi-layer micro-perforated panels (MPP) with a tunable wideband sound absorption behavior. Additionally, applications in medical industry are of high interest. Yang et al. [9] reviewed the use of bone scaffolds manufactured by various additive manufacturing technologies. In terms of LP-PBF-P, semisolid consolidation mechanisms were applied to process polymers with lower melting temperature such as polylactic acid (PLA) or poly(ε-caprolactone) (PCL) [10,11].

The focus of the work at hand is on polyamide 11. It is well-known that many factors, such as the machine, the applied sintering method, and the material itself are influencing the sintering process and thus the quality of the printed parts [12]. Therefore, tensile bars were printed to evaluate the mechanical properties such as the fracture behavior of the sintered components. In addition to material variations, which are indicated by changes in the molecular weight distribution and the melting and crystallization behavior, contaminations and non-optimized process parameters may negatively impact the mechanical properties [12]. Furthermore, the solidification step is a complex process involving a number of mechanisms [13]. Starting with the building steps, the entire part cake remains at elevated temperatures. A temperature gradient within the part cake from the center to the edge is unavoidable, while the center shows the highest temperature. The subsequent cooling phase to the removal temperature of about 40 – 60 °C can take up to 20 h [5]. Furthermore, mixtures of used and unused powder are applied in the sintering process to improve economic efficiency [1]. However, this may lead to poor surface quality of the components and other problems associated with reusing the unsintered powder [1].

A variety of studies cover the material quality and the process in the context of LB-PBF-P. Commonly, good mechanics of the resulting end products require certain physical and

chemical properties such as a complete layer adhesion ensured by coalescence of the powder particles [14,15]. In addition, at the microstructure level a small number of pores results in good mechanical characteristics that are consistent with a high component density [16,17]. Moreover, resistance against oxidation needs to be assured in addition to constant melting and crystallization characteristics [18,19].

The monomer for the polycondensation of polyamide 11 is 11-aminoundecanoic acid, which is synthesized from castor oil [20]. Monomers can be polymerized either in the melt or in aqueous suspension using phosphorous regulators [20]. Since castor oil is considered a renewable raw material, polyamide 11 is classified as a biobased polymer. For LB-PBF-P applications, linear polyamide 11 is used as a living polymer which is defined by the ability to further proceed the polycondensation due to reactive end groups [21]. So far, literature mainly covers the aging studies of polyamide 12 in the field of LB-PBF-P [15,18,22,23].

For uneven polyamides, hydrogen bonding between two adjacent chains in parallel, antiparallel or complete random orientation is possible. Hydrogen bonds between antiparallel molecules of polyamide 11 result in monoclinic unit cells for the β crystals, whereas triclinic forms occur for the α crystals [24]. Triclinic and pseudohexagonal structures can be obtained by crystallization from the melt. Monoclinic unit cells are obtained by precipitation from solution. Beside the most thermodynamically stable triclinic α phase, possible structures include the triclinic α', monoclinic β, pseudohexagonal δ and smectic pseudohexagonal δ' phases. During heating polyamide 11 passes a reversible brill transition in case of α' and δ phases. The structural information can be connected with the mechanical properties such as elongation at break (ε_B) [25–27]. In general, resistance to mechanical stress is related to the ability to dissipate energy in the microscopic and macroscopic structure. During elongation, different structural properties promote brittle or ductile behavior. High crystallinity with improved lamellae thickness induces microscopic cracks during stress which lead to a brittle behavior caused by the incapability to absorb energy by deformation. Amorphous regions, however, promote a ductile behavior by unfolding mechanisms of unoriented polymer chains [28,29].

Moreover, the semi-crystalline nature of polyamides leads to poor solubility in common chromatographic solvents. In general, polyamides exhibit high melting points and a high amount of intermolecular hydrogen bonding between the amide linkages. However, the polymer has to be soluble in the chromatographic solvent for molecular weight determination.

The solvent systems for size exclusion chromatography (SEC) of polyamides can be divided into three categories: high-temperature SEC [30], SEC with common solvents after trifluoroacetylation [31], and fluorocarbon solvents such as trifluoroethanol [32] and

1,1,1,3,3,3-hexafluoroisopropanol (HFIP) [33]. Each solvent has its merits and limitations. Fluorinated solvents are able to dissolve crystalline polymers due to their high polarity and capability of hydrogen bonding [30]. Nevertheless, polyelectrolyte effects can be observed in fluorinated solvents which are prevented by adding salts [33]. Due to its low refractive index, HFIP is an attractive solvent for light scattering detection. Unfortunately, the light scattering detector exhibits low sensitivity for low molar masses. High molar masses are determined more precisely as both molar mass and concentration are affecting the light scattering signal [34]. Chen et al. [34] reported that optimum SEC behavior of polyamides was obtained with HFIP + 0.05 mol L^{-1} KTFAc. Laun et al. [35] tested different polar and non-polar stationary phases for SEC analysis of polyamide 11 and 12 and found that the polar silicagel phase exhibited no hydrophobic interaction. Furthermore, they compared different procedures for molar mass determination and constituted that conventional poly(methylmethacrylate) calibration yielded poor results.

Polyamide 11 is a crystallizable thermoplastic polymer occurring in different structures. Melt and solution processing impact the crystallization frequently leading to lamellar crystals forming a spherulitic structure. Its thermal and thermomechanical properties vary with its structure [26,36]. Analyses of phase transitions and heat capacities are carried out by differential scanning calorimetry (DSC).

Studies by Mollova et al. [37] showed the formation of different morphologies while using various cooling conditions. When chip calorimetry with high cooling rates was applied, mesophases could be formed and analyzed. This leads to a change from heterogeneous to homogeneous nucleation. In addition, Acierno et al. [38,39] investigated the isothermal and non-isothermal crystallization kinetics of focused branching of the polymer backbone. Little information is known about the branching of polyamide 11 by thermal stress. However, it has been shown that short-chain branching slows down crystallization and reduces crystallinity.

In this work, thermally aged powder samples and tensile bars prepared under identical conditions were analyzed by SEC and DSC measurements. Based on the molecular weight distribution as well as the crystallization and melting behavior, aging states could be defined and transferred to the particles of the tensile bars. From this, conclusions could be drawn about the thermal stress of the powder used in the LB-PBF-P process. Regarding mechanical properties, relations between the ε_B and the polydispersity (P) as well as the crystallization onset temperature ($T_{ei,c}$) could be drawn. The results allow to correlate the physico-chemical properties and the LB-PBF-P part quality.

4.4.2 Experimental

4.4.2.1 Powder material and tensile bars

The colorless polyamide 11 powder (commercially available as PA 1101) from EOS (Krailling, Germany) was used for all investigations. The material does not contain reinforcing fillers such as glass or carbon fibers. Melting onset temperature ($T_{ei,m1}$) and weight average molar mass (M_W) were 197.9 °C and 33700 g mol^{-1}, respectively. Tensile bars were printed in vertical direction under identical sintering conditions using an EOS P396 laser sintering machine. The test specimens were dumbbell-shaped with a total length of 170 mm and a thickness of 4 mm according to type 1A of DIN EN ISO 527 [40]. The width at the narrow portion was 10 mm and 20 mm at the ends. A total amount of 13 tensile bars was investigated.

4.4.2.2 Powder heat treatment conditions

The powder tempering was conducted as follows. An amount of 1 g of powder was filled in an aluminum crinkle and inserted into a Micro-Chamber M-CTE250 (Markes, Offenbach am Main, Germany) at fixed temperatures (153, 162, 171, and 180 °C) while applying a nitrogen gas flow of 10 mL min^{-1}. The temperature was checked with a calibrated RS 1316 dual data logger thermometer. Treatment durations of 8, 16, and 24 h were chosen. The samples were cooled in the chamber under nitrogen flow. Afterwards, the powders were stored in argon atmosphere. An overview of the applied treatment conditions is given in Table 4.4.1.

Table 4.4.1 Parameters of the heat treatment for PA 1101 powder samples.

Temperature of heat treatment /°C	Duration of heat treatment /h		
153	8	16	24
162	8	16	24
171	8	16	24
180	8	16	24

4.4.2.3 Sample preparation

The tensile bars were sawn off near the fracture surface. The separated parts were polished gently from all sides to ensure that no surface particles influence the SEC and DSC analyses. During sample preparation, special attention was paid to minimize both mechanical and thermal stress. The aliquots of the samples for SEC and DSC analyses were taken with a scalpel.

4.4.2.4 DSC equipment and measurement

Calorimetric measurements were carried out using a NETZSCH DSC 204 F1 Phoenix calorimeter (Selb, Germany) with a CC300 controller for liquid N_2-assisted cooling. The temperature and sensitivity calibration were done for a heating rate of 10 K min^{-1} by using adamantane, indium, tin, bismuth, and zinc. A purge gas flow of 20 mL min^{-1} N_2 (5.3 purity) guaranteed an inert atmosphere inside the cell. Regarding sample preparation, the polyamide 11 powder was placed into 25 µL aluminum crucibles and sealed with a pierced lid. For higher reproducibility, the powder was evenly distributed at the bottom of the crucible. The samples of 5 ± 0.05 mg were cooled to -20 °C, held isothermally for 10 min, and subsequently heated to 230 °C at a heating rate of 10 K min^{-1}. The heating run was followed by a cooling phase to -20 °C at a rate of 10 K min^{-1}. The melting and crystallization behavior were analyzed by carrying out two heating runs according to DIN EN ISO 11357-1, and DIN EN ISO 11357-3 [41,42]. The initial melting temperature ($T_{i,m}$), melting onset temperature ($T_{ei,m}$), and the enthalpy of melting (H_f) were used to characterize the melting behavior. $T_{i,m}$ describes the first deviation of the curve of the extrapolated initial baseline. $T_{ei,m}$ can be derived from the intersection of the virtual interpolated baseline and the tangent applied at the inflection point of the peak beginning (tangent method). The enthalpy H_f of the melting peak is obtained by integrating the signal using a linear baseline of $T_{i,m}$ to $T_{f,m}$ (last recorded deviation of the curve from the extrapolated final baseline). For the evaluation of the crystallization behavior, the temperature $T_{ei,c}$, which is also determined by the tangent method, was used.

4.4.2.5 SEC equipment and measurement

HFIP from ChemPur (Karlsruhe, Germany) with 0.05 M KTFAc from Alfa Aesar (Kandel, Germany) was used as eluent with a flow rate of 0.35 mL min^{-1}. The measurements were performed with an injection volume of 15 µL and a sample concentration of 5 mg mL^{-1} according to ISO 16014 [43]. The samples were dissolved for at least 16 hours in the eluent and were shaken carefully. A chromatographic Agilent Series 1260 Infinity system (Waldbronn, Germany) equipped with an isocratic pump and a column oven (PSS, Mainz, Germany) at a temperature of 40 °C was employed. The experiments were conducted using the refractive index (RI) detector Optilab T-rEx and the multi-angle laser light scattering (MALLS) detector Dawn HELEOS II (both from Wyatt Technologies, Santa Barbara, USA). The RI detector was set to 40 °C. A precolumn (4 mm x 3.0 mm) and two Phenogel linear columns (300 mm x 4.6 mm, 5 µm) from Phenomenex (Aschaffenburg, Germany) were used as stationary phase. Molar masses were determined in absolute values. For this reason, the dn/dc of new polyamide 11 powder was determined as dn/dc = 0.2374 mL g^{-1} and taken for absolute calculation of the different molar mass values. One advantage of absolute molar

mass determination was that no calibration standards were needed. The selection of such standards for conventional calibration is difficult as they are not commercially available for polyamide 11 [34]. For the SEC measurements and data evaluations ASTRA 7 and HPLC manager software (Wyatt, Santa Barbara, USA) were used.

4.4.2.6 Tensile test equipment and measurement

The tensile tests were performed according to DIN EN ISO 527 [40] using a ZWICK ROELL universal testing machine Z100 with a 100 kN force indicator. The overall testing conditions included a temperature of 23 °C at a relative humidity of about 50%.

4.4.3 Results and discussion

4.4.3.1 Heat-treated polyamide 11 powder

4.4.3.1.1 SEC studies on PA 1101 powder

The evolution of the molar mass distribution of the powder samples has been followed by SEC-MALLS. An increase of the M_w with increasing tempering temperature and time was observed and is shown in Figure 4.4.1 a. Starting with a M_w of 33,700 g mol^{-1} for new PA 1101 powder, the values of M_w increased to up to 166,467 g mol^{-1} at temperatures of 153 °C and 162 °C. Furthermore, a significant increase of M_w at 8 h treatment time was observed upon raising the temperature from 171 °C to 180 °C. Powder processed at a temperature of 180 °C (8 h) showed a three times higher mass compared to the powder processed at a temperature of 171 °C (8 h). However, solubility of samples became a problem at elevated temperatures and durations and is shown in Figure 4.4.1 b. The solubility of the powder samples started to decrease at conditions of a temperature and treatment time of 171 °C and 16 h. The effect increased with increasing duration and temperature. Samples could not be entirely dissolved, instead they became gel-like. This could be confirmed by integrating and comparing the dRI-signals of the samples. For 180°C (8h), 80% of the dRI area signal compared to completely dissolved samples could be measured. Consequently, the M_w value reflected that 80% of the sample showed the significant increase of M_w to up to 446,800 g mol^{-1}. At a temperature of 180 °C applied for 16 h and 24 h, about 45% and 40% of the respective area compared to virgin powder could be measured, indicating low solubility of the tempered polymer powders.

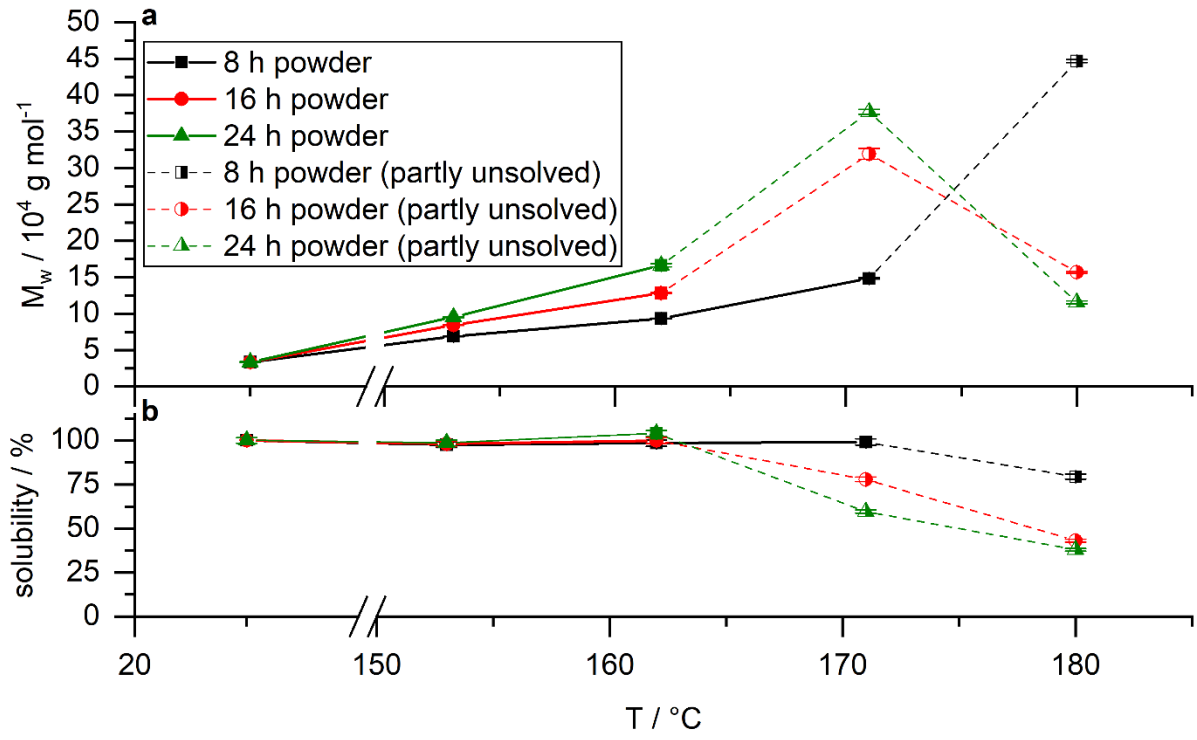

Figure 4.4.1 a Influence of tempering conditions including temperature and time on the development of the weight average molar mass M_w of PA 1101 powder and **b** influence on sample solubility. A constant flow of 10 mL min^{-1} N_2 was applied during heat treatment. Molar masses were determined by means of SEC-MALLS. The average of three measurements is shown.

Table 4.4.2 The values for the weight average molar mass M_w (compare Figure 4.4.1), the number average molar mass M_n, the average molar mass at peak maximum M_p, and the polydispersity P of the PA 1101 powder obtained by SEC-MALLS measurements are depicted.

Temperature of heat treatment /°C	Duration of heat treatment /h	M_n /g mol^{-1}	M_p /g mol^{-1}	M_w /g mol^{-1}	P
virgin powder	—	21,167	29,567	33,700	1.59
153	8	38,667	56,200	68,833	1.78
153	16	46,200	64,800	84,567	1.83
153	24	52,433	71,633	95,333	1.82
162	8	52,633	69,133	93,467	1.78
162	16	62,200	85,433	128,433	2.07
162	24	74,900	97,500	166,467	2.22
171	8	69,233	92,033	148,433	2.14
171*	16	134,067	153,400	319,400	2.38
171*	24	173,900	194,400	376,900	2.17
180*	8	188,467	195,167	446,800	2.37
180*	16	62,567	113,100	156,867	2.51
180*	24	51,000	87,767	115,600	2.27

**powder was not completely dissolved in the SEC solvent, samples became gel-like*

For all powder samples, the values for M_w, the number average molar mass (M_n), the average molar mass at peak maximum (M_p) of the SEC-MALLS measurements, and P are depicted in Table 4.4.2. For new PA 1101 powder, a P value of 1.59 was obtained, corresponding to a polydisperse powder. Higher polydispersities compared to virgin powder were noticed for all samples. M_w increased significantly to 446,800 g mol^{-1} at a temperature of 180 °C applied for 8 h. In general, the obtained values showed that PA 1101 is a reactive material and proved by means of increasing molar masses that post-condensation occurred for tempering conditions up to 180 °C and 8 h [21]. Further reactions related to thermal decomposition e.g. crosslinking could take place, which might have caused the reduced solubility starting at a temperature of 171 °C applied for 16 h and thus affected the molar mass distributions of those samples. In the literature, however, only minor crosslinking is reported for polyamide 11. Furthermore, no generally accepted mechanism for the thermal decomposition of aliphatic nylons and its influence on molar mass distribution is cited [44]. Consequently, SEC experiments solely cannot be used to prove crosslinking as the reason for low solubility of tempered PA 1101 powder samples. Schubert et al. [45] investigated the thermal aging behavior of polyamide 12 powders used for the LB-PBF-P process by means of DSC and SEC. M_w and P increased from 17,000 g mol^{-1} to 25,000 g mol^{-1} and from 2 to 2.2 within an aging duration of 24 h at 170 °C under N_2-atmosphere, respectively. In general, the increase of M_w for polyamide 12 over time under N_2 was much lower compared to the values of polyamide 11 we obtained. As no solubility problems of the aged powders were mentioned, no gelation occurred. Consequently, for aging in air, their measurements indicated a combination of chain extension or radical crosslinking and thermo-oxidative chain decomposition. Moreover, the increase of M_w and P was higher under air compared to nitrogen [45].

In addition to M_w, M_n, and M_p, more information can be obtained from the distribution curves of the light scattering (LS) and differential refractive index (dRI) signals, especially when comparing samples. Thus, the LS and dRI signals at different tempering temperatures and 8 h treatment time are depicted in Figure 4.4.2. Two peaks were visible in the LS curve of the virgin powder. As polymer molecules are separated according to their hydrodynamic volume, the first peak at 14 min elution time could be assigned to a component with high molar mass but in a too low concentration to be detected by refractive index. Wudy et al. [23] also observed a LS peak with missing dRI-signal in the context of polyamide 12 powder used in the LB-PBF-P process and investigated this LS peak in more detail: Powder was stored in the LB-PBF-P build chamber up to 27 h, whereby the high molar mass peak of the LS signal increased with build time. Furthermore, M_w was almost doubled during this process. This region of the LS-signal was interpreted as a sign for amounts of polymer species with very high molar masses [23], which could have a significant influence on polymer properties, such as tensile

strength, impact strength, brittleness, and melt viscosity [46]. In Figure 4.4.2 the LS signals increase with higher temperatures and exhibit shorter elution times. This intensity increase resulted from the signal dependency being proportional to concentration and molar mass [47]. In contrast, the dRI signal showed highest intensities for the virgin powder signal and the powder heat treated at 153 °C. The dRI signal for 180 °C showed the broadest distribution and a slight shoulder in the high molar mass region. Additionally, a decrease of peak height down to 0.5 was obtained, most likely caused by reduced solubility of the powder. The latter could be quantified by comparison of the dRI peak areas of virgin powder compared to heat-treated powder. With reference to the area value, 20% of the sample treated at 180 °C for 8 h remained unsolved.

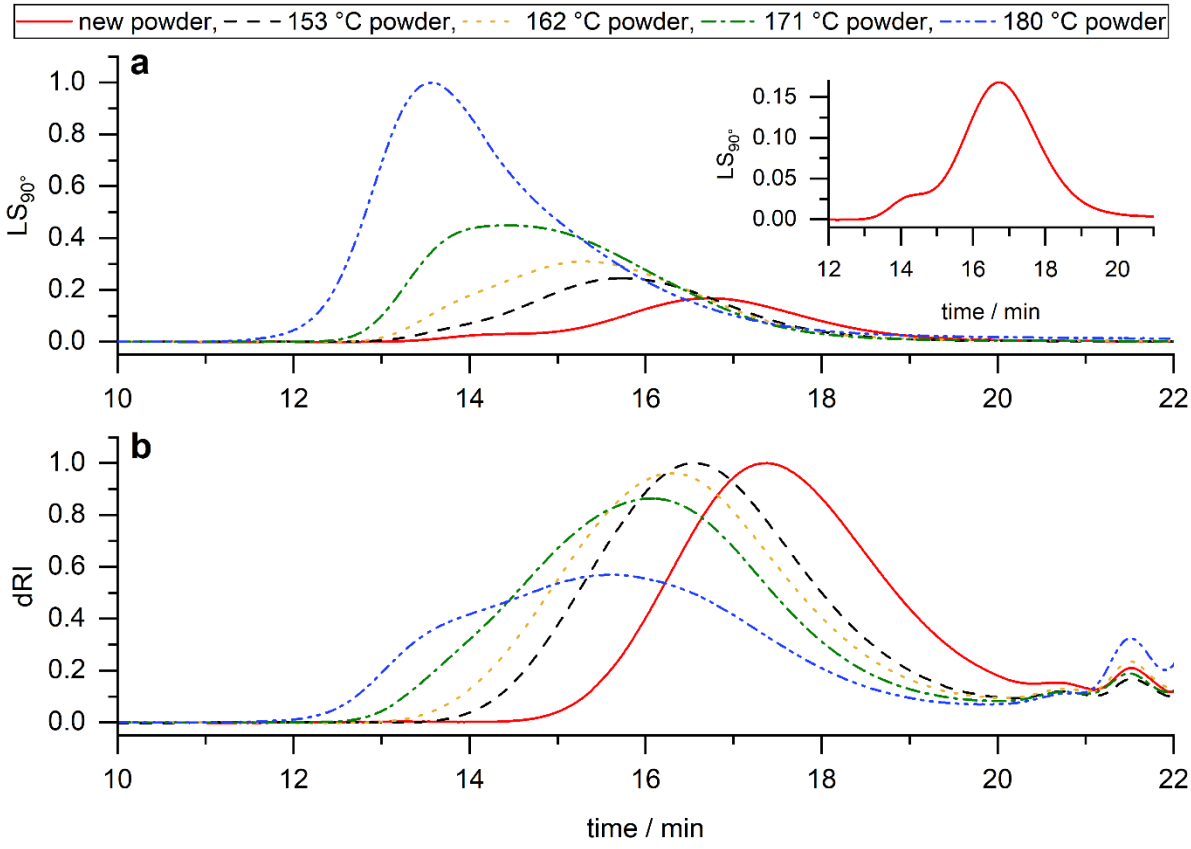

Figure 4.4.2 a $LS_{90°}$ and **b** dRI signals of PA 1101 powders treated at different temperatures under a N_2 gas flow of 10 mL min^{-1} for 8 h. New PA 1101 powder is compared to powders held at temperatures of 153, 162, 171, and 180 °C. The dRI and LS signals were normalized to the respective plots.

4.4.3.1.2 DSC studies on PA 1101 powder

Differential scanning calorimetry (DSC) was used for analyzing the melting and crystallization behavior. Full DSC runs including 2 heating scans were applied to new and heat-treated powder material. Figure 4.4.3 gives insights on the thermal effects occurring for new and aged powders at 171 °C for 8 h.

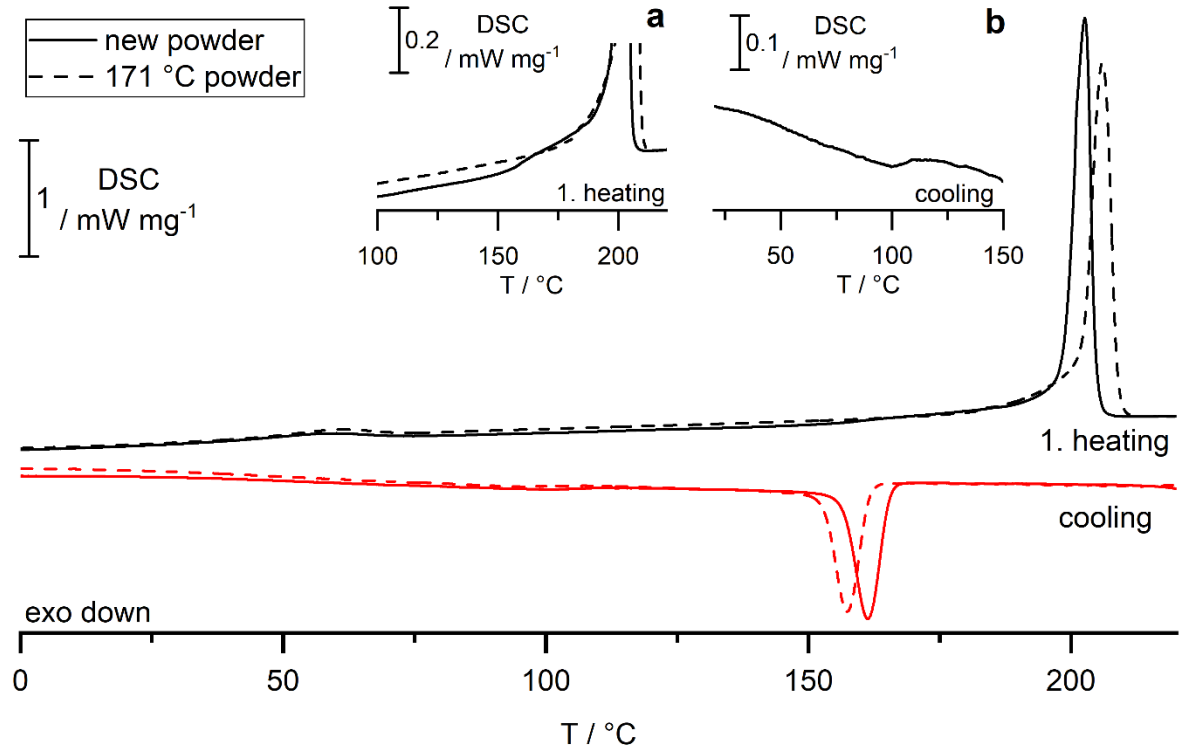

Figure 4.4.3 DSC heat flow of new PA 1101 powder and thermally stressed powder at 171 °C for 8 h. For a better comparison, the data sets were shifted along the y-axis. The insets **a** and **b** show the beginning of the melting process in the first heating run and a detailed curve of the cooling, respectively.

During the first heating, a broad glass transition between 20 °C and 80 °C was observable and accompanied by a relaxation effect. The beginning of the melting process is described by $T_{i,m1}$ and was at 160 °C and 180 °C for virgin powder and aged powder, respectively. The corresponding onset temperatures $T_{ei,m1}$ were 197.9 °C and 202.2 °C. Compared to temperatures stated in the literature, the onset of melting occurred at higher temperatures [48]. In the graph, virgin powder samples showed a shoulder in the first heating step before the main melting peak, resulting from reorganization effects (see Figure 4.4.3 inset a). Thereby, at elevated temperatures, imperfect crystals melt and recrystallize until perfect crystals are formed [48,49]. Since the analyzed powder was tempered at 171 °C, the reorganization effects have already occurred to a significant part and it was not expected that a shoulder would be formed during the first heating. Nevertheless, the shape of the melting peaks was sharp and indicated both a uniform structure and a narrow distribution of crystallite size. In case of virgin powder, the heat of fusion amounted to 125 J g^{-1}, corresponding to a crystallinity of 66%. Tempered powder at 171 °C for 8 h adopted a heat of fusion of 114 J g^{-1} with a crystallinity of 60%. The value of crystallinity was calculated taking a reference value of 189 J g^{-1} into account [50]. In addition to the thermal stress described herein, the polymer powders used in LB-PBF-P

are pretreated by the manufacturer in a pressurized steam atmosphere at an elevated temperature between the glass transition and the melting point to increase the melting temperature and melting enthalpy [51]. Heat treatments promote the growth of the crystallites lamella thickness present in the powder sample. Carrying on, the subsequent cooling step at 10 K min^{-1} during the DSC measurement showed that the crystallization process took place under supercooling. The onset temperatures $T_{ei,c}$ for virgin powder and heat-treated powder were 165.6 °C and 161.9 °C, respectively. Since the full width at half maximum was 5.1 °C for both samples, the crystallization was shifted to lower temperatures without a broadening occuring. Rhoades et al. [52] studied the nucleation process of polyamide 11 for different levels of supercooling. For low supercooling, the nucleation process was mainly driven by the creation of heterogeneous nuclei, which should not change its density during tempering. Furthermore, Paolucci et al. [38] investigated the molar mass dependency of the crystallization kinetics and revealed that isothermal crystallization at high temperatures showed no differences in the growth rate for new and tempered samples of polyamide 12. Assuming similar behavior for polyamide 11 and 12, it could be possible that a restrain of the non-isothermal crystallization was caused by the change of the molecular weight distribution. Both samples showed a second exothermic event in the temperature range between 110 °C and 90 °C (see inset b in Figure 4.4.3). According to Pepin et al. [25], this effect is referred to as the Brill transition. It is also known as a thermally induced crystal transition. The triclinic α' structure transforms reversibly into a high-temperature pseudo-hexagonal δ phase upon heating.

Table 4.4.3 shows the melting onset of the first heating run $T_{ei,m1}$, the melting enthalpy of the first heating run $H_{f,1}$, the crystallization onset of the cooling run $T_{ei,c}$, the melting onset of the second heating $T_{ei,m2}$, and the melting enthalpy of the second heating run $H_{f,2}$ for all heat treated samples. $T_{ei,m1}$ increased with both higher temperatures and longer treatment durations, which could be related to lamellae thickening. Upon cooling, $T_{ei,c}$ first decreased by treatment times and temperatures up to 180 °C for 8 h. Further thermal stress led to a slight increase of $T_{ei,c}$. Onset values of the melting process in the second heating run also decreased for increasing thermal stress, indicating an imperfect crystal structure. The melting enthalpies of the first and second heating were determined as well. $H_{f,1}$ increased for samples treated at 153°C. Analyses of virgin powder samples showed a beginning of the reorganization effects at 160°C. A thermal treatment below this temperature only causes an annealing of the crystallites and consequently an increase of $H_{f,1}$. With higher heat treatment parameters $H_{f,1}$ decreased from 125 J g^{-1} to 111 J g^{-1}, as reorganization effects took place during tempering. The melting enthalpy in the second heating run, $H_{f,2}$ remained constant at around 58 J g^{-1} for samples treated at a temperature exceeding 153 °C.

Table 4.4.3 Thermal properties of different polyamide 11 (PA 1101) powders investigated by DSC. Mean values of a double determination for the melting onset of the first heating run $T_{ei,m1}$, the melting enthalpy of the first heating run $H_{f,1}$, the crystallization onset of the cooling run $T_{ei,c}$, the melting onset of the second heating $T_{ei,m2}$, and the enthalpy of melting of the second heating run $H_{f,2}$ are depicted.

Temperature of heat treatment /°C	Duration of heat treatment /h	$T_{ei,m1}$ /°C	$H_{f,1}$ /J g^{-1}	$T_{ei,c}$ /°C	$T_{ei,m2}$ /°C	$H_{f,2}$ /J g^{-1}
virgin powder	–	197.9	125	165.6	179.2	63
153	8	200.4	124	165.0	178.7	62
153	16	201.0	128	163.3	177.0	61
153	24	201.3	126	162.7	176.8	57
162	8	201.2	122	163.1	177.2	56
162	16	201.7	124	162.3	176.4	58
162	24	201.9	123	162.3	176.2	58
171	8	202.0	114	161.9	176.2	57
171	16	202.5	114	162.0	176.0	56
171	24	202.8	122	161.9	175.6	62
180	8	202.5	111	161.5	175.6	57
180	16	203.2	113	162.0	175.5	58
180	24	203.6	112	162.6	175.7	58

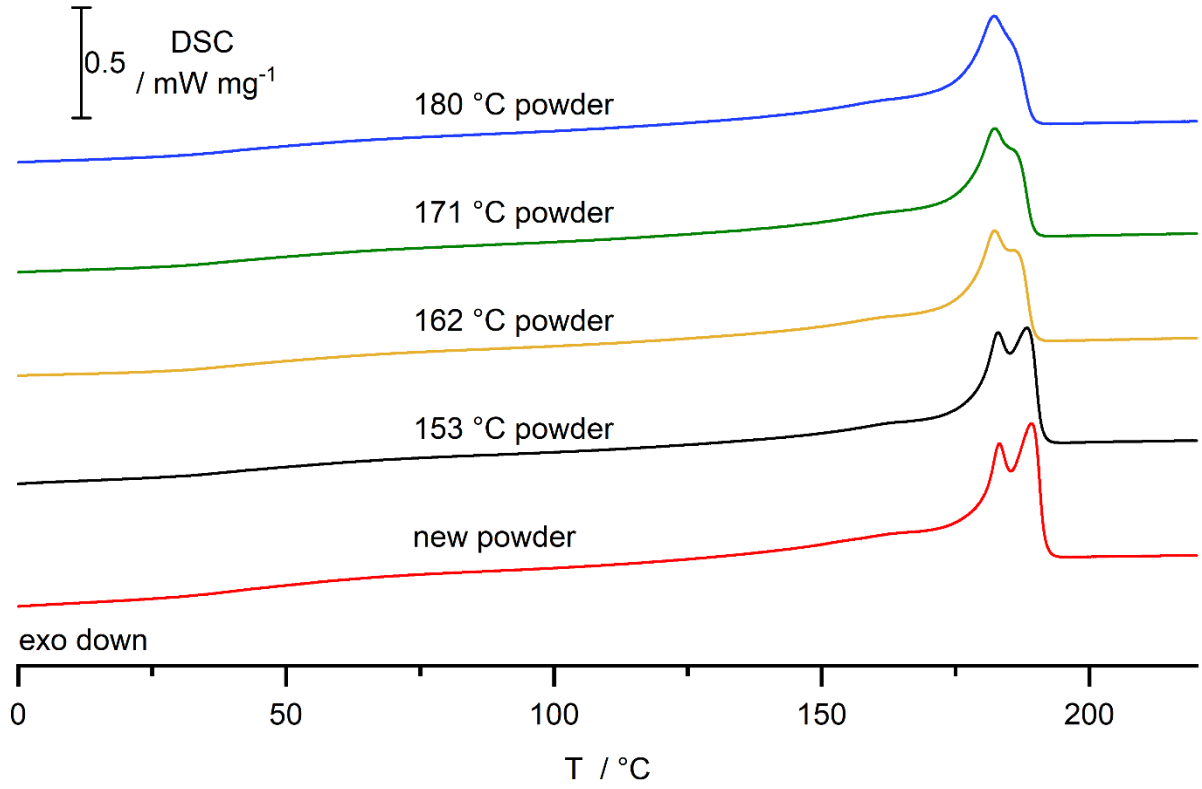

Figure 4.4.4 DSC heat flow of PA 1101 powders tempered at different temperatures for 8 h and new PA 1101 powder. For better comparison, the data sets of these second heating runs were shifted along the y-axis. The second heating step is shown.

Information about the material change during thermal stress experiments can be obtained from Figure 4.4.4 and Table 4.4.3. Figure 4.4.4 shows calorimetric measurements of the second heating curve of specimens that were thermally stressed for 8 h at different temperatures of 153 °C, 162 °C, 171 °C, and 180 °C. The glass transition range extended over a wide temperature range of approx. 20 °C - 80 °C and passes the characteristic $T_{1/2}$ at 45 °C for both samples. A broad glass transition range is typical for semi-crystalline polymers [53]. During melting, a polymorphic behavior was observed, starting with $T_{i,m2}$ at 110°C. The overall melting process was shifted to lower temperatures compared to the melting process from the first heating due to rewriting of the thermal history. Moreover, the bottom curve was obtained with a virgin powder sample without any thermal treatment. Virgin powder samples showed two overlapping melting peaks with peak temperatures of 183 °C and 189 °C. With increasing tempering temperature, the second melting peak decreased in height. Chocinski-Arnault et al. [54] studied the multiple melting behavior of polyamide 11 and proposed that polymorphism occurred when heating a slowly cooled melt. The low temperature peak was a result of mainly δ phase crystals and the high temperature peak representing the smectic δ’ phase. The δ phase correlates to the stable α’ phase at high temperatures. It was suggested that the amount of local chain alignments decreased for annealing at high temperatures in the

melt and led to suppression of the smectic δ' phase. In contrast, Pepin et al. [25] observed the Brill transition of polyamide 11 samples by X-ray diffraction and DSC. Both α' and δ' phases pass a Brill transition upon heating, yielding the δ form. A polymorphism was only assumed for α' crystals which did not transform into δ phase structures due to lack of transition time. In addition, Rhoades et al. [52] suggested that the formation of δ' phase was connected with a high supercooling near the glass transition temperature resulting in a homogeneous nucleation with high nuclei density. Thus, the formation of δ' phase by a non-isothermal cooling at 10 K min^{-1} was hardly probable. SEC studies showed an increase of molecular weight by heat treatment of polyamide 11 powder samples. As a result, the detected decrease of polymorphism could be related to a lower chain mobility restricting the Brill transition of α' crystals.

4.4.3.2 Sintered PA 1101 tensile bars

The 13 analytically characterized tensile bars were fabricated under identical parameters (powder material, sintering machine, build parameters). Selecting criteria were clean fractured surfaces that did not indicate any crack inducing contamination or other external influences. Furthermore, the fractured surfaces were evaluated microscopically. Figure 4.4.5 a and b show examples for ductile and partly brittle fracture mechanisms. In general, high values of ε_B indicate a ductile behavior with a clear necking area and an isotropic fracture pattern on the fractured surface. In contrast, low values of ε_B show a partly brittle or brittle fracture behavior with an even fractured area and anisotropic crack pattern. The mean ε_B value for all 13 tensile bars was 23%. The location of each tensile bar during the build job is depicted in Figure 4.4.12 in the section supporting information.

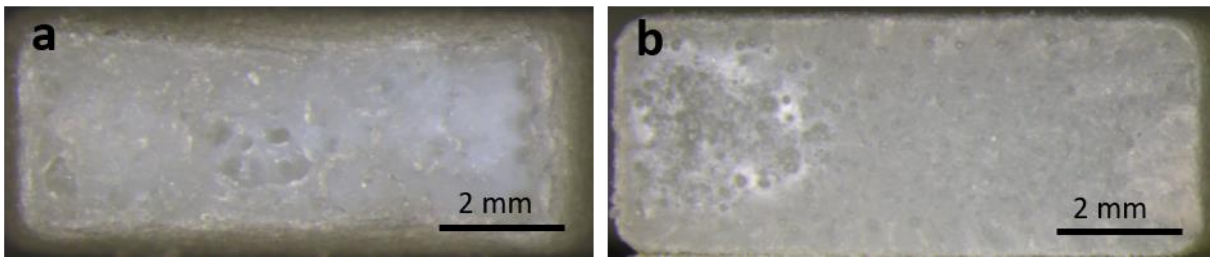

Figure 4.4.5 Microscopic images of ductile (**a**) and partly brittle (**b**) fracture mechanisms of sintered PA 1101 tensile bars.

4.4.3.2.1 SEC studies on PA 1101 tensile bars

Molar mass distribution

The molar mass distribution of tensile bars with different ε_B values was determined, whereby two examples for ductile and partly brittle fracture were investigated in more detail in this

section. In general, the solubility behavior of the tensile bars was different compared to the tested powders. The tensile bar samples were completely dissolved except for some particles sticking to the wall of the sample vessel. A reason for the insolubility could be small amounts of multiple recycled powder that was poorly soluble. However, these portions could not be quantified using the area of the dRI-signals. The plots of LS signal, molar mass, and dRI signal of tensile bar A and B with ε_B values of 39% and 10%, respectively, are shown in Figure 4.4.6. For tensile bar A high LS signal at an elution time of 13 min was detected, whereas tensile bar B showed a much lower intensity. Furthermore, the peak height of B was approximately half of the intensity of A, indicating less amount of high molar species in sample B. Regarding the molar mass curve, an increase of molar mass at higher elution times which does not correspond to the theory of SEC, could be observed. This effect is also known as “anchoring” in literature [46]. It describes the penetration of parts of large polymer chains into the pores of the stationary phase, resulting in anchoring of the entire polymer chain. Consequently, elution of these molecules will be retarded to higher elution times, leading to coelution with molecules that possess lower molar masses [46]. The dRI signal of tensile bar A showed a slight shoulder in the high molar mass region, which indicated that a particularly large amount of molecules was present in this range of molecular weight. Furthermore, the concentration signal of tensile bar A showed a broader distribution compared to tensile bar B.

For all investigated tensile bars the values for ε_B, M_w, M_n, M_p, and P are depicted in Table 4.4.4. The ε_B values were between 9.6% and 39%, showing a broad distribution in their fracture behavior. It was remarkable that low M_n values (compare tensile bars C and K) did not always result in a brittle fracture. Moreover, partly good mechanical behavior ($\varepsilon_b \geq 24.9\%$) was observed with tensile bars including high M_w values in the range between 147,563 g mol^{-1} and 254,007 g mol^{-1}. However, tensile bars D and F showed lower ε_B values with M_w between 173,600 g mol^{-1} and 186,047 g mol^{-1}. No direct relation between M_w and ε_B was found. Instead, the P value has proven as an indicator for ductile or brittle fractures (see plot of P in relation to the ε_B values in Figure 4.4.9). The P values ranged from 1.80 up to 2.21, whereby higher P values correlated with better mechanical characteristics. Comparing the tempered PA 1101 powder samples to the sintered tensile bars, it could be noticed that some of the tensile bars showed M_w values similar to the aged powder samples. For the tensile bars B, C, E, G, H, I, and K, values in the same range as for powder tempered at 162 °C between 16 h and 24 h or up to a temperature of 171 °C tempered for 8 h could be observed. The other tensile bars showed higher M_w values, which could be measured for virgin powder when applying e.g. more than 24 h of heat treatment at 162 °C. Based on the P values, the aging of the particles by the LB-PBF-P process could be compared with powder treated at 162 °C for durations between 8 h and 24 h.

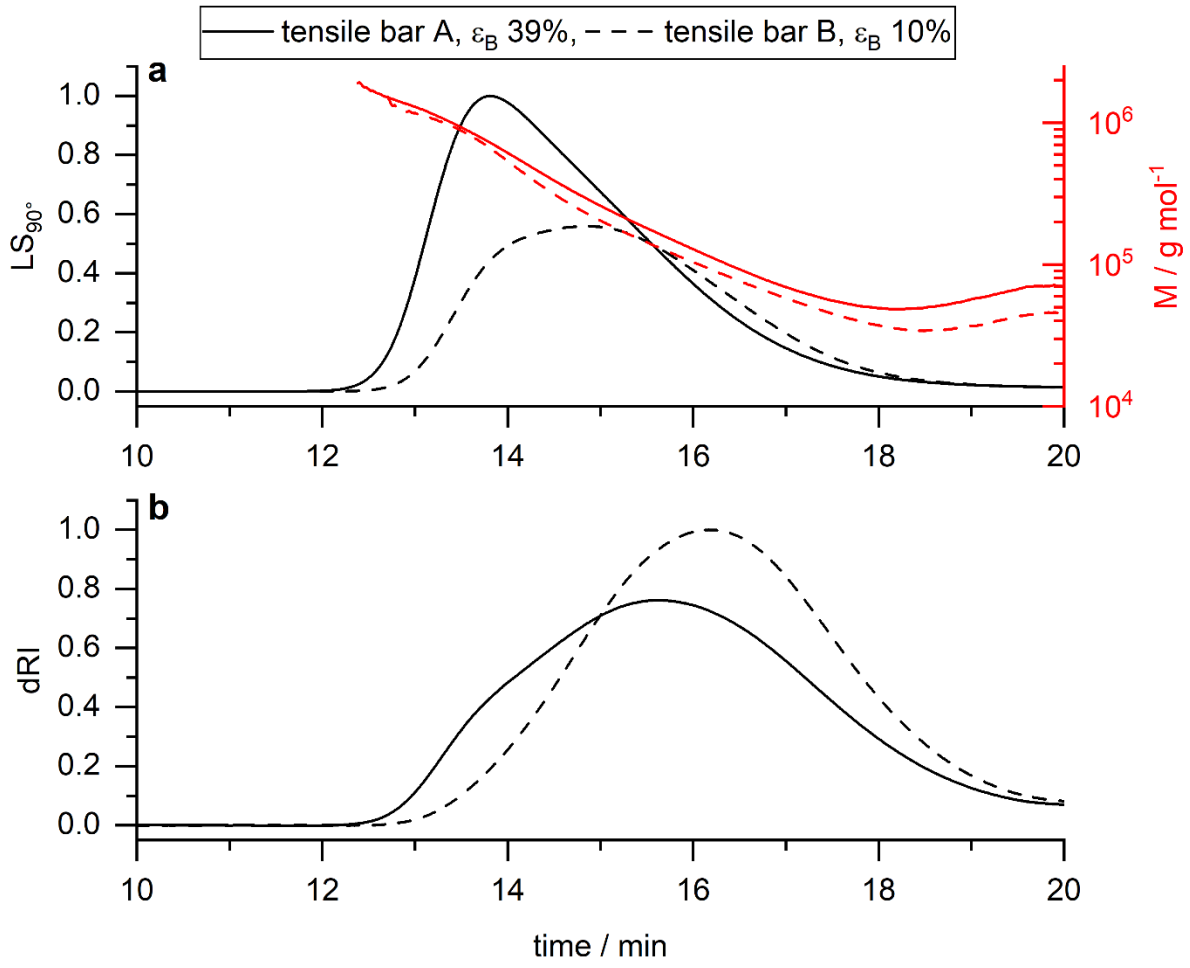

Figure 4.4.6 a $LS_{90°}$ and **b** dRI signals of tensile bar A and B with different ε_B values. Tensile bar A showed an ε_B of 39%, for tensile bar B 10% were measured. The dRI and LS signals were normalized to the highest signal in the plots, respectively. Additionally, the molar mass curves of the two tensile bars are shown in **a**.

Table 4.4.4 Overview of different tensile bars and their corresponding elongation at break ε_B values, weight average molar mass M_w, number average molar mass M_n, average molar mass at peak maximum M_p, and the polydispersity P of the SEC-MALLS measurements.

Tensile bar	ε_B /%	M_n /g mol^{-1}	M_p /g mol^{-1}	M_w /g mol^{-1}	P
A	39.0	114,910	163,627	254,007	2.21
B	10.3	76,850	93,750	139,830	1.82
C	9.6	73,157	89,940	132,020	1.80
D	19.4	85,040	113,920	173,600	2.04
E	19.8	74,010	94,100	140,950	1.90
F	21.3	89,120	118,187	185,190	2.08
G	21.5	75,923	99,263	146,870	1.94
H	22.0	71,997	89,643	137,137	1.91
I	23.4	66,193	87,050	129,500	1.96
J	24.9	86,900	124,353	186,047	2.14
K	30.0	72,570	98,337	147,563	2.04
L	31.0	93,023	130,950	197,333	2.12
M	31.6	104,540	137,927	222,241	2.12

Conformation plots of PA 1101 tensile bars

Conformation plots of tensile bars A and B in comparison to those of new PA 1101 powder and PA 1101 powder aged at 171 °C (8 h) are shown in Figure 4.4.7. Conformation plots depict the dependence of the root mean square (RMS) radius on molar mass and reveal information about the molecular conformation of polymers in solution. Furthermore, it is a method suitable for the determination of branching [46]. As the hydrodynamic volume differs for linear and branched molecules, conformation plots can be used for their differentiation [55]. This is possible as branched molecules possess a smaller RMS radius compared to non-branched molecules with the same molar mass. Thus, different slopes in conformation plots are obtained [56]. However, limitations remain as molecules with radius smaller than 10 nm cannot be characterized [46]. The slope values of the conformation plots in Figure 4.4.7 were determined by linear fitting of the measured data. Tensile bar B (ε_B 10%) showed two different slopes. These were 0.40 for the low and 0.30 for the high molar mass region between $8 \cdot 10^4$ g mol^{-1} and $3 \cdot 10^5$ g mol^{-1}. The different slopes indicated different molecular conformations of the sample [46]. In contrast, tensile bar A (ε_B 39%) showed a single slope of 0.47. Typically, values of 0.5, 1.0, and 0.33 indicate forms of linear random coils, rods, and compact spheres in theta solvents [46]. The slope decreases with increasing degree of branching [46,57]. Considering this information, it could be assumed that tensile bar B

contained partly branched molecules especially in the high molar mass region. The conformation plot of new PA 1101 powder also showed two different slopes (0.38 for the low and 0.13 for the high molar mass region). The slope 0.13 was very flat and extended into the high molar mass range, but with low concentration in this range. Therefore, it was very likely that these conformations were still present in the aged material. However, the effect was superimposed by conformations created during post-condensation, resulting in one slope for PA 1101 powder aged at 171 °C (8 h). Another explanation for the similarities of the conformation plots of tensile bar B and new PA 1101 powder could be powder particles present in tensile bar B, which partly exhibited the structure of virgin powder due to low energy input [58]. This led to unmelted regions in the tensile bar and resulted as a consequence of bad layer adhesion in a low value of ε_B [12]. The slope of tensile bar A and the slope of the low molar mass region of tensile bar B were similar to the conformation plot of PA 1101 powder tempered at 171 °C (8 h). A detailed comparison of conformation plots of the investigated powder samples with 8 h sampling duration is included in Figure 4.4.10. It was shown that the slopes of new PA 1101 powder were characteristic and differed from the heat-treated powder indicating that different molecular conformations were present in the samples.

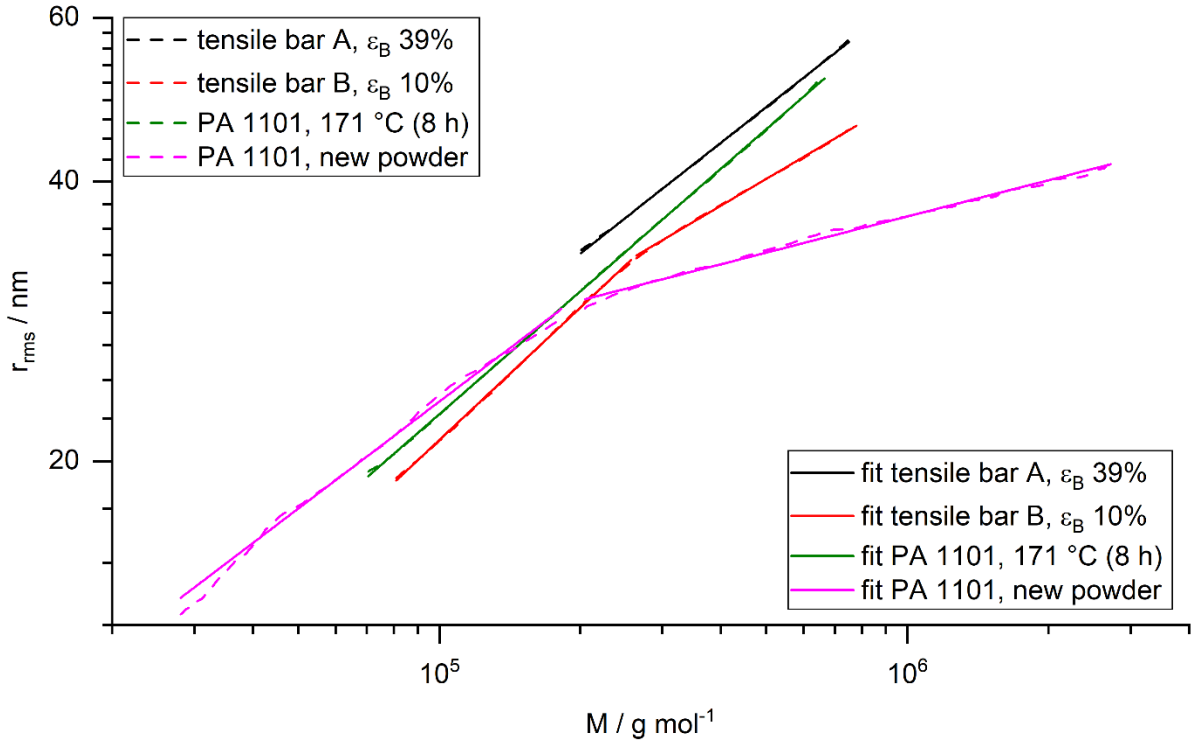

Figure 4.4.7 Conformation plots of tensile bar A (ε_B 39%) and B (ε_B 10%) in comparison to those of new PA 1101 powder and PA 1101 powder aged at 171 °C (8 h). The dashed lines represent the raw data and the solid lines the fit curves. Slopes were 0.30 and 0.40 for tensile bar B and 0.47 for tensile bar A. The slopes of new PA 1101 powder were 0.38 and 0.13, the slope of PA 1101 powder aged at 171 °C (8 h) was 0.44.

4.4.3.2.2 DSC studies on PA 1101 tensile bars

The DSC heat signal is shown as a function of temperature in Figure 4.4.8 and allows for comparison of the thermal behavior of tensile bars A and B with ε_B values of 39% and 10%, respectively.

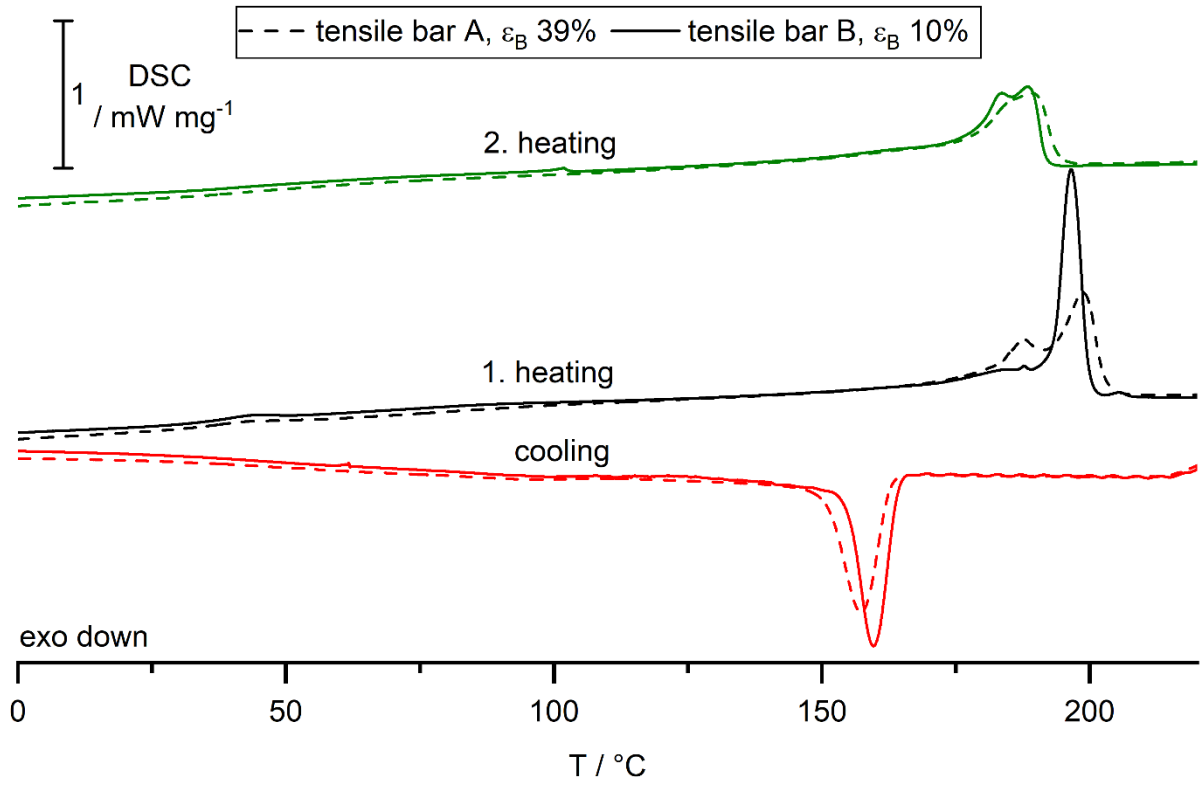

Figure 4.4.8 DSC heat flow signals for two tensile bars A and B with elongation at break values of 39% and 10%, respectively. Heating rate: 10 K min^{-1}. For better comparison, the data sets were shifted along the y-axis.

During the first heating run, sample A showed a polymorphism with peak temperatures of 187.8 °C and 198.8 °C. Tensile bar B in contrast yielded a broad melting peak at 184.7 °C, a sharp melting peak at 193.2 °C, and a separate peak at 203.1 °C. The high temperature peak was probably caused by unsintered but thermally stressed particles. The sharp melting peak in sample B indicated a narrow distribution of crystallite size. The total crystallinity differed slightly between samples with 34% and 39% for tensile bar A and B, respectively. Hocker et al. [59] studied the ductile fracture behavior of polyamide 11 by defining a critical crystallinity χ_c of about 35.4% as a criterion for ductile-brittle-fracture transition by taking a reference enthalpy of 189 J g^{-1} into account. Cooling the melt at a rate of 10 K min^{-1} revealed different crystallization processes. Tensile bar A solidified in a broad transition range which was shifted towards lower temperatures. The crystallization peak of tensile bar B was sharper, resulting in a more intensive signal, and occurred at a higher temperature. In the following heating run, the melting region of tensile bar A was slightly larger and showed a single peak. Tensile bar

B, on the other hand, showed a polymorphic melting peak. The crystallinity was calculated using the heat of fusion obtained during the second heating run, being 33% for both samples. Measured thermal key values for all tensile bars are listed in Table 4.4.5 and plotted in Figure 4.4.11. The crystallization by cooling from the melt is dependent on the cooling rate. Slower cooling rates result in more time being available for organization processes and crystal growth. Consequently, since the cooling rate during LB-PBF-P was approx. 0.2 K min^{-1}, high amounts of crystallinities were achieved [5].

Table 4.4.5 Overview of different tensile bars and their corresponding elongation at break ε_B values. Mean values of a double determination for the melting onset of the first heating run $T_{ei,m1}$, the melting enthalpy of the first heating run $H_{f,1}$, the crystallization onset of the cooling run $T_{ei,c}$, the melting onset of the second heating $T_{ei,m2}$, and the enthalpy of melting of the second heating run $H_{f,2}$ are listed.

Tensile bar	ε_B /%	$T_{ei,m1}$ /°C	$H_{f,1}$ /J g^{-1}	$T_{ei,c}$ /°C	$T_{ei,m2}$ /°C	$H_{f,2}$ /J g^{-1}
A	39.0	192.3	64.1	162.8	176.7	62.7
B	10.3	193.2	68.2	164.2	177.6	62.2
C	9.6	193.2	69.3	163.9	177.5	62.9
D	19.4	194.5	68.2	163.4	177.4	63.7
E	19.8	193.1	68.7	163.8	177.4	62.5
F	21.3	194.7	67.6	163.3	177.1	63.7
G	21.5	192.8	68.3	163.7	177.0	63.0
H	22.0	192.6	67.0	163.5	177.2	61.7
I	23.4	192.6	68.3	163.8	177.4	63.8
J	24.9	194.4	65.4	163.4	177.0	61.9
K	30.0	191.6	64.7	163.6	177.1	63.1
L	31.0	186.6	63.1	163.0	176.8	62.4
M	31.6	193.9	64.5	163.1	176.6	62.3

The melting enthalpy of the first heating run depends on the LB-PBF-P process conditions and represents the crystallinity of the tensile bars. $H_{f,1}$ values between 63.1 J g^{-1} and 69.3 J g^{-1} were determined. Tensile bars with high elongation at break ($\varepsilon_B \geq 24.9\%$) showed a crystallinity below the critical value of 35.4%. In contrast, specimen with a low elongation at break ($\varepsilon_B \leq 10\%$) exhibited a crystallinity above the critical value, leading to brittle fracture mechanism. Regarding the crystallization onsets, tensile specimens with an $\varepsilon_B \geq 24.9\%$ achieved values of maximum 163.1 °C (see tensile bars A, M, L). Brittle fracture samples showed a crystallization onset of 163.9 °C or higher (tensile bars B and C). All other tensile specimens showed values between the described extremes. $T_{ei,m2}$ enables an estimation of the aging state of the powder used in the LB-PBF-P process. Based on the thermal aging of

powder samples, it was observed that $T_{ei,m2}$ was shifted to lower temperatures with increasing thermal stress (see Table 4.4.3). The comparison between tensile bar and powder samples indicated that the aging state of the particles of printed components was in the range of 8 to 16 h at a temperature of 162 °C. In some cases even shorter times could be possible. Samples with low ε_B thus showed a rather low thermal stress (see tensile specimen B and C).

4.4.3.2.3 Correlation between polydispersity P, the crystallization onset $T_{ei,c}$, and elongation at break ε_B values of tested tensile bars

Figure 4.4.9 sets ε_B of different tensile bars and their physico-chemical properties, represented by $T_{ei,c}$ and P, into relation. It is noteworthy that the two tensile bars with the lowest ε_B values of about 10% showed the lowest P values but highest crystallization onset temperatures $T_{ei,c}$. For the tensile bars with the highest values for ε_B, the opposite effects on P and $T_{ei,c}$ could be observed. In Table 4.4.4 it is shown that M_w and M_n do not directly correlate with P.

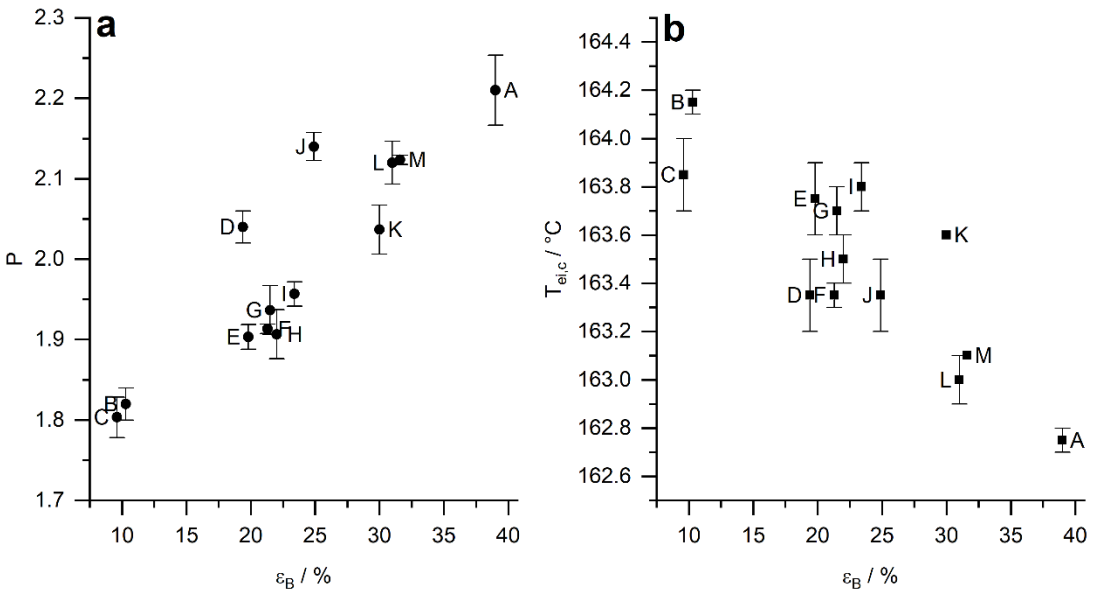

Figure 4.4.9 a Polydispersity P and **b** the crystallization onset temperature $T_{ei,c}$ in relation to elongation at break ε_B values of different tensile bars.

Maiza et al. [60] investigated the influence of aging by thermal stress and storage in aqueous conditions on physico-chemical and mechanical properties of polyamide 11. A decrease of the molecular weight was correlated to decreasing ε_B values. Moreover, it was shown that ε_B decreases with thermal stress. However, the material Rilsan BESNO TL+ grade was tested in the investigation, which is a product containing 0.8% of antioxidant. In our case, the product PA 1101 was examined. Thus, apart from the constitution of the pure polymer, additives may be included in the formulation influencing the characteristics of the PA 1101. In literature,

different kinds of stabilizers are cited to enhance thermal and oxidative stability of the polymer, such as copper salts, phosphites, and hindered phenols [61]. Furthermore, polyamide 11 can also be obtained in form of composites with other materials [7], such as carbon black (PA 1102) or carbon fiber (HP 11-30). However, ε_B is stated highest for the unfilled material [62].

4.4.4 Conclusion

The combination of SEC with a MALLS detector was demonstrated as a powerful method for molecular weight determination and the investigation of polymer conformation [56]. Via SEC-MALLS measurements, changes in molar mass distributions in heat-treated powders could be investigated and compared to the results of sintered tensile bars. Additionally, conformational differences of tensile bars with different ε_B values were shown. An increase of the molecular weight averages by a multiple to the values of new PA 1101 powder was observed as a result of post-condensation. Therefore, it could be demonstrated that PA 1101 is a highly reactive material. Under high thermal stress, however, solubility of the samples in HFIP became problematic, whereby the reason for the solubility issues of corresponding samples still needs to be further investigated. The increase of molar mass values was also determined for the investigated tensile bars, but no direct correlation of M_w values and the mechanical behavior of the tensile bars could be drawn. Instead, tensile bars with good mechanical properties were related to P values of up to 2.21. Furthermore, the SEC characteristics of tensile bars was compared to heat-treated powder samples, comparing the effects of temperatures of 162 °C and 171 °C applied for different durations.

Moreover, the influence of thermal treatment on the melting and crystallization behavior was characterized by DSC measurements. It could be observed that both the $T_{ei,m2}$ and $T_{ei,c}$ are shifted to lower temperatures. Molecular changes resulted in a less distinctive polymorphism in defined melt films due to lack of transition time of α' crystals. Based on the defined aging experiments of powder samples, the thermal stress of printed parts could be estimated by comparing the thermal properties at a temperature of 162 °C applied for 8 h to 16 h. Tensile samples with poor mechanical properties could be identified by high melting and crystallization temperatures. In addition, a sharp and uniform melting peak indicated a brittle fracture mechanism. The overall crystallinities of samples with ε_B values of less than 10.0% were higher than χ_c of 35.4% and vice versa, taking specimen of good mechanics into account [59].

The applied conditions in the micro-chamber could be adapted to typical conditions in the LB-PBF-P process. The duration of heat treatment and the applied temperature were important factors, influencing both the changes in the molecular weight distribution as well as the melting and crystallization behavior of the material. Comparing ε_B, P, and $T_{ei,c}$ of the

analyzed tensile bars, a correlation between the physico-chemical properties and the LB-PBF-P part qualification could be drawn. Low P values of tensile bars implied low ε_B values and thus brittle fracture behavior. The opposite correlation between the $T_{ei,c}$ and ε_B of the tensile bars could be observed.

Acknowledgements

The authors thank the BMW AG for funding analytical equipment and financial support which is gratefully acknowledged. Many thanks are addressed to Gabriele Fruhmann (BMW AG, Munich) and Monika Gessler (EOS, Krailling) for the fruitful discussions and their support by providing polyamide 11 and various other samples.

4.4.5 References

[1] S.C. Ligon, R. Liska, J. Stampfl, M. Gurr, R. Mülhaupt, Polymers for 3D printing and customized additive manufacturing, Chem. Rev. 117 (2017) 10212–10290. https://doi.org/10.1021/acs.chemrev.7b00074.

[2] M. Schmid, Additive Fertigung mit Selektivem Lasersintern (SLS): Prozess- und Werkstoffüberblick, Springer Vieweg, Wiesbaden, 2015.

[3] A. Gebhardt, Generative Fertigungsverfahren: Additive Manufacturing und 3D Drucken für Prototyping - Tooling - Produktion, Carl Hanser Verlag, München, 2013.

[4] 3D-grenzenlos Magazin, MINI Yours Customised - Mit 3D-Druck den MINI personalisieren, 2018, https://www.3d-grenzenlos.de/magazin/zukunft-visionen/mini-yours-customised-auto-personalisieren-27338973/, accessed 9 December 2019.

[5] S. Josupeit, H.-J. Schmid, Temperature history within laser sintered part cakes and its influence on process quality, Rapid Prototyp. J. 22 (2016) 788–793. https://doi.org/10.1108/RPJ-11-2015-0166.

[6] M. Schmid, Selektives Lasersintern (SLS) mit Kunststoffen: Technologie, Prozesse und Werkstoffe, Hanser, München, 2015.

[7] S. Yuan, F. Shen, C.K. Chua, K. Zhou, Polymeric composites for powder-based additive manufacturing: Materials and applications, Prog. Polym. Sci. 91 (2019) 141–168. https://doi.org/10.1016/j.progpolymsci.2018.11.001.

[8] W. Yang, X. Bai, W. Zhu, R. Kiran, J. An, C.K. Chua, K. Zhou, 3D Printing of polymeric multi-layer micro-perforated panels for tunable wideband sound absorption, Polymers 12 (2020). https://doi.org/10.3390/polym12020360.

[9] Y. Yang, G. Wang, H. Liang, C. Gao, S. Peng, L. Shen, C. Shuai, Additive manufacturing of bone scaffolds, Int. J. Bioprint. 5 (2019) 148. https://doi.org/10.18063/IJB.v5i1.148.

[10] Y. Du, H. Liu, J. Shuang, J. Wang, J. Ma, S. Zhang, Microsphere-based selective laser sintering for building macroporous bone scaffolds with controlled microstructure and excellent biocompatibility, Colloids Surf. B Biointerfaces 135 (2015) 81–89. https://doi.org/10.1016/j.colsurfb.2015.06.074.

[11] Y. Du, H. Liu, Q. Yang, S. Wang, J. Wang, J. Ma, I. Noh, A.G. Mikos, S. Zhang, Selective laser sintering scaffold with hierarchical architecture and gradient composition for osteochondral repair in rabbits, Biomaterials 137 (2017) 37–48. https://doi.org/10.1016/j.biomaterials.2017.05.021.

[12] A. Wegner, Theorie über die Fortführung von Aufschmelzvorgängen als Grundvoraussetzung für eine robuste Prozessführung beim Laser-Sintern von Thermoplasten. Dissertation, 2015.

[13] J.-P. Kruth, P. Mercelis, Binding mechanisms in selective laser sintering and selective laser melting, Rapid Prototyp. J. 11 (2005) 26–36. https://doi.org/10.1108/13552540510573365.

[14] M. Schmid, K. Wegener, Additive Manufacturing: Polymers applicable for laser sintering (LS), Procedia Engineering 149 (2016) 457–464. https://doi.org/10.1016/j.proeng.2016.06.692.

[15] S. Dadbakhsh, L. Verbelen, O. Verkinderen, D. Strobbe, P. van Puyvelde, J.-P. Kruth, Effect of PA12 powder reuse on coalescence behaviour and microstructure of SLS parts, Eur. Polym. J. 92 (2017) 250–262. https://doi.org/10.1016/j.eurpolymj.2017.05.014.

[16] D. Rouholamin, N. Hopkinson, An investigation on the suitability of micro-computed tomography as a non-destructive technique to assess the morphology of laser sintered nylon 12 parts, Proc. IME B J. Eng. Manufact. 228 (2014) 1529–1542. https://doi.org/10.1177/0954405414522209.

[17] T. Stichel, T. Frick, T. Laumer, F. Tenner, T. Hausotte, M. Merklein, M. Schmidt, A round robin study for selective laser sintering of polyamide 12: Microstructural origin of the mechanical properties, Optic Laser. Technol. 89 (2017) 31–40. https://doi.org/10.1016/j.optlastec.2016.09.042.

[18] C. Kummert, S. Josupeit, H.-J. Schmid, Thermoplastic elastomer part color as function of temperature histories and oxygen atmosphere during selective laser sintering, JOM 70 (2018) 425–430. https://doi.org/10.1007/s11837-017-2658-2.

[19] R.D. Goodridge, C.J. Tuck, R.J.M. Hague, Laser sintering of polyamides and other polymers, Prog. Mater. Sci. 57 (2012) 229–267. https://doi.org/10.1016/j.pmatsci.2011.04.001.

[20] M. Genas, Rilsan (Polyamid 11), Synthese und Eigenschaften, Angew. Chem. 74 (1962) 535–540. https://doi.org/10.1002/ange.19620741504.

[21] L. Verbelen, S. Dadbakhsh, M. van den Eynde, J.-P. Kruth, B. Goderis, P. van Puyvelde, Characterization of polyamide powders for determination of laser sintering processability, Eur. Polym. J. 75 (2016) 163–174. https://doi.org/10.1016/j.eurpolymj.2015.12.014.

[22] K. Schubert, J. Kolb, F. Wohlgemuth, D. Lellinger, I. Alig, Thermische Alterung und Eigenschaften von Polymermaterialien für das Selektive Lasersintern, in: H.A. Richard, B. Schramm, T. Zipsner (Eds.), Additive Fertigung von Bauteilen und Strukturen, Springer Fachmedien Wiesbaden, Wiesbaden, 2017, pp. 159–172.

[23] K. Wudy, D. Drummer, Aging effects of polyamide 12 in selective laser sintering: Molecular weight distribution and thermal properties, Addit. Manuf. 25 (2019) 1–9. https://doi.org/10.1016/j.addma.2018.11.007.

[24] S. Rhee, J.L. White, Crystalline structure and morphology of biaxially oriented polyamide 11 films, J. Polym. Sci. B Polym. Phys. 40 (2002) 2624–2640. https://doi.org/10.1002/polb.10330.

[25] J. Pepin, V. Miri, J.-M. Lefebvre, New insights into the brill transition in polyamide 11 and polyamide 6, Macromolecules 49 (2016) 564–573. https://doi.org/10.1021/acs.macromol.5b01701.

[26] K. Jariyavidyanont, W. Focke, R. Androsch, Thermal properties of biobased polyamide 11, in: Springer, Berlin, Heidelberg, 2019, p. 139.

[27] R. Brill, Über das Verhalten von Polyamiden beim Erhitzen, J. Prakt. Chem. 161 (1942) 49–64. https://doi.org/10.1002/prac.19421610104.

[28] H.-G. Elias, Macromolecules, Wiley-VCH, Weinheim, 2008.

[29] M.D. Lechner, E.H. Nordmeier, B.J. Schmitt, K.-H. Hahn, C. Lennartz, R. Heering, Das Makromolekül als Festkörper und als Schmelze, in: M.D. Lechner, K. Gehrke, E.H. Nordmeier (Eds.), Makromolekulare Chemie, Springer, Berlin, Heidelberg, 2014, pp. 429–641.

[30] C.-s. Wu (Ed.), Handbook of size exclusion chromatography, Dekker, New York, NY, 1995.

[31] K. Weisskopf, G. Meyerhoff, Molecular weight determinations of polyamides by N-trifluoroacetylation, Polymer 24 (1983) 72–76. https://doi.org/10.1016/0032-3861(83)90083-6.

[32] P.J. Wang, R.J. Rivard, Characterization of nylons by gel permeation chromatography and low angle laser light scattering in 2,2,2-trifluoroethanol, J. Liq. Chromatogr. 10 (1987) 3059–3071. https://doi.org/10.1080/01483918708068297.

[33] T.H. Mourey, T.G. Bryan, Size-exclusion chromatography in 1,1,1,3,3,3-hexafluoro-2-propanol, J. Chromatogr. A 964 (2002) 169–178. https://doi.org/10.1016/S0021-9673(02)00510-1.

[34] J. Chen, W. Radke, H. Pasch, Analysis of polyamides by size exclusion chromatography and laser light scattering, Macromol. Symp. 193 (2003) 107–118. https://doi.org/10.1002/masy.200390044.

[35] S. Laun, H. Pasch, N. Longiéras, C. Degoulet, Molar mass analysis of polyamides-11 and -12 by size exclusion chromatography in HFiP, Polymer 49 (2008) 4502–4509. https://doi.org/10.1016/j.polymer.2008.08.017.

[36] P. Frübing, A. Kremmer, R. Gerhard-Multhaupt, A. Spanoudaki, P. Pissis, Relaxation processes at the glass transition in polyamide 11: from rigidity to viscoelasticity, J. Chem. Physics 125 (2006) 214701. https://doi.org/10.1063/1.2360266.

[37] A. Mollova, R. Androsch, D. Mileva, C. Schick, A. Benhamida, Effect of supercooling on crystallization of polyamide 11, Macromolecules 46 (2013) 828–835. https://doi.org/10.1021/ma302238r.

[38] F. Paolucci, M.J.H. van Mook, L.E. Govaert, G.W.M. Peters, Influence of post-condensation on the crystallization kinetics of PA12: From virgin to reused powder, Polymer 175 (2019) 161–170. https://doi.org/10.1016/j.polymer.2019.05.009.

[39] S. Acierno, P. van Puyvelde, Effect of short chain branching upon the crystallization of model polyamides-11, Polymer 46 (2005) 10331–10338. https://doi.org/10.1016/j.polymer.2005.07.097.

[40] DIN EN ISO 527, Plastics - determination of tensile properties - Part 2: Test conditions for moulding and extrusion plastics 83.080.01, 2012.

[41] DIN EN ISO 11357-1, Kunststoffe - Dynamische Differenz-Thermoanalyse (DSC): Allgemeine Grundlagen 83.080.01, 2016.

[42] DIN EN ISO 11357-3, Kunststoffe - Dynamische Differenz-Thermoanalyse (DSC): Bestimmung der Schmelz- und Kristallisationstemperatur und der Schmelz- und Kristallisationsenthalpie 83.080.01, 2018.

[43] ISO 16014-5, Plastics - determination of average molecular mass and molecular mass distribution of polymers using size-exclusion chromatography - Part 5: Method using light-scattering detection 83.080.01, 2012.

[44] S.V. Levchik, E.D. Weil, M. Lewin, Thermal decomposition of aliphatic nylons, Polym. Int. 48 (1999) 532–557. https://doi.org/10.1002/(SICI)1097-0126(199907)48:7<532:AID-PI214>3.0.CO;2-R.

[45] K. Schubert, J. Kolb, F. Wohlgemuth, D. Lellinger, I. Alig, Thermische Alterung und Eigenschaften von Polymermaterialien für das Selektive Lasersintern, in: H.A. Richard, B. Schramm, T. Zipsner (Eds.), Additive Fertigung von Bauteilen und Strukturen, Springer Fachmedien, Wiesbaden, 2017, pp. 159–172.

[46] S. Podzimek, Light scattering, size exclusion chromatography, and asymmetric flow field flow fractionation: Powerful tools for the characterization of polymers, proteins and nanoparticles, Wiley, Hoboken N.J., 2011.

[47] P.J. Wyatt, Light scattering and the absolute characterization of macromolecules, Anal. Chim. Acta 272 (1993) 1–40. https://doi.org/10.1016/0003-2670(93)80373-S.

[48] A. Xenopoulos, B. Wunderlich, Thermodynamic properties of liquid and semicrystalline linear aliphatic polyamides, J. Polym. Sci. B Polym. Phys. 28 (1990) 2271–2290. https://doi.org/10.1002/polb.1990.090281209.

[49] B. Wunderlich, Macromolecular physics, Academic Press, New York, 1980.

[50] Q. Zhang, Z. Mo, S. Liu, H. Zhang, Influence of annealing on structure of nylon 11, Macromolecules 33 (2000) 5999–6005. https://doi.org/10.1021/ma000298d.

[51] J.-P. Allen, P. Blondel, P. Douais, Process for increasing the melting point and the melting enthalpy of polyamides by water treatment, 1413595B1 (2003), Arkema.

[52] A.M. Rhoades, N. Wonderling, C. Schick, R. Androsch, Supercooling-controlled heterogeneous and homogenous crystal nucleation of polyamide 11 and its effect onto the crystal/mesophase polymorphism, Polymer 106 (2016) 29–34. https://doi.org/10.1016/j.polymer.2016.10.050.

[53] J.D. Menczel, R.B. Prime, Thermal analysis in polymers, Wiley, Oxford, 2009.

[54] L. Chocinski-Arnault, V. Gaudefroy, J.L. Gacougnolle, A. Rivière, Memory effect and crystalline structure in polyamide 11, J. Macromol. Sci., Part B 41 (2002) 777–785. https://doi.org/10.1081/MB-120013064.

[55] S. Mori, H.G. Barth, Size exclusion chromatography, Springer, Berlin Heidelberg, 2013.

[56] S. Podzimek, T. Vlcek, Characterization of branched polymers by SEC coupled with a multiangle light scattering detector. II. Data processing and interpretation, J. Appl. Polym. Sci. 82 (2001) 454–460. https://doi.org/10.1002/app.1871.

[57] S. Podzimek, The use of GPC coupled with a multiangle laser light scattering photometer for the characterization of polymers. On the determination of molecular weight, size and branching, J. Appl. Polym. Sci. 54 (1994) 91–103. https://doi.org/10.1002/app.1994.070540110.

[58] H. Zarringhalam, C. Majewski, N. Hopkinson, Degree of particle melt in nylon-12 selective laser-sintered parts, Rapid Prototyp. J. 15 (2009) 126–132. https://doi.org/10.1108/13552540910943423.

[59] S.J.A. Hocker, W.T. Kim, H.C. Schniepp, D.E. Kranbuehl, Polymer crystallinity and the ductile to brittle transition, Polymer 158 (2018) 72–76. https://doi.org/10.1016/j.polymer.2018.10.031.

[60] S. Maïza, X. Lefebvre, N. Brusselle-Dupend, M.-H. Klopffer, L. Cangémi, S. Castagnet, J.-C. Grandidier, Physicochemical and mechanical degradation of polyamide 11 induced by hydrolysis and thermal aging, J. Appl. Polym. Sci. 136 (2019) 47628. https://doi.org/10.1002/app.47628.

[61] O. Okamba-Diogo, Thermo-oxydation des polyamides. Dissertation, 2015.

[62] EOS, Polyamid 11 Nylon: Nylon im 3D-Druck - Ersatz für ABS oder PA6, https://www.eos.info/de/additive-fertigung/3d-druck-kunststoffe/polymer-material-werkstoffe/pa-11-nylon-3d-druck-abs, accessed 17 July 2020.

4.4.6 Supporting information

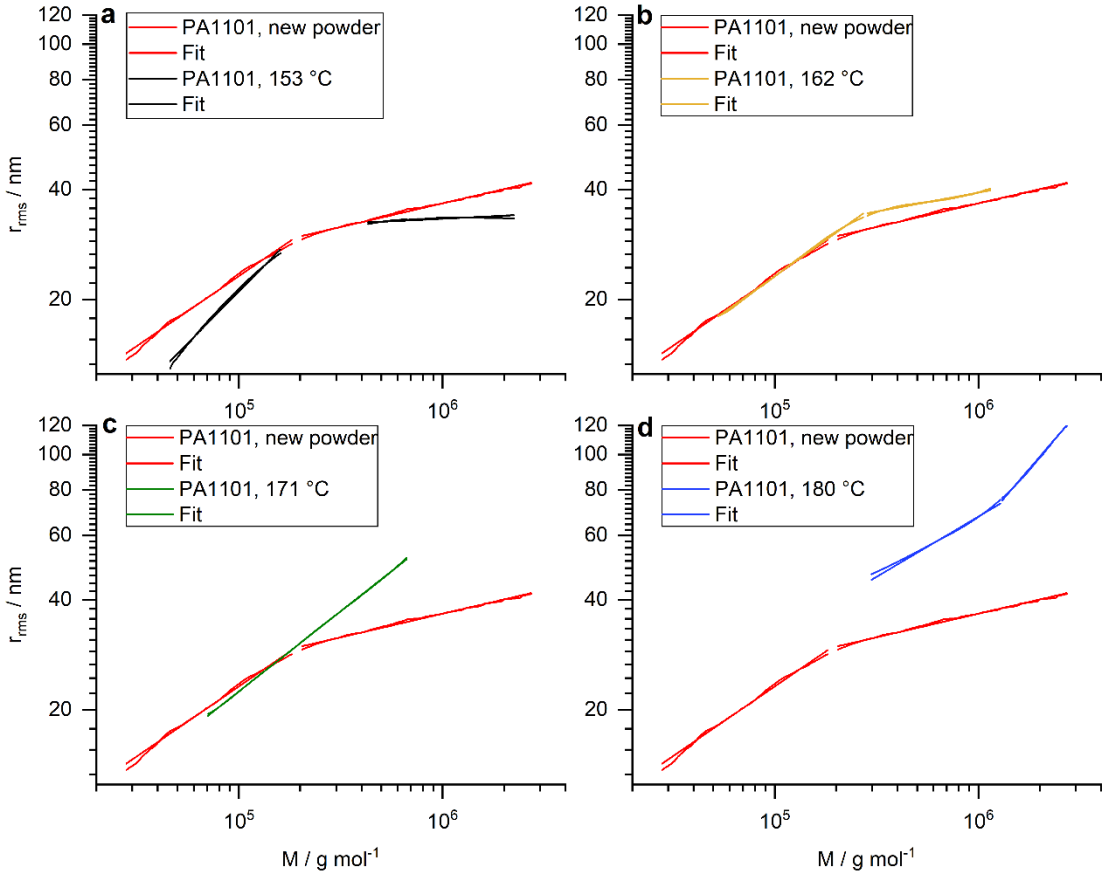

Figure 4.4.10 Conformation plots of PA 1101 virgin powder in comparison to powder tempered at different temperatures for 8 h under a N_2 gas flow of 10 mL min^{-1}; **a** 153 °C, **b** 162 °C, **c** 171 °C, and **d** 180 °C. The different slopes are depicted in Table 4.4.6.

Table 4.4.6 Slopes of the conformation plots according to Figure 4.4.10. In addition, the range of the fit is depicted, respectively.

Corresponding figure	aging conditions	M /g mol^{-1}	slope /g mol^{-1} nm^{-1}
a-d	virgin powder	$2.8 \cdot 10^4$-$1.8 \cdot 10^5$	0.38
		$2.1 \cdot 10^5$-$2.7 \cdot 10^6$	0.13
a	153 °C, 8 h	$4.6 \cdot 10^4$-$1.6 \cdot 10^5$	0.56
		$4.3 \cdot 10^5$-$2.2 \cdot 10^6$	0.03
b	162 °C, 8 h	$5.3 \cdot 10^4$-$2.7 \cdot 10^5$	0.40
		$2.9 \cdot 10^5$-$1.1 \cdot 10^6$	0.10
c	171 °C, 8 h	$7.1 \cdot 10^4$-$6.7 \cdot 10^5$	0.44
d	180 °C, 8 h	$3.0 \cdot 10^5$-$1.3 \cdot 10^6$	0.65
		$1.3 \cdot 10^6$-$3.8 \cdot 10^6$	0.33

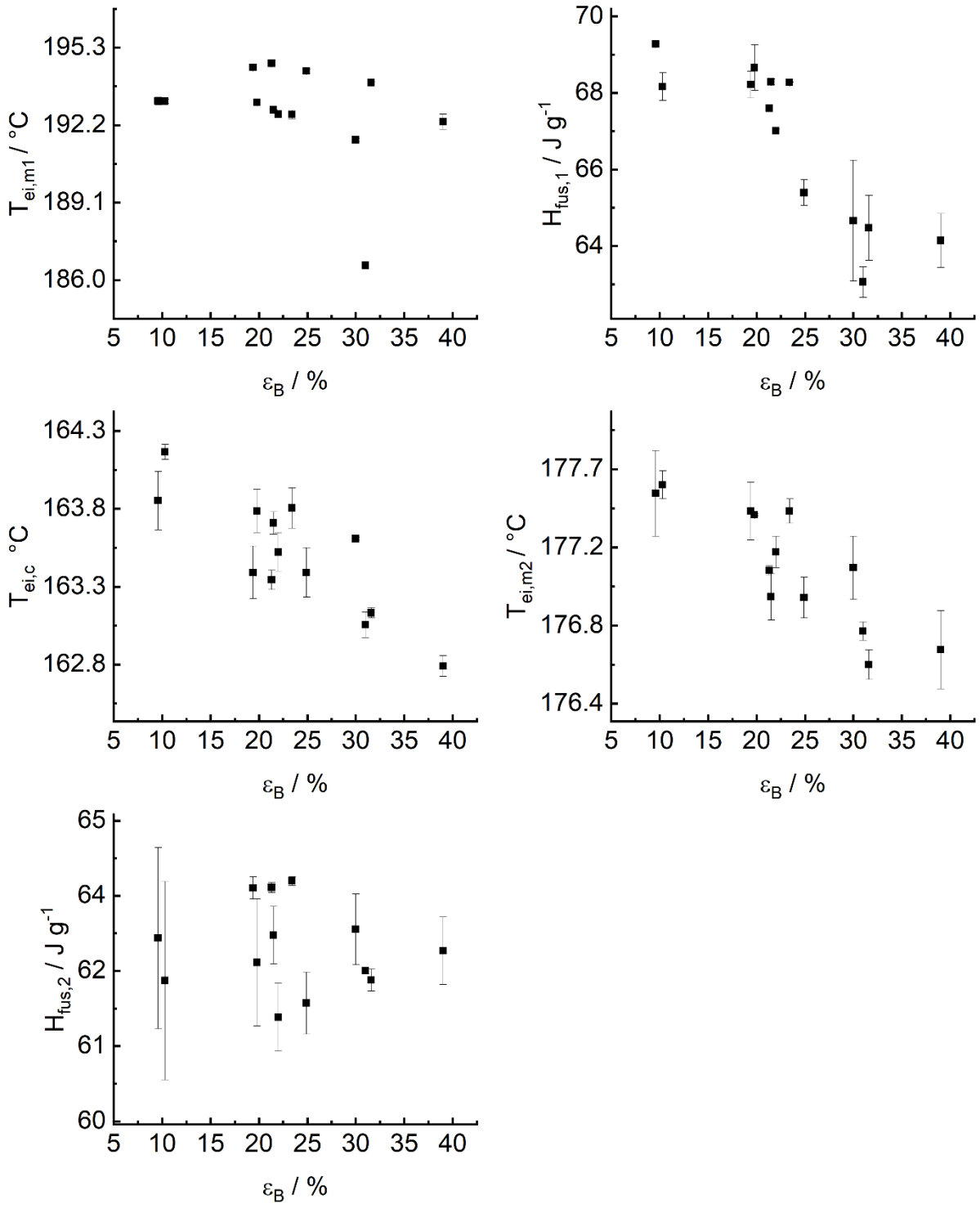

Figure 4.4.11 Overview of different tensile bars and their corresponding elongation at break ε_B values for the melting onset of the first heating run $T_{ei,m1}$, the melting enthalpy of the first heating run $H_{fus,1}$, the crystallization onset of the cooling run $T_{ei,c}$, the melting onset of the second heating $T_{ei,m2}$, and the enthalpy of melting of the second heating run $H_{fus,2}$ are depicted.

	A	B	C	D	E	F	G	H	I
1									
2		H: 22%						K: 30%	
3									
4						J: 24.9%	F: 21.3%		
5	I: 23.4%								
6							M: 31.6%		
7					A: 39%				
8								D: 19.4%	
9	E: 19.8%		L: 31%						B: 10.3%
10									
11									
12	C: 9.6%								
13									
14									
15									
16				G: 21.5%					

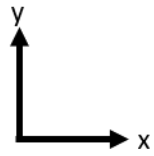

Figure 4.4.12 Scheme of the location and position of each tensile bar in the build chamber of the laser sintering machine. The tensile bars were labeled with their ε_B values. The tensile bars were built in z-direction.

4.5 Investigations of polymer samples of polyamide 11 concerning the content of monomer, oligomers, and the oxidation stabilizer Irganox 1098 by utilizing inverse gradient HPLC in combination with a triple detection system (diode array detection / mass spectrometry / charged aerosol detection)

This subchapter was published in the journal *Talanta Open*. The layout specifications of the journal were changed for uniformity. The corresponding text is adapted from:

B. Scherer, F.-M. Matysik, *Talanta Open* **2021**, 3, 100023.

Abstract

The aim of this work was to develop a method to comprehensively characterize extracts from polyamide 11 powder samples used in the laser sintering process. Firstly, high-resolution mass spectrometry was applied to identify low molecular weight compounds in the material. Secondly, by means of an inverse gradient high-performance liquid chromatography (HPLC) in combination with a triple detection system consisting of a diode array detector (DAD), a mass spectrometer (MS), and a charged aerosol detector (CAD), a method was established to determine the amount of monomer and oligomers up to the linear tetramer and cyclic pentamer. Furthermore, the oxidation stabilizer identified as Irganox 1098 was determined. The DAD was utilized for the quantification of the UV-active oxidation stabilizer. Thus, to be able to extract the low molecular weight compounds, various protocols were studied and finally accelerated solvent extraction was used. As there is a lack of commercial standards of polyamide 11 related oligomers, these compounds were detected with the CAD, taking advantage of its uniform response behavior in conjunction with an inverse gradient HPLC protocol. In addition, the MS was utilized as a qualitative detector for peak identification. The information regarding low molecular weight compounds are required as the powder is subject to the thermal loading of the sintering process, which influences the composition of the low molecular weight compounds. Thus, the method was applied to new and oven-aged polyamide 11 samples. Finally, it was possible to monitor the change of low molecular weight compounds in stressed polyamide 11 powder samples.

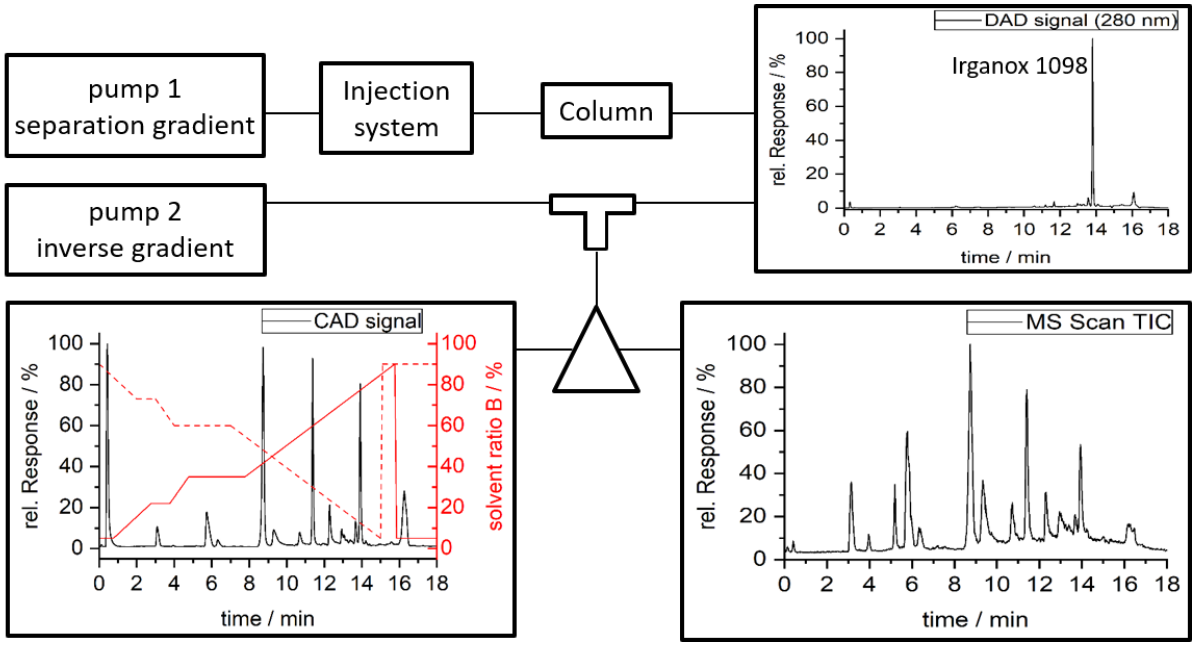

Graphical Abstract: Scheme of the inverse gradient HPLC with the triple detection system.

4.5.1 Introduction

Polyamide 11 derives from renewable raw materials and is thus classified as biobased polymer based on its monomer, 11-aminoundecanoic acid (AUA), which is synthesized from castor oil. The polymeric material is formed via polycondensation [1]. Polyamide 11 is utilized in various products, such as pipelines for oil and gas, textiles, wires, cables, and 3D-printed parts [2–5].

Within the field of additive manufacturing, selective laser sintering is one of the most established and widely used processes. Complex 3D objects are built by selectively and successively fusing layers of powdered material [6]. The building process is performed under inert gas (N_2) and consists of four iterative steps [7]: Firstly, lowering of the building platform by one layer thickness, followed by, secondly, the application of one layer of powder. Thirdly, the applied powder layer is heated up to processing temperature and, finally, the powder particles are selectively melted by a CO_2 laser in the area where needed [8]. Within selective laser sintering, semi-crystalline thermoplastic polymers, such as polyamide 11 and 12 are well established [7]. Especially polyamide 11 offers advantages like high- and low-temperature performance, chemical resistance and high part ductility compared to polyamide 12 [2, 4]. As thermal and thermo-oxidative aging can cause embrittlement resulting in deterioration of the mechanical properties, different additives are added to improve those properties and extend

the range of usability. In literature, a distinction is made between thermal and thermo-oxidative degradation. In practice however, mostly an overlay of these degradation types occurs [9]. Metal salts, phenolic antioxidants, aminic antioxidants, and phosphites are applied individually or in combination to delay aging of polyamides by inhibiting autoxidation [10, 11]. The antioxidants either stop the radical chain reaction or suppress the branching of the reaction by scavenging reactive radicals or by chemically binding the reactive peroxide oxygen. Thus, stabilizer depletion is typically observed [9]. Sterically hindered phenols as classical radical scavengers are the most commonly applied group of heat stabilizers and are utilized in concentrations between 0.25% and 0.75% [9, 10].

Besides different additives, certain amounts of linear and cyclic monomers, and oligomers are present in the product based on the polymerization of polyamide 11 [10]. After synthesis, polyamides contain up to 2% cyclic oligomers [12]. Polyamide 6 is an exception containing 9% - 12% cyclic oligomers without post-treatment of the polymer, such as hot water or vacuum extraction [12]. In general, low molecular weight components influence the processability of the powder by lowering the viscosity of the polymer melts [10]. Consequently, the determination of those compounds is required to detect changes in the polymer and to evaluate the influences on the laser sintering process. Moreover, information on the stabilizer depletion is necessary to identify the main mechanism of stabilizer loss and estimate the remaining lifetime [13, 14].

Related to investigations on oligomers, Zahn and Kunde [15] identified and synthesized the cyclic dimer and cyclic trimer of polyamide 11. Furthermore, the lactam of AUA was extracted from the technical polycondensate “Rilsan” utilizing glacial acetic acid [15]. The method of Mori and Furusawa [16] revealed quantitative results of the cyclic monomers and the individual cyclic oligomers contained in polyamide 6, 66, and 12. For this purpose, the monomers and oligomers were reduced to the corresponding cyclic monoamines and oligoamines by means of $LiAlH_4$, followed by gas chromatography of the amines. In [17], a simple method was developed to determine cyclic oligomers of ε-caprolactam by applying high-performance liquid chromatography (HPLC) and UV-detection. Additionally, this method was applied for the determination of oligomers of laurolactam up to the hexamer [17]. Moreover, a method for quantification of cyclic oligomer content in polyamide materials was introduced using HPLC coupled to a chemiluminesence nitrogen detector in combination with single-substance calibration. The method was applied for the quantification of cyclic oligomers in several polyamide granulates of polyamide 6 and 66 [12]. Further oligomer determinations are described elsewhere [18–23]. Unfortunately, oligomers of polyamide 11 are not commercially available. Consequently, it is not possible to establish external calibration curves for those compounds.

In this context, aerosol techniques as for instance charged aerosol detection (CAD) come into play. They are described as “universal” as they provide an almost uniform response dependent on the mass of the compound irrespective of molecular structures at constant mobile phase conditions. The possibility to obtain uniform response for different compounds enables the quantification of multiple compounds with a single calibrator [24, 25]. This method is typically applied in pharmacy to determine impurities in drugs [26]. The most common HPLC detectors, UV and MS, exhibit non-uniform response behavior which is based on different extinction coefficients and ionization efficiencies caused by the individual chemical structures of the analytes [27].

Samples which consist of nonvolatile compounds are reliably detected via CAD. They typically exhibit properties of a boiling point higher than 400°C [28, 29], a molecular weight higher than 350 g mol^{-1}, and an enthalpy of vaporization higher than 65 kJ mol^{-1} [30]. However, these parameters should not be considered as strict boundaries as the transitions are smooth including unexpected outliers. Moreover, the response behavior of analytes capable of ion pair formation can be increased by the addition of mobile phase additives resulting in salt formation. This can be utilized practically to convert semi-volatile compounds into nonvolatile ones, as the detector response increases proportionally according to the additional molar mass of the counter ion upon salt formation [31]. Solvent gradients, analyte volatility, salt formation, and analyte density are the factors that influence the response behavior of analytes. Among them, analyte density has shown to have only minor and solvent composition to have most influence [24]. The organic content of the mobile phase affects the transport efficiency of the nebulizer and the PSD of the droplets and thus the number of particles reaching the detection chamber [32]. The approach called inverse gradient, applied as post column addition of solvent components, is one way to establish a constant composition of the mobile phase entering the CAD. Therefore, the exact inverse of the separation gradient is applied after the diode array detector (DAD) which makes a second pump and a T-piece necessary to mix both flowing streams [24, 32]. Consequently, by applying the inverse gradient, advantage of the universal response behavior of the CAD can be utilized to determine low molecular weight compounds even if no analytical standards are available.

By combining the CAD with other detectors such as the DAD and the MS, complementary information about the investigated sample can be revealed within one single measurement. Within this setup, UV-active substances can be analyzed by the sensitive DAD, whereas the MS serves as qualitative detector for substance identification and assures right peak assignment. Consequently, in the assembly of the above mentioned detectors the uniform CAD serves for quantification of unknown substances and substances with missing analytical standards.

In this study, the approach of inverse gradient HPLC in combination with a triple detection system (DAD/MS/CAD) was established and characterized. Furthermore, this concept was utilized to develop a method for determination of remaining monomer and oligomers up to the cyclic pentamer and the oxidation stabilizer in polymer samples of polyamide 11. In addition, the extraction of these low molecular weight compounds from polyamide 11 samples was studied in detail.

4.5.2 Methods and material

4.5.2.1 HPLC-electrospray ionization-quadrupole-time-of-flight mass spectrometry (HPLC-ESI-QTOF) screening measurements

4.5.2.1.1 Sample preparation for HPLC-ESI-QTOF measurements

250 mg of each powder sample were added to 5 mL methanol and sonicated in the ultrasonic bath for 15 min. Afterwards the suspension was filtrated using a MS syringe filter (0.2 µm WWPTFE) from Acrodise (Westborough, USA).

4.5.2.1.2 Instrumentation and measurement conditions

A 1260 Infinity LC system in combination with an electrospray ionization (ESI) source and a 6530 Accurate-Mass QTOF detector from Agilent Technologies (Waldbronn, Germany) were applied. The analytical separation was obtained with a reversed-phase SB-C18 RRHD column (2.1 mm × 150 mm, 1.8 µm) from Agilent Technologies. The injection volume was 1 µL and the flow rate 0.45 mL min^{-1}. The conditions for the chromatographic separation were as follows. Solvent A was 0.02% formic acid (FA) in water and solvent B was acetonitrile/tetrahydrofuran (70:30, v:v). The LC gradient was: 0 min: 95% of solvent A + 5% solvent B, 1 min: 95% A + 5% B, and 15 min: 100% B until 20 min, followed by reconditioning the system by applying initial conditions. The column oven temperature was set to 45 °C and UV/VIS spectra were recorded in the range of 200 nm to 640 nm using the DAD. The ESI source was operated in positive ion mode. Source parameters were 250 °C gas temperature, 8 L min^{-1} drying gas flow, 35 psi nebulizer pressure, 350 °C sheath gas temperature, and 11 L min^{-1} sheath gas flow (N_2). The capillary voltage was set to 3,000 V, the fragmentor voltage was 80 V, and the skimmer voltage was 65 V. MS data were received in the range of 20 *m/z* to 1,500 *m/z* with an acquisition rate of 2 spectra/s and an acquisition time of 500 ms/spectrum. Data evaluation was done applying the Agilent MassHunter Qualitative Analysis Navigator B.08.00 and the Agilent MassHunter Qualitative Analysis Workflow B.08.00 in combination with a database research (Agilent accurate mass personal compound database and library for extractable and leachable components).

4.5.2.2 HPLC-DAD/MS/CAD measurements

4.5.2.2.1 Experimental setup

The HPLC-DAD/MS/CAD measurements were controlled with the software OpenLab CDS Version 2.4 from Agilent. For the separation gradient a 1290 pump (Agilent Technologies) was applied. For the inverse gradient, which was applied post-column after the DAD, a second pump (1200, Agilent) was installed. The injection system, the column oven, and the DAD were 1290 systems as well. A flow splitter (Analytical Scientific Instruments, model-No.: 600-PO10-06) purchased from Thermo Fisher (Germering, Germany) was installed before the MS and CAD. An AD converter (1200 Infinity Universal Interface Box II, Agilent Technologies) was used to integrate the CAD signal into the OpenLab software. For all separations the reversed phase column Eclipse Plus RRHD C18 (2.1 mm × 50 mm, 1.8 µm) from Agilent was used. The DAD recorded UV spectra in the range of 190 to 400 nm in steps of 2 nm, whereas the Irganox 1098 signal was quantified at the absorption maximum of 280 nm. The MS signals were recorded using the single quadrupole 6130 LC-MS system in combination with an ESI source from Agilent. The gas temperature was 250 °C, the gas flow was adjusted to 7.0 L min^{-1}, the nebulizer pressure was 40 psi, and the capillary voltage was set to 4,000 V. Fragmentation voltages were 135 V for positive and negative scan (dwell time 200 ms), 160 V for Irganox 1098 (dwell time 10 ms), and 70 V for all other compounds (dwell time 10 ms, respectively). The CAD was a Corona Veo purchased from Thermo Fisher Scientific Dionex (Germering, Germany). For best signal quality, the evaporation temperature was set to 35 °C and the filter constant to 3.6 s. The power function value was set to 1.0 and a data collection rate of 20 Hz was applied. The scheme of the overall setup is shown in Figure 4.5.1. The two streams of the mobile phase were combined before the splitter, but after the DAD. The second stream was supplied by the additionally installed pump. Mixing took place in a T-piece. The lines from the two pumps were connected to the opposite arms of the T-piece, and the line to the splitter was connected to the perpendicular arm.

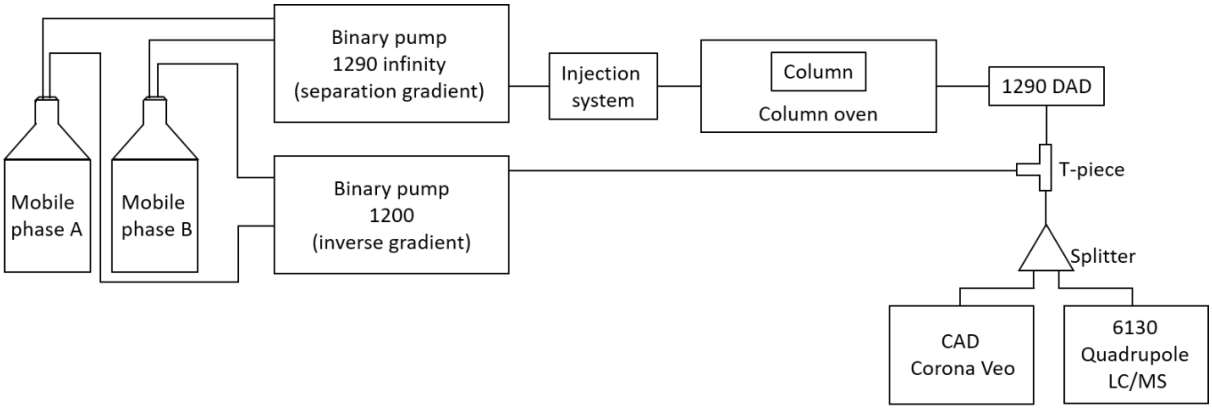

Figure 4.5.1 Scheme of the triple detection system including the separation HPLC gradient, the inverse gradient and a triple detection system with a diode array detector (DAD), a single quadrupole mass spectrometer (MS), and the charged aerosol detector (CAD).

4.5.2.2.2 Determination of the delay volume

The aim of the determination of the delay volume was to ensure proper compensation of the two gradient systems resulting in a constant concentration of the organic solvents in the CAD during analyte detection. The separation column was removed for the determination of the delay volume. The delay volume of the separation column was experimentally determined by using uracil as a non-retarding substance and corresponds to a void volume factor of 0.63. The void volume factor is defined as the ratio between the volumes occupied by the mobile and stationary phase inside the column and represents the total porosity of the interior of the separation column [33]. The calculated term for the void volume was added to the delay of the separation gradient. The volume of the separation and the inverse gradient was determined individually, respectively. The gradients were run at 100% A at a flow rate of 0.45 mL min^{-1}, followed by a short pulse (about 3 s) to 100% B and back. A signal rise and fall was observed after a certain time and the duration from the pulse of eluent B to the peaks' apex was determined, respectively. By subtracting the volumes of the separation and the inverse gradient, the delay volume for the analytical gradient was calculated. The analytical gradient was programmed for a delay equivalent to 341 µL which equals a delay time of 0.76 min to ensure a constant content of the organic components in the mobile phase in the CAD.

4.5.2.2.3 Verification of the determined delay volume

An additional experiment was conducted to verify the determination of the delay volume (see section 4.5.3.2.2 for results). In this context, the organic mobile phase B (MeOH/ACN/THF (30:30:40) +0.02% FA) further contained 0.05 mg mL^{-1} uracil. Measurements were conducted without injection of any sample solution. Firstly, the system was solely run applying the separation gradient. Secondly, the inverse gradient compensation was applied. The CAD

signal and the MS signal of uracil were recorded (*m/z* 113) applying ESI in positive mode. The fragmentor voltage was set to 70 V and the dwell time was 25 ms.

4.5.2.3 Extraction procedures

4.5.2.3.1 Ultrasonic extraction

The amount of powder sample was weighed (about 0.6 g) and a defined volume of 5 mL MeOH was added. Afterwards, the sample was sonicated in the ultrasonic bath for at least 15 min, followed by filtration using a 0.2 µm PTFE syringe filter from VWR.

4.5.2.3.2 Soxhlet extraction

For the Soxhlet extractions the automated extraction system B-811 from Büchi (Essen, Germany) was applied. The extraction was programmed for 40 cycles and the heat rate was adjusted to the properties of the chosen extraction solvents according to the user manual provided by the manufacturer [34]. An amount of powder of 0.6 g (the exact quantity was noted) was filled into extraction thimbles (603 Standard Cellulose Extraction Thimbles) manufactured from high-quality cellulose with a size of 33 mm x 94 mm from VWR (Darmstadt, Germany), respectively. The cooling system was a recirculating chiller F-114 from Büchi.

4.5.2.3.3 Accelerated solvent extraction (ASE)

For accelerated solvent extraction the ASE 200 accelerated solvent extractor from Dionex (Dreieich, Germany) was applied. Extraction conditions were as follows. The sample was preheated for 5 min at 80 °C. The sample was loaded into an extraction cell with a volume of 11 mL together with Ottawa sand and sodium sulphate. The solvent was pumped into the preheated cell. The extraction was conducted under a pressure of 1,500 psi. After the static extraction time of 1 min, the cell was flushed with 150% of its volume and purged for 60 sec. The procedure was repeated three times and the extracts were collected.

4.5.2.4 Chemicals

For HPLC-ESI-QTOF measurements all solvents were LC-MS grade. All solvents used in further experiments were HPLC grade. ACN, MEOH, and non-stabilized THF were purchased from Merck (Darmstadt, Germany) and used without further purification. FA (98-100%) and heptafluorobutyric acid (HFBA) (for synthesis) were also acquired from Merck. Trifluoroacetic acid (TFA) (HiPErSolv CHROMANORM) was used with 100% purity and was purchased from VWR (Darmstadt, Germany). Sodium sulphate anhydrous, obtained from VWR, was of analytical grade and Ottawa sand, (Resprop, size 20/30 Mesh) was purchased from Restek (Bad Homburg v. d. Höhe, Germany). Furthermore, uracil of analytical grade was from Fluka

(Buchs, Schweiz) and AUA from Sigma-Aldrich with a purity of 97%. Irganox 1098 was obtained from BASF (Ludwigshafen, Germany).

4.5.2.5 Polymer samples

The polyamide 11 powder PA 1101 from EOS (Krailling, Germany), which is commonly applied in the laser sintering process, was used. Moreover, the powder was aged under the conditions given in Table 4.5.1. An amount of 1 g powder was filled in an aluminum crinkle and inserted into a Micro-Chamber M-CTE250 (Markes, Offenbach am Main, Germany) at fixed temperatures (153, 162, 171, and 180 °C). The temperature was checked with a calibrated RS 1316 dual data logger thermometer. All powder samples were aged applying a nitrogen gas flow and a compressed air gas flow of 10 ml min^{-1}, respectively. Aging durations of 8 and 24 h were chosen. The samples were cooled in the chamber to 40 °C and afterwards stored in argon atmosphere.

Table 4.5.1 Aging conditions of PA 1101 powder samples.

Temperature of heat treatment / °C	Durations of heat treatment / h		Aging under nitrogen gas flow (10 mL min^{-1})	Aging under compressed air gas flow (10 mL min^{-1})
153	8	24	yes	yes
162	8	24	yes	yes
171	8	24	yes	yes
180	8	24	yes	yes

4.5.2.6 Sample processing for quantitative investigations

All samples, extracted with Soxhlet or ASE, were processed in the same way. The extraction solvent was evaporated using a Syncore system together with the Vacuum Pump V-700 and the Vacuum Controller V-855 from Büchi. Afterwards the samples were stored in the vacuum drying oven from Binder (Tuttlingen, Germany) for at least 12 h at 40 °C to ensure the completeness of solvent evaporation. 5 mL of (MeOH +0.02% FA) were added to the dried extracts. Mixing was ensured by applying the Vortex-T Genie 2 (Scientific Industries, Bohemia, USA). After ultrasonification for 15 min, the extracts were cooled down for at least 2 h before filtering. This step was important as it prevents dissolved polymer parts from precipitating after filtration in the HPLC vial. The samples were filtrated using a 0.2 µm PTFE syringe filter and a glass syringe into the HPLC vial. The usage of glass syringes was preferred as disposable plastic syringes showed a blank signal in the CAD.

4.5.3 Results and discussion

4.5.3.1 Qualitative HPLC-ESI-QTOF screening measurements

The qualitative investigations on PA 1101 powder were started in terms of characterizing the methanol extracts of virgin powder by high-resolution mass spectrometry. For this purpose, the prepared methanol extracts (see section 4.5.2.1.1 for sample preparation) were measured by HPLC in combination with positive ESI-QTOF mass spectrometry. The corresponding total ion chromatogram (TIC) recording is illustrated in Figure 4.5.2 a. An overview of detected monomers, oligomers, and oxidation stabilizer together with their molecular structures is shown in Figure 4.5.2 b-l. All masses were extracted in the form of $[M+H]^+$ with a mass range interval of ± 100 ppm. The linear oligomers eluted before the cyclic ones, which is caused by higher hydrophilicity of the linear forms. The signal of AUA (*m/z* 202.180) is depicted in Figure 4.2.5 b and was found in intensities of $4 \cdot 10^6$ counts as it is the monomer of the polymerization process. Additionally, the cyclic monomer (*m/z* 184.170) was detected (compare Figure 4.5.2 c). Within the EIC of the cyclic dimer (e), however, two peaks were detected starting with the first peak at the retention time of the aminoundecanolactam. Thus, the aminoundecanolactam could also form the cyclic dimer during the ionization process in the ESI chamber. The oligomers were able to be detected up to the linear and cyclic pentamer with the applied setup. Moreover, a decrease in intensity was observed for the oligomers up to the pentamer and generally the cyclic oligomers showed higher intensities compared to the linear forms. However, all the detected oligomer compounds are side products of the polymerization process [10]. Additionally, an overlay of some oligomers was observed. The cyclic dimer showed an overlay with the linear trimer, the cyclic trimer an overlay with the linear tetramer, and the cyclic tetramer with the linear pentamer. Consequently, further method development was needed to achieve a complete separation by HPLC to be able to establish quantitative determination of those compounds. In Figure 4.5.2 l the EIC of the identified oxidation stabilizer Irganox 1098 is depicted. Its identity could be proven by comparison of the UV-spectra and the retention time of a reference standard. Irganox 1098 is typically used for polyamide stabilization as its amide functions provide compatibility with the polymer matrix [35]. Furthermore, it improves the long-term stability of the polymer which is a key factor for the application in the selective laser sintering process based on the thermal loading during the process. Moreover, material is recycled and reused in the process. Hence, long-term stability is also an important factor [11, 36, 37].

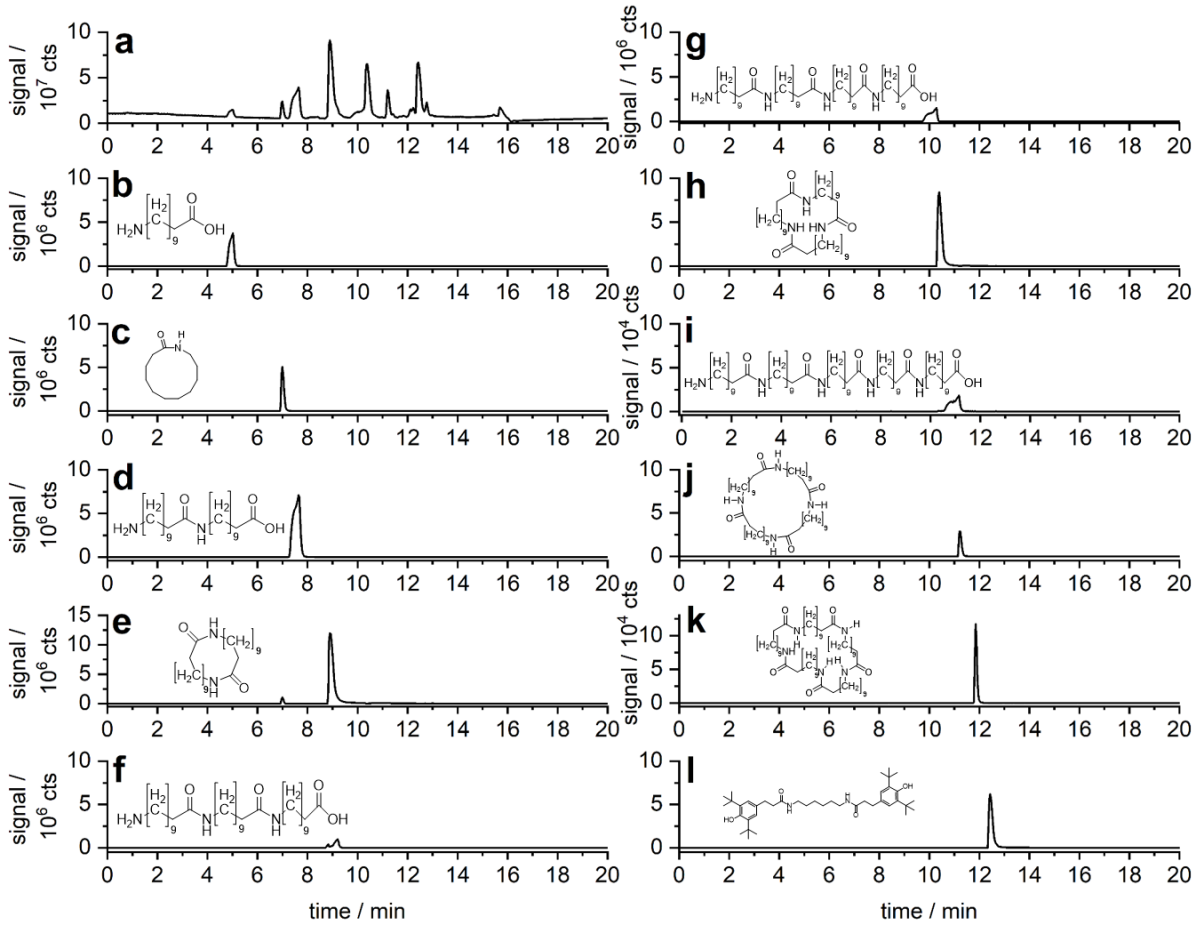

Figure 4.5.2 a, Total ion chromatogram (TIC) of a methanol extract of new PA 1101 powder. The extracted ion chromatogram (EIC) traces of the monomers, oligomers, and the oxidation stabilizer are depicted: **b**, aminoundecanoic acid (*m/z* 202.180); **c**, aminoundecanolactam (*m/z* 184.170); **d**, linear dimer (*m/z* 385.343); **e**, cyclic dimer (*m/z* 367.332); **f**, linear trimer (*m/z* 568.505); **g**, linear tetramer (*m/z* 751.667); **h**, cyclic trimer (*m/z* 550.494); **i**, linear pentamer (*m/z* 934.829); **j**, cyclic tetramer (*m/z* 733.657); **k**, cyclic pentamer (*m/z* 916.819); **l**, Irganox 1098 (*m/z* 637.494). The EIC traces were extracted with a mass range interval of ± 100 ppm.

4.5.3.2 Method development for chromatographic separation of polyamide 11 related monomers, oligomers, and the oxidation stabilizer Irganox 1098

4.5.3.2.1 Optimization of chromatographic separation

The aim was to obtain best possible resolution by optimizing the separation gradient. Therefore, the chromatographic method of the qualitative investigations was used as starting point. Samples were prepared as described in section 4.5.2.3.1. Firstly, the method was transferred to the HPLC-DAD/MS/CAD system by applying a reversed phase Eclipse Plus C18 column. As a result, insufficient separation of the linear trimer and the cyclic dimer was obtained. Furthermore, an impurity identified as a degradation product of Irganox 1098 [38] was not baseline separated from the oxidation stabilizer itself. In a second step, several experiments were conducted to optimize the analytical separation. Moreover, different

compositions of the organic mobile phase were tested on trial as coelution was still a problem. A mixture of methanol and tetrahydrofuran resulted in separated peaks of the cyclic dimer and the linear trimer. However, the cyclic trimer and the linear tetramer showed co-elutions. Consequently, a mixture of methanol, acetonitrile and tetrahydrofuran was applied and showed the best results. Within method development, the MS was solely used for peak identification to assure correct peak assignment in all experiments. The optimized gradient protocol and the corresponding chromatogram are depicted in Figure 4.5.3. The composition of the organic mobile phase was adjusted to methanol/acetonitrile/tetrahydrofuran (30:30:40, v:v:v) with an injection volume of 1 µL of sample solution. Furthermore, the column oven temperature was set to 30°C. The modified eluent B and the optimized gradient program led to complete separation of the linear trimer and cyclic dimer. Moreover, the impurity 2 was separated from Irganox 1098. Unfortunately, aminoundecanolactam could not be detected by CAD due to too high volatility and low molecular weight [24].

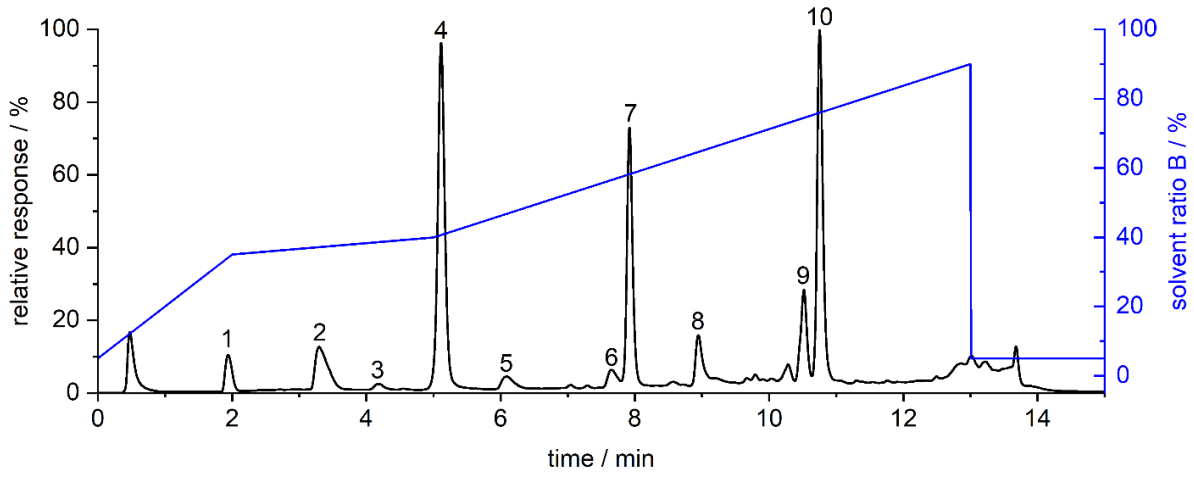

Figure 4.5.3 Optimization of the separation gradient program and the organic mobile phase composition for the HPLC-DAD/MS/CAD determination of (1) aminoundecanoic acid, (2) linear dimer, (3) impurity 1, (4) cyclic dimer, (5) linear trimer, (6) linear tetramer, (7) cyclic trimer, (8) cyclic tetramer, (9) impurity 2, (10) Irganox 1098. A reversed phase Eclipse Plus C18 column was used; eluent A was H_20 + 0.02% FA, and eluent B methanol/acetonitrile/tetrahydrofuran (30:30:40, v:v:v). The CAD recording is depicted.

A prerequisite for quantitative determination of the linear monomer, the oligomers, and the Irganox 1098 is the quantification by external calibration with analytical standards. However, standards were available only for AUA and Irganox 1098 but not for the other oligomers. Thus, the next step was to take advantage of the universal response of the CAD. It was aimed to use one calibration curve for the quantification of the linear monomer and polyamide 11 oligomers. Consequently, it was needed to eliminate the dependency of the signal response from the content of the organic components in the mobile phase entering the CAD. Therefore,

in the next step an inverse gradient was applied to be able to draw quantitative conclusions of the oligomer composition in PA 1101.

4.5.3.2.2 Verification of correctness of the determined delay volume

For universal response in the CAD a constant content of the organic components in the mobile phase entering the detector was mandatory during the HPLC experiments. Therefore, the analytical gradient was compensated by combining the effluent flow of the separation column with a mobile phase whose composition was modified through the run as the inverse of the gradient applied for the separation column [32]. For this purpose, the installation of a second pump and an inverse gradient were needed to ensure universal response of the CAD. Thus, in the setup (compare Figure 4.5.1) a T-piece was placed behind the DAD to combine the two effluents. The T-piece was positioned after the DAD to prevent broadening and dilution of the DAD signal caused by the doubled flow through the measuring cell. Figure 4.5.4 shows a comparison of the CAD signals resulting from the inverse gradient compensation, and the signal of the analytical gradient without gradient compensation using uracil as a marker in the organic mobile phase representing the content of eluent B in the combined flowing stream. This configuration was applied to all quantitative determinations in this work. While the response of uracil in the run without the compensation gradient increased with an increasing organic content in the mobile phase, the signal remained practically constant in the run with compensation. Consequently, the proposed method including the experimentally determined delay volume worked efficiently and formed the basis for a uniform response behavior in the CAD.

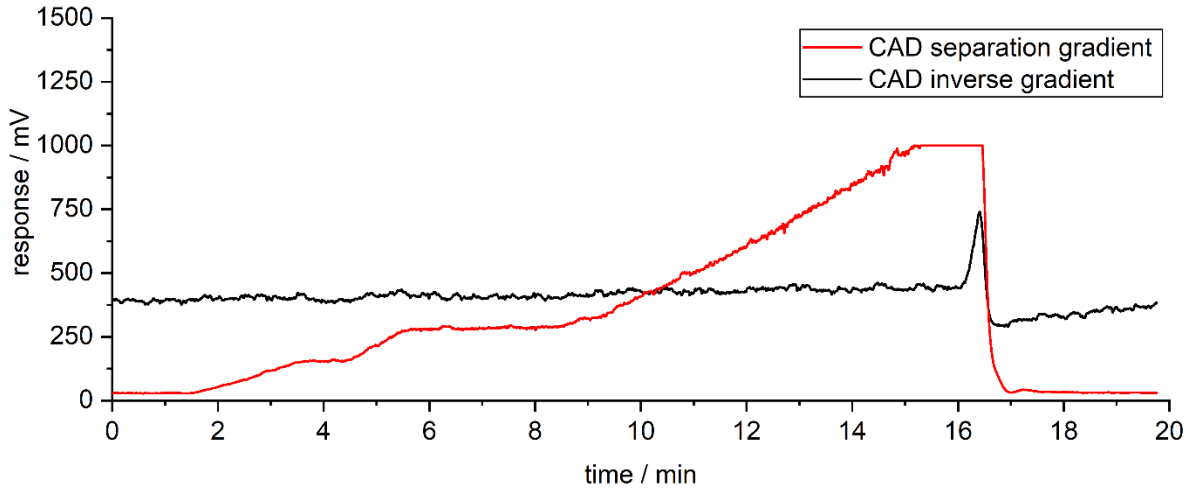

Figure 4.5.4 CAD recordings of uracil added as a marker to the organic mobile phase component (eluent B) at a concentration of 0.05 mg mL^{-1}. The recording for the analytical gradient without (red trace) and with inverse gradient (black trace) application are shown for separation conditions as specified in section 4.5.3.4.

4.5.3.2.3 Final optimization of the chromatographic separation applying the inverse gradient

After implementation of the inverse gradient, the delay volume had to be integrated into the separation gradient. The separation gradient was programmed for a delay equivalent to 341 µL which equaled an isocratic period of 0.76 min after injection to ensure a constant content of organic solvents in the CAD. Furthermore, 0.02% FA was added to eluent B resulting in a final composition of methanol/acetonitrile/tetrahydrofuran (30:30:40, v:v:v) + 0.02% FA. In addition, the injection volume was doubled to 2 µL. This led to a more pronounced signal for the cyclic pentamer (labeled with number 11 in Figure 4.5.5). However, the delay time, which was needed to adjust the two gradient systems to each other, affected the chromatographic separation negatively, which is shown in Figure 4.5.5 a and b. The isocratic period of 0.76 min lead to an overlay of the cyclic dimer and linear trimer. Moreover, an overlay of the linear dimer and cyclic monomer was observed in the MS traces. Consequently, the analytical gradient again had to be optimized. Additionally, the temperature of the column oven was lowered to 25 °C as this change showed a positive effect on the separation.

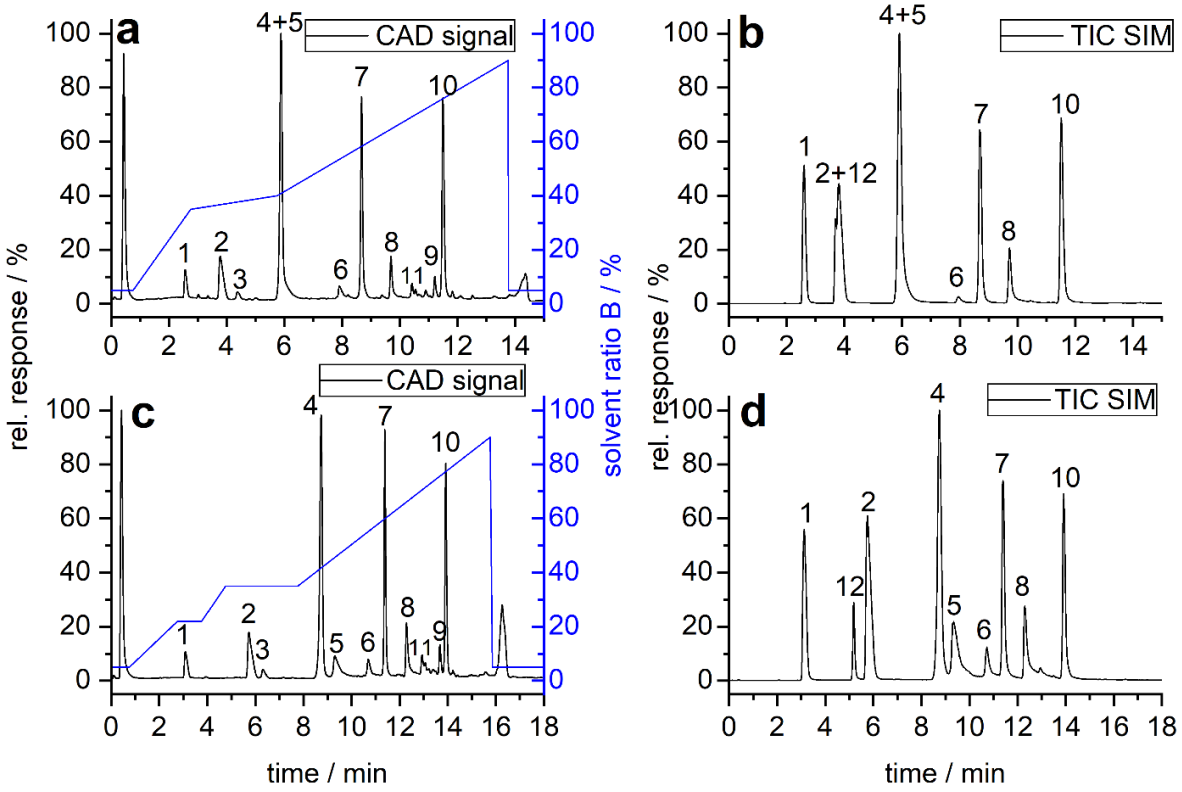

Figure 4.5.5 Transfer of the separation method to the inverse gradient (**a**: CAD signal; **b**: TIC SIM signal). Optimized separation of the oligomers and oxidation stabilizer (**c**: CAD signal; **d**: TIC SIM signal). Detected compounds are (1) aminoundecanoic acid, (2) linear dimer, (3) impurity 1, (4) cyclic dimer, (5) linear trimer, (6) linear tetramer, (7) cyclic trimer, (8) cyclic tetramer, (9) impurity 2, (10) Irganox 1098, (11) cyclic pentamer, and (12) aminoundecanolactam. (3) and (9) were not recorded in SIM mode.

The final separation gradient, the CAD, and MS signals are shown in Figure 4.5.5 c and d. It was possible to detect separate signals of the oxidation stabilizer, linear monomer, oligomers up to the linear tetramer, cyclic pentamer, and some impurities. The established method was applied to all further experiments.

4.5.3.3 Optimization of the extraction procedure

Different extraction solvents were tested regarding Soxhlet extraction of new PA 1101 powder. The aim was to investigate which solvent was able to extract low molecular weight compounds quantitatively. Tested solvents were methanol, methanol/acetonitrile (1:1, v:v), ethanol, ethanol/H_2O (85:15, v:v), ethyl acetate, acetone, and chloroform. Water has shown to be more difficult to be removed during sample processing, which was time-consuming. Methanol showed satisfactory results for AUA, oxidation stabilizer and oligomers up to cyclic pentamer. This was proven by comparison of the two consecutive Soxhlet extractions (first extraction and second extraction) of the same new polyamide 11 powder sample depicted in Figure 4.5.6 a and b. AUA, the linear dimer, the cyclic dimer, and Irganox 1098 could not be detected in the second extraction. Consequently, these compounds were extracted quantitatively with methanol. As an example for an extraction solvent which showed insufficient results, the chromatograms of the extraction with chloroform are depicted in Figure 4.5.6 c and d. Especially in Figure 4.5.6 d it becomes obvious that none of the compounds except impurity 1 could be removed completely, as those peaks could still be detected in the second extraction of the PA 1101 powder material. Thus, methanol was chosen as the extraction solvent of choice. As an efficient alternative to the Soxhlet extraction ASE was used as described in section 4.5.2.3.3. The results of Soxhlet and ASE studies were compared. It can be concluded that the results of Soxhlet extractions are comparable to ASE. However, ASE is much faster than the Soxhlet extraction.

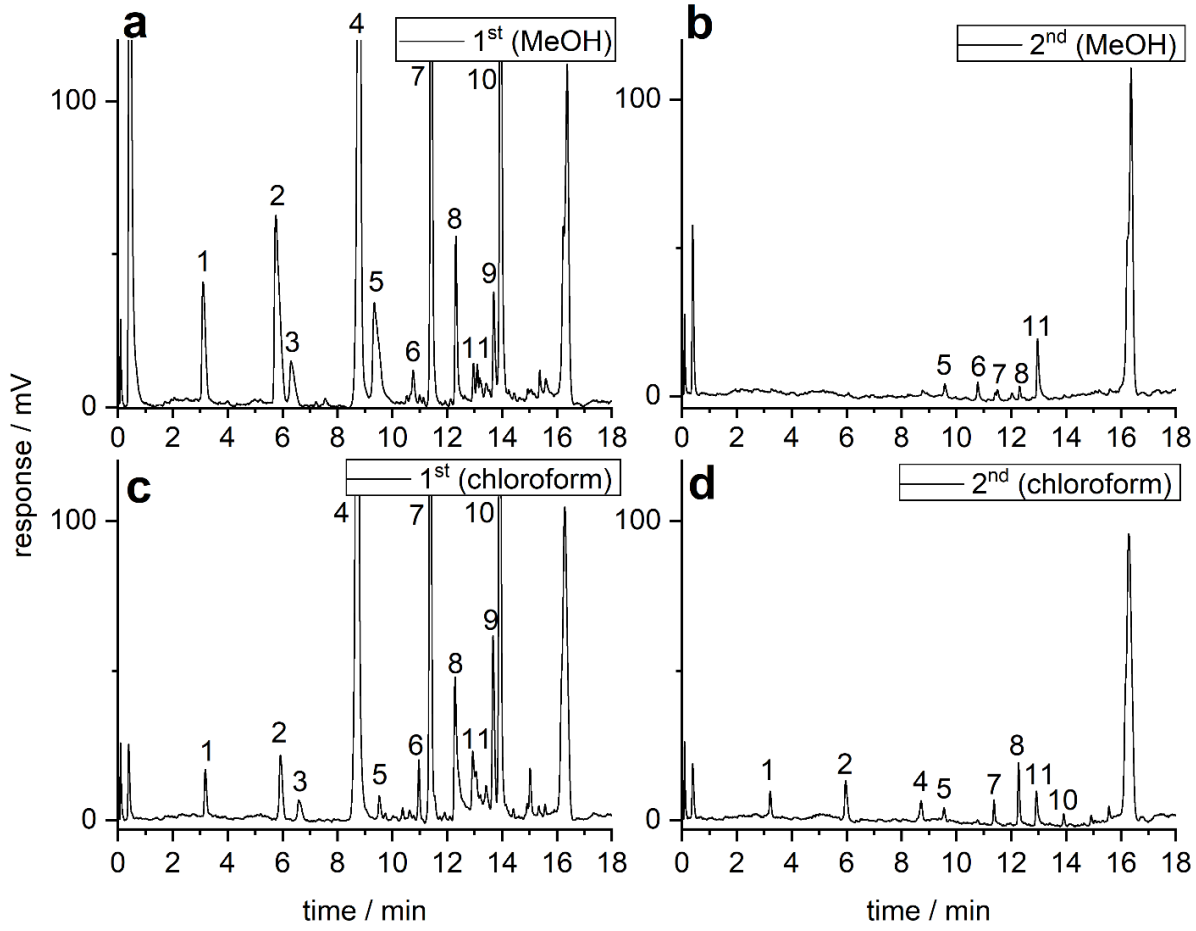

Figure 4.5.6 Comparison of extraction efficiency of two different extraction solvents. One PA 1101 virgin powder sample was extracted twice by Soxhlet extraction with the same extraction solvent. Chromatograms with the CAD signals of the extracts were recorded, respectively: **a**, 1st extraction with methanol; **b**, 2nd extraction with methanol as best extraction solvent; **c**, 1st extraction with chloroform; **d**, 2nd extraction with chloroform as example for a worse extraction solvent. Detected compounds were (1) aminoundecanoic acid, (2) linear dimer, (3) impurity 1, (4) cyclic dimer, (5) linear trimer, (6) linear tetramer, (7) cyclic trimer, (8) cyclic tetramer, (9) impurity 2, (10) Irganox 1098, (11) cyclic pentamer.

4.5.3.4 Determination of low molecular compounds by HPLC-DAD/MS/CAD

4.5.3.4.1 Determination of aminoundecanoic acid, oligomers, and Irganox 1098 via CAD and DAD (280 nm) by application of response factors

Salt formation can be used to transform compounds that behave as semi-volatile ones into more non-volatile ones. Consequently, this can impact the response behavior significantly. As AUA and some of the other oligomers behave as semi-volatile compounds different mobile phase additives, such as FA, TFA, and HFBA were tested to decrease volatility. Such volatile acids are commonly used to control the pH of the mobile phase and to improve peak shape and resolution [24]. These additives can be a source of counter ions for the target analytes. Consequently, salt formation in the aerosol droplets can be realized to establish comparable

response factors to enable quantification. The signal increase is directly depending on the mass of the counter ion for salt formation [25,31]. However, it was not obvious which oligomers would build ion pairs. Consequently, this was checked by the influence of different mobile phase additives on the retention times [24]. In Table 4.5.2 it is shown whether compounds were forming ion pairs or not. The retention times of the oligomers were recorded for the different added ion pair builders and were used as an indicator for salt formation. A shift of retention times based on the formation of ion pairs was observed for all linear oligomers and impurity 1. No shift of retention times of all cyclic oligomers, impurity 2, and Irganox 1098 was obtained. FA was chosen as ion pair building compound as the principle of equal response worked best for FA. Furthermore, the baseline noise was lowest for FA. It increased with the mass of the mobile phase additive and was highest for HFBA. Moreover, the molecular formulas, molar masses, and response factors of the target compounds are given in Table 4.5.2.

Table 4.5.2 Overview of compounds including their molecular formula, mass, calculated response factors, capability of ion pair formation, calculated response factors ($RF_{calc,\ FA}$) with formic acid (FA) as ion pairing substance, and the calculated response factor related to AUA ($RF_{AUA,\ FA}$). Retention times were related to different mobile phase additives such as FA, trifluoracetic acid (TFA), and heptafluorobutyric acid (HFBA).

Compound	Molecular formula	Mass /g mol^{-1}	ion pair formation	$RF_{calc,FA}$	$RF_{AUA,FA}$	RT_{FA}^{*} / min	RT_{TFA}^{*} / min	RT_{HFBA}^{*} / min
aminoundecanoic acid	$C_{11}H_{23}NO_2$	201.31	yes	0.839	1.000	3.2	3.9	5.3
linear dimer	$C_{22}H_{44}N_2O_3$	384.33	yes	0.893	1.064	5.9	6.9	9.0
impurity 1 related to Irganox 1098 [38]	$C_{23}H_{40}N_2O_2$	376.31	yes	0.891	1.062	6.7	8.6	10.0
cyclic dimer	$C_{22}H_{42}N_2O_2$	366.32	no	1.000	1.192	8.8	8.8	8.8
linear trimer	$C_{33}H_{65}N_3O_4$	567.50	yes	0.925	1.102	9.6	10.3	10.8
linear tetramer	$C_{44}H_{86}N_4O_5$	750.66	yes	0.942	1.123	10.8	11.3	11.6
cyclic trimer	$C_{33}H_{63}N_3O_3$	549.49	no	1.000	1.192	11.4	11.4	11.4
cyclic tetramer	$C_{44}H_{84}N_40_4$	732.65	no	1.000	1.192	12.3	12.3	12.3
cyclic pentamer	$C_{55}H_{105}N_5O_5$	915.81	no	1.000	1.192	13.1	13.0	13.0
impurity 2 related to Irganox 1098	$C_{40}H_{64}N_2O_5$	652.48	no	1.000	1.192	13.7	13.7	13.7
Irganox 1098	$C_{40}H_{64}N_2O_4$	636.96	no	-	-	13.9	13.9	13.9

* Retention times are depicted as mean value of three determinations

The factors for response correction were calculated as depicted in the following formula.

$$RF = \frac{Molar\ mass\ (compound)}{\frac{Molar\ mass\ (compound)+molar\ mass\ (formic\ acid)}{Purity\ (compound)}}$$ [31]

The response factors were calculated for all target compounds based on their molar mass and the molar mass of FA. As the quantification of all compounds except the Irganox 1098 was done with the calibration curve of AUA, all response factors were related to the value of the linear monomer. If no ion pair formation was found, then the response factor was set to 1.000. However, this factor was also set into relation to the response factor of AUA for quantitative determinations.

4.5.3.5 Application of the overall analytical protocol to various samples of polyamide 11

4.5.3.5.1 Results of quantitative investigations on new PA 1101 powder

The MS was a helpful tool for the identification of the oligomers. Furthermore, the MS spectra were used in combination with the QTOF measurements for the identification of some impurities. As expected, Irganox 1098 showed signals in the DAD and CAD. The oxidation stabilizer was determined by external calibration using the DAD signal at a wavelength of 280 nm, which corresponds to the absorption maximum. The DAD signal was taken for quantification of Irganox 1098 as it was more sensitive compared to the CAD signal and showed a linear dependency in the relevant concentration range. However, the CAD was applied for quantification of all other compounds due to its universal response behavior. Therefore, the external calibration of AUA with an analytical standard was used for all other oligomers and impurities in terms of quantification. According to literature, the response behavior of non-volatile components is very similar if the mobile phase composition in the detector stays the same during separation [24,39]. However, ion pair formation and corresponding response factors had to be considered [31]. Consequently, the calculated response factors related to AUA were applied for the quantitative calculation of the contents of the oligomers. The results for new PA 1101 powder, the relative standard deviation, the retention times, and the limits of detection are shown in Table 4.5.3. A sum of 1.92% of monomer, oligomers, impurities, and oxidation stabilizer was determined. It became obvious that the quantities of the cyclic dimer, Irganox 1098, and cyclic trimer were the highest with up to 0.79% in virgin powder. Impurities were detected in low amounts of 0.01% (impurity 1) and 0.02% (impurity 2). The linear oligomers were detected in rather low amounts up to 0.09% for the linear dimer.

Table 4.5.3 Overview of low molecular weight compounds determined under conditions of tenfold complete processing of new PA 1101 powder (starting with ASE, processing of the sample, one sample measured three times respectively) and the corresponding relative standard deviation (RSD). Limit of detection (LOD = 3*signal/noise, calculated peak to peak) values were experimentally determined.

Compound	%[a] (powder)	RSD[a] / %	RT[a] / min	$LOD_{CAD/DAD}$[b] / ppm
AUA	0.02	6.8	3.1	6.0
linear dimer	0.09	4.1	5.8	18.7
impurity 1[d]	0.01	30.3	6.5	x [c]
cyclic dimer	0.79	3.6	8.4	15.9
linear trimer	0.06	10.0	9.2	15.0
linear tetramer	0.02	15.8	10.3	9.0
cyclic trimer	0.38	4.7	11.2	46.4
cyclic tetramer	0.07	5.6	12.0	37.6
cyclic pentamer	0.01	12.7	12.7	19.4
impurity 2[d]	0.02	41.8	13.5	x [c]
Irganox 1098[e]	0.55	6.0	13.7	2.7
sum of quantified compounds	1.92	-	-	-

[a] all measurements were done in triplicate for each extraction. The data are presented as the average of 30 measurements from ten extracts (mean value and relative standard deviation (RSD)).
[b] LOD values of AUA (CAD Signal) and Irganox 1098 (DAD signal) were determined by diluting standard solution, LOD of the oligomers (CAD signal) were determined by diluting a PA 1101 sample.
[c] LOD values of the impurities were not determined.
[d] related to Irganox 1098.
[e] quantified by UV signal at 280 nm, all other substances were quantified by their CAD signals.

Additionally, the split ratio of the CAD and the MS detector was determined as (2.66 ± 0.01) which corresponds to a 2.7 fold flow velocity through the CAD compared to MS. Moreover, the peak widths at half maximum of the CAD and MS were compared to each other. The CAD delivered narrower peaks compared to the MS detector although almost thrice of the HPLC flow arrived at the CAD. Comparing the peak widths at half maximum of the Irganox 1098 signal in the DAD and in the CAD, 3.8 s were determined for the DAD signal and 4.3 s for the CAD signal. This indicated that just a minor band broadening was introduced by the combined streams of the analytical and inverse gradients. The peak width at half maximum for the DAD signal was quite low as the T-piece, resulting in a doubled flow, was placed behind the DAD detector. Furthermore, the CAD was taking advantage of that higher flow rate regarding peak widths as the contact time in the detector itself was minimized [40].

4.5.3.5.2 Application of the protocol to aged polyamide 11 samples

PA 1101 powder samples were aged according to conditions given in Table 4.5.1. The aging was conducted to simulate the thermal loading of the laser sintering process for different time periods in different environments. Moreover, the influence on the monomer, oligomer, and stabilizer content was investigated. The results are shown in Figure 4.5.7, Figure 4.5.8, and Figure 4.5.9. Starting points were the values of new PA 1101 powder, respectively. The AUA and linear oligomers (see Figure 4.5.7 a) were found with values up to 0.09% in virgin powder. Under thermal treatment the amount decreased to 0% as the AUA and linear monomers can be implemented into the polymer due to post-condensation processes [37].

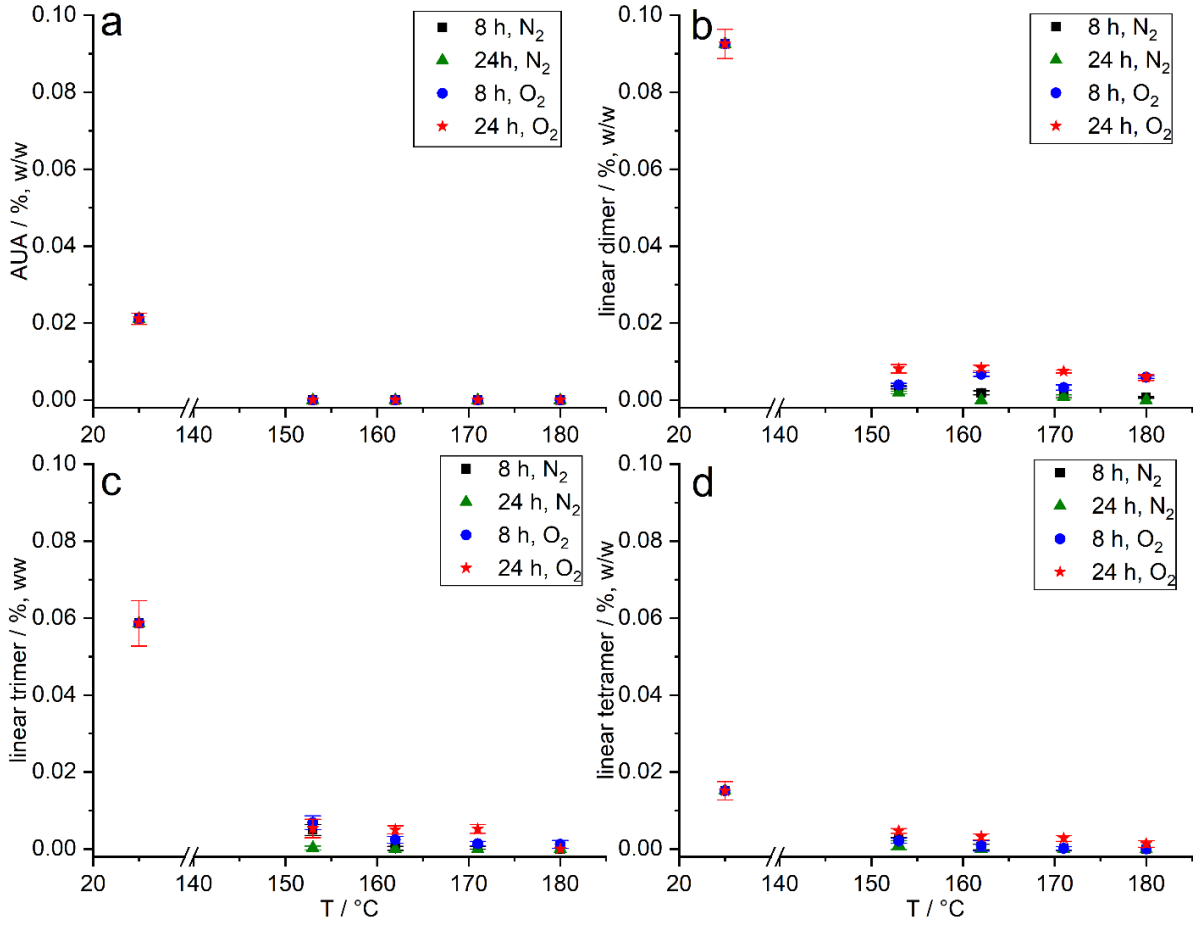

Figure 4.5.7 Change of content of AUA (**a**), linear dimer (**b**), linear trimer (**c**), and linear tetramer (**d**) determined in tempered PA 1101 powder samples.

The cyclic oligomers were present in a higher amount in the PA 1101 samples compared to the linear forms. The content of the cyclic dimer (compare Figure 4.5.8 a) was the highest at 0.79% and remained at a high level even in the aged samples. Moreover, no remarkable difference was observed for samples aged under N_2 and compressed air gas flow. The cyclic trimer (see Figure 4.5.8 c) showed the same tendencies as the cyclic dimer. The cyclic

tetramer showed quite stable values even under thermal treatment for different durations. In Figure 4.5.8 d the cyclic pentamer behaved similar to the cyclic tetramer. It is assumed that the saturation concentration was achieved in methanol resulting in values in the range of 0% and 0.01% for the tempered powders. Furthermore, it must be considered that the oligomers from the linear trimer up to the cyclic pentamer were not extracted quantitatively and traces could be detected in the 2nd Soxhlet extraction (compare Figure 4.5.6 b).

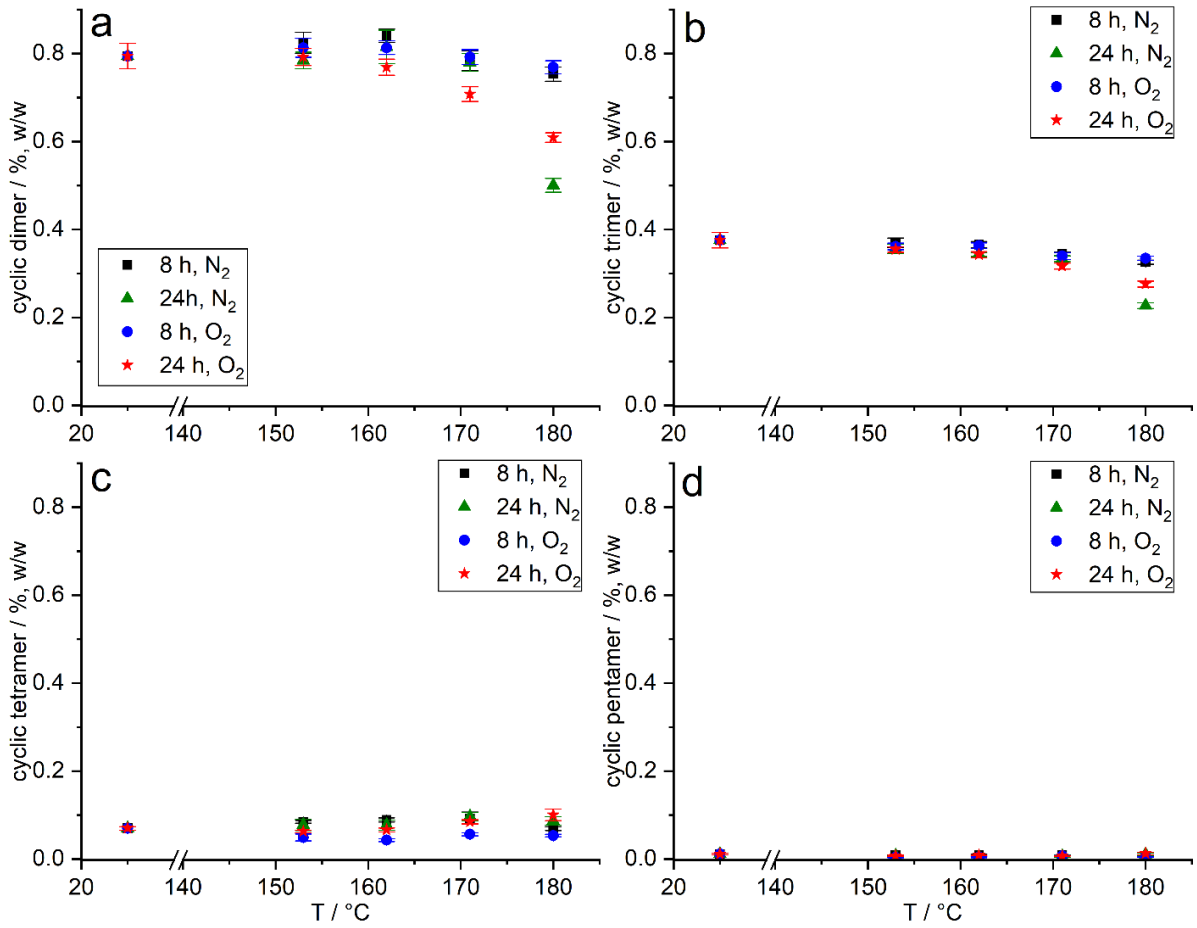

Figure 4.5.8 Change of content of cyclic dimer (**a**), cyclic trimer (**b**), cyclic tetramer (**c**), and cyclic pentamer (**d**) determined in tempered PA 1101 powder samples.

In Figure 4.5.9 a, a decrease of Irganox 1098 was observed depending on the aging temperature and aging duration. The effect of the different aging durations was highest for a temperature of 180 °C. One possible explanation could be that the stabilizer was consumed during thermal treatment in dependence on the aging durations. However, evaporation or sublimation of low molecular weight compounds could also be a reason for depleting stabilizer and oligomer contents. In Figure 4.5.9 b, an overview of the sum of all determined compounds is given. It was shown that the sum of extractable low molecular compounds was decreasing with both the temperature and the duration of heat treatment. The highest difference was obtained for the samples aged at 180 °C. The samples treated for 8 h showed similar values

no matter if aged under nitrogen or compressed air gas flow. Considering the samples that were aged for 24 h, the value of 1.0% for aging under nitrogen was the lowest compared to 1.2% for aging under compressed air gas. Impurity 1 (compare Figure 4.5.9 c) showed a partial increase based on the thermal treatment whereby the values showed considerable fluctuations. For impurity 2, the initial value was highest with 0.02% and showing a relatively high standard deviation. A decrease down to 0% was observed for PA 1101 samples tempered at 24 h under N_2.

Moreover, an increase of yellowing was observed for powders aged under compressed air gas in dependency of the aging durations and temperatures. Okamba-Diogo et al. [13,35] conducted several studies investigating polyamide 11. In one of their studies, the stabilizer was extracted from the polymer matrix by a dissolution/precipitation method. After thermal oxidation at 110 °C the stabilizer depletion was quantified by HPLC using the UV signal at 280 nm [13]. The same method was applied for investigating the effect of hindered phenols on the stabilization of polyamide 11 aged at temperatures from 90 °C up to 165 °C. It was constituted that phenols significantly contribute to yellowing. Moreover, the influence of phenol concentration was compared to Irganox 1010 and Irganox 245. Remarkably, the authors admitted that within the dissolution/precipitation reaction, residues of the stabilizer might be physically trapped between crystalline lamellae or chemically linked by a transamidation reaction. Consequently, their determinations might be underestimated [35].

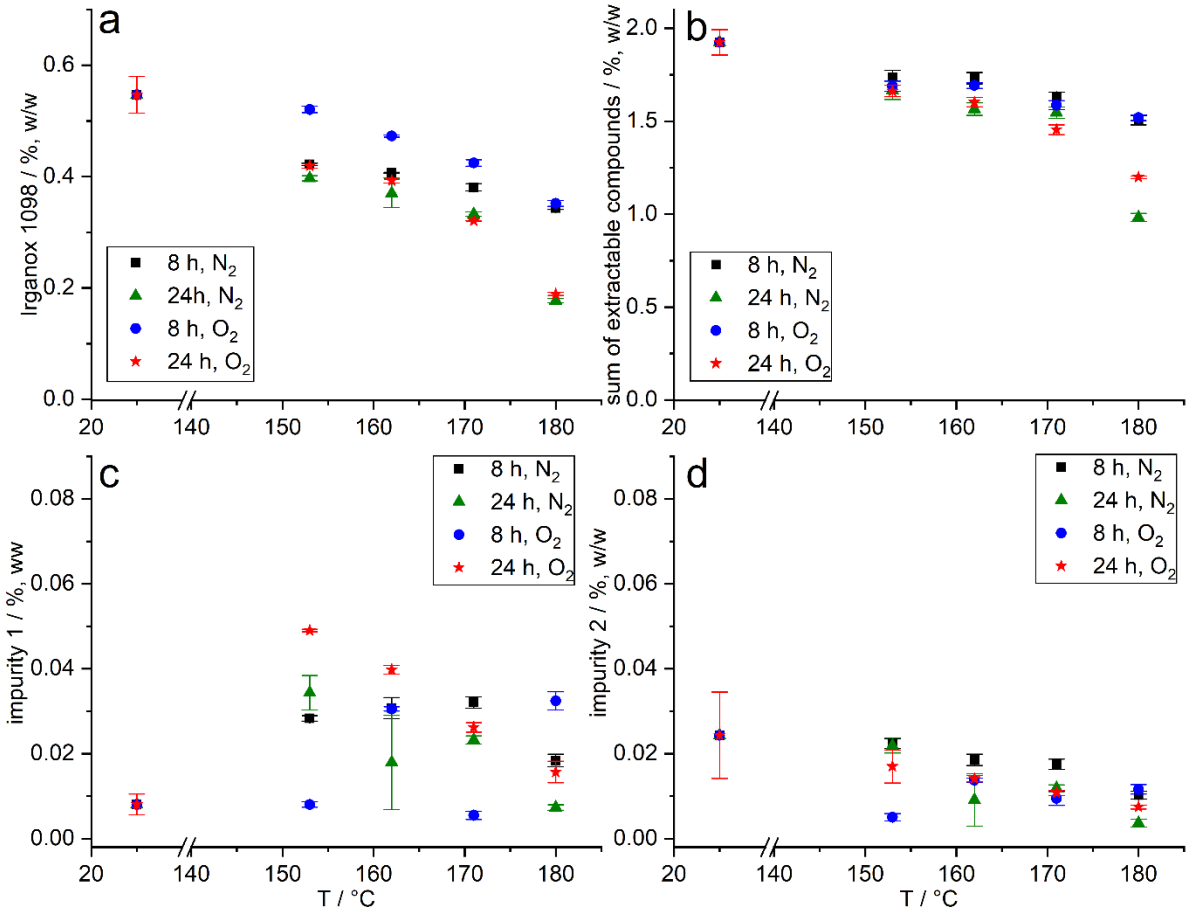

Figure 4.5.9 Change of content of Irganox 1098 (**a**), the sum of the determined extractable compounds (**b**), impurity 1 (**c**), and impurity 2 (**d**) determined in tempered PA 1101 powder samples.

4.5.4 Conclusion

A triple detection system in combination with inverse gradient HPLC was established to develop a method for the determination of low molecular weight compounds in polyamide 11 identified by high-resolution mass spectrometry.

The development of a suitable extraction method was a prerequisite to enable the subsequent analytical determination of the content of oligomer compounds in PA 1101 powder samples. ASE was found to be an efficient extraction method being less time-consuming compared to Soxhlet extraction.

Moreover, it was taken advantage of the different detectors of the triple detection system including DAD, MS, and CAD. The DAD was applied for the determination of Irganox 1098 and the MS was used for peak identification of signals in the CAD. Furthermore, the uniform response behavior in the CAD due to inverse gradient compensation was utilized for the quantification of low molecular weight compounds where no analytical standards were available. Based on the application of an inverse gradient HPLC protocol, the calibration curve

of AUA could be applied to all other oligomer compounds in consideration of response factors, which were determined for the CAD. In this context, investigations concerning the formation of ion pairs with mobile phase additives were conducted, as ion pair formation is a key factor to reduce the volatility of the linear monomer.

By combination of the ASE extraction protocol and the inverse gradient HPLC triple detection method, it was possible to monitor the change of low molecular weight compounds in new and stressed PA 1101 powder samples. Concerning the aging studies, it was found that the atmosphere, e.g. N_2 or compressed air gas flow under thermal load, had only minor influence on the remaining amount of the stabilizer Irganox 1098. Consequently, it could not be identified if evaporation or consumption were the main reasons for the depletion of low molecular weight content. However, the high surface to volume ratio and the gas flow in the micro chamber might have led to evaporation of the oxidation stabilizer. In the sintering process, the cyclic oligomers are suspected to cause contamination of the sintering machine. Moreover, it would be interesting if the decrease of linear oligomers can be directly correlated to the increase of molecular weight due to post condensation processes

Acknowledgements

The authors thank the BMW AG for funding analytical equipment and financial support which is gratefully acknowledged. Special thanks are expressed to Katherine Lovejoy und Sylvia Grosse from Thermo Fisher Scientific for helpful discussions. Further thanks go to BASF for providing the sample of Irganox 1098.

4.5.5 References

[1] M. Genas, Rilsan (Polyamid 11), Synthese und Eigenschaften, Angew. Chem. (1962) 535–540.

[2] S. Tencé-Girault, S. Lebreton, O. Bunau, P. Dang, F. Bargain, Simultaneous SAXS-WAXS experiments on semi-crystalline polymers: Example of PA11 and its Brill transition, Crystals 9 (2019). https://doi.org/10.3390/cryst9050271.

[3] W. Romão, E.V.R. Castro, E.A.S. Filho, R.C.L. Guimarães, A.L.N. Silva, S.C.S. Teixeira, M.-A. de Paoli, G.L. de Sena, Ageing of polyamide 11 used in the manufacture of flexible piping, J. Appl. Polym. Sci. 114 (2009) 1777–1783. https://doi.org/10.1002/app.30793.

[4] A. Wegner, R. Harder, G. Witt, D. Drummer (Eds.), Determination of optimal processing conditions for the production of polyamide 11 parts using the laser sintering process, 2015.

[5] L. Martino, L. Basilissi, H. Farina, M.A. Ortenzi, E. Zini, G. Di Silvestro, M. Scandola, Bio-based polyamide 11: Synthesis, rheology and solid-state properties of star structures, Eur. Polym. J. 59 (2014) 69–77. https://doi.org/10.1016/j.eurpolymj.2014.07.012.

[6] R.D. Goodridge, C.J. Tuck, R.J.M. Hague, Laser sintering of polyamides and other polymers, Prog. Mater. Sci. 57 (2012) 229–267. https://doi.org/10.1016/j.pmatsci.2011.04.001.

[7] M. Schmid, Selektives Lasersintern (SLS) mit Kunststoffen: Technologie, Prozesse und Werkstoffe, Hanser, München, 2015.

[8] M. Schmid, Additive Fertigung mit Selektivem Lasersintern (SLS): Prozess- und Werkstoffüberblick, Springer, Wiesbaden, 2015.

[9] G.W. Ehrenstein, S. Pongratz, Beständigkeit von Kunststoffen, Hanser, München, 2007.

[10] G.W. Becker, D. Braun (Eds.), Technische Thermoplaste Polyamide: Kunststoff Handbuch ¾, Hanser, München, 1998.

[11] R.D. Maier, M. Schiller, Kunststoff Additive Handbuch, Hanser, München, 2016.

[12] M. Heimrich, M. Bönsch, H. Nickl, T.J. Simat, Cyclic oligomers in polyamide for food contact material: quantification by HPLC-CLND and single-substance calibration, Food Addit. Contam Part A 29 (2012) 846–860. https://doi.org/10.1080/19440049.2011.649496.

[13] O. Okamba-Diogo, E. Richaud, J. Verdu, F. Fernagut, J. Guilment, F. Pery, B. Fayolle, Quantification of hindered phenols in polyamide 11 during thermal aging, Polym. Test. 52 (2016) 63–70. https://doi.org/10.1016/j.polymertesting.2016.03.023.

[14] O. Okamba Diogo, Thermo-oxydation des polyamides. Dissertation, 2015.

[15] H. Zahn, J. Kunde, Cyclische Amide aus ω-Amino-undecansäure, Chem. Ber. 94 (1961) 2470–2477. https://doi.org/10.1002/cber.19610940920.

[16] S. Mori, M. Furusawa, T. Takeuchi, Reduction-gas chromatographic determination of cyclic monomer and oligomers in polyamides, Anal. Chem. 42 (1970) 661–662. https://doi.org/10.1021/ac60288a037.

[17] V. Krajník, P. Božek, J. Kondelíková, j. Králíček, High-performance liquid chromatography of 12-dodecanelactam and its cyclic oligomers present in polymide 12, J. Chromatogr. A 250 (1982) 138–140. https://doi.org/10.1016/S0021-9673(00)95224-5.

[18] Y. Mengerink, S. van der Wal, H.A. Claessens, C.A. Cramers, Analysis of higher polyamide-6 oligomers on a silica-based reversed-phase column with a gradient of formic acid as compared with hexafluoroisopropanol, J. Chromatogr. A 871 (2000) 259–268. https://doi.org/10.1016/S0021-9673(99)01072-9.

[19] V.R. Feldmann, R. Feinauer, Cyclische Monomere und Oligomere in Polyamid-11 und Polyamid-12, Die Angewandte Makromolekulare Chemie 34 (1973) 9–18. https://doi.org/10.1002/apmc.1973.050340102.

[20] S. Mori, T. Takeuchi, Gel permeation chromtography of the linear monomer and oligomers in polyamides, J. Chromatogr. A 50 (1970) 419–428. https://doi.org/10.1016/S0021-9673(00)97967-6.

[21] H. Zahn, G.B. Gleitsman, Oligomers and pleionomers of synthetic fiber-forming polymers, Angew. Chem. Int. Ed in English 2 (1963) 410–420. https://doi.org/10.1002/anie.196304101.

[22] P. Peng, P. Hodge, Cyclic oligo(undecanamide)s (nylon 11 s) and cyclic alternating oligo(undecanamide-undecanoate)s: their synthesis using high dilution conditions and their analysis, Polymer 39 (1998) 981–990. https://doi.org/10.1016/S0032-3861(97)00365-0.

[23] Mengerink Y., R. Peters, C.G. deKoster, S. van der Wal, H.A. Claessens, C.A. Cramers, Separation and quantification of the linear and cyclic structures of polyamide-6 at the critical point of adsorption, J. Chromatogr. A 914 (2001) 131–145. https://doi.org/10.1016/S0021-9673(01)00622-7.

[24] P.H. Gamache (Ed.), Charged aerosol detection for liquid chromatography and related separation techniques, Wiley, Hoboken, 2017.

[25] R.D. Cohen, Y. Liu, X. Gong, Analysis of volatile bases by high performance liquid chromatography with aerosol-based detection, J. Chromatogr. A 1229 (2012) 172–179. https://doi.org/10.1016/j.chroma.2012.01.036.

[26] J. Loughlin, H. Phan, M. Wan, S. Guo, K. May, B. Lin, Evaluation of charged aerosol detection (CAD) as a complementary technique for high-throughput LC-MS-UV-ELSD analysis of drug discovery screening liraries.

[27] A. de Villiers, T. Górecki, F. Lynen, R. Szucs, P. Sandra, Improving the universal response of evaporative light scattering detection by mobile phase compensation, J. Chromatogr. A 1161 (2007) 183–191. https://doi.org/10.1016/j.chroma.2007.05.078.

[28] E. Grushka, N. Grinberg (Eds.), Advances in chromatography: Advances in aerosol-based detectors, CRC Press, Boca Raton, 2014.

[29] J.P. Hutchinson, J. Li, W. Farrell, E. Groeber, R. Szucs, G. Dicinoski, P.R. Haddad, Universal response model for a corona charged aerosol detector, J. Chromatogr. A 1217 (2010) 7418–7427. https://doi.org/10.1016/j.chroma.2010.09.056.

[30] A.W. Squibb, M.R. Taylor, B.L. Parnas, G. Williams, R. Girdler, P. Waghorn, A.G. Wright, F.S. Pullen, Application of parallel gradient high performance liquid chromatography with ultra-violet, evaporative light scattering and electrospray mass spectrometric detection for the quantitative quality control of the compound file to support pharmaceutical discovery, J. Chromatogr. A 1189 (2008) 101–108. https://doi.org/10.1016/j.chroma.2007.11.017.

[31] M. Menz, B. Eggart, K. Lovejoy, I. Acworth, P. Gamache, F. Steiner, Technical Note 72806: Charged aerosol detection - factors affecting uniform analyte response.

[32] T. Górecki, F. Lynen, R. Szucs, P. Sandra, Universal response in liquid chromatography using charged aerosol detection, Anal. Chem. 78 (2006) 3186–3192. https://doi.org/10.1021/ac060078j.

[33] S. Kromidas (Ed.), The HPLC Expert: Possibilities and limitations of modern high performance liquid chromatography, Wiley, Weinheim, 2016.

[34] Büchi (Ed.), Betriebsanleitung Extraktionssystem B-811, 2016.

[35] O. Okamba-Diogo, F. Fernagut, J. Guilment, F. Pery, B. Fayolle, E. Richaud, Thermal stabilization of polyamide 11 by phenolic antioxidants, Polym. Degrad. and Stab. 179 (2020) 109206. https://doi.org/10.1016/j.polymdegradstab.2020.109206.

[36] B. Scherer, I.L. Kottenstedde, W. Bremser, F.-M. Matysik, Analytical characterization of polyamide 11 used in the context of selective laser sintering: Physico-chemical correlations, Polym. Test. (2020) 106786–106795.

[37] K. Wudy, D. Drummer, Aging effects of polyamide 12 in selective laser sintering: Molecular weight distribution and thermal properties, Addit. Manuf. 25 (2019) 1–9. https://doi.org/10.1016/j.addma.2018.11.007.

[38] H. Wang, J. Yuan, Identification and quantification of unknown antioxidants in plastic materials by ultrasonic extraction and ultra-performance liquid chromatography coupled

with quadrupole time-of-flight mass spectrometry, Eur. J. of Mass Spectrom. 22 (2016) 19–29. https://doi.org/10.1255/ejms.1404.

[39] S. Meding, K. Lovejoy, F. Steiner, M. Ruehl, Application Note 72869: A multi-detector platform comprising UV/Vis, charged aerosol, and single quadrupole mass spectrometric detection for comprehensive sample analysis.

[40] M. Lísa, F. Lynen, M. Holcapek, P. Sandra, Quantitation of triacylglycerols from plant oils using charged aerosol detection with gradient compensation, J. Chromatogr. A 1176 (2007) 135–142. https://doi.org/10.1016/j.chroma.2007.10.075.

5 Summary

In order to meet the quality requirements for polymers used in AM, especially in laser sintering and MJF, as well as to guarantee high quality of printed parts, a comprehensive characterization of the intrinsic properties of the applied materials is necessary. In this thesis, therefore, methods were developed and optimized to investigate polyamide 11 and 12 both at the macromolecular and the low molecular weight range.

In one project, a sawtooth gradient for HRP-HPLC was developed that allowed the separation and analysis of polyamide 11 and 12 samples. This special type of gradient program paved the way for the distinction of polyamide 11 processing powders. It was possible to distinguish between virgin, mixed, and used polyamide 11 powder samples which are applied in the laser sintering process. Additionally, SEC-MALLS as a complementary method gave information about the molar mass distribution of the investigated polyamide 11 and 12 samples.

In another project, HPLC in combination with high-resolution MS was utilized for the identification of individual components of materials applied in the MJF process. Within these investigations, residues of the identified components of fusing and detailing agents could still be detected in the printed parts.

Moreover, SEC-MALLS was a powerful tool to characterize aged PA 1101 powder samples in terms of molecular weight distribution after thermal treatment. PA 1101 was identified as a highly reactive polymer, which was proven by the increase of molar mass under artificial aging conditions due to post-condensation. The observed results were transferred to the investigated printed parts and related to their mechanical performance described by the corresponding ε_B values. The increase of molar mass values was also proven for the investigated tensile bars, but high M_w values could not be identified as the reason for brittle fracture of printed parts. Instead, tensile bars with good mechanical performance were related to comparatively high P values.

In the last part of this work, different extraction methods were studied to ensure a quantitative extraction of low molecular weight compounds from PA 1101 powder samples. Extracts of different aging states were characterized with respect to their stabilizer, monomer, and oligomer content. To achieve this, a quantitative method was developed in conjunction with a triple detection system consisting of a DAD, a MS, and a CAD. The results revealed that cyclic oligomers were stable against thermal treatment whereas the linear ones decrease already at a low thermal load. Moreover, it is possible that the low molecular weight compounds evaporate due to their low vapor pressure and condensate again within components of the sintering machine. The depositions in the machine could be one reason for a bad mechanical

performance of printed parts. Consequently, the low molecular weight content should be kept as low as possible within the polymer powder.

Within this thesis, methods for characterization of the material properties of PA 1101 and related polymers were established. The gained results and methods help to improve the quality of powder materials and stability of the laser sintering process.

6 Zusammenfassung in deutscher Sprache

Um den Qualitätsanforderungen für Polymere gerecht zu werden, die für die additive Fertigung und insbesondere für das Lasersintern und MJF verwendet werden, sowie um eine hohe Qualität der gedruckten Teile garantieren zu können, ist eine umfassende Charakterisierung der intrinsischen Eigenschaften der verwendeten Materialien notwendig. In der vorliegenden Arbeit wurden daher Methoden entwickelt und optimiert, um Polyamid 11 und 12 sowohl auf makromolekularer als auch niedermolekularer Ebene zu untersuchen.

Im ersten Projekt wurde eine Sägezahngradientenmethode für HRP-HPLC entwickelt, die eine Trennung und Analyse von Polyamid 11 und 12 Proben ermöglichte. Dieses spezielle Gradientenprogramm erlaubte eine Unterscheidung von Polyamid 11 Prozesspulvern. Es war möglich mittels HRP-HPLC zwischen neuen, gemischten und gebrauchten Polyamid 11 Pulverproben aus dem Lasersinterprozess zu unterscheiden. Zusätzlich wurden mit SEC-MALLS als komplementäre Methode Informationen hinsichtlich der Molmassenverteilung der untersuchten Polyamid 11 und 12 Proben erhalten.

Im nächsten Projekt wurden mit HPLC in Verbindung mit hochauflösender MS einzelne Inhaltsstoffe der Materialien identifiziert, die im MJF Prozess Anwendung finden. Mit Hilfe dieser Untersuchungen wurden selbst Rückstände der Inhaltsstoffe der Fusing und Detailing Agenzien im gedruckten Bauteil festgestellt.

Des Weiteren wurde SEC-MALLS angewandt, um gealterte PA 1101 Pulverproben hinsichtlich ihrer Molgewichtsverteilung nach thermischer Belastung zu bestimmen. PA 1101 wurde als hochreaktives Polymer charakterisiert, was durch den Anstieg der Molmasse durch Postkondensation unter der künstlichen Alterung belegt werden konnte. Die erhaltenen Ergebnisse wurden auf die gedruckten Prüfkörper in Bezug auf deren mechanisches Verhalten, welches über die korrespondierenden ε_B Werte beschrieben wurde, übertragen. Die Molmassenzunahme wurde auch für die gedruckten Prüfkörper bestätigt, wobei eine hohe Molmasse nicht als Grund für Sprödbrüche benannt werden konnte. Stattdessen zeigten gedruckte Prüfkörper mit einem guten mechanischen Verhalten vergleichsweise hohe P Werte.

Im letzten Teil dieser Arbeit, wurden verschiedene Extraktionsmethoden untersucht, um eine quantitative Extraktion der niedermolekularen Anteile aus PA 1101 Pulverproben sicherzustellen. Die erhaltenen Extrakte wurden hinsichtlich ihres Stabilisator-, Monomer- und Oligomergehaltes charakterisiert. Um dies zu ermöglichen, wurde eine Methode bestehend aus einer HPLC mit inversen Gradienten und einem Tripledetektionssystem mit einem DAD, einem MS und einem CAD entwickelt. Die Ergebnisse zeigten, dass die zyklischen Oligomere

stabil gegenüber thermischer Belastung sind, während die linearen Oligomere bereits bei niedriger thermischer Belastung abnehmen. Dabei ist es auch möglich, dass sich die niedermolekularen Bestandteile aufgrund ihres niedrigen Dampfdrucks verflüchtigen und an anderer Stelle in der Sintermaschine wieder kondensieren. Folglich können Ablagerungen innerhalb der Sintermaschine ein Grund für ein schlechtes mechanisches Verhalten von gedruckten Bauteilen sein. Deshalb sollte der Anteil an den genannten Verbindungen im Polymerpulver so gering wie möglich gehalten werden.

In der vorliegenden Arbeit wurden Methoden für eine umfassende Charakterisierung der Materialeigenschaften von PA 1101 und ähnlichen Polymeren entwickelt. Die erhaltenen Ergebnisse und Methoden tragen dazu bei die Qualität der Pulvermaterialien und die Prozessstabilität im Lasersintern zu verbessern.

Eidesstattliche Erklärung

Ich habe die Arbeit selbstständig verfasst, keine anderen als die angegebenen Quellen und Hilfsmittel benutzt und bisher keiner anderen Prüfungsbehörde vorgelegt. Von den in §27 Abs. 5 vorgesehenen Rechtsfolgen habe ich Kenntnis genommen.

Regensburg, den 29.04.2021 ……

(Beate Scherer)